

NAPOLI | IN-VENTO 2018

XV CONFERENCE OF THE ITALIAN ASSOCIATION FOR WIND ENGINEERING

ABSTRACTS



September
9-12
2018
NAPOLI
CASTEL DELL'OVO



NAPOLI | IN-VENTO 2018

XV CONFERENCE OF THE ITALIAN ASSOCIATION FOR WIND ENGINEERING

ABSTRACTS

with the patronage of:



Scientific Committee

Alberto Maria Avossa
Gianni Bartoli
Marco Belloli
Claudio Borri
Luca Bruno
Massimiliano Burlando
Luca Caracoglia
Yaojun Ge
Christos T. Georgakis
Massimiliano Gioffrè
Vittorio Gusella
Horia Hangan
Rüdiger Höffer
Ahsan Kareem
Giampiero Manara
Francesco Petrini
Maria Pia Repetto
Francesco Ricciardelli
Daniele Rocchi
Giovanni Solari
Ted Stathopoulos
Yukio Tamura
Alberto Zasso

Organizing Committee

Alberto Maria Avossa
Stefania Di Ronza
Caterina Eramo
Giovanna Giugliano
Carmela Maienza
Francesco Ricciardelli (Chair)
Marco Vigliotti

Contacts

Department of Engineering
www.in-vento-2018.org
invento2018@unicampania.it

INDEX

- L. Amerio, G. Lamberti, A. Zasso and C. Gorlé	1
Comparison of high-resolution pressure peak events measurement in closed section and open section wind tunnels	
- T. Andrianne, F. Rigo and V. Denoël	3
VIV response of a suspended sphere nearby the critical Reynolds number	
- T. Argentini, S. Omarini, A. Zasso and M. Petrangeli	7
Aerodynamic tailoring of a bluff deck section subjected to inclined winds due to the complex orography of the construction site	
- D. Astolfi, F. Castellani and L. Terzi	9
A SCADA-based method for estimating the energy improvement from wind turbine retrofitting	
- S. Attrill, K. Reipas and V. Tang	11
How Stack Effect and Wind Impacts in Tall Buildings can Affect Occupant Comfort and Smooth Building Operation	
- A. Balbi, M. P. Repetto, G. Solari and A. Freda	13
Wind effects on containers stability	
- G. Barbanti, E. Marino and C. Borri	15
Mooring system optimization for a spar-buoy wind turbine in rough wind and sea conditions	
- M. Barbato, F. Petrini and J. E. K. Antoun	17
Performance-Based loss estimation for tall buildings under wind	

- G. Bartoli, C. Mannini and A. M. Marra STEELWAR project: wind tunnel tests on automated rack supported warehouses	19
- I. Bayati, L. Bernini, A. Facchinetti, A. Fontanella, H. Giberti, A. Zasso and M. Belloli Hybrid/HIL Testing of Floating Wind Turbines: the LIFES50+ project	21
- L. Bernini, G. Tomasini and D. Tarsitano Design and experimental optimisation of a cm-scale wind turbine for energy harvesting	23
- G. Bordogna, S. Muggiasca, S. Giappino and M. Belloli Wind-tunnel experiments on a large-scale Flettner rotor	25
- R. Buccolieri, T. Massai, A. Giachetti, F. Quarta and G. Bartoli The effect of lift-up buildings on wind-induced forces and ventilation in simple urban geometries	27
- A. Buljac, H. Kozmar, W. Yang and A. Kareem Wind, wave and sea current loads on offshore wind turbines	29
- A. Buljac, H. Kozmar, M. Macháček and S. Pospíšil Self-excited vibrations of bridge deck with single and double wind barriers	31
- M. Burlando, D. Romanić, H. Hangan and G. Solari Wind tunnel experimentation on stationary downbursts at WindEEE	33
- I. Calotescu Damage from recent thunderstorms in Romania	35
- S. Cammelli, H. Nguyen-Sinh and J. Garcia Navarro Full-scale measurements of a 63-storey mixed-use high-rise under wind	37
- N. Caterino, G. Pugliano and U. Robustelli Design and assessment of real time monitoring systems for structural control of wind turbines	39
- E. Cheynet, J. Bogunović Jakobsen and J. Snæbjörnsson Influence of the bridge deck on the flow characteristics monitored by sonic anemometers installed on a long-span bridge	41
- E. Cheynet Estimation of the vertical wind coherence in an offshore environment	45

- P. Churin, O. Egorychev, O. Poddaeva and J. Gribach	49
Design and experimental studies of wind impact to unique buildings	
- M. Ciano, M. Giofrè and M. Grigoriu	51
Modeling and simulation of non-stationary thunderstorm outflows	
- M. Cid Montoya, F. Nieto and S. Hernández	53
On the aerostructural design of long-span cable-stayed bridges: The contribution of parameter variation studies with focus on the deck design	
- M. Cindori, I. Džijan, F. Juretić and H. Kozmar	55
A novel steady RANS model for the computational modeling of the homogeneous atmospheric boundary layer flow over hilly terrain	
- D. P. Coiro, F. Scherillo, G. Troise, N. Bizzarrini and G. Calise	57
Experiences in designing, manufacturing, installation and testing of wind turbines	
- M. Como	59
On the Flutter Wind Speed of Long Span Suspension Bridges	
- C. Demartino and F. Ricciardelli	61
Probabilistic assessment of the galloping stability of ice-accrete bridge hangers	
- A. Denis, G. Piccardo and G. Solari	63
Numerical simulation of cable dynamics induced by synoptic and thunderstorm events	
- A. Eltayesh, M. Burlando, F. Castellani, M. Becchetti and H. M. El-Batsh	65
Experimental and numerical study of the wind tunnel blockage effects on the behaviour of a horizontal axis wind turbine	
- A. Fenerci and O. Øiseth	67
Wind field variability in complex terrain: Lessons from the Hardanger Bridge	
- G. Ferri, A. Chiaracane, F. Lupi, U. Winkelmann, C. Borri and R. Hoeffler	69
Validated numerical simulation of aerodynamic and aeroelastic characteristics of Rhein-crossing bridge in Leverkusen	
- G. Frison, A. M. Marra, G. Bartoli and R. Scotta	71
Aerodynamic and aeroelastic response of CAARC building – Comparison between numerical simulation and wind tunnel measurements	
- C. T. Georgakis, J. Chen, N. Caterino and M. Spizzuoco	73
Mitigation of structural demand to wind turbines: experimental investigation of three control strategies	

- A. Giachetti, C. Mannini and G. Bartoli Experimental study on the aerodynamics of rectangular prisms with a forebody screen	75
- S. Giappino, A. Manenti and S. Muggiasca Aerodynamic instability of cables fitted with pipes	77
- S. Giappino, S. Omarini, P. Schito, C. Somaschini, M. Belloli and M. Tenni Cyclist aerodynamics: a comparison between wind tunnel tests and CFD for helmet design	79
- J. B. Holmes Extreme wind speed prediction – the Australian experience	83
- M. Horvat, L. Bruno, S. Khris and A. Lo Giudice Computational simulation of windblown sand erosion, transport, and sedimentation around dunes	85
- G. Hu, K. C. S. Kwok and K. T. Tse Application of aerodynamic modification on slender structures for wind energy harvesting	87
- L. Ierimonti, I. Venanzi and L. Caracoglia Life-cycle cost-based wind design of tall buildings	89
- M. Karami, L. Carassale, H. Hangan and M. Refan An approximate model for large-scale fluctuations in tornado-like vortices	91
- YC Kim, YL Lo and CH Chang Characteristics of unsteady aerodynamic force on tall building	93
- G. Lamberti and C. Gorié Uncertainty quantification in RANS simulations for predicting wind loads on buildings	95
- S. Lin, H. Liao, N. Nikitas and Qi Wang Effects of amplitude on the spectral characteristics of motion-induced force for oscillating 5:1 rectangular cylinder	97
- F. Lupi, H. J. Niemann and R. Höffer A model extension for vortex-induced vibrations	99
- T. M. Lystad, A. Fenerci and O. Øiseth Aerodynamic effect of non-uniform turbulent wind profiles for long-span bridges	101

- C. Maienza, A. M. Avossa, F. Ricciardelli, F. Scherillo and C. T. Georgakis	103
A comparative analysis of construction costs of onshore and shallow- and deep-water offshore wind farms	
- F. Malizia, H. Montazeri and B. Blocken	105
A numerical analysis of different approaches for rotation modelling on the aerodynamic drag of a spoked cycling wheel	
- G. Manara	107
Some topics about wind engineering that Curtain Walling design might be longing for in standards	
- C. Mannini	109
Numerical investigation of transverse galloping in turbulent flow	
- A. Mariotti, G. Buresti and M. V. Salvetti	111
Flow separation delay and drag reduction through contoured transverse grooves	
- K. Matsuda, K. Kato, N. Cao and R. Higashimura	113
Experimental Study on the Effect of Secondary Vortices at Trailing Edge on Motion-Induced Excitation	
- A. Mockutè, C. Borri, E. Marino and C. Lugni	115
Wind-wave loading and response of OWT monopiles in rough seas	
- M. Cid Montoya, S. Hernández, C. López, A. Álvarez and J. Á. Jurado	117
Design optimization of a reduced model of a wind mill tower for wind tunnel testing	
- D. M. Moore, C. W. Letchford and M. Amitay	119
Transitional shear layers on rectangular sections	
- M. Mulas and R. Zucca	121
CFD applications for Building and Environment	
- B. Nicese, C. Mannini, A. M. Marra and G. Bartoli	123
A critical database for the Strouhal number of bridge decks	
- L. Patruno and M. Ricci	125
Synthetic turbulence generation using spectral methods	
- F. Petrini, Z. Wang and A. Giaralis	127
Simultaneous vibration suppression and energy harvesting under wind excitation in tall buildings equipped with the tuned mass damper inerter (TMDI)	

- L. Pigolotti, C. Mannini and G. Bartoli Some advances in the study of classical-flutter-based generators	129
- L. Raffaele and L. Bruno A semi-probabilistic framework for windblown sand action	131
- M. P. Repetto and M. Damele Wind-induced fatigue verification standard methods	133
- A. Rezaeiha, H. Montazeri and B. Blocken Effect of Solidity on Aerodynamic Performance of Vertical Axis Wind Turbines	137
- A. Ricci and B. Blocken Predicting microscale wind conditions to improve ship navigation in the largest vault in the world	139
- L. Riefolo, M. Vardaroglu, A. M. Avossa, D. Vicinanza, F. Ricciardelli, and G. R. Tomasicchio Experimental tests on the wave-induced response of a Tension Leg Platform supporting a 5MW wind turbine	141
- F. Rigo, T. Andrianne and V. Denoël Mixture model in high-order statistics for peak factor estimation on low-rise building	143
- F. Rigo, V. Denoël and T. Andrianne Vortex induced vibrations of rectangular cylinders arranged on a grid	147
- D. Romanić and H. Hangan The interplay between background atmospheric boundary layer winds and downburst outflows. A first physical experiment	151
- R. Sasaki, K. Miyashita and R. Yoshie Field measurement of gas dispersion in the Atsugi area	155
- P. Schito, L. Rosa and A. Zasso Definition of wind loads on the Riyadh Western Metro Station	157
- V. Sepe, F. Rizzo, F. Ricciardelli and A. M. Avossa Characterization of mean wind profiles and surface roughness assessment from wind LIDAR measurements	159

- Y. Uematsu and R. Yamamura	161
Experimental study of wind loads on domed free roofs	
- L. Viviani, F. Dorigatti, J. Kilpatrick and J. Galsworthy	163
Aerodynamic Optimization of Tall Buildings	
- A. Zasso, F. Perotti, L. Rosa, P. Schito, G. Pomaranzi and N. Daniotti	165
Wind Pressures Distribution on a Porous Double Skin Façade System	
- X. Zheng, H. Montazeri and B. Blocken	167
Numerical study of wind-induced pressure on a high-rise building with balconies: comparison of LES, RANS and experiments	
- S. Zhou, L. Tan and S. Li	169
On effects of Correction Factor for VIV Amplitude from a Prototype Prism and 2D Section Model	

ABSTRACTS

Comparison of high-resolution pressure peak events measurement in closed section and open section wind tunnels

L. Amerio¹, G. Lamberti², A. Zasso³ and C. Gorié²

¹Advanced Technology + Research group, ARUP, London, UK

²Department of Civil and Environmental Engineering, Stanford University, California

³Department of Mechanical Engineering, Politecnico di Milano, Italy

Corresponding author: L. Amerio, luca.amerio@arup.com

Abstract

Wind tunnel measurements are an established technique for the assessment of wind induced pressure on building façades. Despite having been used for more than fifty years, there are still some open questions. One of these are the so-called pressure peaks (or spikes) occurring in the leeward faces of the models.

These events have been observed by numerous authors in several works, who proposed different interpretations. They have been investigated with different techniques, such as wind tunnel pressure tests ((Lin, et al., 1995), (Lin & Surry, 1998), (Gavanski & Uematsu, 2014) and (Peng, et al., 2014)), flow visualization (Banks, et al., 2000), Computation Fluid Dynamic (Ono, et al., 2008) or even full-scale tests ((Lin & Surry, 1998), (Wu, 2000) and (Wu, et al., 2001));

Most of these works investigate the pressure distributions on the roofs of low-rise buildings. Here, these events have been generally linked to the conical vortexes that forms behind the roof leading edge. This was confirmed by the simultaneous flow visualization and pressure measurement performed by (Banks, et al., 2000). However, (Surry & Djakovich, 1995) observed a relationship between the pressure spikes occurring on the lateral surfaces of slender high-rise buildings and the vortex shedding frequency associated with the geometry, suggesting that also other phenomena takes part in the production of these events.

During a high-resolution pressure field measurement at Politecnico di Milano, unusually strong suction events up to $-15 C_p$ have been observed on the lateral surface of a prismatic high-rise building (Amerio, 2018). These events were characterized by an extremely short duration and small spatial extension.

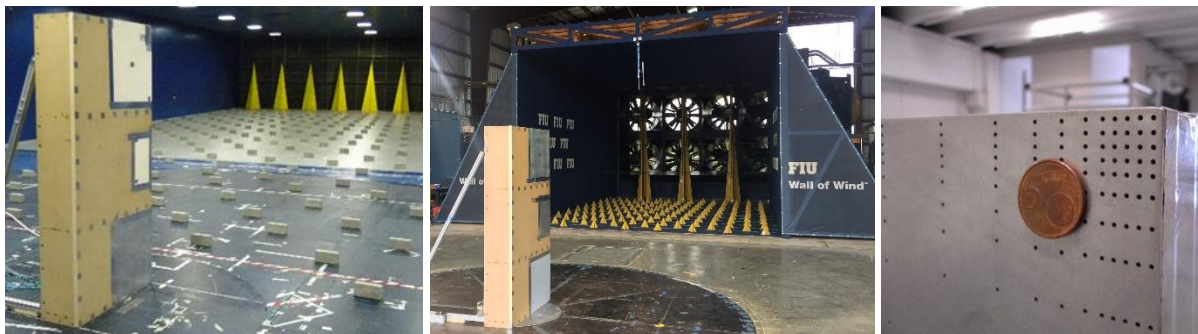


Figure 1 – Left) The test performed at PoliMi GVPM; Centre) The second test in FIU WoW; Right) A closeup view of the instrumented area

The experiment has been replicated in the Florida International University Wall of Wind in an open section facility. The experiment has been repeated both at the same Reynolds number used in Politecnico di Milano GVPM and at higher Reynolds numbers to study the dependency of these events from it.

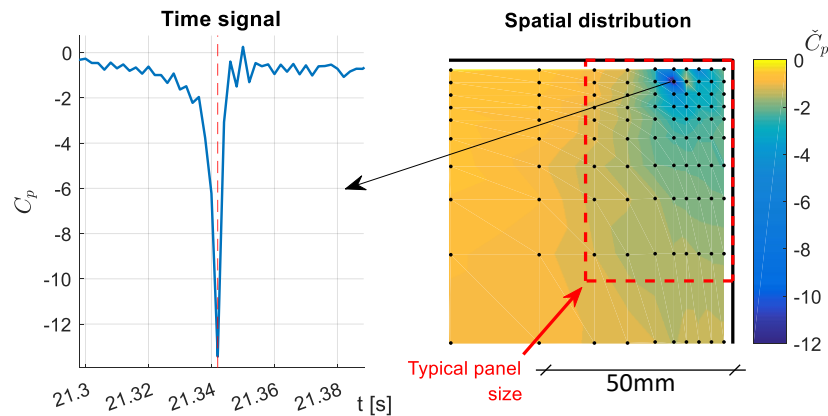


Figure 2 – An example of pressure peak occurring in the corner region of the model

In this paper a comparison of the results of the two experiments is performed, with special regard to the extreme pressure spikes occurring in the corner region of the model and to the Reynolds dependency of these phenomena.

References

- Amerio, L., 2018. *Experimental high resolution analysis of the pressure peaks on a building scale model façades (Ph.D. thesis, unpublished)*. Milano: s.n.
- Banks, D. et al., 2000. Flow visualization of conical vortices on flat roofs with simultaneous surface pressure measurement. *Journal of Wind Engineering and Industrial Aerodynamics*, 1, 84(1), pp. 65-85.
- Gavanski, E. & Uematsu, Y., 2014. Local wind pressures acting on walls of low-rise buildings and comparisons to the Japanese and US wind loading provisions. *Journal of Wind Engineering and Industrial Aerodynamics*, 9, Volume 132, pp. 77-91.
- Lin, J. & Surry, D., 1998. The variation of peak loads with tributary area near corners on flat low building roofs. *Journal of Wind Engineering and Industrial Aerodynamics*, Volume 77, pp. 185-196.
- Lin, J., Surry, D. & Tieleman, H. W., 1995. The distribution of pressure near roof corners of flat roof low buildings. *Journal of Wind Engineering and Industrial Aerodynamics*, 5, 56(2-3), pp. 235-265.
- Ono, Y., Tamura, T. & Kataoka, H., 2008. LES analysis of unsteady characteristics of conical vortex on a flat roof. *Journal of Wind Engineering and Industrial Aerodynamics*, 10, 96(10-11), pp. 2007-2018.
- Peng, X. et al., 2014. A comparison of methods to estimate peak wind loads on buildings. *Journal of Wind Engineering and Industrial Aerodynamics*, 3, Volume 126, pp. 11-23.
- Surry, D. & Djakovich, D., 1995. Fluctuating pressures on models of tall buildings. *Journal of Wind Engineering and Industrial Aerodynamics*, Issue 58 (1-2), pp. 81-115.
- Wu, F., 2000. Full-Scale Study of Conical Vortices and Their Effects near Roof Corners. *Wind and Structures*, 4(2), pp. 131-146.
- Wu, F., Sarkar, P., Mehta, K. & Zhao, Z., 2001. Influence of incident wind turbulence on pressure fluctuations near flat-roof corners. *Journal of Wind Engineering and Industrial Aerodynamics*, 4, 89(5), pp. 403-420.

VIV response of a suspended sphere nearby the critical Reynolds number

T. Andrianne¹, F. Rigo¹ and V. Denoël²

¹Wind Tunnel Lab, Dept. of Aerospace and Mechanical Engineering, University of Liège, Belgium

²Stochastic and Structural Dynamics, Dept. of Urban and Environmental Engineering, University of Liège, Belgium

Corresponding author: T. Andrianne, t.andrianne@uliege.be

Abstract

The Vortex-Induced Vibration of a sphere connected to a flexible beam is investigated in air for Reynolds numbers including the critical value. For this value ($Re_c=3 \cdot 10^5$), wake disorganization is expected in a static configuration. This fundamental fluid-structure interaction characterised by an axisymmetric configuration leads to vibrations in the lateral and longitudinal directions. Similarly to the well-known circular cylinder, a lock-in phenomenon will take place due to the effect of the motion of the body on the shedding process. An experimental aeroelastic model is designed, instrumented and tested in the wind tunnel of University of Liège. The objective is twofold: (i) solve a practical wind-engineering problem (a spherical suspended streetlight) and (ii) propose a fundamental investigation of the VIV of a smooth sphere for sub-critical and critical Reynolds numbers.

1 Introduction

The configuration of a rigid sphere supported in a fluid by a flexible beam can be encountered in many hydrodynamic applications, where tethered bodies are concerned: marine buoys, balloons, objects behind ships, underwater mines, etc.. Williamson, Govardgan and Jauvtis [1-3] carried out important experimental works on this topic, shedding light on the occurrence of three regimes of vibration. Behara and co-workers recently published numerical investigations of the same systems [4,5]. All these works concern the behaviour of a sphere, suspended or tethered at low Reynolds numbers ($300 \leq Re \leq 1200$). These experimental/numerical simulations are performed in water and characterised by low mass ratio ($m^* = \text{mass of the sphere} / \text{mass of the fluid} < 1$).

In the scope of this work, the Reynolds number ranges between $4 \cdot 10^4$ and $6 \cdot 10^5$, enclosing the critical regime of a smooth sphere [6]. The application motivating this study concerns a spherical luminaire (diameter 60cm) suspended to a cylindrical tube (diameter 4cm, length 370cm) and the above-mentioned Reynolds range corresponds to the wind speed range of 0.25m/s up to 15m/s of urban environment. The mass ratio ($m^* \sim 50$) is much higher than the values found in the literature. The purpose of this work is to analyse the Vortex-induced Vibration (VIV) response of this sphere in order to quantify the peak responses and the extent of the lock-in range of the phenomenon throughout the critical Reynolds range.

2 Methodology

The analysis is based on wind tunnel tests of an aeroelastic model representative of the full-scale prototype. For that purpose, a reduced scale model is designed and built. Figure 1 shows a sketch of the model and its instrumentation. It consists in a wireless 3 components accelerometer located inside the sphere, a force balance connected to the supporting beam and a cobra probe in the wake of the sphere.

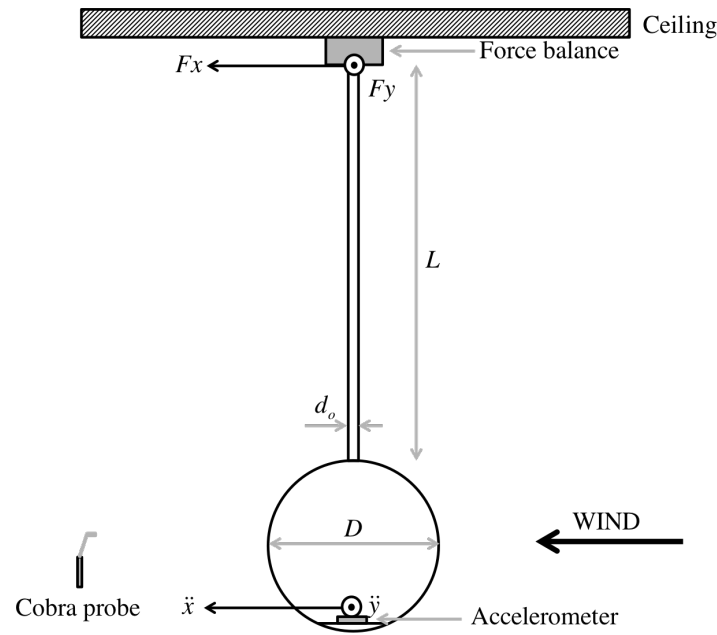


Figure 1. Sketch of the model and instrumentation.

The Reynolds and Scruton similarity laws are enforced in order to transpose directly the measured VIV responses into useful results for the design of the prototype. In addition the Strouhal relation must be conserved because of the unsteadiness features of the flow and the resulting vibrations of the structure.

The left part of table 1 shows the ratios of length, velocity, frequency and mass. The right part of the table presents the characteristics of the prototype and the model. These quantities will be verified on the experimental model through a modal analysis at wind-off conditions.

λ_L	1/4						
λ_U	4						
λ_f	16						
λ_M	1/64						
		D	d_o	d_i	L	M	f
Prototype		600mm	40mm	32mm	3700mm	8kg	1.46Hz
Model		150mm	10mm	8mm	375mm	145g	21.0Hz
Error		-	-	-	-	+15.7%	-0.95%

Table 1. Scaling factors and characteristics of the prototype/model

3 Challenges of the study

Figure 2 depicts the flow characteristics of a static smooth sphere as a function of the Reynolds number. It is observed that the Reynolds number corresponding to the frequency matching and apparition of VIV (denoted $Re_{VIV} = 2 \cdot 10^5$, in red in figure 2) is close to the critical Reynolds number ($Re_C \sim 3 \cdot 10^5$). Hence the flow regime will change during the VIV lock-in and influence the VIV response of the sphere. The opposite situation is also true: VIV vibrations will affect the shedding process, as it is well-known for circular cylinders.

The perfect matching of the Reynolds similarity law is enforced by a velocity ratio of $\lambda_U=4$, balancing the geometric scaling ($\lambda_L=1/4$). The surface roughness of the model (measured to $k/d=5 \times 10^{-5}$) corresponds to a smooth surface, in comparison with the works of Achenbach [6]. The dynamic part of the scaling is reached by adapting the length L of the supporting tube. Consequently the aerodynamics is adequately scaled and the effect of the disorganisation of the flow will be captured during the wind tunnel test campaign.

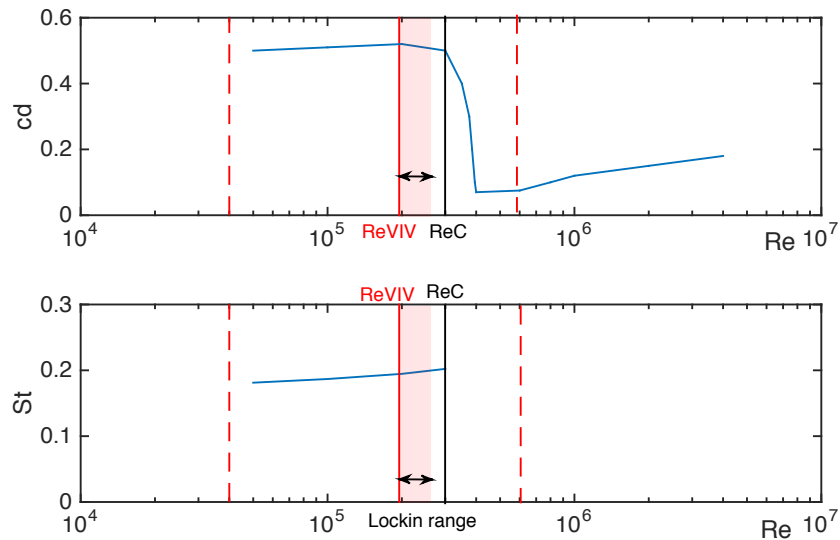


Figure 2. C_d and St for a static smooth sphere vs Reynolds number (reproduced from [6])

4 Outputs of the study

Two types of answers will be given at the end of this work:

Practical application of the streetlight:

- What are the peak displacements along x and y when the sphere undergoes VIV?
- What is the extent of the lock-in range for this specific configuration?
- What is the effect of VIV on the fatigue life of the structure?

Fundamental study of the VIV of a smooth sphere for sub-critical and critical Reynolds numbers:

- What is the effect of the flow disorganisation on the VIV response (extent of the lock-in range and amplitude of vibration)?
- What is the effect of the mass ratio?
- What is the effect of the flow regime on the VIV response? The scaling of the aeroelastic system can be changed by reducing the velocity ratio (λ_U taking values of 3, 2 and 1) and adapting the length of the supporting tube.

References

- [1] C.H.K. Williamson, R. Govarghan, Dynamics and forcing of a tethered sphere in a fluid flow, *Journal of Fluids and Structures* (1997) vol. 11, pp. 293-305
- [2] N. Jauvtis, R. Govarghan, C.H.K. Williamson, Multiple modes of Vortex-induced vibrations of a sphere, *Journal of Fluid Mechanics* (2001) vol. 15, pp. 555-563
- [3] R. Govarghan, C.H.K. Williamson, Vortex-induced vibrations of a sphere, *Journal of Fluid Mechanics* (2005) vol. 531, pp. 11-47
- [4] S. Behara, I. Borazjani, F. Sotiropoulos, Vortex-induced vibrations of an elastically mounted sphere with three degrees of freedom at $Re = 300$: hysteresis and vortex shedding modes, *Journal of Fluid Mechanics* (2011), vol. 686, pp. 426-450
- [5] S. Behara, F. Sotiropoulos, Vortex-induced vibrations of an elastically mounted sphere: The effects of Reynolds number and reduced velocity, *Journal of Fluids and Structures Mechanics* (2016), vol. 66, pp. 54-68
- [6] E. Achenbach, The effects of surface roughness and tunnel blockage on the flow past spheres, *Journal of Fluid Mechanics* (1974), vol. 65, part 1, pp. 113-125

Aerodynamic tailoring of a bluff deck section subjected to inclined winds due to the complex orography of the construction site

T. Argentini¹, S. Omarini¹, A. Zasso¹ and M. Petrangeli²

¹Department of Mechanical Engineering, Politecnico di Milano, Italy

²Mario Petrangeli & Associati s.r.l., Roma, Italy

Corresponding author: T. Argentini, tommaso.argentini@polimi.it

Abstract

Bridges crossing steep valleys in mountainous regions may be subjected to large angles of attack of the incoming wind flow, because of the complex orography of the region where the structure is located. Therefore, the aerodynamic analysis of bridges in this kind of regions should account for this peculiarity. In this paper, the aerodynamic characterization of a bluff deck section of a railway bridge, with angles of attack ranging from -6 to $+6$ degrees is discussed. It is shown that standard analyses that consider only angles of attack near 0 degree only are not sufficient to ensure optimal aerodynamic performances. Indeed, with such large angles of attack the flow field near the deck may change consistently, also leading to aeroelastic instabilities or strong vortex-induced vibrations. To mitigate the aeroelastic issues, without an abrupt change of the deck section, several aerodynamic appendices were tested, and a tailored section with acceptable behaviour was selected.

1 Introduction

The project in consideration is located in a mountainous region, as shown in Figure 1a. Due to its location in a steep valley, the local mean flow approaches the deck with a mean angle of attack α that ranges from -6 degrees to $+6$ degrees (see conventions in Figure 1b). This fact is not common for standard bridges, that are generally subjected to nearly horizontal mean wind flows. Therefore, it may happen, as in this case, that a section with acceptable aerodynamic performances at 0 degree angle of attack may not behave properly when large mean angles of attack are considered. Since the aerodynamic tests in wind tunnel were commissioned at a late stage of the design, only small modifications of the deck were possible, and to improve the aerodynamics small aerodynamics appendices were successfully tested, exploiting devices already tested on similar bridges (see Zasso et al 2016, and Amerio et al. 2017).

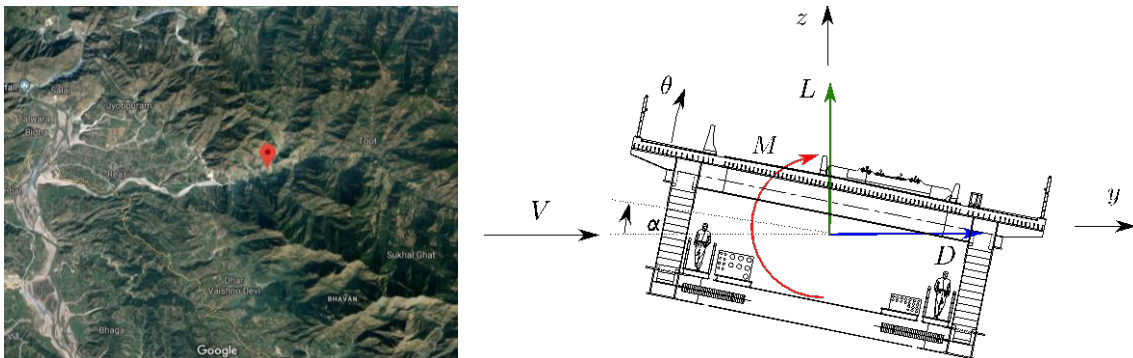


Figure 1. The construction site and the deck cross section.

2 Aerodynamic behaviour before and after optimization

As it can be noticed in Figure 2, the original deck section (Config 00) shows a stall of the moment and lift coefficient. This negative slopes at positive α are an index of likely 1-dof aeroelastic stability at relatively low reduced velocities, as it was verified during wind tunnel tests on suspended sectional model. To change this characteristic behaviour, several aerodynamic appendices were tested (8 in total), with the idea of changing the flow pattern around the deck.

Two successful solutions (Config 03 and 06) are sketched in Figure 2: the upper deck is extended by means of a nose with a beneficial effect on the slope of the static coefficients, and also on the aeroelastic behaviour, as it will be presented in the full paper.

Without considering the large positive mean angle of attack, the original deck section would have performed satisfactorily, and no tailoring would have been necessary. This test case highlights the necessity of considering the possible inclination of the mean flow in bridges crossing steep and deep valleys during the design stage of the structure.

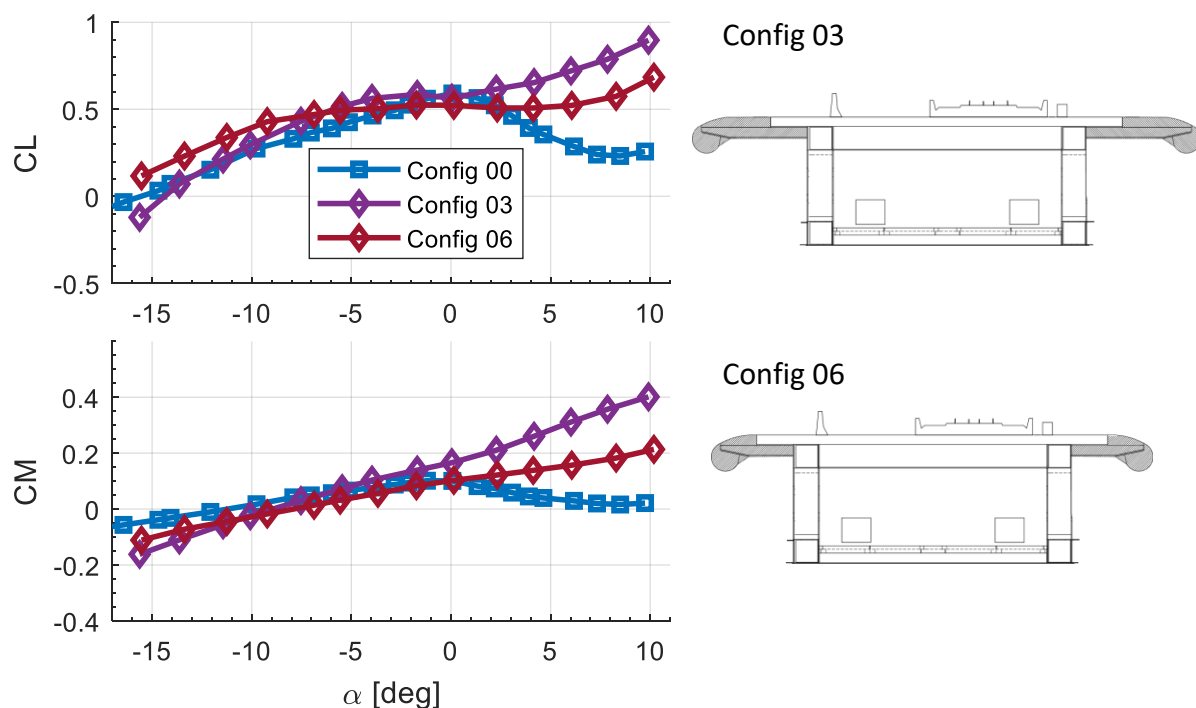


Figure 2. Lift and moment coefficients of the original and optimized cross sections.

References

- Zasso, A.; Rocchi, D.; Argentini, T.; Giappino, S. and Costantini, T. (2016) Experimental and numerical aerodynamic analysis of a concrete railway bridge in tandem arrangement with a truss road bridge. *8th International Colloquium on Bluff Body Aerodynamics and Applications*
- Amerio, L.; Argentini, T.; Rocchi, D. and Zasso, A. (2017) Experimental and numerical aerodynamic optimization of a post-tensioned concrete railway bridge in tandem arrangement with a truss road bridge. *7th European African Conference on Wind Engineering*

A SCADA-based method for estimating the energy improvement from wind turbine retrofitting

Davide Astolfi¹, Francesco Castellani¹ and Ludovico Terzi²

¹University of Perugia - Department of Engineering, Via G. Duranti 93 - 06125 Perugia (Italy)

²Renvico srl, Via San Gregorio 34 – 20124 Milano (Italy)

Corresponding author: Davide Astolfi, davide.astolfi@unipg.it

Abstract

Full scale wind turbines technology has been widely improving in the recent years and condition monitoring techniques assist at the scope of making 100% technical availability a realistic perspective. In this context, several retrofitting techniques are also being used for improving the efficiency of wind kinetic energy conversion. This kind of interventions is costly and therefore a precise quantification of the benefits is needed, in order to know if the retrofitting has an advantageous return of investment. For quantifying ex post the benefits, two elements are needed: SCADA data before and after the retrofitting and a reliable model for simulating how much the wind turbine would have produced without the retrofitting. In this work, a model is formulated for estimating the improvement in energy production provided by a start-up upgrade of the control system. Three full-scale wind turbines sited onshore are studied: the upgrade is quantified and the statistical soundness of the method is discussed.

1 Introduction

The target of improving the efficiency of wind kinetic energy extraction has stimulated a certain boost in full-scale wind turbines retrofitting. This kind of interventions has material and labour costs and producible energy is lost during installation. Therefore, wind farm owners have the necessity of quantifying the benefits with precision, but this is difficult because of the unsteady conditions under which wind turbines operate. Commonly, the procedure is as follows: certain test wind turbines inside a wind farm are retrofitted and the possible extension of the retrofitting to the whole wind farm is examined on the grounds of the estimation of the improvement on the test wind turbines. To do this, SCADA data are helpful because they describe the operation before and after the upgrade. A further element is needed, indeed: a reliable model for estimating how the wind turbine would have operated, under the post-upgrade wind conditions, if the upgrade didn't take place. Straightforward power curve analysis, although qualitatively useful, commonly is not precise enough to quantify upgrades that are of the order of the per cent. Therefore, more sophisticated models are employed as for example in Lee, 2015. The present work deals with this kind of problem: the upgrade of the start-up for three full-scale wind turbines sited in a gentle terrain is studied. A model is formulated and consequently the energy improvement is estimated and the statistical soundness of the results is estimated.

2 The method

Three SCADA data sets are employed:

- D0 goes from 05/05/2016 to 05/05/2017 and is used for training the model;
- D1 goes from 05/05/2017 to 05/09/2017 and is used for testing the model;
- D2 goes from the installation of the improved start-up (27/09/2017) to 03/12/2017 and is used for validating the model.

The model is a feedforward Artificial Neural Network, with this structure:

- $y(\mathbf{x})$ is the power output;
- The inputs are the wind speed (renormalized with the temperature for referring to standard atmospheric conditions) and the wind directions. $\mathbf{x}=(v, \sin\theta, \cos\theta)$.

The residuals between the simulations and the measurements are analysed before and after the installation of the improved start-up and this allows to estimate the percentage of energy improvement during the D2 data set.

The data are filtered on the $[3, 7]$ m/s interval, because the improved start-up acts at low wind speeds.

3 Results

In Figure 1, the power curves in the $[3, 7]$ m/s interval are reported. The power measurements are averaged within wind speed interval of 0.25 m/s. The blue line refers to the period before the upgrade (D0 and D1 data sets), the orange line refers to the period post upgrade (D2 data set), the aqua line is the difference of the two. On the left, WTG2 is one of the three turbines that have been upgraded with the improved start-up. On the right, WTG4 is a turbine that hasn't been upgraded. From Figure 1, the improvement for WTG2 with respect to itself and with respect to WTG4, is visible. In order to quantify the improvement precisely, the model described in Section 2 is adopted and the estimates are reported in Table 1.

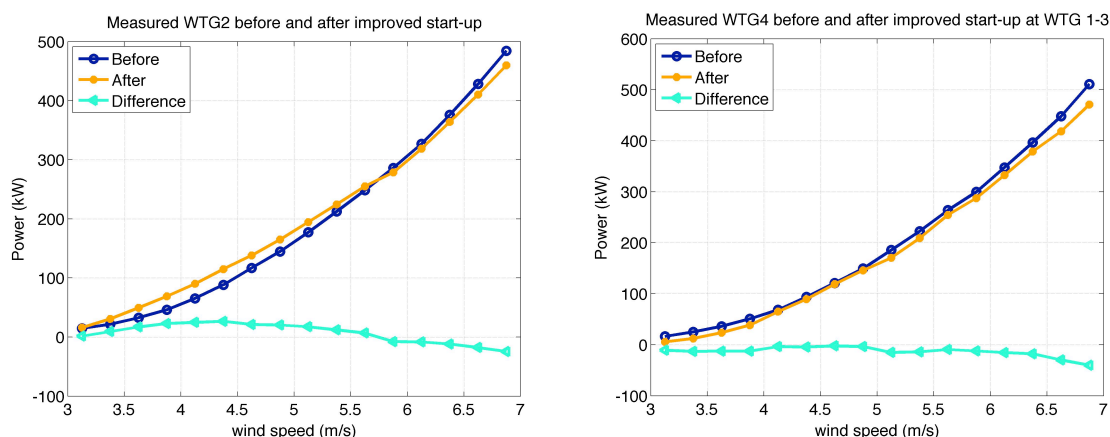


Figure 1. Power curve during the D0 and D1 data set (before upgrade) vs D2 data set (after upgrade). On the left, WTG2 has upgraded. On the right, WTG4, hasn't been upgraded with the improved start-up.

Table 1. Percentage energy improvement in the $[3, 7]$ m/s interval

WTG1	4%
WTG2	5.5%
WTG3	3.5%

References

Lee, G., Ding, Y., Xie, L., & Genton, M. G. (2015). A kernel plus method for quantifying wind turbine performance upgrades. *Wind Energy*, **18**(7), 1207-1219

How Stack Effect and Wind Impacts in Tall Buildings can Affect Occupant Comfort and Smooth Building Operation

S.Attrill, K.Reipas and V.Tang

RWDI

Corresponding author: S.Attrill, Steven.Attril@RWDI.com

Abstract

Tall buildings can be prone to adverse impacts (including cold draughts, lift door operability issues, and aeroacoustic “whistling” noise at doors) on their internal environments resulting from their exposure to high wind speeds and tendency to suffer from stack effect. Use of computational modelling tools at design stage can be an effective way to examine a buildings’ response to these environmental effects. This can assist in identifying and resolving inherent areas of weakness pre-construction, making design improvements to reduce risk. Similarly, if a problem has already occurred, on-site measurements of pressure differentials and leakage flows, combined with computational modelling where appropriate, can also be used to diagnose and test solutions for mitigating existing issues. This case study will examine some of these real-world issues in existing schemes, including a number of residential towers in London and discuss what approaches can be put into action to limit potential for such issues.

1 Introduction

High wind speeds and stack effect, a buoyancy-driven flow phenomenon, can lead to unintended internal airflows through the building and a range of adverse impacts including wintertime cold draughts, lift door operability issues, aeroacoustic “whistling” noise at doors, as well as more dangerous conditions (such as slamming doors and reduced access to emergency egress paths). The latter, particularly in residential buildings, can have a serious impact on occupant health and wellbeing.

Stack effect is a phenomenon that can exist in all buildings and is driven by the height of a building and the interior-exterior temperature difference and is not fundamentally caused by a building’s design. A conceptual image illustrating typical impacts of stack effect during heating seasons (when the exterior temperature is colder than interior) is shown in Figure 1a. During cooling seasons (when the exterior temperature is warmer than interior) stack effect related airflows are the reverse of that shown in Figure 1a.

Positive pressure zones are created as wind impacts the windward façades of a building. This wind flow accelerates around and off the building corners, which can create a suction (negative pressure zone, as shown in Figure 1b) on the leeward façades of the building. Individually these factors can result in a net positive or negative pressurisation within the building (especially where direct openings are provided). The combination of these factors can result in uncontrolled flow through a building from the positively pressurised areas to the negative pressure zones.

Stack effect induced problems are most severe on very cold or very hot days when the difference between indoor and outdoor temperatures is the greatest. Whilst windier conditions are often associated with winter in the UK (with the focus of this review being case study buildings in London), high wind speeds and therefore air flow issues resulting from wind flow can occur throughout the year.

The case study buildings are representative of complete or partial occupied residential buildings with existing airflow related issues. Site visits to these buildings were conducted to take pressure and airflow measurements to investigate and understand the likely cause of the existing airflow issues.

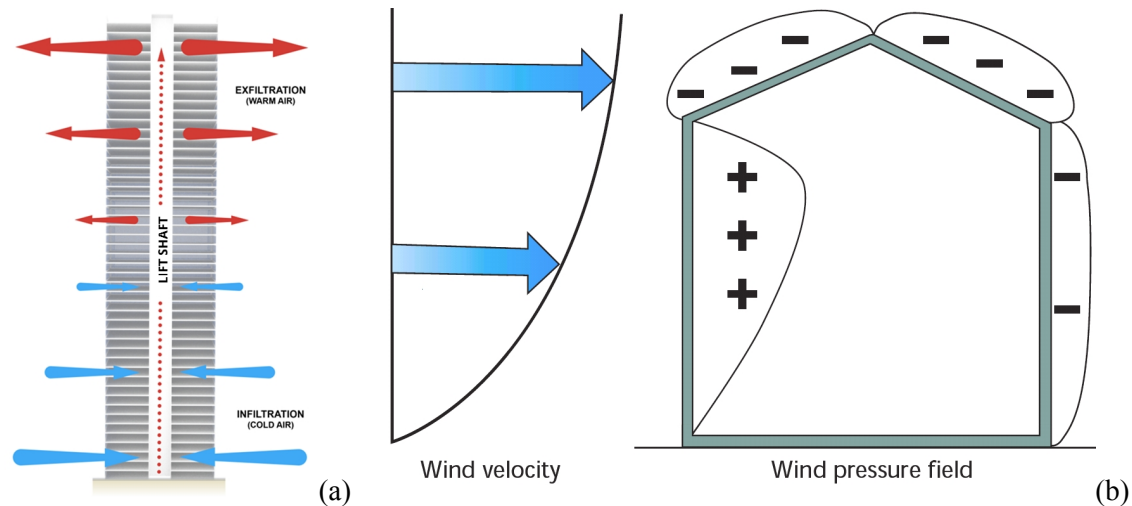


Figure 1. Conceptual image of heating season stack effect (on cold days) airflows in buildings (a) and example of wind pressure on building (b) (CIBSE, 2005)

2 Analysis

As part of the analysis the meteorological data were reviewed for the case study sites in London, UK, with the temperature range in the UK indicating that both winter and summer stack effect can occur. However, in the UK winter temperatures provide a larger interior to exterior temperature difference which would be expected to result in stronger stack effect. Meteorological data for London indicate that the prevailing wind direction throughout the year is from the southwest with a secondary peak from north easterly winds (especially during the spring), which is typical for many areas of southern England.

Onsite measurements are also required to review the effect of the numerous penetrations typically present in residential buildings facades (such as exhaust vents and operable windows) and the unique challenges such as occupant behaviour like leaving windows and doors open. On-site measurements of pressure differentials and leakage flows (using micromanometers, anemometers and flow visualisation equipment) were combined with a review of the project drawings and information for the case study buildings to diagnose the likely cause of the existing airflow issues.

3 Conclusions

Based on the observations of the site visits and information reviews the problems observed within the case study buildings were generally related to how the corridor and apartments were being ventilated and if / how the perimeter gaps around the interior apartment and stairwell doors were sealed. The development of mitigation for these existing buildings is ongoing. It is noted that although the flow of air through a building can be reduced, due to the interactions between elements within a building, reducing airflow related issues can be an iterative process (of investigation, implementation and development of additional measures for specific residual issues). This future investigation and development of mitigation would likely consist of further on site measurements and testing combined with computational modelling.

References

CIBSE. (2005). Natural Ventilation of non-domestic buildings. *AM10*.

Wind effects on containers stability

Alberto Balbi¹, Maria P. Repetto¹, Giovanni Solari¹, Andrea Freda¹

Department of Civil, Chemical and Environmental Engineering (DICCA)
University of Genova (Italy)

Corresponding author: Alberto Balbi, alberto.balbi@dicca.unige.it

Abstract

Due to their natural location, Seaports are continuously threatened by natural hazards. Considering in particular terminal containers, the piled containers can fall and get damaged under strong wind. This paper describes a wide research activity on terminal resilience, aimed at the formulations of the critical wind velocity for the containers stability. The analytical formulation of the critical velocities causing container's sliding, tilting and lifting is firstly developed, showing that they are dependent from three parameters: the wind field and turbulence parameters, the coefficient of friction between the containers surface and the piled containers aerodynamic coefficients. The coefficient of friction has been analysed by means of in situ tests on the piled containers. The aerodynamic coefficients have been studied by means of wind tunnel test on scaled models. By combining these parameters, a series of critical wind speed values is obtained.

1 Introduction

The Seaports are critical infrastructures very exposed to extreme weather actions like wind; their consequences can be very destructive for all the terminal activities. Terminal containers are one of the crucial area in the Seaports due to the strategic importance of the movement of goods.

Containers piled in the terminal yard can fall and get damaged under strong wind, causing serious safety problems for port operators and economic damage. However in literature there is a lack of information about wind stability of the piled containers (Zhen 2011) and the critical wind velocity values at the basis of the safety systems are still affected by many uncertainties.

2 Methodology

This work describes a wide research activity aimed at the formulations of the critical wind velocity for the containers stability. The analytical formulation of the critical velocities causing container's sliding, tilting and lifting is firstly developed. Considering the container as a rigid body, the balance of forces with respect translation and rotation can be imposed. Sliding, tilting and lifting occur when the wind peak actions F_{xy} (horizontal force), F_z (vertical suction force) and M_y (overturning moment with respect to the long side of the container itself) respectively exceed the horizontal friction resistant force, the vertical weight force P of an empty container and the stabilizing moment due to the weight itself. The limit states can be expressed as:

$$F_{xy} = (P - F_z)C_a \quad (1)$$

$$F_z = P \quad (2)$$

$$M_y = P \frac{l}{2} \quad (3)$$

where C_a is the coefficient of static friction between stacked containers, l is the transverse width of the container. On their turn, the wind peak actions are dependent from the incoming wind field and turbulence parameters, aerodynamic coefficients of the stacked containers. Writing in explicit form Eq. (1)-(3) and solving the equations with respect the wind velocity, an analytical expression of the critical wind velocity can be obtained. The paper develops the methods and analyses the input parameters.

The static friction coefficient between two stacked containers is a key parameter for assessing the stability of the container; however, the data provided in the literature present a considerable dispersion, inducing an important uncertainty in the analyses. Therefore, an on-site experimental campaign was carried out to experimentally measure the friction coefficient between stacked containers. In order to take into account the variability induced by natural and physical conditions, several containers were subjected to a sliding tests where an horizontal force was applied to each test container staked one of them, measuring for which force values the sliding occurred. Tests were carried out under different natural conditions (conditions of dry or wet surfaces), containers surface conditions and configurations, in order to obtain a representative distribution of the coefficient values.

The value of the aerodynamic coefficient for the container is not known in the literature and is difficult to assess using the current regulations, given the peculiarities of the shape and the surface of the container, and the variability of the configurations that the stacked containers can take in the port yard. In order to evaluate reliable values, the aerodynamic coefficients have been studied by means of wind tunnel tests on scaled model of 1:50. Several set-up conditions have been reproduced, considering seven different container storage configurations, two different incoming wind profiles and two different container's tier, obtaining as many aerodynamic coefficients values.

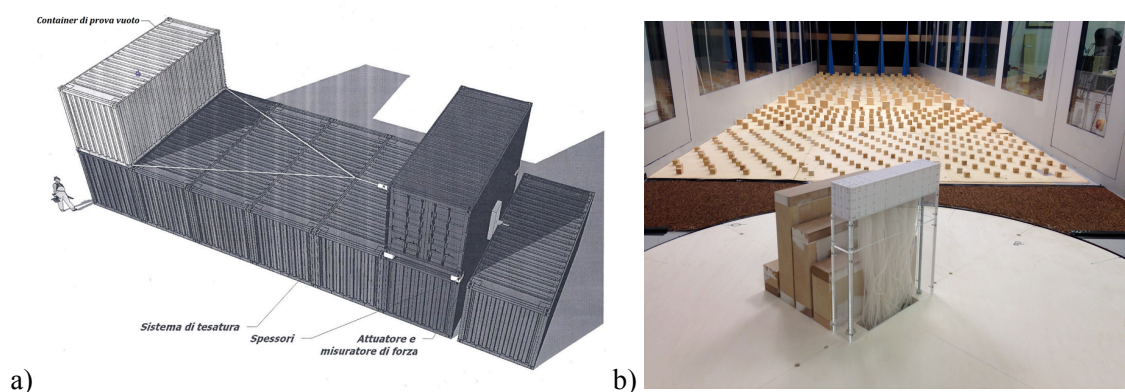


Figure 1. a) On-site experimental test for friction coefficient; b) wind tunnel test on stacked containers

3 Final Results

By combining the wind field and its turbulence intensity, the friction coefficients and the aerodynamic tests, a series of critical wind velocity values is obtained, whose variability represent the uncertainties in the input parameters. Model uncertainties are taken into account as well, furnishing a probabilistic description of the critical wind speed. The study has been applied and discussed with reference to the Terminal VTE, Port of Genoa.

References

Zhen, W., Xingqian, P., & Chunhui, Z. (2011, April). Overturning analysis of Harbor Containers based on wind tunnel test of rigid models. In *Electric Technology and Civil Engineering (ICETCE), 2011 International Conference on* (pp. 544-548). IEEE.

Mooring system optimization for a spar-buoy wind turbine in rough wind and sea conditions

G. Barbanti, E. Marino and C. Borri

Department of Civil and Environmental Engineering, University of Florence, Italy

Corresponding author: G. Barbanti, gbarbanti@dicea.unifi.it

Abstract

In this paper the dynamic response of a spar-buoy floating offshore wind turbine (FOWT) is investigated in order to optimize the design of the deep water mooring system.

The variation of several mooring system design parameters is considered within prescribed boundaries with the aim to minimize the platform motions and the bending moments in the tower for operational and survival environmental conditions. Emphasis will be put on mooring system sensitivity and design optimization to both wind and waves conditions.

1 Introduction

Floating offshore wind turbine have the potential to greatly expand the siting possibilities for offshore wind energy plants and thus become one of the more important resource of sustainable renewable energy. Using a floating support platform, the wind turbine can be installed in water deeper than 30m, exceeding the limit of conventional bottom-fixed offshore wind turbines opening new opportunities for the installation in areas characterized by deep water (e.g. the Mediterranean Sea). In October 2017, Hywind Scotland built the first floating offshore wind park making the spar-buoy concept one of the most promising floating platform technology. Offshore wind turbines are subject to a variety of environmental conditions, which cause a significantly different response depending on the turbine state (operational or parked), making the hydro-aero-servo-elastic analysis not a trivial task.

Karimirad and Moan (2011) compared the response of the floating wind turbine in both survival and operational conditions and emphasized the importance of analyzing the structural response in survival conditions to obtain lifetime evaluation. Fylling and Berthelsen (2011) presented an integrated design tool for the optimization of moored spar-buoy type support structures for wind turbines including the mooring system. The optimization was performed in the frequency domain to determine the minimum material cost by the minimization of the objective functions, defined by the costs of spar buoy, mooring line, and cable using a gradient method. Brommundt (Brommundt et al., 2012) described a tool for the optimization of a catenary moored semi-submersible floating wind turbine using a frequency domain approach with the purpose to minimize the line lengths under site specific environmental loads. In these two studies a large number of different scenarios can be efficiently simulated due to the linear approximation made in the frequency domain analysis, but the inability to simulate the nonlinear behaviour of the system could be a disadvantage for the optimization reliability. Kvittem and Moan (2012) showed substantial differences in the motion response of a floating wind turbine modelled with a linearized mooring line and a nonlinear model for different mooring line configurations. In (Chen, et al., 2017) the mooring line is optimized for a spar-buoy FOWT, limiting the analysis only for surge, heave and pitch motions and simplifying the aerodynamic and the overall structure dynamics. The results showed that the spar dynamic response and the mooring line tension can be improved relative to a non-optimized mooring system.

The purpose of the present study is to optimize the mooring system of a spar-buoy floating wind turbine in order to enhance the structure response to operational and survival environmental condition using a hydro-aero-servo-elastic time-domain modelling. Optimizations will be performed considering different wind and wave conditions, reproduced through different mean wind speeds and turbulence intensities, and associated significant wave heights and spectral periods.

2 Methodology

In this study the OC3-Hywind spar-buoy featuring the NREL 5-MW baseline wind turbine is investigated using FAST, a fully coupled hydro-aero-servo-elastic time-domain simulator for horizontal axis wind turbines developed by the National Renewable Energy Laboratory (NREL). The wind turbine properties, platform properties and mooring system properties are kept the same as described in OC3 Hywind (Jonkman, 2010). To achieve a more accurate estimation of the loads in the mooring lines the multi-segmented lumped-mass module MoorDyn is used. This module can model the mooring lines dynamic improving the mooring load predictions (Wendt, et al., 2015).

The mooring system is optimized varying the design parameters within prescribed boundaries and given specific constraints.

The primary design parameters of the system configuration are:

1. geometries of the mooring lines (unstretched length, horizontal distance from fairlead to anchor, percentage resting on the seafloor);
2. mooring lines type (chains, ropes);
3. number and size of the mooring lines and fairlead position along the spar-buoy draft.

Several constraints are adopted in the simulation:

1. line maximum tension of the cables must not be exceeded;
2. drag embedded anchors reactions must be solely horizontal;
3. translational and rotational motions of the floater must be within certain limits (e.g. due to power cables constraints);
4. depth to top of taper below the mean surface level must remain the same (i.e. the spar-buoy should remain in the same static equilibrium position)

The goal of the optimization is to minimize the platform motion and the bending moment in the tower. Indeed, these measures can be representative as a fatigue index for the wind turbine tower. In a second step the influence of mooring line buoyancy/ballasting positioning and their amounting along the cables will be investigated. Later the optimization procedure will be extended to the worst scenario found to take stock of the more suitable mooring system design.

3 References

- Brommundt, G., Krause, L., Merz, K., & Muskulus, M. (2012). Mooring system optimization for floating wind turbines using. *Energy Procedia* 24, 289 – 296.
- Chen, D., Gao, P., Huang, S., Fan, K., Zhuang, N., & Liao, Y. (2017). *Dynamic response and mooring optimization of spar-type substructure under combined action of wind, wave, and current* (Vol. 9). Journal of Renewable and Sustainable Energy .
- Fylling, I., & Berthelsen, P. (2011). WINDOPT - an optimization tool for floating support structures for deep water wind turbines. *Proceedings of the ASME 2011 30th International Conference on Ocean, Offshore and Arctic Engineering* (p. 1-10). Rotterdam, Netherlands: OMAE2011.
- Jonkman, J. (2010). *Definition of the Floating System for Phase IV of OC3*. Technical Report NREL/TP-500-47535.
- Karimirad, M., & Moan, T. (2011). Extreme Dynamic Structural Response Analysis of Catenary Moored Spar Wind Turbine in Harsh Environmental Conditions. *Journal of Offshore Mechanics and Arctic Engineering*, Vol.133.
- Kvittem, M. I., & Moan, T. (2012). Effect of Mooring Line Modelling on Motions and Structural Fatigue Damage for a Semisubmersible Wind Turbine. *Proceedings of the Twenty-second (2012) International Offshore and Polar Engineering Conference* (p. 273 - 278). Rhodes, Greece : International Society of Offshore and Polar Engineers (ISOPE).
- Wendt, F., Robertson, A., Jonkman, J., & Hayman, G. (2015). Verification of New Floating Capabilities in FAST v8. *Proc. AIAA SciTech 2015* (p. 1 - 11). Florida, USA: American Institute of Aeronautics and Astronautics.

Performance-Based loss estimation for tall buildings under wind

Michele Barbato¹, Francesco Petrini² and Jad E.K. Antoun¹

¹ Department of Civil & Environmental Engineering, Louisiana State University, USA

² Department of Structural and Geotechnical Engineering, Sapienza University of Rome, Rome, Italy

Corresponding author: Francesco Petrini, francesco.petrini@uniroma1.it

Abstract

In this paper, a rigorous procedure based on the general Performance-Based Wind (Hurricane) Engineering (PBWE, PBHE) framework is developed to perform a loss analysis for high-rise buildings by considering both hurricane and regular wind hazards. This study employs: (1) well-established models that are available in the literature for hazard and interaction analyses, (2) finite element analysis in conjunction with a frequency-domain approach for the structural analysis phase, and (3) existing models available in literature for damage and loss evaluations. An application example consisting of the performance assessment of a 74-story building subjected to both hurricane and non-hurricane wind hazard is presented to illustrate the proposed procedure.

1 Introduction

In recent years, performance-based engineering (PBE) approaches have been receiving significant attention by researchers in wind and hurricane engineering (Ciampoli et al. 2011, Smith and Caracoglia 2011, Barbato et al. 2013, Spence and Kareem 2014). In particular, the performance of high-rise buildings under wind actions is crucial in driving the design, and a probabilistic risk assessment analysis becomes necessary to ensure appropriate serviceability and safety in combination with an economic design. A coherent and rigorous evaluation of performance in monetary terms is of paramount importance to design optimal structural systems that maintain an acceptable performance during their whole life cycle. Thus, a PBE approach can be very beneficial in the analysis and design of this building typology.

In the fields of wind and hurricane engineering, Bashor and Kareem (2007) developed a probabilistic framework to evaluate the performance of tall buildings in terms of occupants' comfort. The random variables considered were the wind speed and structural damping. Reliability analyses based on the First-Order Reliability Method (FORM) and Monte-Carlo simulation (MCS) were used to assess the probability of failure, i.e., the probability of occupants' discomfort. Ciampoli et al (2011) developed a performance-based wind engineering (PBWE) framework by extending the performance-based earthquake engineering (PBEE) approach proposed by Pacific Earthquake Engineering Research Center (PEER). As a further evolution of PBWE, Barbato et al. (2013) developed a probabilistic Performance-Based Hurricane Engineering (PBHE) framework based on the total probability theorem, which can be used for the risk assessment and loss analysis of structural systems subject to hurricane hazard. This framework considered the multi-hazard nature of hurricane events, the interaction of different hazard sources, and the possible sequential effects of these distinct hazards. The PBHE framework was employed to compare the performance of different storm mitigation techniques for low-rise residential buildings (Unnikrishnan and Barbato 2016) and to investigate the effects of hazard interaction on the loss analysis for wood-frame houses (Unnikrishnan and Barbato 2017).

In this paper, the PBHE framework is used for the risk assessment of tall buildings subjected to both hurricane and non-hurricane wind hazards. The general multi-layer Monte-Carlo simulation (MCS) approach is specialized for the risk assessment of engineered buildings such as high-rise buildings. The problem of risk assessment is disaggregated into the following basic probabilistic components: (1) hazard analysis, (2) structural characterization, (3) interaction analysis, (4) structural

analysis, (5) damage analysis, and (6) loss analysis. The different random parameters involved in these analysis phases are identified and their statistical characteristics are obtained from the literature. A story-based loss estimation method is used for the loss analysis in conjunction with damage and loss functions taken from HAZUS® (FEMA 2007).

An application example consisting of a 74-story building located in Miami County, Florida, is presented to illustrate the framework. The annual probabilities of exceedance of the response in the along and across wind directions are calculated. For this application example, it was observed that: (1) the annual probabilities of exceedance of the displacements in the along wind direction are significantly larger than the corresponding probabilities for the displacements in the across wind direction, due to the effects of the mean wind speed on the response; and (2) the annual probabilities of exceedance of the accelerations in the across wind direction are significantly larger than the corresponding probabilities for the accelerations in the along wind direction, due to the effects of the vortex shedding on the structural response.

The expected losses for the target building for different limit states were also calculated.

References

- Barbato, M., Petrini, F., Unnikrishnan, V. U., and Ciampoli, M. (2013). Performance-based hurricane engineering (PBHE) framework. *Structural Safety* **45**, 24-35.
- Bashor, R., and Kareem, A. (2007). Probabilistic performance evaluation of buildings: An occupant comfort perspective. *Proc., 12th International Conference on Wind Engineering (12-ICWE)*, Cairns, Australia.
- Ciampoli, M., Petrini, F., and Augusti, G., (2011). Performance-Based Wind Engineering: towards a general procedure. *Structural Safety* **33** (6), 367-378.
- FEMA. (2007). Multi-hazard estimation methodology –hurricane model. *HAZUS-MH-MR4 technical manual*, Federal Emergency Management Agency (US), Department of Homeland Security, Washington D.C.
- Smith, M. A., and Caracoglia, L. (2011). "A monte carlo based method for the dynamic "fragility analysis" of tall buildings under turbulent wind loading." *Engineering Structures* **33** (2):410-420
- Spence, S. M. J., and Kareem, A. (2014). Performance-based design and optimization of uncertain wind-excited dynamic building systems. *Engineering Structures* **78**, 133-144.
- Unnikrishnan, V.U. and Barbato, M. (2016). Performance-based comparison of different storm mitigation techniques for residential buildings. *Journal of Structural Engineering* **142**(6), p. 4016011.
- Unnikrishnan, V.U. and Barbato, M. (2017). Multihazard interaction effects on the performance of low-rise wood-frame housing in hurricane-prone regions. *Journal of Structural Engineering* **143**(8), p. 4017076.

STEELWAR project: wind tunnel tests on automated rack supported warehouses

Gianni Bartoli^{1,2}, Claudio Mannini^{1,2} and Antonino Maria Marra^{1,2}

¹Department of Civil Engineering and Environmental Engineering, University of Florence, Italy

²CRIACIV, Inter-University Research Centre on Building Aerodynamics and Wind Engineering, Italy

Corresponding author: Antonino Maria Marra, antoninomaria.marra@unifi.it

Abstract

Automated rack supported warehouses (ARSW) are nowadays a very popular typology of buildings for massive storage of goods. Their large dimensions, together with the property of having the racks as load bearing structure, implies that Recommendations and Codes for the usual warehouses are not entirely applicable. STEELWAR project is aimed at increasing the safety, reliability and economy of ARSW. The analysis of actual design practices, unconventional loading conditions, constructional phases and seismic design are the objectives of the project. In addition, a significant effort is devoted to the wind effects on ARSW by modelling and measuring actions on structures with different characteristics and extension. The present work deals with the wind tunnel modelling of ARSW.

1 Introduction

A warehouse is a building where massive amount of goods can be stored. The necessity of storage space is always increasing due to the rapid growing of e-commerce markets. The trend in the warehouse sector goes towards reduced running costs, automation and larger sizes. At present, automated rack supported warehouses (ARSW) or clad rack warehouses are usually built by manufactures specialized in the usual warehouse storage pallet racks. ARSW can be much larger and taller than the classical pallet rack systems. Heights of 40 m, widths of 100 m and lengths of 150 m can be reached. In addition, unlike the warehouse storage pallet racks, the load bearing structure of an ARSW coincides with the rack itself, and then it supports not only the weight of the goods but also the weight of all building elements (clads, roof, etc.) and the external loads (e.g., wind, snow and earthquake). Therefore, partial or total collapse of these structures can occur if the aforementioned actions are not correctly accounted for. As for the wind action, the construction phases have also been demonstrated to be critical (Figure 1 shows a partial collapse of an ARSW). It is evident that the effects of wind during both construction and operational life should be properly considered in the early stages of the design.

The STEELWAR project (“Advanced structural solutions for automated STEELrack supported WAREhouses”, funded by the European Commission) faces the aforementioned problems with the aim of increasing the safety, reliability and economy of ARSW. The analysis of actual design practices, unconventional loading conditions, constructional phases and seismic design are the objectives of the project. In addition, a significant effort is devoted to the wind effects on ARSW by modelling and measuring actions on structures with different characteristics and extension (30 case studies will be analysed during the project).



Figure 1. Partial collapse of an ARSW during construction phase.

2 Experimental activity

Wind tunnel tests will be carried out at the CRIACIV boundary layer wind tunnel in Prato, Italy. No accurate scaled models for wind tunnel tests can be manufactured due to the complex geometry of large ARSW structures. In addition, the significant mismatch of the Reynolds number between the model and the prototype leads to a questionable validity of the experiments. In order to overcome these problems, the experimental procedure will require a two-step approach. First, equivalent porous panels will be calibrated in order to produce the same wind effects, in terms of drag force and drop of static pressure, of selected portions of ARSW frames. This approach has already been applied in reproducing the wind effects on porous barriers and other structures (Allori et al., 2013; Richards and Robinson, 1999; Telenta et al., 2014). In the second step, wind tunnel tests on models of entire ARSWs at a scale of 1:100 - 1:200, conceived based on the equivalent porous panels defined in the first step, will be conducted within a suitable reproduced atmospheric boundary layer.

References

- Allori, D., Bartoli, G., and Mannini, C. (2013). Wind tunnel tests on macro-porous structural elements: a scaling procedure. *Journal of Wind Engineering and Industrial Aerodynamics* **123**, 291–299.
- Richards, P. J., and Robinson, M. (1999). Wind loads on porous structures. *Journal of Wind Engineering and Industrial Aerodynamics* **83**, 455–465.
- Telenta, M., Duhovnik, J., Kosel, F., and Šajin, V. (2014). Numerical and experimental study of the flow through a geometrically accurate porous wind barrier model. *Journal of Wind Engineering and Industrial Aerodynamics* **124**, 99–108.

Hybrid/HIL Testing of Floating Wind Turbines: the LIFES50+ project

I. Bayati^{1*}, L. Bernini¹, A. Facchinetti¹, A. Fontanella¹, H. Giberti², A. Zasso & M. Belloli¹

¹Department of Mechanical Engineering, Politecnico di Milano, Italy

²Università degli studi di Pavia, Pavia, Italy

*Corresponding author: ilmasandrea.bayati@polimi.it

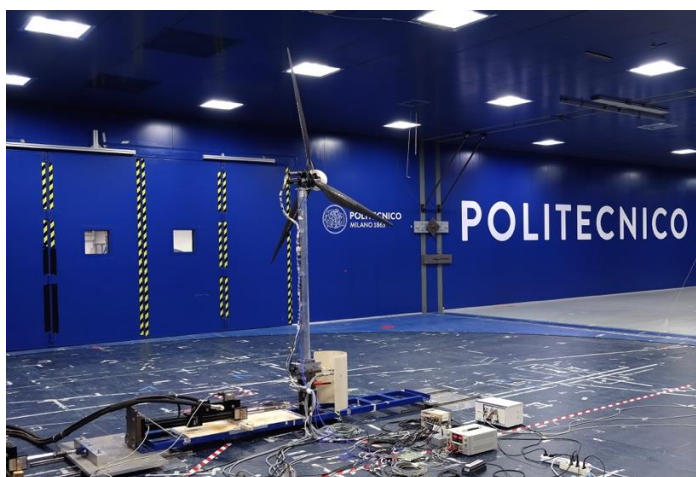
Abstract

This paper describes the innovative experimental approach, introduced by the authors within the EU H2020 project LIFES50+, that was used to study the integrated Floating Offshore Wind Turbine (FOWT) dynamics inside the Politecnico di Milano (PoliMi) Atmospheric Boundary Layer (ABL) wind tunnel. Unsteady aerodynamic loads were extensively investigated for different imposed-motion conditions. A 6-DOFs Hardware-In-the-Loop (HIL) system was designed and used to directly measure the global FOWT response for combined wind and wave conditions.

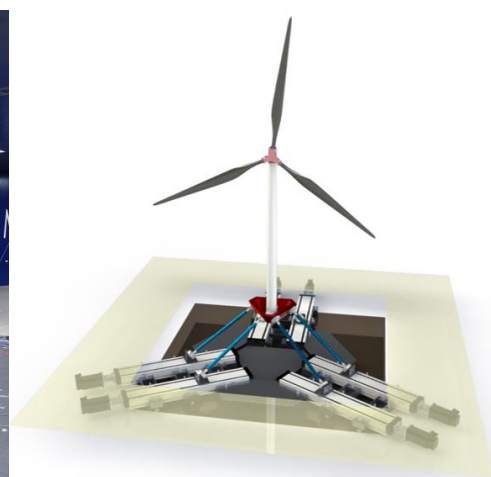
1 Introduction

LIFES50+ is an EU H2020 project born to make economically and technologically feasible installing a 10MW wind turbine, defined in Bak (2013), in coastal areas with water depths greater than 50 meters. Two innovative platform concepts are designed and qualified by means of specific aero-servo-hydro-elastic simulation models conceived to reproduce with high fidelity the multiple interconnected phenomena experienced by FOWTs. In this contest, experimental data are of fundamental importance to validate numerical models and ensure the reliability of the codes used for design and certification.

LIFES50+ favours the rise of hybrid/HIL testing to overcome the scaling issues typical of traditional ocean-basin model tests. Aerodynamic loads or hydrodynamic loads are reproduced exploiting a dedicated facility (respectively wind tunnel or ocean basin) while complementary forces are computed in real-time and provided to the scale model by means of a proper actuation system.



(a)



(b)

Figure 1. General view of the wind turbine scale model inside the PoliMi wind tunnel (a) and 6-DOFs hybrid HIL setup (b).

2 Unsteady aerodynamics

The low frequency dynamics introduced by platform rigid-body motion modes cause the wind turbine rotor to operate under unsteady flow regimes resulting in a variable thrust force that, in turn, greatly affects the motion of the entire structure.

A 1/75th scale model of the DTU 10MW Reference Wind Turbine (RWT) was designed and built at PoliMi, as described in Bayati (2017a), to investigate, inside the ABL test section of the PoliMi wind tunnel (GVPM), the unsteady aerodynamic loads experienced by FOWTs (see Bayati 2017b). An optimization procedure was developed to design an aero-elastic rotor and match the full-scale machine performance at low-Reynolds conditions. Rotor torque and thrust were measured for imposed mono-harmonic motion considering different combinations of amplitude and frequency. From experimental data, it was possible to study how the aerodynamic forcefield affects the FOWT dynamic response.

3 Global FOWT dynamics

The wind turbine scale model was also coupled with an HIL system, described in Bayati (2017c) and Bayati (2014), that makes possible to reproduce the floating system response inside the wind tunnel. Aerodynamic loads generated by the wind turbine model are continuously measured and combined with computed hydrodynamic forces. Real-time integration of a numerical model of the floating subsystem allows to simulate inside the wind tunnel the FOWT dynamic response.

A specific mechatronics system, designed in Fontanella (2018), allows to control the scale model with the same regulation principles adopted by modern multi-megawatt machines making possible to directly investigate how the wind turbine control system affects the FOWT response in different environmental conditions.

4 Conclusions

The experimental set-up developed by the authors to investigate FOWT dynamics inside a wind tunnel is presented. A fully-controlled 1/75 scale model of the DTU 10MW RWT was designed and built to be used for measuring unsteady aerodynamic loads due to floating platform motion. The same model was combined with a 6-DOFs HIL system to study the FOWT response for different operating and environmental conditions.

References

- Bak, C. et al. (2013). Description of the DTU 10MW Reference Wind Turbine. *DTU Wind Energy Report*.
- Bayati, I., Belloli, M., Bernini, L. et al. (2017a). Scale model technology for floating offshore wind turbines. *IET Renewable Power Generation*.
- Bayati, I., Belloli, M., Bernini L. et al. (2017b). Unsteady Aerodynamics of Floating Offshore Wind Turbines: Focusing on the Global System Dynamics. *Proceedings of 36th International Conference on Ocean, Offshore & Arctic Engineering, OMAE 2017*.
- Bayati, I., Belloli, M., Ferrari, D. et al. (2014). Design of a 6-DoF Robotic Platform for Wind Tunnel Tests of Floating Wind Turbines. *Energy Procedia* **53**, 313–323.
- Bayati, I., Belloli, M., Facchinetti, A. (2017c). Wind Tunnel 2-DOF Hybrid/HIL tests on the OC5 floating offshore wind turbine. *Proceedings of 36th International Conference on Ocean, Offshore & Arctic Engineering, OMAE 2017*.
- Fontanella, A., Bayati, I., and Belloli, M. (2018). Control of Floating Offshore Wind Turbines: Reduced-order Modeling and Real-time Implementation for Wind Tunnel Tests. *Proceedings of 37th International Conference on Ocean, Offshore & Arctic Engineering, OMAE 2018, forthcoming*.

Design and experimental optimisation of a cm-scale wind turbine for energy harvesting

Luca Bernini¹, Gisella Tomasini¹ and Davide Tarsitano¹

¹Department of Mechanical Engineering, Politecnico di Milano, via La Masa,1, I-20156, Milano, Italy

Corresponding author: Gisella Tomasini, gisella.tomasini@polimi.it

Abstract

Wind turbine is a good choice for energy harvesting on trains. The air flow is generated by the train movement and it is quite simple to find places with high flow speed near the wireless sensor nodes location which are typically mounted on bogies and wheelsets. The requested amount of energy is relatively small, in the order of 0.1-1 W, allowing for wind turbines with very small diameter, between 2 to 6 cm. In the present work a newly designed turbine is described. The turbine is placed in an enclosed duct with protection purposes and it has a symmetrical design that results in power production independently from the train movement direction.

1 Introduction

This work deals with the design and the optimisation by means of wind tunnel tests of a centimetre scale wind turbine to be used as energy harvester in autonomous sensor nodes for diagnostic/monitoring of freight trains.

The state of the art in the field of small scale wind turbines for energy harvesting is focused on the performance analysis of off-the-shelf cm-scale turbines using commercially available components small scale rotors [1] [2]. Few recent studies [3] analyse the aerodynamics of the blades, using the Blade Element Momentum based code to design and built a customized cm-scale turbine to optimize its efficiency for a low wind speed air-ventilation application.

With respect to the cited works, in this research the aerodynamic design of a centimetre scale blade is carried out using an inhouse BEM code and the layout is specifically studied to be adopted in railways applications (wide range of wind speed, bidirectional operation). Different prototypes of rotors are tested in wind tunnel both in open field tests and with different configurations of ducts.

2 Numerical design with BEM code

In the first part of the work, the rotor is designed by means of the BEM code. This code allows to calculate the steady loads and, thus, also the thrust and the power for different settings of the wind speed, rotational speed and pitch angle. Providing as input the blades number, the rotor diameter, the nominal rotation speed and the design wind velocity, it is possible to use the BEM algorithm for rotor shape optimization. Different design options were considered, finally three of them were finalized: one 3 cm and one 4 cm diameter rotors employed low Reynolds airfoil, SD7032 from Selig catalogue [4] and one 4cm symmetrical rotor with constant blade pitch fixed at 45° and flat plate blade section. Note that the symmetrical rotor was not optimized using the BEM code for lack of knowledge about the flat plate response at the considered conditions. The main driver for the symmetrical design was the ability to work with both the train running directions, All the rotors prototypes have been produced with metal rapid prototyping technique (see Figure 1) with high precision and good mechanical strength characteristics.

3 Wind tunnel tests

The rotors performance have been tested in the “Sergio De Ponte” wind tunnel of Politecnico Di Milano, the tunnel test section is 1.5 by 1 m with a maximum wind speed of 55 m/s.

Firstly, the 3cm and 4 cm diameter rotors were tested, Figure 2(a) shows the comparison of the power output with the numerical simulation for the 4 cm one. The agreement is not perfect but BEM is in general able to correctly catch the results trend confirming its capability as optimising tool.

The symmetric turbine was not compared to any numerical simulation, but it was tested both in open field and placed in the duct that will be used in the final application. The duct, showed in Figure 1, is necessary to protect the rotor in the final placement under the train body.



Figure 1 Rotor placed in the duct

Moreover, the testing duct has a modular design allowing to change the duct total length and the inlet geometry, allowing to test different solutions optimizing for the rotor performances. Figure 2(b) shows the power output for the open-field symmetrical rotor (red symbols) and the ducted set-up (blue symbols): it is evident how the ducted rotor performance is enhanced by the duct presence.

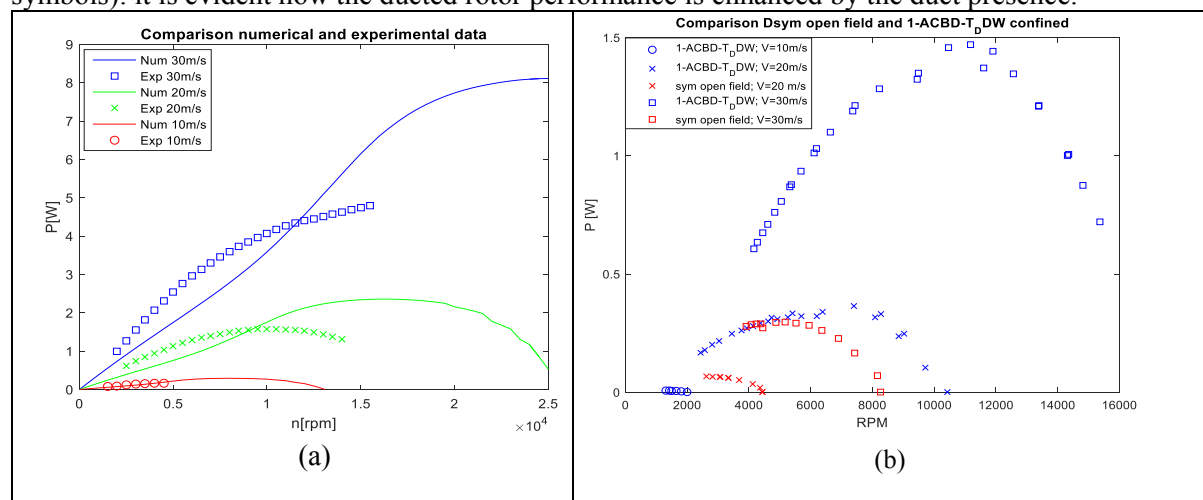


Figure 2 . Open field (a) and duct (b) wind tunnel setup.

4 References

- [1] D. Rancourt, A. Tabesh and L. Fréchette, “Evaluation of centimeter-scale micro wind mills: Aerodynamics and electromagnetic power generation,” pp. 93-96, 1 2007.
- [2] F. J. Xu, F. G. Yuan, J. Z. Hu and Y. P. Qiu, “Miniature horizontal axis wind turbine system for multipurpose application,” *Energy*, vol. 75, pp. 216-224, 2014.
- [3] F. J. Xu, F. G. Yuan, J. Z. Hu and Y. P. Qiu, “Design of a miniature wind turbine for powering wireless sensors,” 2010.
- [4] C. A. Lyon, A. P. Broeren, P. Giguere, A. Gopalathnam and M. S. Selig, Summary of Low-Speed Airfoil Data – Volume 3, 1997.

Wind-tunnel experiments on a large-scale Flettner rotor

G. Bordogna¹, S. Muggiasca², S. Giappino², M. Belloli²

J.A. Keuning¹, R.H.M. Huijsmans¹ and A.P. van 't Veer¹

¹Section of Ship Hydromechanics and Structures, Delft University of Technology, The Netherlands

²Department of Mechanical Engineering, Politecnico di Milano, Italy

Corresponding author: G.Bordogna, g.bordogna@tudelft.nl

Abstract

Experiments on a large-scale Flettner rotor were carried out in the boundary-layer test section of Politecnico di Milano wind tunnel. The Flettner rotor is a device that makes use of the Magnus effect in order to generate a lift force and it finds several applications in a variety of different industries. The rotor tested (referred to as Delft Rotor) had a diameter of 1 m and a span of 3.73 m. Such large dimensions were necessary to study the influence of different Reynolds numbers on the aerodynamic forces generated by the rotor. The Delft Rotor was equipped with two purpose-built force balances and two different measurement systems to measure the pressures on the rotor's outer skin. The highest Reynolds number achieved was $Re=9.2 \cdot 10^5$. These experiments are part of an on-going cooperation between Delft University of Technology and Polytechnic University of Milan within the Sail Assist project.

1 Introduction

In recent years, wind energy as an auxiliary form of propulsion for commercial ships has attracted attention as a viable response to volatile fuel prices and to drastically reduce pollutant emissions produced by the shipping industry. Nevertheless, the lack of a robust performance prediction method, i.e. an accurate estimate of how much fuel can be saved given a certain weather condition, is one of the most relevant aspects affecting the further uptake of this promising technology. In this context, the experiments carried out on the Delft Rotor are aimed at gaining a better understanding of the aerodynamic forces generated by a full-scale Flettner rotor. Previous experimental results available in the literature are limited to low Reynolds numbers (Badalamenti and Prince, 2008) or to low (not useful from a real application point of view) spinning ratios (Swanson, 1961). It should be pointed out that the present paper focuses on the various experimental techniques employed during the wind-tunnel tests. A following journal article will be published in which all the results will be presented with the aim to offer a useful benchmark for CFD computations.

2 The Delft Rotor

The Delft Rotor is a large Flettner rotor, i.e. a spinning cylinder, with diameter $D=1.0$ m and span $H=3.73$ m. The Delft Rotor was comprised of three main parts: a fixed part, that was made of an upper and a lower structure where the two balances were located, a rotating internal frame, and an outer skin, that is where the pressure taps were installed. The outer skin, the internal frame and the two balances were built with alloy whereas the other fixed parts were built with steel. To be able to assembly the rotor and to install all the necessary measuring instruments, the outer skin was made of four separated calendered sheets that were eventually mounted on the internal frame to construct the cylinder. Two different pressure measurement systems were installed, i.e. (one ESP scanner with 32 pressure

sensors and one single sensor AMS 4711: both use piezoresistive silicon chip as sensing element). Images of the Delft Rotor are given in Figure 1 and Figure 2.

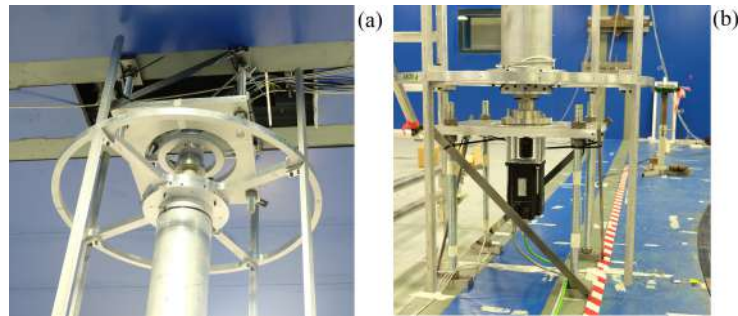


Figure 1. Upper force balance (a) and lower force balance together with the electric engine (b).



Figure 2. Complete setup of the Delft Rotor.

3 Test matrix

The aim of the experiments was to study the influence of the Reynolds number on the aerodynamic forces generated by a Flettner rotor. The lift and the drag forces produced depend on the spinning ratio k , that is the ratio between the tangential velocity of the spinning cylinder and the incoming flow velocity. In Table 1 the entire test matrix is given. In particular, it is shown the rpm of the Flettner rotor depending on the four Reynolds numbers and the seven spinning ratios tested. For the largest Reynolds number, $Re=9.2 \cdot 10^5$, the highest spinning ratio achieved was $k=2.0$ due to the very large inertial forces involved that would have caused structural problems to the outer skin of the rotor.

Table 1. Delft Rotor test matrix

Re	Rotor rpm VS Reynolds number and spinning ratio						
	$k=1.0$	$k=1.25$	$k=1.5$	$k=1.75$	$k=2.0$	$k=2.25$	$k=2.5$
$1.6 \cdot 10^5$	48	60	72	84	95	107	119
$3.3 \cdot 10^5$	95	119	143	167	191	215	239
$5.0 \cdot 10^5$	143	179	215	251	286	322	358
$9.2 \cdot 10^5$	267	334	401	468	535	-	-

References

- Badalamenti, C. and Prince, S.A. (2008). The Effects of Endplates on a Rotating Cylinder in Crossflow. *26th AIAA Applied Aerodynamic Conference, Aug. 18-21, Honolulu, Hawaii.*
- Swanson, W.M. (1961). The Magnus Effect: A Summary of Investigations to Date. *Journal of Basic Engineering* **83**, 461–470.

The effect of lift-up buildings on wind-induced forces and ventilation in simple urban geometries

Riccardo Buccolieri¹, Tommaso Massai², Andrea Giachetti², Francesca Quarta¹, Gianni Bartoli²

¹Dipartimento di Scienze e Tecnologie Biologiche ed Ambientali, University of Salento, Lecce, Italy

²Department of Civil and Environmental Engineering, University of Florence, Florence, Italy

Corresponding author: Tommaso Massai, tommaso.massai@unifi.it

Abstract

This paper is devoted to the study of lift-up building design. Wind-induced forces are first measured in wind tunnel and then linked to ventilation conditions evaluated through Computational Fluid Dynamics (CFD) simulations around isolated buildings and urban-like street canyons with open spaces at both ground and higher floors.

1 Introduction

Modern big cities are characterized by high-rise and closely-spaced buildings which can affect the ventilation at the ground-level causing accumulation of pollutants or discomfort for pedestrian.

A solution to minimize the ground-level wind flow obstruction and improve the wind circulation (frequently used in the sub-tropical cities of South-East Asia), is the design of buildings with a “lift-up” shape, in which the entire structure is maintained by a central core, columns or cutting walls. In this context, in the present work both wind tunnel experiments and Computational Fluid Dynamics (CFD) simulations are performed to assess the mean wind velocity at the pedestrian-level and the wind induced forces (drag, lift, torque, ...) exerted by several configurations of lift-up buildings.

2 A brief overview of recent literature studies on lift-up buildings

Only few recent studies have looked at the effects of open spaces on flow and pollutants dispersion by using wind tunnel measurements and CFD simulations.

Wind tunnel experiments have been recently performed to have an insight on the effects of different configurations of lift-up buildings on flow and pedestrian comfort under several wind directions. Du et al. (2017a) investigated the effects of lift-up design taking Hong Kong Polytechnic University campus as study area suggesting that the lift-up design can effectively improve the thermal conditions in the campus. Tse et al. (2017) considered isolated buildings with different dimensions of the central lifting core and showed that a lift-up building modifies the surrounding wind environment differently than a building without lift-up design. Increases in size and intensity of high wind speed areas were found enhancing ventilation conditions around lift-up buildings. The wind tunnel study of Zhang et al. (2017) investigated the influence of lift-up buildings with different aspect ratios (height on width building dimensions) and with a central core to elevate the main structure from the ground which was preferred over columns or shear wall designs because it induces minimum disturbance to the wind conditions in the lift-up area. Lift-up designs adopted for short and wide buildings produced larger areas of pedestrian wind comfort.

CFD simulations were performed by Liu et al. (2017) considering an isolated building lifted-up by three structural pillars showing that the wind flow can blow freely through the open space and small vortices were produced behind each pillar; many vortexes occurred in the wake region of the lift-up building. The flow pattern was in fact strongly modified by the lift-up design, which can lead to different

pedestrian-level wind comfort. Du et al. (2017b) using CFD simulations showed that the improvement of pedestrian-level wind comfort in the wind-speed lift-up area and in the surrounding areas also depend on the approaching wind direction. A last study coupling CFD simulations with response surface methodology has recently proposed a multi-variable optimization method to determine optimum wind comfort and the corresponding lift-up design variables for an isolated building (Du et al., 2018).

3 Description of the cases investigated and analysis

The studies mentioned above clearly indicate that the lift-up design has a significant influence on pedestrian level wind environment and thermal comfort, and that such applications are quite recent in the literature. In this context, the wind velocity at the pedestrian-level and the wind induced forces exerted by lift-up high-rise buildings as control parameters are investigated in the proposed work, taking into account several wind directions.

Starting from the base case of an isolated high-rise building (*e.g.* width:depth:height ratio = 2:1:5), we firstly lift-up the whole building leaving an open space between the ground and the first floor, then we consider several open spaces at higher floors. The geometry is progressively complicated by adding a second building forming a sort of street canyon.

Wind-induced aerodynamic forces are measured in wind tunnel experiments using a HFFB (ATI FT-Delta) and integrating pressure measurements on several heights, to be compared with those computed by CFD, equipped with RANS (Reynolds-Averaged Navier-Stokes) turbulence models. First, wind tunnel measurements are used for modelling validation, then CFD is employed to evaluate the link between forces and lift-up designs, and their influence on ventilation conditions.

References

- Du, Y., Mak, C.M., Huang, T., and Niu, J. (2017a). Towards an integrated method to assess effects of lift-up design on outdoor thermal comfort in Hong Kong. *Building and Environment* **125**, 261-272.
- Du, Y., Mak, C.M., Liu, J., Xia, Q., Niu, J., and Kwok, K.C.S. (2017b). Effects of lift-up design on pedestrian level wind comfort in different building configurations under three wind directions. *Building and Environment* **117**, 84-99.
- Du, Y., Mak, C.M., Li, Y., 2018. Application of a multi-variable optimization method to determine lift-up design for optimum wind comfort. *Building and Environment* **131**, 242–254.
- Liu, J., Niu, J., Mak, C.M., and Xia, Q. (2017). Detached eddy simulation of pedestrian-level wind and gust around an elevated building. *Building and Environment* **125**, 168-179.
- Tse, K.T., Zhang, X., Weerasuriya, A.U., Li, S.W., Kwok, K.C.S., Mak, C.M., and Niu, J. (2017). Adopting ‘lift-up’ building design to improve the surrounding pedestrian-level wind environment. *Building and Environment* **117**, 154-165.
- Zhang, X., Tse, K.T., Weerasuriya, A.U., Li, S.W., Kwok, K.C.S., Mak, C.M., Niu, J., and Lin, Z. (2017). Evaluation of pedestrian wind comfort near ‘lift-up’ buildings with different aspect ratios and central core modifications. *Building and Environment* **124**, 245-257.

Wind, wave and sea current loads on offshore wind turbines

Andrija Buljac¹, Hrvoje Kozmar¹, Wenxian Yang² and Ahsan Kareem³

¹Faculty of Mechanical Engineering and Naval Architecture, University of Zagreb, Croatia

²School of Engineering, Newcastle University, UK

³Department of Civil and Environmental Engineering and Earth Sciences,
University of Notre Dame, USA

Corresponding author: Andrija Buljac, andrija.buljac@fsb.hr

Abstract

This study investigated coupling features of wind, wave and tidal current loads and their combined effects on the structural response of a bottom-fixed monopile supported offshore wind-turbine. A small-scale model of an offshore wind turbine was developed and systematic laboratory tests were carried out in the Wind-Wave-Current Tank (WWC) at Newcastle University, UK. In the experiments, the aerodynamic loads in six degrees of freedom of the wind-turbine model were measured. The measurement results have shown that the tidal current and waves have a significant contribution to the static loads on the wind-turbine model. The dominant frequency of the drag force acting on the wind-turbine model is the same as the wave frequency. This suggests the natural frequency of the wind turbine should be designed far away from the wave frequency to enhance its structural safety.

1 Introduction

Offshore wind turbines have been increasingly used due to a strong initiative on renewable energy production, as indicated by Lewis et al. (2011). Offshore wind turbines with horizontal axis are commonly exposed to a harsh marine environment including wind, wave and sea current loads. To extend their lifetime and increase efficiency, it is necessary to carefully analyze the effects of environmental loads on these structures. The focus of this study is to analyze simultaneous wind, wave and sea current loads on a single offshore wind-turbine model and its structural response.

2 Experimental setup

The small-scale laboratory experiments were performed in the Wind-Wave-Current Tank (WWC) at Newcastle University, UK. The Siemens Sapiens FFA W3 small-scale model of the offshore wind turbine was designed with monopile support structure and placed in the lateral center of the test section, as shown in Figure 1. The wind-turbine model was attached to the six-component high-frequency force balance. The sampling frequency was 500 Hz. The wave height and frequency were determined using the wave probe placed next to the wind-turbine model.

3 Experimental results and discussion

The results for the drag force are shown in Figure 2a for the average wind velocity of 8.5 m/s (AH); tidal current velocity of 0.7 m/s (CM) and without the current (C0); wave amplitude and frequency of 0.15 m and 0.6 Hz (WH) and without the waves (W0). The power spectra of the drag forces measured for various wave conditions (i.e. different wave frequencies f_w) were calculated and shown in Figure 2b. The wave drag force spectra exhibits contribution from nonlinearity in drag as noted by the presence of sub and super harmonics, Kareem et al. (1995).

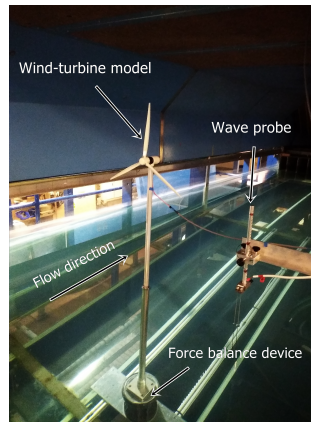


Figure 1. Experimental setup for the WWC measurements of aerodynamic loads on a bottom-fixed monopile offshore wind-turbine model.

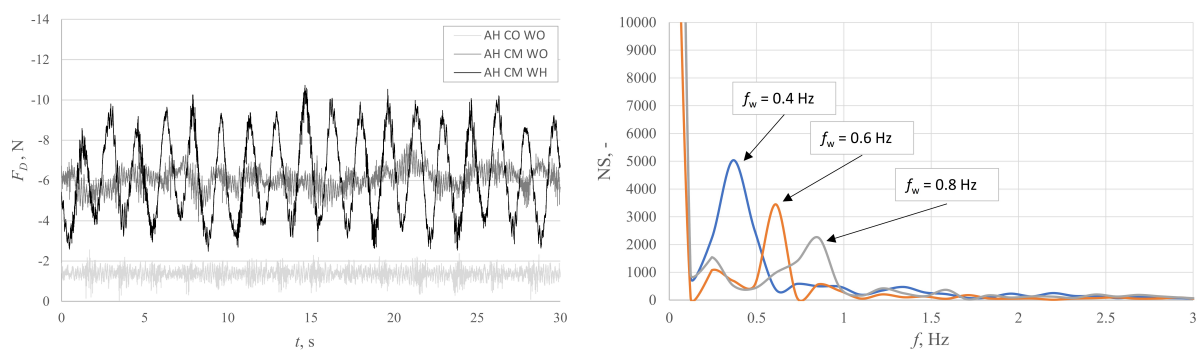


Figure 2. a) Drag force acting on the wind-turbine model for various airflow, waterflow and wave characteristics, b) Power spectrum of the drag force fluctuations for various frequencies of the waves.

The drag force of the wind-turbine model significantly increased when the waterflow was present in addition to the airflow, while the deviations with respect to the mean value were increased as well. The waves played an important role in the resultant static loads of the wind-turbine model, as they increased the peak drag force up to 30%. The dominant frequency of the drag force of the wind-turbine model matched the wave frequency f_w . This suggests the natural frequency of the wind turbine should be designed far away from the wave frequency to enhance its structural safety.

Acknowledgement

The authors acknowledge the support by the Croatian Science Foundation IP-2016-06-2017 (WESLO). Special thanks is extended to the WWC technical staff for their help in the experiments and to Mr. Peter Bowes for his kindness with respect to coordinating the WWC tests.

References

- Lewis, A., Estefen, S., Huckerby, J., Musial, W., Pontes, T., Torres-Martinez, J. (2011). *Ocean energy, IPCC Special Report on Renewable Energy Sources and Climate Change Mitigation*. Cambridge University Press, Cambridge, United Kingdom, 497-534.
- Kareem, A., Zhao, J., Tognarelli, M.A. (1995). Surge response statistics of tension leg platforms under wind and wave loads: a statistical quadratization approach. *Probabilistic Engineering Mechanics* **10** (4), 225-240.

Self-excited vibrations of bridge deck with single and double wind barriers

A. Buljac¹, H. Kozmar¹, Michael Macháček, Stanislav Pospíšil

¹Faculty of Mechanical Engineering and Naval Architecture, University of Zagreb, Croatia

²Institute of Theoretical and Applied Mechanics Prague, Academy of Science, Czechia

Corresponding author: Andrija Buljac, andrija.buljac@fsb.hr

Abstract

Wind-tunnel experiments are carried out to study the influence of wind barriers on the flutter susceptibility of a streamlined bridge-deck section. The wind barriers of various heights and constant porosity of 30% are placed at the a) windward bridge-deck edge, b) leeward bridge-deck edge, c) both windward and leeward bridge-deck edges. The results indicate that the studied bridge deck remains dynamically stable with respect to the heave motion for all configurations of wind barriers. The configurations with wind barriers at both edges are more sensitive to torsional flutter when compared to configurations with single wind barriers placed either at the windward or at the leeward bridge-deck edge.

1 Introduction

Strong winds that commonly blow on bridges may deteriorate dynamic stability of vehicles crossing the bridge. Hence, wind barriers are commonly placed on bridges to protect vehicles from adverse cross-winds effects. These barriers, often used with various heights and porosities, proved to be successful in sheltering vehicles on bridges, e.g. Kozmar et al. (2014). However, long-span cable-supported bridges, characterized by low natural frequencies and low mechanical damping, are particularly sensitive to wind effects, and even a small change in the bridge-deck design may trigger the dynamic instability, Jones et al. (1995).

Wind barriers may be placed in various arrangements at the bridge deck to be suitable for wind and terrain characteristics on a certain geographic location. In the area where the wind blows predominantly from one direction, wind barriers are usually placed at the windward bridge-deck edge only. The windward-placed wind-barriers proved to significantly influence the aerodynamic and aeroelastic characteristics of bridges, Buljac et al. (2017).

For wind barriers placed both at the windward and leeward bridge-deck edges, the shear layer that separates from the windward wind-barrier top may remain captured at the bridge deck between the windward and leeward wind barriers, e.g. Avila-Sanchez et al. (2016). This issue is expected to influence the dynamic stability of long-span bridges. To investigate this issue, wind-tunnel experiments on the influence of wind-barrier configurations on flutter susceptibility of a streamlined bridge-deck section were carried out. The studied bridge deck section model is used together with 30% porous wind barriers with various heights (3, 5 and 7 m in full-scale).

2 Experimental setup

The bridge-deck model was placed on the custom-made mechanism for measurements of complex aeroelastic phenomena. This mechanism allows for a dynamic motion of the bridge-deck model in two-degrees of freedom (heave and pitch). It is designed to allow for large deflections with a linear behavior. The dynamic response of the bridge-deck model under the influence of the airflow was measured using the free-vibration method. It included an initial displacement of the bridge-deck section in both degrees of freedom and measurements of the free-decay oscillations due to the flow.

Eight flutter derivatives were obtained from the measured signal using the modified unifying least-squares method.

3 Experimental results and discussion

The direct H_1^* and A_2^* derivatives are reported in Figure 1 for various configurations of wind barriers.

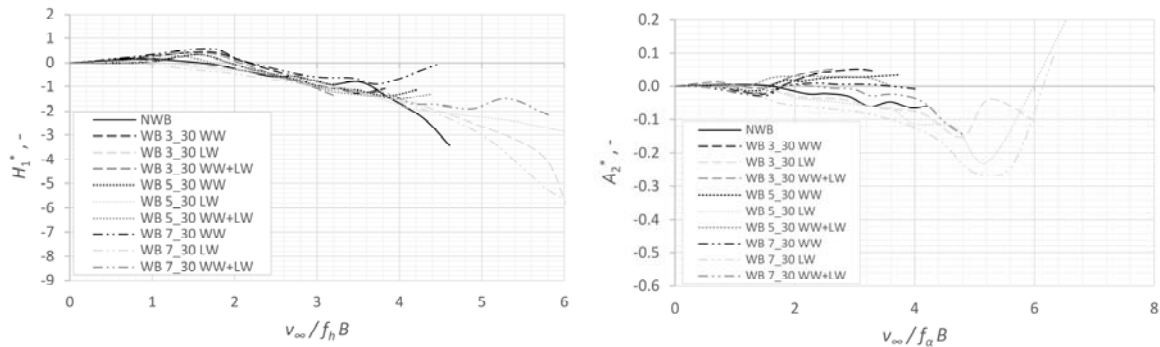


Figure 1. The H_1^* and A_2^* derivatives for bridge-deck with wind barriers.

The H_1^* derivative remains negative at large reduced flow velocities v/fB , which indicates that the studied bridge-deck remains dynamically stable with respect to the heave motion for all the studied configurations of wind barriers. Positive values of this derivative at lower reduced flow velocities are likely due to the vortex-shedding frequency that is nearly equal to the heave natural frequency of the bridge-deck section, as this instability vanishes with further increase of the flow velocity.

The wind barriers deteriorate the dynamic stability in torsional motion, as the A_2^* derivative becomes positive at relatively large reduced flow velocities. Lower wind barriers increase the susceptibility to torsional flutter for the studied bridge-deck section, while the configurations with wind barriers at both bridge-deck edges are more sensitive to torsional flutter when compared to the configurations with single wind barriers placed either at the windward or at the leeward bridge-deck section edge only.

Acknowledgement

The support of the Croatian Science Foundation, GAČR No. 17-26353J, CET sustainability project LO12 (SaDeCET) is gratefully acknowledged.

References

- Avila-Sanchez, A., Lopez-Garcia, O., Cuerva, A., and Meseguer, J. (2016). Characterisation of cross-flow above a railway bridge equipped with solid windbreaks. *Engineering Structures* **126**, 133-146.
- Buljac, A., Kozmar, H., Pospíšil, S., and Macháček M. (2017). Flutter and galloping of cable-supported bridges with porous wind barriers. *Journal of Wind Engineering & Industrial Aerodynamics* **171**, 304-318.
- Jones, N.P., Scanlan, R.H., Sarkar, P.P., and Singh, L. (1995). The effect of section model details on aeroelastic parameters. *Journal of Wind Engineering & Industrial Aerodynamics* **54/55**, 45-53.
- Kozmar, H., Procino, L., Borsani, A., and Bartoli, G. (2014). Optimizing height and porosity of roadway wind barriers for viaducts and bridges. *Engineering Structures* **81**, 49-61.

Wind tunnel experimentation on stationary downbursts at WindEEE

Massimiliano Burlando¹, Djordje Romanić², Horia Hangan² and Giovanni Solari¹

¹Department of Civil, Chemical and Environmental Engineering, University of Genoa, Italy

²Wind Engineering, Energy and Environment (WindEEE) Research Institute, Western University,
London, Ontario, Canada

Corresponding author: M. Burlando, massimiliano.burlando@unige.it

Abstract

In the context of the European Project THUNDERR a scientific collaboration between the Wind Engineering and Structural Dynamics (Windyn) Research Group of the University of Genoa (Italy) and the Wind Engineering, Energy and Environment (WindEEE) Research Institute of the Western University (Canada) has been established to study experimentally at the WindEEE Dome facility how the main geometrical and mechanical properties of downbursts are affected by different cloud base outflows for stationary thunderstorms.

The downburst that occurred in Livorno on 13 September 2015, measured by means of the ultrasonic anemometers and the LiDAR wind profiler belonging to the “Wind, Ports and Sea” wind monitoring network of the Port of Livorno, has been chosen as test-case to be replicated and compared to results in WindEEE Dome. At present, the analysis of the downbursts simulated experimentally is ongoing and some preliminary elaborations have been obtained concerning the qualitative interpretation of the corresponding signals.

1 Introduction

In 2017, in the framework of the European Project THUNDERR – Detection, simulation, modelling and loading of thunderstorm outflows to design wind-safer and cost-efficient structures (Solari et al. 2018), a first set of experiments has been carried out at WindEEE to study the class of downbursts induced by stationary thunderstorm outflows. This class of phenomena comprehends all thunderstorms that are stationary in meteorological terms, which means that their vertical axis does not move with respect to the ground, while the flow field is not steady as it changes according to the time evolution of the cumulonimbus cloud as it passes from mature to dissipative stage.

In the following, a short description of the experimental settings used to simulate downbursts at WindEEE Dome is reported in Section 2 and some measurements and preliminary results are shown in Section 3.

2 Experimental settings

The WindEEE Dome is a hexagonal wind tunnel with an inner diameter of about 25 m, which is intended to reproduce, at large scale and under controlled inflow and boundary conditions, time-dependent swirling winds like tornadoes, downbursts and gust fronts (Hangan et al, 2017).

The presented experiments were carried out in 2017 at WindEEE Dome and they focused mainly on the simulation of downbursts generated by stationary, but unsteady thunderstorm outflows. In terms of experimental inflow conditions, such downbursts are generated producing a dynamic (sudden) vertical flow downward from the bell mouth mounted at the ceiling of the test chamber, which is kept fixed. From similarity point of view, the velocity, time and geometric scales of the reproduced events in the laboratory need to be established in order to accurately investigate the life-cycle of the real downburst in the atmosphere. This information was deduced from the analysis of a real downburst that occurred in Livorno (Italy) on 13 September 2015 at about 1100 UTC (Burlando et al. 2017). In order to simulate as close as possible this particular event, the downburst ring diameter, D , was chosen equal to 3.2 m and the time of louveres to open

and close was approximately 10 s. Two vertical wind speeds of the downward flow (i.e., jet velocities) were tested corresponding to 20% and 40% of the nominal fans power.

3 Downburst measurements and preliminary results

In this section, some measurements and preliminary results of the experimental case corresponding to the 20% fans power are reported. Figure 1 shows the wind speed time series measured by means of Cobra probes at 10 cm above the tunnel floor at a distance from the downburst centre, R , equal to $R/D = 1.0$ (left) and 2.0 (right). The experiment has been repeated 20 times in order to capture the variability of this transient phenomenon. The black line corresponds to the mean values over the whole repetitions.

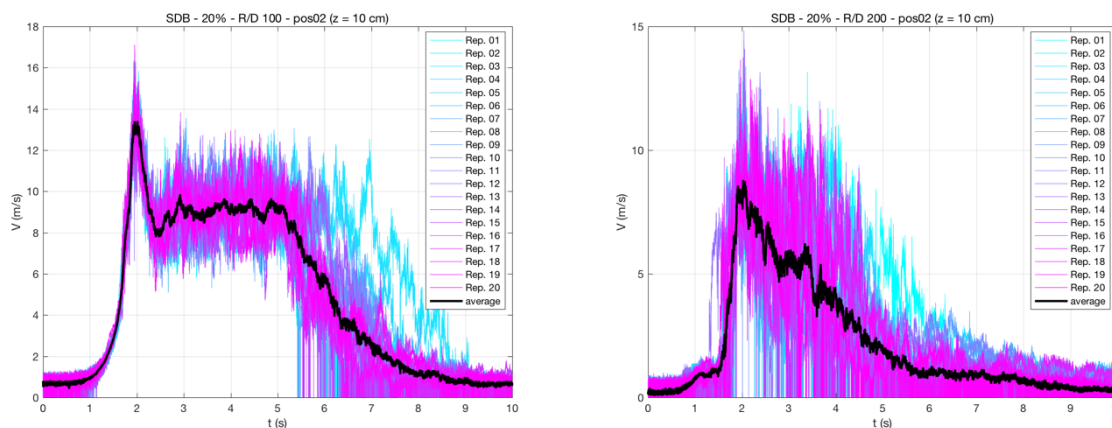


Figure 1. Time series of the wind speed measured at $R/D = 1.0$ (left) and at $R/D = 2.0$ (right) and their mean.

Both the mean time series (black lines), which correspond to the deterministic part of this phenomenon, as well as the statistical repeatability of the simulations show that the signal associated to downbursts consists of three main parts: (1) a sudden ramp-up followed by a rapid decrease of the wind speed, which determine the first maximum of the signal; (2) a plateau that can be more or less pronounced according to the distance from the downburst centre; and (3) a tail during the downburst dissipation stage.

4 Perspectives

The systematic analysis of the time series measured in the wind tunnel is ongoing and will be presented in the full paper. Moreover, by the end of 2018 a set of new experiments will be performed at WindEEE in order to study more complex, but also more realistic, meteorological conditions associated with real downbursts, such as the case of background flows superimposed to thunderstorm outflows.

References

- Burlando, M., De Cio, A., Pizzo, M., and Solari, G. (2017). Analysis of wind vertical profiles of thunderstorm events in the Mediterranean. *9th Asian-Pacific Conference on Wind Engineering*, Dec. 3-7, Auckland, New Zealand.
- Hangan, H., Refan M., Jubayer, C., Romanic, D., Parvu D., LoTufo, J., and Costache, A. (2017). Novel Techniques in Wind Engineering, *J. Wind Eng. Ind. Aerodyn.* **171**, 12–33.
- Solari, G., Burlando, M., and Repetto, M. P. (2018). THUNDERR: an ERC Project for the “detection, simulation, modelling and loading of thunderstorm outflows to design wind-safer and cost-efficient structures”. *International Workshop on Wind-Related Disasters and Mitigation*, Mar. 11-14, Sendai, Japan.

Damage from recent thunderstorms in Romania

Ileana Calotescu¹

¹Department of Steel Structures, Management and Engineering Graphics, Technical University of
Civil Engineering Bucharest, Romania

Corresponding author: Ileana Calotescu, ileana.calotescu@utcb.ro

Abstract

The paper presents an overview of wind-induced damage to the natural and the built environment caused by thunderstorms that occurred in Romania in the past five years (2013-2017). To this aim, a vast online search of mass-media reports is performed in order to identify the date, location and damage type produced by each storm. Due to the lack of measured data, a thunderstorm is identified by means of descriptions of the event provided by interviewed witnesses, by images posted online by the newspaper or by the pattern of damage caused by the storm. The types of damage associated with thunderstorms include damage to buildings and transmission lines produced by strong winds, damage produced by large hail to buildings, cars as well as crops and flooding produced by heavy rainfall. Strong winds may also uproot trees producing considerable damage to forests.

1 Introduction

In this paper, an overview of damage produced by recent thunderstorms that have occurred in Romania in the past five years (2013-2017) is presented. Unfortunately, measured data related to thunderstorms is not yet available in Romania. At most, the Romanian National Meteorology Administration may provide the maximum gust speed related to a particular event when journalists ask for this information. Thunderstorms are localized events that may produce damage both to the man-made (Tamura, 2009) as well as the natural environment (Dupont et. al, 2015). In a previous accompanying study Calotescu (2018) showed that the most affected part of the country with respect to the number of thunderstorms that occurred within the past five years (2013-2017) is the western part. This paper focuses on the damage pattern that emerged from the investigated events.

2 Methodology

Iliescu (1989) showed that thunderstorm season in Romania generally occurs between months March to September. The methodology used within this paper involved making use of the Google engine to perform a vast online search of newspaper articles describing thunderstorms that have occurred in Romania recently. A two-step process was used. First, dates of strong storms were identified by setting a custom search time frame such as the first and last day of each considered month (March-September) for each year (2013-2017). Then, for each identified event, a detailed search was performed and information about location, casualties and damage type from several newspapers was documented.

3 Recent thunderstorms

By applying the methodology presented in Section 2, eleven wind storms were identified in each of the years 2013 to 2016 and 10 storms identified in 2017 (Calotescu, 2018). On *September 14th, 2013* a “tornado” that lasted approximately 40 seconds destroyed 5 houses and damaged other 40 in Tulcea county. On *July 22nd 2014*, a thunderstorm that occurred in Suceava county damaged 55 hectares of

forest (Fig. 1a). Hail was responsible for the damage of approximately 600 houses and 400 hectares of strawberry fields in Satu Mare county on *May 25th, 2015*. On *June 19th, 2016* a particularly strong thunderstorm produced the collapse of several transmission towers in Mureş county (Fig. 1b). The most severe thunderstorm in Romania in recent years occurred on *September 17th, 2017* with the most affected county being Timiş where velocities of 117-122km/h were reported and 5 people lost their lives. Financial support dispatched from the government amounted to 7800000 Euros.

4 Damage associated with recent thunderstorms

Depending on the storm intensity, damage associated with thunderstorms, as resulted from the present study included: complete collapse of poorly engineered family houses, damage to roof tiles, damage to steel sheet roofing as well as partial or overall roof lift-off, partial or total collapse of transmission towers, damage to power lines, collapse of reinforced concrete electricity poles and wooden telephone poles, damage to cladding and roofs of houses due to large hail, damage to cars due to wind breakage of trees, windthrow and damage to crops.

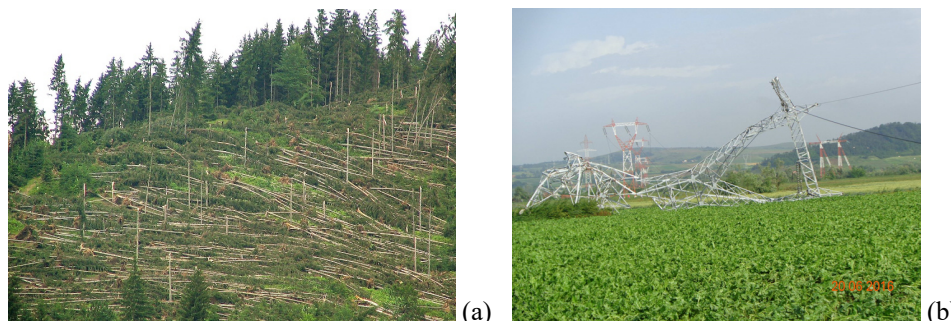


Figure 1. (a) Windthrow, July 22nd 2014 (b) Collapsed tower, June 19th 2016 ©Energy for Romania

5 Conclusions

This paper presents the most frequent types of damage produced by thunderstorms as resulted from the investigation of mass-media reports related to events that occurred in Romania in the past five years (2013-2017). Results showed that strong intensity events produced the collapse of transmission towers as well as non-engineered family houses whereas the most common type of damage associated with medium intensity events was damage to the roofs of buildings. Low intensity events generally produce breakage or uplift of trees damaging cars located nearby. Wind related phenomena such as large hail produced damage to roofs and claddings of buildings as well as damage to crops.

References

- Calotescu, I. (2018). Overview of recent wind-induced damage in Romania based on mass-media reports. *International Workshop on Wind-Related Disasters and Mitigation, March 11-14, Sendai, Japan*.
- Dupont, S., Pivato, D., Brunet, Y. (2015). Wind damage propagation in forests, *Agricultural and Forest Meteorology* **214-215**, 243-251.
- Iliescu, M.C. (1989). *Manifestări electrice atmosferice pe teritoriul României*, Editura Academiei Republicii Socialiste România. (in Romanian)
- Tamura, Y. (2009). Wind-induced damage to buildings and disaster risk reduction. *The Seventh Asia-Pacific Conference on Wind Engineering, November 8-12, 2009, Taipei, Taiwan*.

Full-scale measurements of a 63-storey mixed-use high-rise under wind

Stefano Cammelli¹, Hung Nguyen-Sinh² and Jessica Garcia Navarro¹

¹BMT Fluid Mechanics, Teddington, UK

² BMT Fluid Mechanics, New York City, USA

Corresponding author: Stefano Cammelli, Stefano.Cammelli@bmtglobal.com

Abstract

Despite the hundreds of wind tunnel studies conducted every year on tall- and super-tall buildings globally, the number of full-scale measurements conducted on these structures is still somewhat limited. Full-scale measurements, even for a short duration, have in fact tremendous value as they can be used to validate the structural frequencies predicted during the design stage through Finite Element Model (FEM) analysis and, at the same time, they can provide very valuable information on the level of damping these structures can inherently exhibit once built. In the assessment of the wind-induced response of tall- and super-tall buildings, damping does in fact constitute one of the most uncertain variables. In this technical paper, the findings of a 3-month full-scale monitoring campaign conducted on a 63-storey high-end residential tall building will be presented and discussed.

1 Introduction

During the design of a slender 63-storey high-rise in North America, wind tunnel studies highlighted the potential for wind-induced sway to cause discomfort to the residents of the uppermost occupied levels of the building. In order to mitigate such excessive vibrations, a Tuned Liquid Column Damper (TLCD) in the form of a 'U-tube' water tank with a total effective mass of ~ 410,000 kg was proposed and designed for this structure (Cammelli and Li, 2016).

After the topping out of the structure, the installation of the façade system was well progressed on site and the TLCD casted but lying empty: this was the perfect timing for a short campaign of full-scale measurements to take place. This technical paper summarises the findings of this short-term campaign of full-scale measurements which was aimed at confirming a number of structural parameters assumed during the design of the TLCD (e.g. structural frequencies and damping).

2 The Monitoring Campaign

The instrumentations (see Figure 1) which have been used during the 3-month monitoring campaign discussed within this technical paper were:

- Two (2) three-axis accelerometers and tilt sensors mounted on the 62nd floor;
- A weather station installed at roof level;
- A 3G router and data logger located on the 62nd floor.

Accelerations (sampled at 20Hz), angular accelerations (sampled at 10Hz) and weather statistics (which included: 10-minute averaging wind speed and direction; maximum / minimum wind speed and direction within each 10-minute window; temperature; humidity; atmospheric pressure; rain and its duration) were continuously and simultaneously recorded and stored on a cloud-based server.

3 Data Analysis

During the monitoring period, a number of storms have been identified and analysed making use of the Bayesian Fast Fourier Transform Approach (BFFTA) (Yuen and Katafygiotis, 2003 and Au, 2011 & 2012). The probability density function (PDF) of the measured ambient data for a given set of modal parameters can be approximated by an appropriately selected multi-variate Gaussian distribution. Using Bayes Theorem, the PDF of the modal parameters for a given set of actual measurements (usually referred as the likelihood function) can then be calculated based on the PDF of the actual measurements for a given set of modal parameters. By maximising the likelihood function, the most probable modal parameters were obtained.



Figure 1. Instrumentations used during the monitoring campaign.

References

- Cammelli, S., and Li, Y.F. (2016). Experimental and numerical investigation of a large tuned liquid column damper. *Proceedings of the Institution of Civil Engineers - Structures and Buildings*, Vol. 169, Issue SB8, pp 635-642.
- Yuen, K. V., and Katafygiotis, L.S. (2003). Bayesian Fast Fourier Transform Approach for Modal Updating Using Ambient Data. *Advances in Structural Engineering*, Vol. 6, No. 2.
- Au, S. (2011). Fast Bayesian FFT Method for Ambient Modal Identification with Separated Modes. *Journal of Engineering Mechanics*, Vol. 137, No. 3.
- Au, S. (2012). Fast Bayesian Ambient Model Identification in the Frequency Domain, Part I: Posterior Most Probable Values. *Mechanical Systems and Signal Processing*, Vol. 26, pp 60-75.

Design and assessment of real time monitoring systems for structural control of wind turbines

N. Caterino^{1,2}, G. Pugliano¹ and U. Robustelli¹

¹Department of Engineering, University of Naples “Parthenope”, Naples, Italy

²Institute of Technologies for Construction, National Research Council, San G. Milanese, Milan, Italy

Corresponding author: N. Caterino, nicola.caterino@uniparthenope.it

Abstract

The adoption of wind turbines to produce electric energy nowadays represents one of the most promising alternatives to the use of the exhausting fossil fuel stocks. The actual tendency is toward the design of taller towers, that can produce more power because excited by stronger winds. There is the need of designing these structures in a cost effective way, aiming to reduce the wind induced growing structural demand. A semi-active (SA) control technique recently proposed by the authors (Caterino 2015; Caterino et al. 2016) is based on the use of a cylindrical hinge at the base of the wind tower and magnetorheological (MR) dampers installed in parallel with linear springs. The aim is realizing a time-variant base restraint (Figure 1). A purposely written control logic aims at reducing the base bending moment by relaxing - in selected intervals of time - the base restraint. This causes rocking of the base and dissipation of energy due to cyclic demand of deformation to MR devices. Such SA control strategy has been tested at the Structural Dynamics Laboratory of the Denmark Technical University by means of a shaking table facility (Figure 1), leading to really encouraging results in terms of percentage reduction of structural demand in respect to the “fixed base” configuration.

This control strategy requires that the tower is instrumented so as to monitor in real time the state of stress and deformation and to allow the algorithm to make the decision regarding the optimal calibration, moment by moment, of the variable devices. As regards, in particular, the displacement measurements, in the laboratory they can be carried out, on scaled models, easily with normal transducers and fixed external reference structures. However, for real applications, on- or off-shore wind turbines, making reliable high frequency measurements of the horizontal displacement of points placed at a height of tens of meters can be not so trivial.

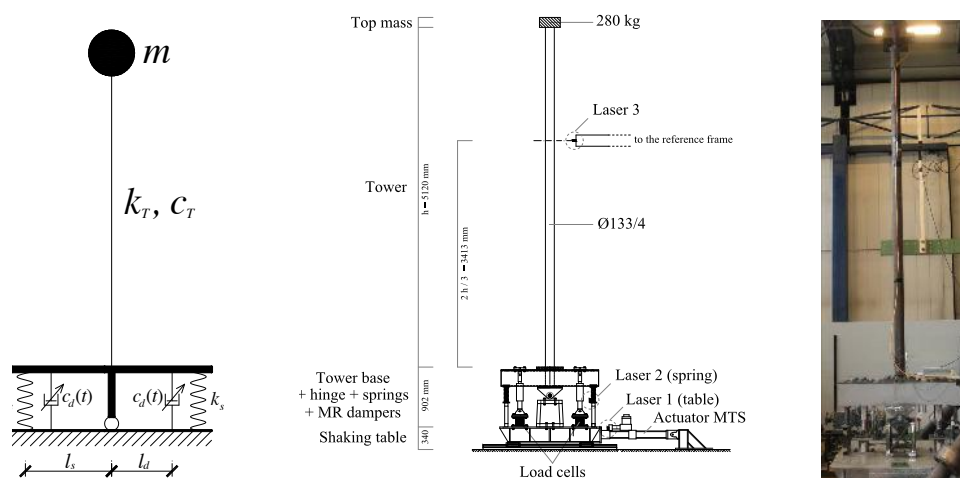


Figure 1. Smart base restraint including semi-active MR dampers: schematic idea, set-up drawing and picture

Among the available geodetic technologies, very few are those can fully satisfy the required monitoring criteria for the above goal. Global Navigation Satellite Systems (GNSS) are among the

most advanced for fully automated and continuous monitoring. Many GNSS-based applications for continuous monitoring of the dynamic behaviour of civil structures were developed in recent years, mainly for long-span bridges and tall buildings (Yu et al. 2014). GNSS actually has the advantage of directly measuring absolute 3-D position coordinates, thereby providing displacement measurements in real-time and full scale.

Usually, GNSS geodetic dual frequency receivers have been used as reliable tool for providing accurate and timely information on the actual status of the structure. The capability of measuring changes in position with high level of accuracy is extensively achieved by adopting the real-time kinematic (RTK) positioning with the need of dedicated base stations in differential GNSS mode. In particular, using the relative GNSS positioning method two GNSS receivers are required, one placed on the deformable object and the other being a nearby reference station. Precise point positioning (PPP) is another efficient method to compute a kinematic position with high accuracy. Compared to precise relative positioning, PPP requires a single GNSS receiver avoiding the use of a reference station (Kaloop et al. 2017). GNSS monitoring receivers are used typically gathering high-rate data at 10-20 Hz. Acquiring data at the maximum sampling rate, up to 50-100 Hz (ultra-high-rate), receivers could identify the high structural vibration frequencies of up to 10 Hz (Psimoulis et al. 2008; Yi et al. 2015).

For achieving the purpose of the article, a properly configured GNSS measurement system can meet most of the possible dynamic measurement needs for relative displacement. In this case, the use of dual frequency GNSS receivers may be expensive and vulnerable to some undesired effects like cycle slips and multipath error, difficult to be removed by current differencing techniques (Wang et al. 2017). More recently, research has also been carried out investigating the use of single frequency receivers (code and phase) to detect dynamic behaviour. Further to this, trials have been carried out investigating the use of low-cost GPS receivers as it is now possible to output the carrier phase from these receivers. In contrast with classical GNSS observables, the use of GNSS intermediate frequency (IF) data is also an interesting topic to investigate for dynamic applications. Intermediate frequency data is the most basic type of GNSS data that can be recorded since it is completely unprocessed and thus allows for many processing options.

With the aim of evaluating the efficiency and feasibility of GNSS-based systems for structural control of wind turbines, this paper try to obtain insight into the characteristics (receiver type, type of observables, sampling data rate) and data processing techniques (differencing method, filtering techniques) that can make the GNSS useful for such application.

References

- Caterino, N. (2015). Semi-active control of a wind turbine via magnetorheological dampers. *Journal of Sound and Vibration* **345**, 1–17, doi:10.1016/j.jsv.2015.01.022
- Caterino, N., Georgakis, C.T., Spizzuoco, M., and Occhiuzzi, A. (2016). Design and calibration of a semi-active control logic to mitigate structural vibrations in wind turbines. *Smart Structures and Systems* **18** (1).
- Kaloop MR, Elbeltagi E, Hu JW, Elrefai A. (2017). Recent Advances of Structures Monitoring and Evaluation Using GPS-Time Series Monitoring Systems: A Review. *ISPRS Int J Geo-Inf.*, **6**, 382.
- Psimoulis P, Pytharouli S, Karambalis D, Stiros S. (2008). Potential of Global Positioning System (GPS) to measure frequencies of oscillations of engineering structures. *J. of Sound and Vibration*, **318**: 606–623.
- Wang D, Meng X, Gao C, Pan S, Chen Q. (2017). Multipath extraction and mitigation for bridge deformation monitoring using a single-difference model. *Adv.s in space research*, **60**: 2882-2895.
- Yi TH, Li HN, Gu M. (2013). Experimental assessment of high-rate GPS receivers for deformation monitoring of bridge. *Measurement*, **46**: 420-432.
- Yu J, Meng X, Shao X, Yan B, Yang L. (2014). Identification of dynamic displacements and modal frequencies of a medium-span suspension bridge using multimode GNSS processing. *Engineering Structures*; **81**:432-443.

Influence of the bridge deck on the flow characteristics monitored by sonic anemometers installed on a long-span bridge

Etienne Cheynet¹, Jasna Bogunović Jakobsen¹ and Jónas Snæbjörnsson^{1,2}

¹Department of Mechanical and Structural Engineering and Materials Science, University of Stavanger, Norway

²School of Science and Engineering, Reykjavík University, Iceland

Corresponding author: Etienne Cheynet, etienne.cheynet@uis.no

Abstract

The present paper discusses the influence of a closed box bridge girder on the flow characteristics recorded by sonic anemometers installed on the bridge hangers. It is found that an anemometer installed on the downwind side of the 12.3 m wide and 2.76 m high bridge girder measures a flow distorted by the girder even when the sensor is located 10 m above the deck. For a sensor located 6 m above the deck, on the windward side of the deck, the flow distortion is, however, much smaller.

1 Introduction

Measurements of wind turbulence acting on the bridge deck girder of long-span cable-suspended bridges are fundamental to assess the wind loads in full-scale. However, the inherent influence of the bridge deck structure on the turbulence monitored by the sonic anemometers has been investigated in only a few studies (Kristensen & Jensen, 1979; Hay, 1981, 1984; Frandsen, 2001), with dissimilarities in the findings. Different shapes and aspect ratios of bridge girders disturb the flow in different ways. This motivates a more thorough analysis of the conditions recorded during a specific measurement campaign, conducted on the Lysefjord suspension bridge in Norway. A set of sonic anemometers are installed above either side of the bridge girder, to study the turbulence on both the upwind and downwind side of the deck. The goal is to investigate the impact of the bridge deck on the turbulence data acquired, to scrutinize the impact of the local terrain, and provide some guidance regarding the installation of sonic anemometers on a cable-suspended bridge with a similar bridge girder shape.

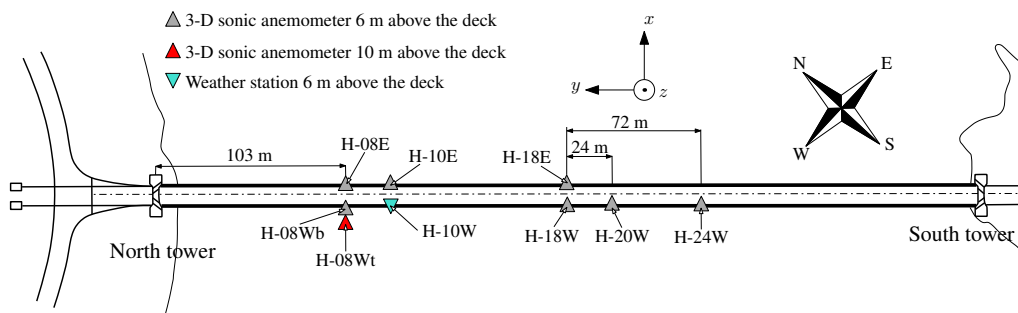


Figure 1. Instrumentation of the Lysefjord Bridge since June 2017. Each anemometer is named with respect to the hanger on which it is installed.

2 Instrumentation and methods

The Lysefjord suspension bridge has a main span of 446 m, oriented from north-west to south-east. The bridge is located at the inlet of a narrow fjord in southwestern Norway and is, therefore, surrounded by mountains and steep hills. The complex topography imposes two main wind directions: north-northeast and south-west. Since June 2017, the bridge instrumentation (fig. 1) allows to simultaneously study the wind turbulence on the upwind side and the downwind side of the deck. Turbulent statistics are studied using an averaging time of 20 min.

3 Results

Figure 2 shows the ensemble averaged one-point power spectral densities (PSD) recorded by the two anemometers located at mid-span. The error bar represents the interquartile range. The samples chosen correspond to stationary wind records from the north-northeast and a mean wind velocity above 6 m s^{-1} . The turbulence intensity recorded is above 20 %, meaning that the turbulence generated by the terrain is likely predominant over the one generated by buoyancy. The solid lines in Figure 2 are the Simiu spectra S_v and S_u (Simiu & Scanlan, 1996), Busch-Panofsky spectrum S_w (Busch & Panofsky, 1968) and Kaimal co-spectrum S_{uw} (Kaimal et al., 1972). The values of $\beta_i = \sigma_i^2 / u_*^2$, where u_* is the friction velocity, are arbitrarily set to $\beta_u = 5.76$, $\beta_v = 3.61$, and $\beta_w = 1.69$, which are commonly found in the literature.

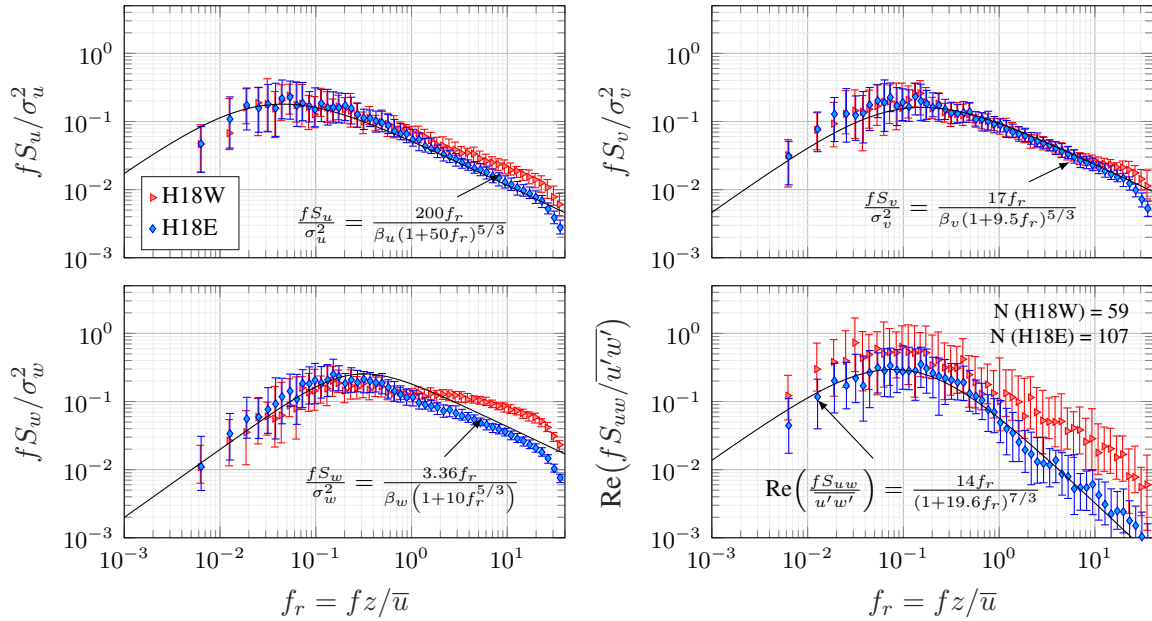


Figure 2. PSD estimates of the turbulent wind velocities on the upwind side (H-18E) and downwind side (H-18W) of the Lysefjord Bridge for a wind from north-northeast recorded between July and December 2017.

In Figure 2, a clear discrepancy between the data recorded on the upwind side and the downwind side of the bridge deck is observed. Whereas the longitudinal turbulence intensity is almost the same on H18E and H18W, the vertical turbulence intensity is lower on H18W than on H18E. It should be noted that for a flow from a north-northeast direction, the anemometer located at H08t, i.e. 10 m above the deck, measures a similar flow distortion as on H08b, located 6 m above the deck.

4 Conclusions

Since June 2017, wind turbulence has been investigated on the Lysefjord Bridge using sonic anemometers mounted on both sides of the girder, at heights of ca. 6 m and 10 m above the deck. It is found that the flow measured on the downwind side of the deck, up to 3.6 bridge deck heights above the deck surface,

is distorted by the presence of the girder. For this reason, a full-scale study of the wind conditions on a bridge deck would benefit from mounting anemometers on both sides of the girder. The full-length paper will address the case of a wind from both south-southwest and north-northeast as well as other aspects of the bridge deck influence on the flow field in terms of one-point turbulent statistics.

References

- Busch, N. E., & Panofsky, H. A. (1968). Recent spectra of atmospheric turbulence. *Quarterly Journal of the Royal Meteorological Society*, **94**, 132–148.
- Frandsen, J. (2001). Simultaneous pressures and accelerations measured full-scale on the Great Belt East suspension bridge. *Journal of Wind Engineering and Industrial Aerodynamics*, **89**, 95 – 129.
- Hay, J. S. (1981). The wind-induced response of the Erskine Bridge. In *Bridge Aerodynamics* (pp. 81–90).
- Hay, J. S. (1984). Analyses of wind and response data from the Wye and Erskine Bridges and comparison with theory. *Journal of wind engineering and industrial aerodynamics*, **17**, 31–49.
- Kaimal, J. C., Wyngaard, J., Izumi, Y., & Coté, O. (1972). Spectral characteristics of surface-layer turbulence. *Quarterly Journal of the Royal Meteorological Society*, **98**, 563–589.
- Kristensen, L., & Jensen, N. O. (1979). Lateral coherence in isotropic turbulence and in the natural wind. *Boundary-Layer Meteorology*, **17**, 353–373.
- Simiu, E., & Scanlan, R. H. (1996). *Wind effects on structures*. Wiley.

Estimation of the vertical wind coherence in an offshore environment

Etienne Cheynet

Department of Mechanical and Structural Engineering and Materials Science, University of Stavanger,
Norway

Corresponding author: Etienne Cheynet, etienne.cheynet@uis.no

Abstract

The vertical wind coherence estimated from full-scale measurements on an offshore platform in the North Sea is compared to the Davenport coherence model, the Mann spectral model and a modified exponential decay function taking explicitly into account the dependency of the coherence with the height. The latter two models are in good agreement with the estimated coherence, but they also show that the coherence models advised in the IEC standard for the design of offshore wind turbines may not be appropriate.

1 Introduction

The coherence, which according to Ropelewski et al. (1973), “can be thought as a correlation in frequency space”, is widely used to describe the spatial structure of wind turbulence. Nowadays, the wind coherence is a key element of the buffeting theory (Davenport, 1964; Scanlan, 1978). The coherence of natural wind has been mostly studied on land and there is, therefore, little knowledge about the wind coherence in an offshore environment. Nevertheless, the ongoing development of large offshore wind turbines justifies the need to investigate more in details the adequacy of the established coherence models, such as the one prescribed in the IEC standard (IEC, 2005, 2009) for the design of wind turbines. Using two years of sonic anemometer records from the offshore platform FINO1 (North Sea), the present study assesses the validity of the Mann spectral model in the offshore environment under neutral conditions as well as the applicability of two empirical coherence models proposed by Davenport (1961) and Bowen et al. (1983).

2 Instrumentation

2.1 selection of the data set

The FINO1 platform is located in the North Sea ca. 45 km north of the German coast. An 81 m high steel lattice tower is mounted on the 20 m high jacket platform. Among the different sensors installed on the mast, three Gill R3-50 sonic anemometers are mounted at 40 m, 60 m and 80 m above the mean sea level. Each sonic anemometer monitors the three wind velocity components and the sonic temperature with a sampling frequency of 10 Hz (Neumann & Nolopp, 2007). The wind coherence is studied using the sonic anemometer data obtained in 2007 and 2008. Only samples characterized by a wind direction from 190° to 359° are considered to avoid flow disturbance by the mast. The data set considered, associated with a neutral atmospheric stratification and stationary fluctuations, corresponds to ca. 1000 hours of records.

2.2 Modelling of the wind coherence

In the present study, three coherence models are examined for vertical separations. The first one is the classical Davenport coherence model (Davenport, 1961). The second one is derived from the one proposed

by Bowen et al. (1983) and is here referred to as the “modified Bowen model”:

$$\gamma_{ii}(z_1, z_2, f) = \exp \left\{ - \left[\frac{d_z}{\bar{U}(z_1, z_2)} \sqrt{(c_1^i f)^2 + (c_3^i)^2} \right] \right\} \exp \left(- \frac{c_2^i f d_z^2}{z \bar{U}(z_1, z_2)} \right) \quad (1)$$

$$\bar{U}(z_1, z_2) = \frac{1}{2} [\bar{u}(z_1) + \bar{u}(z_2)] \quad (2)$$

where $d_z = |z_1 - z_2|$ and the coefficient c_1^i, c_2^i, c_3^i ($i = \{u, v, w\}$) are empirical constants to be determined. The third coherence model is based on the uniform-shear model (Mann, 1994), sometimes denoted as the “Mann spectral model” in the literature. Whereas the first two coherence models are directly fitted to the estimated co-coherence, the third model is computed using the information provided by the one-point auto- and cross-spectra of the three wind turbulent components.

3 Results

In Figure 1, the root-coherence estimates for the u and w components are compared to the three models investigated. A remarkable agreement is obtained with Equation (1). The uniform-shear model, associated with the fitted parameters $L = 21$, $\alpha \epsilon^{3/2} = 0.047$ and $\Gamma = 3.6$ at $z = 60$ m, agrees fairly well with the estimated coherence, especially for $k_1 d_z < 0.1$, where $k_1 = 2\pi f / \bar{u}$. The Davenport model shows a good agreement with $\gamma_{uu}(f, z_1, z_2)$ but fails to represent accurately $\gamma_{ww}(f, z_1, z_2)$.

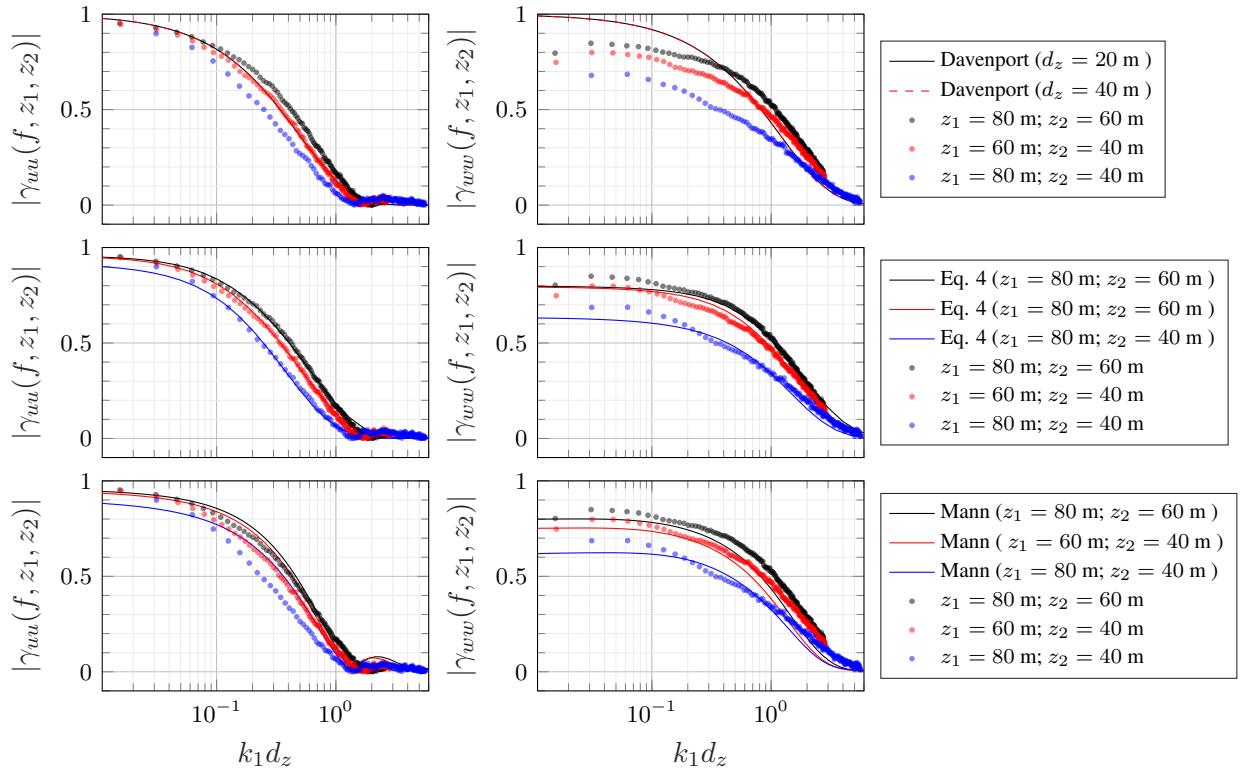


Figure 1. Estimated and fitted root-coherence for neutral conditions with the Davenport model (top panels), the modified Bowen model (middle panels) and the uniform-shear model (bottom panels).

4 Conclusions

The vertical coherence of the wind fluctuations has been investigated in full-scale in an offshore environment. The coherence computed after fitting the Mann spectral model to the estimated one-point spectra

showed a fairly good agreement with the estimated coherence. It also indicates that the parameters prescribed in the IEC standard (IEC, 2005) may not be appropriate. An empirical coherence model inspired from Bowen et al. (1983) provides an excellent fit with the coherence of the along-wind component obtained from the full-scale data.

Acknowledgments

The author would like to acknowledge the Federal Ministry for Economic Affairs and Industry and the Projektträger Jülich for funding the FINO project, and UL DEWI for providing the sonic data.

References

- Bowen, A. J., Flay, R. G. J., & Panofsky, H. A. (1983). Vertical coherence and phase delay between wind components in strong winds below 20 m. *Boundary-Layer Meteorology*, **26**, 313–324.
- Davenport, A. (1964). The buffeting of large superficial structures by atmospheric turbulence. *Annals of the New York Academy of Sciences*, **116**, 135–160.
- Davenport, A. G. (1961). The spectrum of horizontal gustiness near the ground in high winds. *Quarterly Journal of the Royal Meteorological Society*, **87**, 194–211.
- IEC (2005). *IEC 61400-1 Wind turbine—Part 1: Design requirements*.
- IEC (2009). *IEC 61400-3 Wind Turbines—Part 3: Design Requirements for Offshore Wind Turbines*.
- Mann, J. (1994). The spatial structure of neutral atmospheric surface-layer turbulence. *Journal of Fluid Mechanics*, **273**.
- Neumann, T., & Nollop, K. (2007). Three years operation of far offshore measurements at FINO1. *DEWI Mag*, **30**, 42–46.
- Ropelewski, C. F., Tennekes, H., & Panofsky, H. (1973). Horizontal coherence of wind fluctuations. *Boundary-Layer Meteorology*, **5**, 353–363.
- Scanlan, R. (1978). The action of flexible bridges under wind, ii: Buffeting theory. *Journal of Sound and vibration*, **60**, 201–211.

DESIGN AND EXPERIMENTAL STUDIES OF WIND IMPACT TO UNIQUE BUILDINGS

P. Churin¹, O. Egorychev¹, O. Poddaeva¹ and J. Gribach¹

¹ NRU MGSU, 129337, 26, Yaroslavskoe sh., Moscow, Russia

Corresponding author: J. Gribach¹, js-995@mail.ru

Abstract

In this paper, we present a methodology for performing a computational and experimental study of the wind impact on unique buildings and structures. The publication contains a detailed numerical simulation main stages description of wind loads on the objects under investigation in specialized software complexes. A diagram of all stages of conducting experimental studies of the air flows effects on unique objects in a specialized architectural and construction type wind tunnel with subsequent results verification obtained with the data of the analytical study also presented in this article. On the algorithm basis presented, the described methodology was implemented using the Sberbank technopark unique building under construction in Moscow at the Skolkovo Innovation Center as an example. Also obtained results, which include total forces and aerodynamic drag coefficients are given. Based on the work results, conclusions are presented.

1 Introduction

Nowadays, the unique buildings and structures design is one of the most difficult areas of the construction industry. The main problem at each working stage from the object concept creation to its introduction into operation is the analogues constructive and (or) planning solutions lack.

2 Methods

This paper presents a methodology for performing computational and experimental wind impacts studies on unique buildings and structures, developed and tested in the Educational, scientific and industrial laboratory of aerodynamic tests of buildings structures at the Moscow State University of Civil Engineering.

3 The investigated object

The investigated object is the Technopark Sberbank building in the Innovation Center "Skolkovo", authored by the Zahi Hadid Agency. The structure is a 7-storeyed array, divided into two parts. Communication between them occurs at the expense of 5 bridges overhanging the pedestrian boulevard and the roadway, located from the 3rd to the 7th level of the building (fig.1).



Figure 1. The investigated object

4 Approbation

4.1 Numerical simulation

The nonstationary flow pattern and the corresponding distribution of the dimensionless pressure coefficient C_p on facades along the horizontal section building perimeter and along the building height are calculated, as well as the integral aerodynamic forces and moments coefficients acting on the building.

Also, computational studies of the entrance groups bioclimatic comfort and through passage were carried out.

4.2 Experimental study

Using the strain gauges, the pressure on object under study model surface in the drainage points allows us to judge the aerodynamic pressure distribution along the facades of the object at the angles of attack of the air flow from 0° to 360° .

4.3 Verification

The obtained experimental data on the mean pressure distribution in drainage points were used to validate the applied numerical simulation technology in a package of hydro-gas dynamic analysis.

5 Results and conclusions

In the course of the study were obtained:

- average distribution, maximum and minimum aerodynamic coefficients C_p , $C_p +$ and $C_p -$ values over the object under study facade surface;
- maxima and minima estimated wind loads distribution;
- maxima and minima peak wind load distribution;
- velocity fields distribution picture.

Based on the work results, conclusions are presented.

Modeling and simulation of non-stationary thunderstorm outflows

M. Ciano¹, M. Gioffrè¹ and M. Grigoriu²

¹Department of Civil & Environmental Engineering, University of Perugia, Italy

²Department of Civil & Environmental Engineering, University of Cornell, Ithaca, USA

Corresponding author: Matteo Ciano, matteo.ciano@unipg.it

Abstract

Methods currently applied to evaluate wind actions on structures are still mostly based on models related to the stationary phenomena at the synoptic scale that occur in neutral atmospheric conditions with velocity profiles in equilibrium with the atmospheric boundary layer. Nevertheless when thunderstorm outflows are concerned the wind induced load description should take into account its inherent non-stationary features. In this paper a non-stationary model is proposed to describe wind velocity fluctuations of a typical thunderstorm in the northern Italian coast. This model can be obtained by modulating both amplitude and frequency of a stationary process. The responses of tall slender structures to stationary and non-stationary wind loads are finally compared.

1 Introduction

Thunderstorms are non-stationary phenomena at the mesoscale that occur in convective conditions with totally different velocity profiles with respect to synoptic winds. The wind non-stationary problem was faced by several authors in the literature, but the topic is still fragmented and not completely assessed (e.g. Letchford et al., 2002; Chen, 2008, Kwon and Kareem, 2009). Recently this topic has been addressed in (Solari et al., 2017) where the maximum response of vertical slender structures affected by thunderstorm outflows is estimated based on wind velocity data coming from a significant experimental work in northern Italian coast (Solari et al., 2015).

Some of this data are used in this work to model a non-stationary process to be used to generate virtual samples of wind velocity thunderstorm time histories. The top panel of Figure 1a shows the typical wind velocity fluctuations that clearly indicates non-stationary features in the mean (middle panel in Figure 1a) and standard deviation components. The lower panel of Figure 1a is the process

$$u(t) = U(t) - U_m(t) \quad (1)$$

where $U(t)$ is the original time series and $U_m(t)$ is its average component. The non-stationarity of the process $U(t)$ is also evident in the spectrogram of the $u(t)$ component (Figure 1b).

In this paper the non-stationary process $X(t)=u(t)$ is first modeled using the approach presented in (Grigoriu et al., 1988) for seismic loads, where the time-varying spectral density function is described by modeling amplitudes and frequencies with suitable time varying functions. This non-stationary process is defined by

$$X(t) = c(t)Y(\phi(t)) \quad (2)$$

where $Y(t)$ is a real-valued zero-mean wide sense stationary process with variance σ_y^2 and one sided spectral density $G_y(\omega)$, $c(t)$ and $\phi(t)$ are the amplitude and frequency modulating functions, respectively. The function $G_y(\omega)$ is calibrated on the experimental data. Second, virtual time histories of the process (2) are generated using

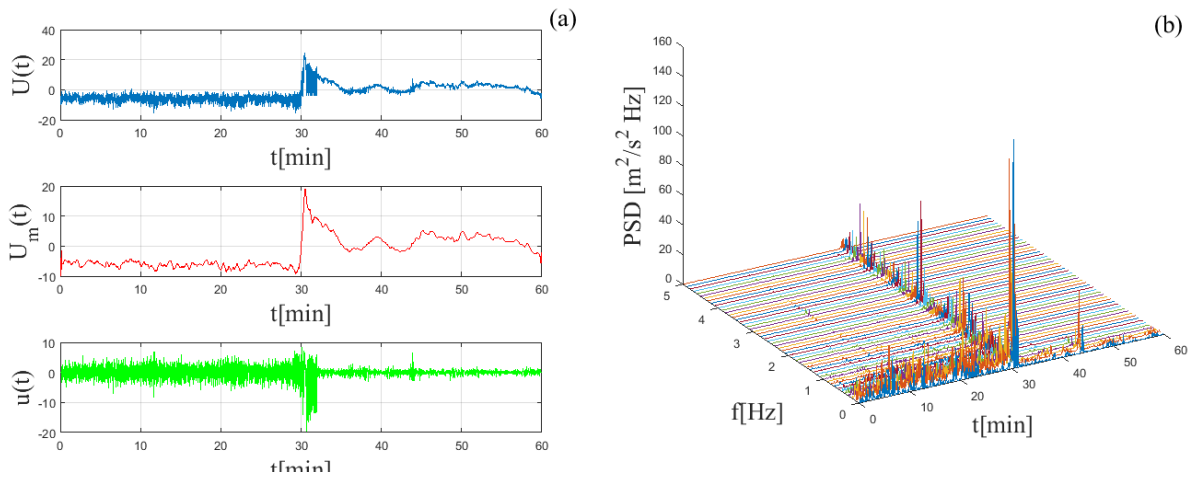


Figure 1. Thunderstorm outflow: a) wind velocity time series (top), mean component (middle), meanless component (bottom); b) spectrogram of $u(t)$.

$$X(t) = c(t) \sum_{q=1}^Q \sigma_q (V_q \cos \omega_q(t)t + W_q \sin \omega_q(t)t) \quad (3)$$

with the time dependent frequencies $\omega_q(t)$, $q = 1, \dots, Q$, where $\omega_q(t) = \omega_q \phi(t) / t$ and V_q and W_q are uncorrelated random variables with zero mean and unit variance. Finally, these wind velocity samples are used to estimate structural response time histories using Monte Carlo simulation. The effect of this kind of non-stationarity is evaluated through a parametric study on a cantilever beam with varying natural frequencies.

2 Acknowledgments

These Authors are indebted to Prof. Giovanni Solari for providing the wind velocity time series used in this work. The support of Ing. Stefano Fioravanti is also gratefully acknowledged.

References

- Chen X. (2008). Analysis of alongwind tall building response to transient non-stationary winds. *Journal of Structural Engineering ASCE*, 134(5), 782-791.
- Grigoriu M., Ruiz S.E., Rosenbueh E., EERI M. (1988). The Mexico earthquake of September 19, 1985 – Nonstationary models of seismic ground acceleration. *Earthquake Spectra*, Vol. 4, No. 3.
- Kwon D.K., Kareem A. (2009). Gust-front factor: new framework for wind load effects on structures. *Journal of Structural Engineering ASCE*, 135(6), 717-732.
- Letchford CW, Mans C, Chay MT (2002). Thunderstorms—their importance in wind engineering (a case for the next generation wind tunnel). *J Wind Eng Ind Aerodyn*, 90:1415–1433.
- Solari G., Burlando M., De Gaetano P., Repetto M.P. (2015). Characteristics of thunderstorms relevant to the wind loading of structures. *Wind and Structures*, Vol. 20, No. 6 763-791.
- Solari G., Rainisio D., De Gaetano P. (2017). Hybrid simulation of thunderstorm outflows and wind excited response of structures. *Meccanica*, 1–24.

On the aerostructural design of long-span cable-stayed bridges: The contribution of parameter variation studies with focus on the deck design

M. Cid Montoya¹, F. Nieto¹ and S. Hernández¹

¹Structural Mechanics Group, School of Civil Engineering, University of La Coruña, La Coruña, Spain

Corresponding author: M. Cid Montoya, miguel.cid.montoya@udc.es

Abstract

The design of long-span bridges consists of dealing with a large number of design variables and it is conditioned by responses of structural and aeroelastic nature. A deep knowledge about the influence of these variables governing the bridge responses is crucial to achieve efficient and safe designs. Apart from heuristic rules, numerical approaches, such as parameter variations studies, sensitivity analysis and optimization algorithms, can provide reliable information to improve designs. This work studies the effects on the flutter and structural responses of a cable-stayed bridge when the mechanical, mass, aerodynamic and aeroelastic properties of a streamlined mono-box deck are modified. These results are used to understand qualitatively and quantitatively the effects caused by the variation of the deck plate thickness and cross-section shape on the bridge responses.

1 Introduction

The aerostructural design of long-span bridges deals with a large number of design variables and design constraints. Among the different constraints, some of them can be recognized to be the most influential on the bridge design. In the case of cable-stayed bridges, these could be the axial load acting on the deck, the deflection of the deck at the centre of the main span, the maximum stress in the deck, or the aeroelastic response, among others. In the same manner, some design variables can be identified to be the most adequate to be modified in order to change certain responses aiming to obtain safer and more feasible designs. Particularly, in the case of the deck, the shape of the cross-section seems to be the most adequate to improve the mechanical properties and/or the deck aerodynamics to deal with structural and aeroelastic constraints. However, every modification on the deck design has consequences in the full set of structural and aeroelastic responses and can also affect to the cost of the structure. The criteria usually used for these modifications have been based on heuristic rules or experience-based approaches. Alternatively, the use of numerical techniques, such as parameter variation studies, sensibility analysis and optimization algorithms, can provide useful information to the designer beyond his previous knowledge. This work analyses the relationships between deck properties and bridge structural and aeroelastic responses of a super-long-span cable-stayed bridge. The main span is 1316 m, and the layout is shown in Figure 1. The deck cross-section geometry considered is the well-known Scanlan's G1 section. The shape variations considered are the width and the depth, as well as the thickness of the steel plates.

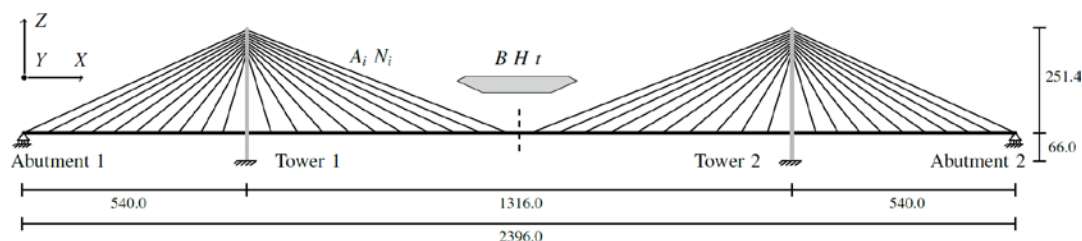


Figure 1. Layout of the bridge model.

2 Parameter variation studies and sensitivity analyses: Results and discussion

Parameter variation studies consist of computing the responses of a model for a set of values of the parameters or design variables under study in order to explore the relationship between the design variables and the responses analysed in the design domain. This allows the designer to have qualitative and quantitative information to take adequate decisions to improve designs. Application examples in the wind engineering field can be found in Wang et al. (2014), or in the authors' previous work Cid Montoya et al. (2018). Some results of the last reference can be found in Figure 2, where a parameter variation study of the flutter response with regards to deck properties is shown.

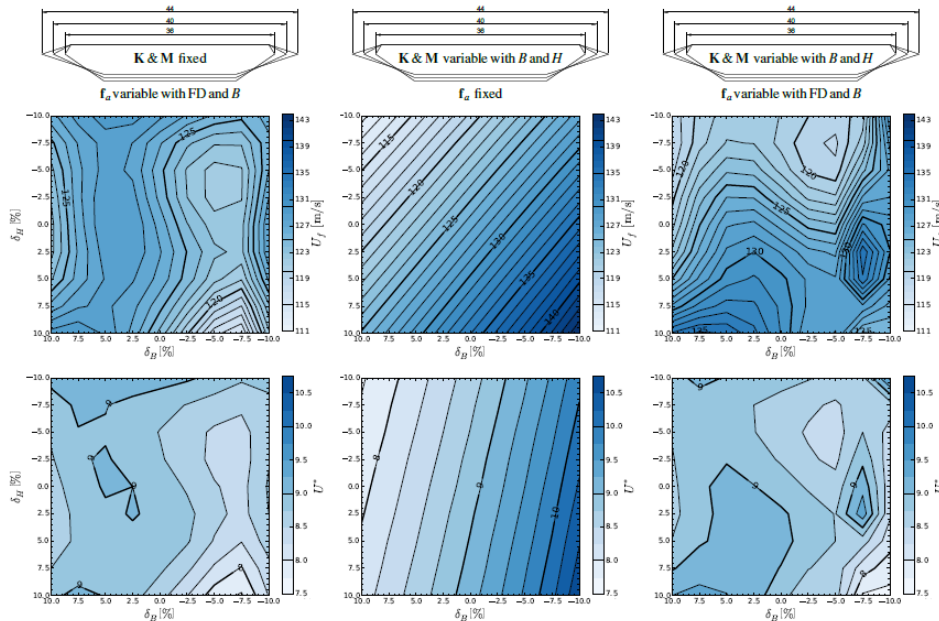


Figure 2. Parameter variation study of the flutter response with regards to deck shape variations.

Sensitivity analyses study the way a response is affected by the variation of a design variable. These studies provide quantitative information of the relationship of a response with a design variable in the neighbourhood of the current value of the design variable in the design domain. This can be carried out analytically or by means of the finite difference method (Jurado et al. (2008), Nieto et al. (2011)).

This work will provide the results of parameter variation studies and sensitivity analyses of some relevant bridge responses, including bridge flutter velocity, deck axial load, deck deflection and deck volume, among others, with regards to mechanical (A_x , I_y , I_z & J_x), mass (M & I_M), aerodynamic (C_L , C_M , C_D , C'_L , C'_M & C'_D) and aeroelastic (H^*_1 , H^*_2 , H^*_3 , A^*_1 , A^*_2 , A^*_3 ...) deck properties and deck design variables including shape and plate thickness.

References

- Wang, H., Tao, T., Zhou, R., Hua, X., and Kareem, A. (2014). Parameter sensitivity study on flutter stability of a long-span triple-tower suspension bridge. *J Wind Eng Ind Aer.* **128**, 12-21.
- Cid Montoya, M., Hernández, S., and Nieto, F. (2018). Shape optimization of streamlined decks of cable-stayed bridges considering aeroelastic and structural constraints. *J Wind Eng Ind Aer* IN PRESS.
- Jurado, J. Á., Nieto, F., Hernández, S., and Mosquera, A. (2008). Efficient cable arrangement in cable stayed bridges based on sensitivity analysis of aeroelastic behaviour. *Advan. Eng. Soft.* **39**, 757-763.
- Nieto, F., Hernández, S., Jurado, J. Á., and Mosquera, A. (2011). Analytical approach to sensitivity analysis of flutter speed in bridges considering variable deck mass. *Advan. Eng. Soft.* **42(4)**, 117-129.

A novel steady RANS model for the computational modeling of the homogeneous atmospheric boundary layer flow over hilly terrain

M. Cindori, I. Džijan, F. Juretić and H. Kozmar

Faculty of Mechanical Engineering and Naval Architecture, University of Zagreb,
Ivana Lučića 5, 10000 Zagreb, Croatia

Corresponding author: M. Cindori, mihael.cindori@fsb.hr

Abstract

A new computational model for the simulation of the neutrally-stratified atmospheric boundary layer (ABL) is developed. It is based on the implementation of the wind-source term in the momentum equation of the steady Reynolds-averaged Navier-Stokes (RANS) model. The wind-source term allows for establishing the profiles of the mean velocity, Reynolds shear stress and turbulent kinetic energy for various terrain exposures. The obtained computational results are in good agreement with the available wind-tunnel measurements.

1 Introduction

Previous methodologies for the computational modeling of the neutrally-stratified atmospheric boundary layer (ABL) were, in part, dealing with the issues of inhomogeneity in the computational domain, together with the establishing of the flow properties that are in agreement with the experimental measurements. The methodology reported in the present work deals with the source-term modeling to overcome some of the noted issues, as originally proposed by Juretić and Kozmar (2013). They concluded that the flow subjected to the appropriate loading can reproduce the decay of the turbulent kinetic energy and the Reynolds shear stress along the height, when the standard $k-\varepsilon$ turbulence model is used. Accordingly, they proposed implementation of the set of source terms in the momentum equation to produce appropriate loading. Cai et al. (2014) briefly analyzed physical significance of an additional force term in the momentum equation and confirmed that such a constant source term can reproduce decay of the turbulent kinetic energy with the negligible pressure gradient along the computational domain. Cindori et al. (2018) performed additional corrections of the source term to achieve the proper Reynolds shear stress distribution. This approach proved its suitability in computations of the pressure distribution at the cubic building model subjected to the suburban ABL flow.

2 Computational model

The model equations were developed using the incompressible steady-state RANS equations for the homogeneous flow and the $k-\varepsilon$ turbulence model. The wind-source was derived under presumption of the zero-pressure gradient in the computational domain, and it was implemented in the momentum equation. The initial value for the wind-source term was calculated from the wind-tunnel Reynolds shear stress measurements,

$$WS_x^{\text{init}}(z) = \frac{1}{\rho} \frac{d\tau_{zx}^{\text{exp}}(z)}{dz}. \quad (1)$$

The precursor domain technique was used, together with the periodic boundary conditions applied at the inlet and the outlet boundary of the domain to obtain the homogeneous profiles of the mean velocity, turbulent kinetic energy and Reynolds shear stress.

3 Results and discussion

The wind-source term was calibrated during the periodic computations to achieve a good match between the experimental and computational Reynolds shear stress. The calculated mean velocity, Reynolds shear stress and turbulent kinetic energy profiles for rural, suburban and urban ABL flow are in good agreement with the available wind-tunnel measurements, as the mean relative error is not larger than 4.1% for mean velocity, 5.6% for turbulent kinetic energy and 2.2% for Reynolds shear stress. The mean velocity profiles agree well with the respective power-law profiles, Figure 1.

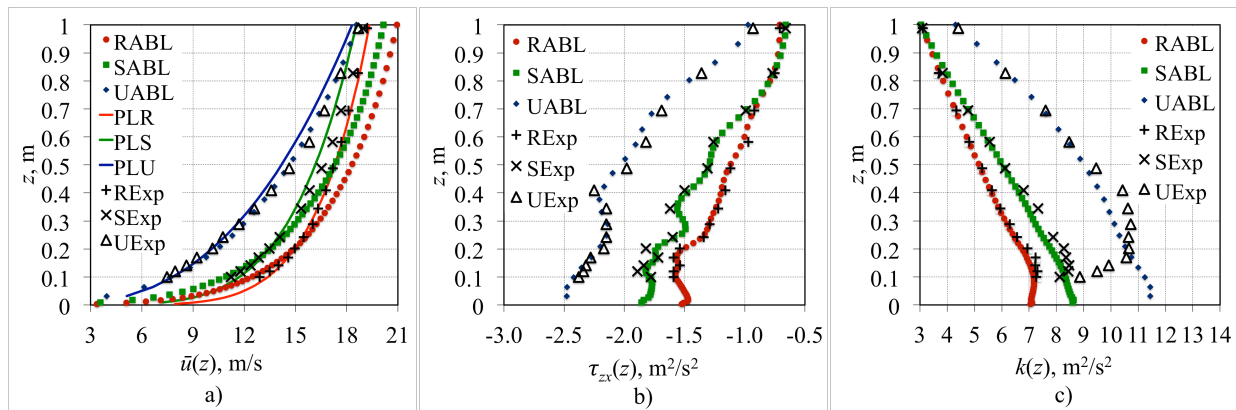


Figure 1. Mean velocity $\bar{u}(z)$ (a), Reynolds shear stress $\tau_{zx}(z)$ (b) and turbulent kinetic energy $k(z)$ (c) profiles obtained in 2D computations for the rural (RABL), suburban (SABL) and urban (UABL) terrain type; wind-tunnel results for the rural (+), suburban (\times) and urban ABL flow (Δ); power-law profiles for mean velocity (PLR – rural ABL, PLS – suburban ABL and PLU – urban ABL).

The calculated profiles of the mean velocity, turbulent kinetic energy, and dissipation rate are set at the inlet boundary of the computational domain and a hilly object is subjected to the rural, suburban and urban ABL flow. These computations are currently underway and the results will be presented at the conference.

4 Acknowledgements

The authors acknowledge the Croatian Science Foundation IP-2016-06-2017 (WESLO) support.

References

- Cai, X., Huo, Q., Kang, L. and Song, Y. (2014). Equilibrium Atmospheric Boundary-Layer Flow: Computational Fluid Dynamics Simulation with Balanced Forces. *Boundary-Layer Meteorology* **152**(3), 349-366.
- Cindori, M., Juretić, F., Kozmar, H., Džijan, I. (2018). Steady RANS model of the homogeneous atmospheric boundary layer. *Journal of Wind Engineering and Industrial Aerodynamics* **173**, 289-301.
- Juretić, F. and Kozmar, H. (2013). Computational modeling of the neutrally stratified atmospheric boundary layer flow using the standard k - ϵ turbulence model. *Journal of Wind Engineering and Industrial Aerodynamics* **115**, 112-120.

Experiences in designing, manufacturing, installation and testing of wind turbines

D.P. Coiro¹, F. Scherillo², G. Troise², N. Bizzarrini² and G. Calise¹

¹Department of Industrial Engineering, Aerospace Division, University of Naples Federico II, Italy

²Seapower scarl, no-profit research consortium with the University of Naples Federico II, Italy

Corresponding author: *Ferdinando Scherillo*, f.scherillo@seapowerscarl.com

Abstract

Small to medium wind turbine market is relatively new for Italy and a number of incidents has occurred during these last years following the deployment of a brand new designed wind turbines. During the past 25 years, the research group at the University of Naples Federico II has gained large experience on such renewable energy devices, being involved during the whole development process, starting from conceptual design, manufacturing, installation and, finally testing of the device in real environment. During the design of small wind turbines, the temptation of using some simplified assumptions on the device operating conditions (e.g. steady wind flow, stream tube flow, rigid blades and tower) is high due to the small size of the turbine whereas, in real situations, both the flow conditions and the structure don't match those hypotheses: the instantaneous wind field is very far from being uniform and steady, as well as the tower and the blades are not rigid at all.

Moreover, second order effects, like gravity forces and gyroscopic loads, need to be considered and make the design of small/medium wind turbines particularly challenging. Finally, wind turbines represent highly complex systems and the interaction of each part with the others in a highly turbulent flow should be considered.

In terms of turbine power performance, all these phenomena can produce a real power vs. wind speed curve with large spread range and very different from that evaluated using the ideal assumptions (see Figure 1).

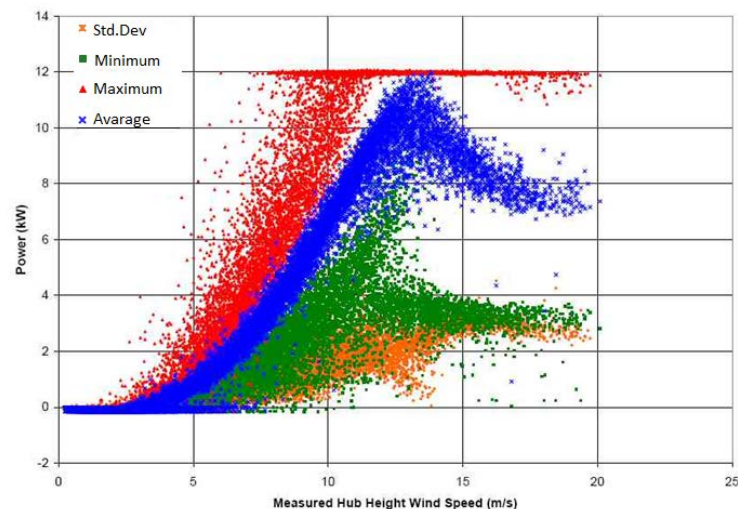


Figure 1 - A measured power vs. wind speed curve

In term of loads acting on the turbine, these simplified assumptions lead to use considerable high safety factors during the design phase, which imply over-dimensioned structures with related excessive manufacturing costs.

In light of this, an accurate aeroelastic analysis of the complete device operating in turbulent flow is necessary, in order to consider the dynamic behavior of the wind turbine and to accurately predict performance, extreme and fatigue loads.

All the issues previously illustrated are even more problematical in the case of small wind turbines. These are installed at lower heights and rotate at considerably higher rotational speeds compared to large wind turbines; therefore, they operate in a higher turbulent flow and are affected by stronger centrifugal and gyroscopic forces.

From aerodynamics point of view, the design of small wind turbine is complex due to the low local Reynolds number along the blade, causing a lower airfoil aerodynamic efficiency and the overall aerodynamic behavior more complicated and uncertain (e.g., laminar separation bubbles at the blade leading edge). Furthermore, the fatigue lifetime of such device is lower than a large wind turbine, being the number of fatigue cycle very high.

Finally, an appropriate control system is needed to prevent power output peaks and this is not an easy task due to the fast dynamics normally involved in this type of turbines

The aerodynamic and structural design of small wind turbines has been carried out by Seapower srl, a research consortium born from University researchers, combining well-assessed techniques for designing turbine blades (e.g. BEM method, potential flow analysis, FEM analyses) with new design trends based on Computational Fluid Dynamics (CFD) to improve both the performance predictions and blade structural strength. (see Figure 2). The structural design involves also the design of the composite material (lamination layup) with which the blade is made up, along with load estimations on the tower and the wind turbine foundation.

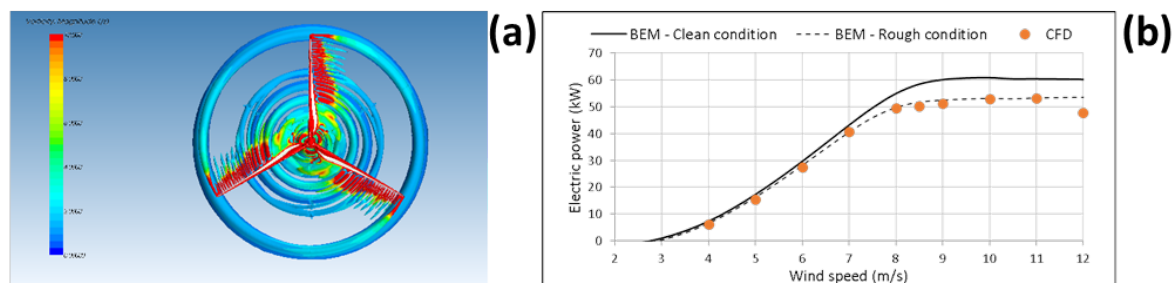


Figure 2 – An example of CFD analysis (a) and simulation outputs (b)

Blade aerodynamic measurements and bench tests are carried at the University of Naples Federico II, using the low speed wind tunnel test facility. The wind tunnel test section allows to test both two-dimensional models up to 1.4m with suction system at wall intersection and, also, three-dimensional scaled blade models, using also measurement techniques based on PIV. To reduce wind tunnel blockage effects, some of the prototypes have been tested in “free air” conditions, as well: the comparison between measured data and numerical data has shown a highly good agreement. Bench tests on the generator allow to test several control strategies to improve wind turbine power production and protection in off-design conditions. The experience gained on a 60kW variable pitch turbine shows that control system improvements can drastically reduce the fatigue and extreme loads. Regarding the blade, Seapower is able to perform structural static, dynamic and fatigue tests, using direct and indirect measurements (e.g. modal analysis): such results are of matter of importance for a correct tuning between blade induced loads and tower modal response. Using strain gauges on both the tower and the wind turbine blade, a set of load measurements are acquired during operation of the wind turbine into a real environment following the IEC 61400-13 (*Measurement of Mechanical Loads*) guidelines. These measurements are used to validate the aeroelastic model and the load estimation and, if necessary, to perform appropriate design fixes.

In the light of this, a low wind speed 60kW wind turbine, named SIMPLY 60 has been recently designed, manufactured and successfully installed in a test area in the south of Italy. The SIMPLY 60 device is a downwind passive stall regulated wind turbine with high performance blades, whose aerodynamic and aeroelastic behavior has been deeply investigated. The SIMPLY 60 operative range is from 4.5 m/s up to 15 m/s, and the rated power of 60 kW is reached at 8.5 m/s. Due to an innovative blade design, the blade cost is similar to a shorter blade and this has allowed to use a larger rotor than similar rated power turbines. The reduced costs of both blades and the nacelle, along with the reduced time required for assembling the parts, make the SIMPLY 60 a low-cost wind turbine, with high reliability and low maintenance effort.

On the Flutter Wind Speed of Long Span Suspension Bridges

Mario Como¹

¹ Department of Civil Engineering and
Computer Science Engineering, University of Rome Tor Vergata, Italy
como@ing.uniroma2.it

Abstract

This paper aims to evaluate the flutter wind speed of very long span suspension bridges. Two relevant aspects of the problem are investigated:

- the dynamical response of the bridge by means of a suitable continuous model, able to express with a simple formula one of the more relevant factor that conditions the flutter response of the bridge: the ratio between its fundamental periods of the vertical and torsional oscillations of the bridge in still air.
- the formulation of the aerodynamic forces acting on the girder section oscillating in the wind under large values of the reduced velocity U_R . This formulation, already proposed by Como et al. (2005), permits suitable asymptotic expansions of the Scanlan (1971) flutter derivatives.

Connected to both the above aspects of the problem, the corresponding flutter velocity is then given in a simple form. Comparisons among the flutter velocities of some modern suspension bridges, particularly the Akashi bridge, with those obtained with the proposed approach, are then given. Finally, a discussion on the main structural and aerodynamic problems, crucial to the design project of very long span suspension bridges, ends the paper.

References

- Como, M., Del Ferraro S., Grimaldi A. (1995). A parametric analysis of the flutter velocity for long span suspension bridges. *Wind and Structures*, Vol. 8, **1**, 1–12.
- Scanlan, R.H. (1971). Airfoil and bridge deck flutter derivatives. *J.Eng. Mech. Div.: Proc. of the American Society of Civil Engineers*, 1717–1737.

Probabilistic assessment of the galloping stability of ice-accrete bridge hangers

Cristoforo Demartino¹, and Francesco Ricciardelli²

¹College of Civil Engineering, Nanjing Tech University, Nanjing 211816, P.R. China

²Department of Civil Engineering, Design Building and Environment, University of Campania, Italy

Corresponding author: Cristoforo Demartino, cristoforo.demartino@me.com

Abstract

Galloping vibrations have recently been identified as a potential problem for ice-accreted bridge hangers. The analysis of the forces causing them is usually made using the quasi-steady theory. Several deterministic models have been developed with the aim of predicting cable aerodynamic instabilities, each of which consider different aspects of the dynamic and aerodynamic behaviour. Starting from wind tunnel measurements of the aerodynamic coefficients of an ice accreted HDPE cable hanger, the random nature of the aerodynamics is shown. Then, a framework based on Monte Carlo simulations is applied for probabilistic assessment of the minimum structural damping required to prevent galloping of bridge hangers based on the output of a 2-DoFs sectional quasi-steady aeroelastic model. All the variables required to define the hanger dynamics, the sheath aerodynamics and the local wind climate are considered. Because of the large uncertainties and of the non-linear nature of the problem, the distribution of the minimum structural damping required to prevent galloping is obtained. The results highlight the advantages of the probabilistic procedure in terms of reliability quantification, compared to the deterministic approach.

1 Introduction

Wind-induced cable vibrations have been the topic of many studies carried out in the last decades. These mainly focus on the unstable behaviour deriving from a variety of causes, e.g. vortex shedding, galloping (in its many forms), shape modifications due to rain and ice. In particular, undesirable wind-induced vibrations of bridge cables can occur when atmospheric conditions are such to generate ice accretion. These vibrations are generated by the complex aerodynamics of circular cylinders that is particularly sensitive to small variations of the superficial characteristics (Demartino and Ricciardelli, 2017).

Galloping-induced instabilities are often modelled using the Quasi-Steady (QS) theory (Blevins, 1977). A pioneering approach was derived by Den Hartog (1932), that presented a first mathematical description of the Single Degree of Freedom (SDoF) acrosswind galloping mechanism, together with a criterion for the assessment of its possible occurrence, i.e.:

$$C_D(\alpha) - \frac{\partial C_L(\alpha)}{\partial \alpha} < 0 \quad (1)$$

where C_D and C_L are the mean drag and lift coefficients, function of the angle of attack, α .

Following this approach, EN1991 Part 1-4 (CEN, 2005) defined the onset wind velocity, U_{CG} , is expressed as a function of the acrosswind dimension of the structure (D), of the Scruton number (Sc), of the acrosswind fundamental frequency of the structure ($f_{1,y}$), and of the factor of galloping instability (a_G), which depends on cross section geometry:

$$U_{CG} = \frac{2Sc}{a_G} f_{1,y} D \quad \text{with } a_G = - \left(C_D(\alpha) - \frac{\partial C_L(\alpha)}{\partial \alpha} \right) \quad (2)$$

EN1991 Part 1-4 (CEN, 2005) defines that a structure is considered stable against galloping, if U_{CG} is at least 25% larger than the mean wind velocity evaluated at the height where galloping excitation is expected to occur, likely to coincide to the point of maximum amplitude of oscillation.

In some circumstances, code approaches are not sufficiently accurate and more sophisticated analyses must be undertaken. In this context, a number of models have been derived for the prediction of galloping instability of bridge cables based on the QS theory; these were reviewed and compared in Demartino and Ricciardelli (2015) and in Piccardo et al. (2015).

However, although many authors demonstrated the role of uncertainties in the evaluation of the minimum damping required to prevent galloping instability of ice accreted bridge cables, the development of a probabilistic framework has never been explored.

In this paper, a procedure for the probabilistic assessment of the minimum structural damping required to prevent galloping of dry bridge hangers is presented. The procedure is based on the calculation of the minimum structural damping required to prevent galloping of bridge hangers using a 2-DoFs sectional QS aeroelastic model. The aerodynamic data of ice accreted stay cable used in the calculations derived from wind tunnel tests performed at the DTU/Force Technology collaborative Climatic Wind Tunnel (CWT) in Lyngby, Denmark (Demartino 2015a,b). The experimental procedure and results are fully described in Demartino (2014).

The probability distribution of the minimum required structural damping is evaluated through Monte Carlo simulations; this allows for realistic worst case conditions among different scenarios, and their probabilistic definition. The calculation will be carried out according to a prototype suspended bridge located in Copenhagen, where the climatic conditions are characterized by large probability of ice formation on the cables.

Using a normal and log-normal model of capacity, the probability of failure is calculated. In the definition of the framework, all the variables required to define (i) the hanger dynamics, (ii) the ice accreted sheath aerodynamics and (iii) the local wind climate are considered. Finally, a simplified closed form equation for the evaluation of the minimum structural damping required to prevent galloping in a probability-based performance approach is proposed.

The results highlight the advantages of the probabilistic procedure in terms of reliability quantification, compared to the deterministic approach. Moreover, the proposed procedure allows for a probabilistic safety check, based on reliability requirements given by International Standards, and it can be incorporated into performance-based design frameworks. Full results will be shown in the full paper.

References

- Blevins, R., 1977. Flow-induced vibration. New York, Van Nostrand Reinhold Co., 1977. 377.
- CEN, 2005. Eurocode 1: Actions on structures. Comité Européen de Normalisation.
- Demartino, C., 2014. Aerodynamics and aeroelastic behaviour of ice-accreted bridge cables. Ph.D. thesis. University of Naples Federico II University of Naples Federico II - Department of Structures for Engineering and Architecture.
- Demartino, C., Koss, H., Georgakis, C., Ricciardelli, F., 2015a. Effects of ice accretion on the aerodynamics of bridge cable. *Journal of Wind Engineering and Industrial Aerodynamics*.
- Demartino, C., Ricciardelli, F., 2015b. Aerodynamic stability of ice-accreted bridge cables. *Journal of Fluids and Structures* 52, 81–100.
- Demartino, C., Ricciardelli, F., 2017. Aerodynamics of nominally circular cylinders: A review of experimental results for civil engineering applications. *Engineering Structures* 137, 76–114.
- Den Hartog, J., 1932. Transmission line vibration due to sleet. *Electrical Engineering* 51, 413–413.

Numerical simulation of cable dynamics induced by synoptic and thunderstorm events

Andrés Denis¹, Giuseppe Piccardo² and Giovanni Solari²

¹IET, Universidad de la República, Montevideo, Uruguay

²DICCA, University of Genoa, Italy

Corresponding author: Giuseppe Piccardo, giuseppe.piccardo@unige.it

Abstract

The dynamic response of suspended cables has received a great attention in the last decades leading to the formulation of sophisticated mechanical models. Concerning the actions, many studies are dedicated to analyse the effects of deterministic loading, even in the wind field (e.g., self-excited oscillations and galloping phenomena). Nevertheless, suspended cables are often particularly vulnerable to random loading such as turbulent winds and thunderstorms. This paper intends to deal with the response of a shallow cable subject to simulated synoptic and thunderstorms events. Particular attention is paid to the analysis of the dynamic component of the response.

1 Introduction

Cables are convenient structural solutions used in many applications, where the wind is the main design load. The scientific literature is rich in contributions to aeroelastic phenomena, such as galloping and vortex-induced vibrations. Nevertheless, cables are extremely vulnerable even to high winds, as in the case of transmission lines. These events can be divided in extratropical depressions (ED) and thunderstorms (TH). In the TH field above all, several efforts to include this action into structural design are still to be done.

On the other hand, it is well known that the governing equations for dynamic motions of a cable have important nonlinearities (e.g., Luongo and Zulli, 2013) that make their application complex for design purposes. Concerning ED and TH events, the dynamic response is obtained by finite-element numerical analyses (e.g., Aboshosha and El Damatty, 2015) and quasi-static techniques (e.g., Wang et al. 2017).

Using a modal approach, this paper analyses the nonlinear dynamical behaviour of aluminium horizontal cable conductors excited by random forces representative of ED and TH measured events. Results from different type of simulations are critically compared, pointing out the role of nonlinearities and of the dynamic component of the response.

2 Mechanical model

An approximate nonlinear model of shallow cable can be deduced introducing classic hypotheses (e.g., Luongo and Zulli, 2013), among which the static condensation of the cable tangential displacement; in the intrinsic basis it reads:

$$(\bar{T} + EAe_0)v'' + EAe_0\bar{k} + \bar{p}_v = m\ddot{v} \quad (1)$$

$$(\bar{T} + EAe_0)w'' + \bar{p}_w = m\ddot{w} \quad (2)$$

where E , A and m are the modulus of elasticity, the cross-sectional area and the mass per-unit-length of the cable, respectively; e_0 is the strain which, as a result of the assumptions, is expressed by integrals over the curvilinear abscissa s (then, it is a function of time only); \bar{k} is the Frenet curvature assumed constant (and small) along the cable; \bar{T} is the static prestress; $v(s, t)$ and $w(s, t)$ are the in-

plane and out-of-plane cable displacements, respectively; \bar{p} are the corresponding external forces. The prime symbol expresses derivatives with respect to the abscissa s , whereas the dot symbol indicates time-derivative. The integro-differential equations (1)-(2) can be numerically solved by a standard Galerkin procedure using the linear eigenfunctions of the cable.

3 Wind velocity model

Using the classic decomposition rule, a real record of wind velocity is expressed as the sum of the slowly-varying mean component $\bar{v}(t)$, considered as deterministic, and the residual fluctuation related to the high-frequency harmonic content. In its turn, the residual fluctuation can be expressed as the product between the slowly-varying standard deviation and the reduced turbulent fluctuation $\tilde{v}'(t)$ which is a standard Gaussian random field. Then the wind velocity is given by:

$$v(y, t) = \bar{v}(t)[1 + I_v(t)\tilde{v}'(y, t)] \quad (3)$$

where I_v is referred to as the slowly-varying turbulence intensity. Assuming that \bar{v} and I_v do not vary along the cable and extending the method proposed by Solari (2016) from a vertical beam to a horizontal cable, the generalised equivalent spectrum technique (GEST; Piccardo and Solari, 1998) allows us to define an equivalent mono-dimensional field:

$$v(y, t) = \bar{v}(t)[1 + I_v(t)\tilde{v}'_{eq}(t, \delta)] \quad (4)$$

where $y \in [0, L]$ is the external space coordinate along the cable length L ; \tilde{v}'_{eq} is the equivalent reduced turbulent field, written as an explicit function of the size factor δ , which depends on the longitudinal exponential decay coefficient, on the cable length, on the maximum value of \bar{v} and on a non-dimensional modal shape factor. Passing from Eq. (3) to Eq. (4) is a formidable simplification whose correctness was proved by Solari (2016) for vertical beams. If used in a non-stationary field, the GEST approximation allows to apply the sole stationary part of the turbulent fluctuation.

4 Work in progress

The work in progress concerns comparisons among different kind of wind field simulations starting from real measurements of both synoptic events and thunderstorm outflows (e.g., hybrid simulations mixing measured values with Monte Carlo simulations of the reduced turbulent fluctuation or of the equivalent one). The response of some selected cable conductors is under investigation by analysing the probability distributions of cable displacements and tension and verifying the effective contribution of the dynamic component of the response.

References

- Aboshosha, H. and El Damatty, A (2015). Dynamic response of transmission line conductors under downburst and synoptic winds. *Wind and Structures* **21**: 241-272.
- Luongo, A., and Zulli, D. (2013). *Mathematical Models of Beams and Cables*. First ed. ISTE & Wiley.
- Piccardo, G. and Solari, G. (1998). Generalized equivalent spectrum technique. *Wind and Structures* **1**: 161-174.
- Solari, G. (2016). Thunderstorm response spectrum technique: theory and applications. *Engineering Structures* **108**: 28-46.
- Wang, D., Chen, X. and Xu, K. (2017). Analysis of buffeting response of hinged overhead transmission conductor to nonstationary winds. *Engineering Structures* **147**: 567-582.

Experimental and numerical study of the wind tunnel blockage effects on the behaviour of a horizontal axis wind turbine

Abdelgalil Eltayesh¹, Massimiliano Burlando², Francesco Castellani³, Matteo Becchetti³ and Hesham M. El-Batsh¹

¹Mechanical Engineering Department, Benha University, Egypt

²Department of Civil, Chemical, and Environmental Engineering, University of Genoa, Italy

³Department of Engineering, University of Perugia, Italy

Corresponding author: Abdelgalil Eltayesh, abdelgalil.youssef@bhit.bu.edu.eg

Abstract

This study presents an experimental and numerical investigation of the effects of tunnel blockage, defined as the ratio of the free portion of a wind tunnel cross-section with and without the rotor of a small-size (diameter 2 m, nominal power 2 kW) horizontal-axis turbine (HAWT). Experimental measurements were performed on three rotors with different number of blades, namely three, five and six, and different tip speed ratios, in the closed-loop open-test section wind tunnel of the University of Perugia. Numerical wind tunnel simulations were performed at the University of Genoa through a steady-RANS method with SST k- ω turbulence model by means of the CFD solver OpenFOAM. The wind turbine was represented numerically by the actuator disc method. Simulations have been compared to experimental results for validation.

1 Introduction

In wind tunnel experiments of wind turbine behaviour, the most important factor affecting measurements is the blockage effect. The flow field in a wind tunnel differs from the one that would occur in unbounded free air under the same operating conditions due to the presence of wind tunnel walls (Glauret 1935). Therefore, it is usually required to correct measurements for blockage (Chen and Liou 2011, Zaghi et al. 2016).

In the following, a brief description of experimental and numerical setup used for study the tunnel blockage are presented in Section 2, and some preliminary results are reported in Section 4.

2 Experimental and numerical setup

The experiments were carried out in the wind tunnel “R. Balli” of the University of Perugia. This is a closed-loop configuration, driven by a 375 kW electric motor so that the wind can be adjusted up to a maximum speed of 47 m/s. The inlet section of the open test chamber has an area of 5 m² while the recovery section is 7 m². The inflow conditions are measured through two pitot tubes and a cup anemometer in the inlet section while all the atmospheric parameters (static air pressure, temperature and relative humidity) are collected on a station point in the testing room. An honeycomb upstream the test section is able to keep turbulence level below 0.4%.

Numerical studies were carried out using the CFD solver OpenFOAM. The three-dimensional structured grid was generated using the preprocessor software ICEM 14. Figure 1 illustrates the 3D computational domain and the corresponding boundary conditions. The computational domains were designed to match the exact shape of the wind tunnel in order to represent properly the experimental setup and to account for blockage effects. The mesh was generated in a multi-block topology. The

domain was divided into fifty-one blocks and the grid was generated in each block individually. At each side of the domain a boundary layer region were employed. The size of the first layer near wall was chosen in order to obtain dimensionless wall distance y^+ in the logarithmic layer region (30 – 300). The first cell centre was around 0.0003 m from the wall and the growth factor of the grid was kept below 1.2 everywhere. The actuator disk region is modelled as a very thin disk and the properties of the wind turbine were defined in terms of power and thrust coefficients according to the experimental measures.

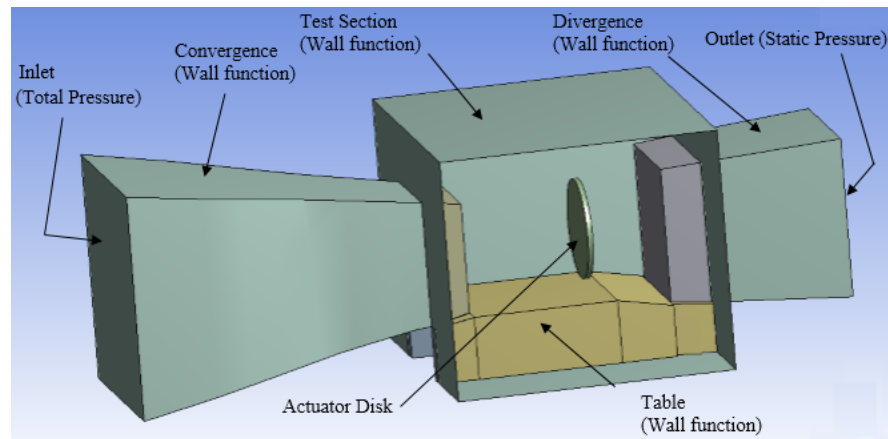


Figure 1. Three-dimensional computational domain and boundary conditions used for the numerical simulations.

3 Results

At present some preliminary experimental and numerical results of the wind tunnel blockage effect have been analysed. In particular, in the wind tunnel the incoming flow velocity at the convergence exit, i.e. at the entrance of the test chamber, has been measured for the case of flow free from obstacles (no wind turbine in the chamber) and when the wind turbine operates with a three blade rotor. The measurements show that there is a difference of wind speed with and without wind turbine of about 0.38 m/s. The numerical simulations, carried out with and without actuator disk, presents a difference at the same position of about 0.41 m/s.

4 Conclusions and perspectives

The preliminary results obtained so far seem to confirm that the numerical wind tunnel simulation of the facility in Perugia can be considered suitable for evaluating the blockage effects numerically. The model, however, has to be validated more extensively and further measurements and simulations are ongoing considering different kind of wind turbines, using three, five and six rotor blades. The complete validation of the model will be presented in the final paper as well as a qualitative and quantitative analysis of the flow affected by blockage around the wind turbine.

References

- Chen, T., and Liou, L. (2011). Blockage corrections in wind tunnel tests of small horizontal axis wind turbines, *Exp. Therm. Fluid Sci.* **35**, 565-569.
- Glauert, H. (1935). *Airplane propellers*. Aerodynamic Theory, vol 4, Division L, Julius Springer, Berlin.
- Zaghi, S., Muscari, R., and Di Mascio, A. (2016). Assessment of blockage effects in wind tunnel testing of wind turbines, *Journal of Wind Engineering and Industrial Aerodynamics* **154**, 1-9.

Wind field variability in complex terrain: Lessons from the Hardanger Bridge

Aksel Fenerci¹ and Ole Øiseth¹

¹Department of Structural Engineering, Norwegian University of Science and Technology, Norway

Corresponding author: Aksel Fenerci, aksel.fenerci@ntnu.no

Abstract

Along the Coastal Highway E39 in the western coast of Norway, Norwegian Government is planning to build several extreme bridges spanning from 1.5 to 5 km. The region is typically mountainous with deep fjords seeping inland. Here, experienced gained from a 5-year monitoring campaign on the Hardanger Bridge in Norway is summarized in this context. The analysis of data provided valuable knowledge on the wind characteristics, which can be generalized for the whole region. Insight has also been gained on the dynamic behaviour of the bridge and how it is influenced by the wind conditions. The results are presented and discussed here with the future bridges in mind.

1 Introduction

Structural health monitoring of large or lifeline structures has been extensively carried out in the last two decades. Long-span cable-supported bridges in particular received considerable attention such that almost every major bridge in the world has a monitoring system installed in it. Although the main purpose of such systems are to monitor the structural health and identify any damage or unexpected phenomena, valuable data on environmental conditions and bridge behaviour is collected as a by-product. Such data are commonly used by researchers to improve the state-of-the-art techniques for structural design and assessment such as the wind-resistant design of long-span cable supported bridges.

In 2013, one such project was initiated on the Hardanger Bridge (HB), the longest suspension bridge in Norway, for the sole purpose of research. The data acquired during the monitoring campaign is used to study the wind characteristics and the terrain effects, validity of common assumptions in wind engineering of such structures, performance of buffeting response predictions and also the design methodology. In this paper, conclusions drawn from the monitoring campaign and their implications on future bridge designs in Norwegian fjords are discussed.

2 Hardanger Bridge Monitoring Project

The Hardanger Bridge is a 1308 meter long-span suspension bridge located in the western coast of Norway. The bridge is crossing the Hardangerfjord and surrounded by a mountainous terrain, which resembles that of the planned E39 bridge locations. The bridge is equipped with a monitoring system composed of 20 accelerometers and 9 anemometers installed on different locations along the bridge deck and the towers.

Wind and acceleration data have been collected from the bridge for a period of 5 years as of today and the data were presented in several papers (Fenerci et al. 2017; Fenerci and Øiseth 2017). More detailed information on the bridge and the monitoring project can be found elsewhere (Fenerci and Øiseth 2017).

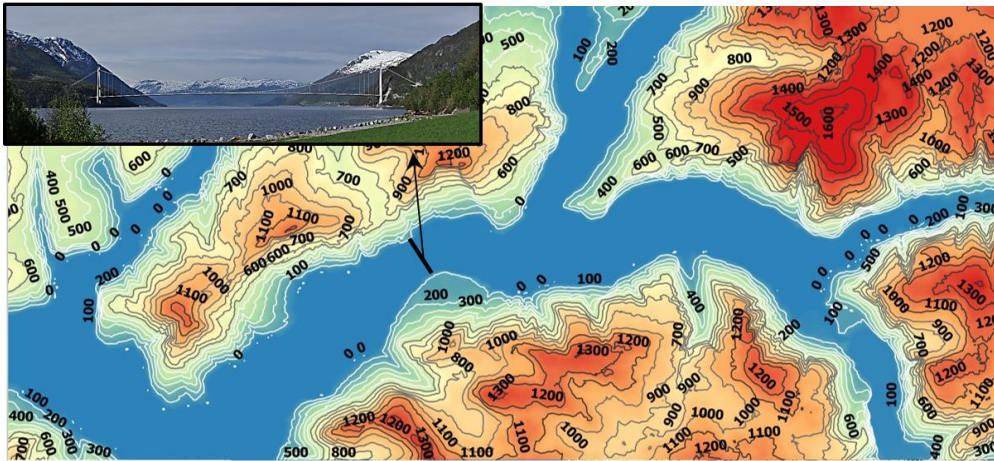


Figure 1. The Hardanger Bridge and its surroundings

3 Insights, challenges and prospects

Traditional structural design against buffeting actions requires prediction of the buffeting response for the design wind speed, where other turbulence parameters such as the turbulence intensity, length scale and coherence of turbulence are modelled deterministically. On the contrary, a look of the data from the HB showed significant variability of the turbulence parameters, which was also reflected into the dynamic response of the bridge (Fenerci and Øiseth 2017). Therefore, it is suggested that the turbulence field along the bridge is modelled probabilistically, taking into account the variations in turbulence parameters.

The data from the HB were also used to evaluate the analytical predictions using state-of-the-art methods. For such applications, the wind field was modelled with maximum possible accuracy using the on-bridge measurements. Despite this, significant discrepancy was found between measured and predicted responses. Identifying the sources of such discrepancies and improving the predictions poses a great challenge and more research is needed on this topic, exploiting the vast amount of data available.

The wind measurements also showed nonstationary and span-wise non-uniform features (Fenerci and Øiseth 2018). Although they seem to be of secondary importance, possibility of inclusion of such effects into the design should be investigated. Moreover, when the bridge is not in place such as in the design process, the transfer of full probability distributions of turbulence characteristics from measurement locations to the bridge location should be handled with care (Lystad et al. 2017).

4 References

- Fenerci, A., and Øiseth, O. (2017). "Measured Buffeting Response of a Long-Span Suspension Bridge Compared with Numerical Predictions Based on Design Wind Spectra." *Journal of Structural Engineering (United States)*, 143(9).
- Fenerci, A., and Øiseth, O. (2018). "Strong wind characteristics and dynamic response of a long-span suspension bridge during a storm." *Journal of Wind Engineering and Industrial Aerodynamics*, 172.
- Fenerci, A., Øiseth, O., and Rønnquist, A. (2017). "Long-term monitoring of wind field characteristics and dynamic response of a long-span suspension bridge in complex terrain." *Engineering Structures*, 147, 269–284.
- Lystad, T. M., Fenerci, A., Saetran, L., and Øiseth, O. (2017). "Wind field characteristics at the Hardanger Bridge site: Comparison of wind tunnel terrain mode tests with full-scale measurements." *7th European and African Conference on Wind Engineering (EACWE 2017)*

Validated numerical simulation of aerodynamic and aeroelastic characteristics of Rhein-crossing bridge in Leverkusen

G. Ferri¹ & A. Chiaracane¹, F. Lupi² & U. Winkelmann², C. Borri¹ & R. Hoeffler²

¹Department of Civil and Environmental Engineering, University of Florence, Italy

²Faculty of Civil and Environmental Engineering, Ruhr-Universität Bochum, Germany

Corresponding author: First Author, giulio.ferri@stud.unifi.it

Abstract

This paper presents the results of numerical investigation of the aeroelastic characteristics of an aged bridge deck: the study is developed on the hand of the Rhein-crossing bridge in Leverkusen (Germany), which is undergoing major investigations and will be likely demolished after 53 years of service. Static coefficients and instationary flutter derivatives are determined by means of both forced vibration tests at WIST wind tunnel (Ruhr-Universität Bochum, Germany) and CFD analysis (Unsteady-Reynolds-Averaged-Navier-Stokes, URANS), by performing this last as two-dimensional simulations. Pressure measurements in a cross-section in the middle of the bridge model are performed in the wind tunnel experiments, in order to analyse the wind flow pattern. Results are compared with literature. The numerical model uses the Finite Volume discretization and the turbulence is simulated by the $k-\omega$ -SST model. Force and pressure measurements from wind tunnel tests are used for validating the numerical model. The main and original contribution of the study consists in assessing the aerodynamic, as well as aeroelastic, behaviour of an aged bridge deck (with rather unusual “old-fashion” profile) and to verify the performance of CFD-URANS method to determine the bridge flutter derivatives.

1 Introduction

With the increasing of slenderness of modern structures, such as bridges, fluid structure interaction becomes more and more important. In addition, the need : i) of checking the diminished performances of aged structures, ii) to detect their deterioration level, or iii) even to reinforce, renew and/or entirely substitute them, makes unavoidable to carry out aerodynamic/aeroelastic tests in wind tunnel. In this work, the attention is focused on the aeroelastic characteristics of Rhein-crossing bridge in Leverkusen, Germany. Results in terms of flutter derivatives are presented, a comparison between numerical simulations and wind tunnel tests is provided.

2 Experimental setup for wind tunnel experiments

The experimental campaign is conducted at the WIST Boundary Layer Wind Tunnel at Ruhr-Universität Bochum. It is an open circuit wind tunnel with a total length of 9.4 m, 1.8 m width and 1.6 m height. All the tests are performed with a turbulence intensity of about 3.5%. High speed additional tests in wind tunnel will likely be performed in order to reach a higher quality/evidence of the dynamic features of the developed separated flow.

The bridge model (in scale 1:150) has a total width B of 0.251 m, a height of 0.033 m and a length L of 1.8 m. Inclined struts are placed at a regular interval of 0.04 m. The total mass of the model is around 2.0 kg. The model is instrumented with 26 pressure taps, two force balances and two laser sensors at its ends. By pressures integration wind induced forces and flutter derivatives are evaluated as well as by force measurements. A comparison between the two methods is provided. Differences between the results are presented and explained. Furthermore, flutter derivatives obtained with pressure integration are deeply analysed for evaluating the effective contribute of each pressure tap to the derivatives.

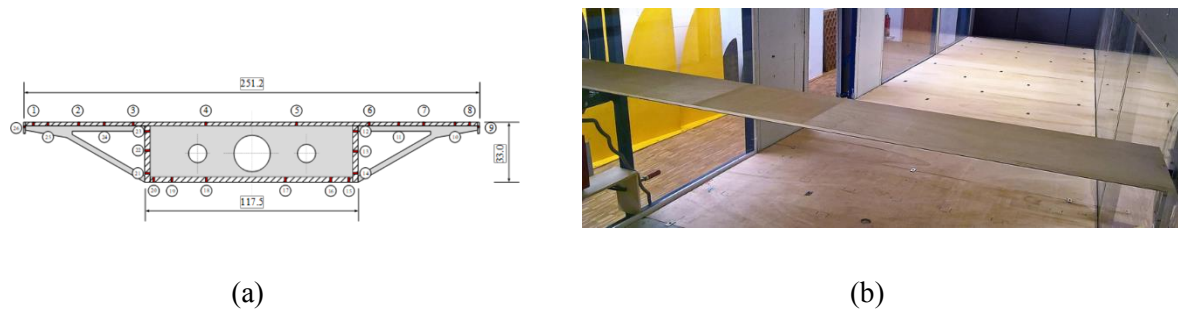


Figure 1. Rhein-crossing bridge wind tunnel model and pressure taps position (a); bridge model placed in the wind tunnel (b).

3 Identification of flutter derivatives from forced-vibration wind tunnel tests

Flutter derivatives are determined experimentally through forced vibration wind tunnel tests in heave and pitch. Forces, pressures and displacements are simultaneously measured during the experiments. Two sets of measurements are conducted to separate the aeroelastic force signals from the larger inertial force signals. First, reference measurements with forced vibration in still air allow to identify inertial forces, then measurements are repeated under the wind flow, measuring inertial and aeroelastic forces together. The aeroelastic forces are obtained by calculating the vectorial difference between the two sets of measurements (Šarkić et al, 2017 and Lupi et al, 2018). Aeroelastic forces time histories are used to validate the numerical simulations.

4 CFD simulations and validation

CFD simulations (2D-URANS with $k-\omega$ -SST turbulence model) are performed on the fixed bridge deck section and on the bridge deck in motion (Šarkić et al, 2012 and Winkelmann et al, 2017).

Both numerical simulations and wind tunnel tests at the fixed bridge deck are performed under different angle of attack, from -10° to $+10^\circ$. Stationary coefficients c_D , c_L and c_M are compared.

In forced vibration CFD simulations a harmonic motion is imposed to the numerical model at 0° angle of attack. All the simulations have the same configuration as in the wind tunnel tests, in terms of flow velocities, oscillation amplitude and motion frequency. Time histories of the force coefficients c_D , c_L and c_M , are compared with the fitted sinusoidal time history calculated from forced vibration wind tunnel tests. Furthermore, flutter derivatives calculated from CFD simulations are compared forced vibration experiment.

References

- Šarkić A., Fisch R., Höffer R., Bletzinger K-U. (2012). Bridge flutter derivatives based on computed, validated pressure fields. *Journal of Wind Engineering and Industrial Aerodynamics* vol. 104-106, pag. 141-151.
- Šarkić A., Höffer R., Brčić S. (2017). Identification of flutter derivatives by forced vibration tests. *Gradevinar* vol.69, pag. 267-280.
- Lupi F., Niemann H.-J., Höffer R. (2018). Aerodynamic Damping Model in Vortex-Induced Vibrations for Wind Engineering Applications. *Journal of Wind Engineering and Industrial Aerodynamics*, (accepted for publication).
- Winkelmann U., Glumac A., Lupi F., Höffer R. (2017). Vortex induced vibrations on circular structures: Numerical modeling of aerodynamic loads. *Proceedings of the European African Conference for Wind Engineering, Liege*.

Aerodynamic and aeroelastic response of CAARC building – Comparison between numerical simulation and wind tunnel measurements

Giovanni Frison¹, Antonino Maria Marra², Gianni Bartoli², Roberto Scotta¹

¹Department of Civil and Environmental Engineering, University of Padova, Italy

²CRIACIV - Department of Civil and Environmental Engineering, University of Florence, Italy

Corresponding author: Giovanni Frison, giovanni.frison@dicea.unipd.it

Abstract

The present work exhibits the comparison between numerical and experimental simulations of the aerodynamic and aeroelastic response of CAARC (Commonwealth Advisory Aeronautic Council) building, a standard in the research of wind effects over tall buildings. At the 12th International Conference on Wind Engineering (Cairns, Australia, July 2007), J.D. Holmes proposed a blind test to 7 wind tunnel facilities around the globe with the purpose of comparing wind action data over the CAARC standard tall building, through the HFBB technique [1]. The outcome of the project highlight a good agreement over the measurement of base moments. However, the measurements of accelerations at the top of the buildings, a key element in the design of high-rise structures in regards of occupant discomfort, shown a significant deviation [2]. Starting from these data, the author intent is to contribute to the study of wind effects on tall buildings through the comparison of wind tunnel experiments and the validation of computational methods. Numerical results obtained with FEM Software Kratos Multiphysics [3] are compared with wind tunnel measurements conducted in the open-circuit boundary layer wind tunnel of CRIACIV located in Prato, Italy.

1 Introduction

Since the early fifties, wind engineering has seen an exponential growth in civil engineering applications. On the one hand, new technologies and the awareness in reliable and refined structural solutions, together with architectural evolution, have brought to an escalation of challenging in the construction industry. On the other, the development of cutting edge experimental techniques, acquisitions devices and the advancement in computational resources, have introduced new tools suited for the study of wind effects on structures. Starting from a pure analytical approach, the field moved gradually to wind tunnel experimentation. The latter, after decades of scientific research, has consolidate its efficiency in a reasonable number of civil application. However, inherent errors of approximation, mainly due to a scaling factors, are most probably the main weak spot for experimentalist, when it comes to the study of flexible structures, where aeroelastic effects tend to dominate the solution. Room of improvement is certainly left, as a matter of fact, few outstanding examples of full aeroelastic models of tall building are part of literature [5]. In the last years, the availability of computational resources has grown beyond any expectation. This has inevitably driven a considerably share of the scientific community to the development of outstanding numerical solutions in many fields. In fluid-dynamic the solution of the Navier-Stokes equation has been tackled from several research groups all over the world. However, while in many industrial applications Computational Fluid-Dynamic (CFD) is nowadays an accepted design tool, in civil engineering a shade of skepticism persists. It is therefore essential to establish an extended and systematic validation process in order to ease the application of Computational Wind Engineering (CWE) in the structural and architectural design practice. The CAARC standard tall building represents a consolidate benchmark for the calibration of several wind tunnel experimental technique. Since the work presented

by Wardlaw and Moss [6] in the seventies, an extensive period of experimentation has followed. Several authors explored every angle of the aerodynamic features of the CAARC building, starting from pressure measurements [7], base forces and moments on rigid models [8], to the study of the dynamic response on aeroelastic model [9]. As a proof of the up-to-date interest in the topic, in 2007 J.D. Holmes proposed a challenge: compare the predicted wind action over two types of tall building, of increasing complexity. The results, presented in 2011, show a good agreement in the prediction of base moments. However, a significant deviation in the measurement of acceleration at the top corner of the model is found, thus highlighting the major issue in the downscaling of dynamic property in experimental aeroelastic models. Therefore, given the vastity and the variety of literature data on the subject, the CAARC building is the perfect candidate for a cross-comparison that could add a piece of wind tunnel literature with the development of a full aeroelastic model and show the potential of computational methods. As a matter of fact, many research have been published recently on the topic. Among the others, Braun in 2009 [10] shows one of the first attempt of fluid-structure interaction, coming to the more recent works of Dagnew et al. [11] and Zang et al. [12]. The present work wants to be a contribution to decades of researches on the CAARC building. This include the design of a novel experimental setup and the validation of computational methods, engineered together in order to provide new insight in practical applications to civil engineering, with a focus on tall buildings and the identification of design challenges related to wind-structure interaction.

References

- [1] Benchmark Buildings for an International HFBB Comparison (2007) - *12th International Conference on Wind Engineering, Cairns, Australia*
- [2] Holmes, J.D., Tse, Tim K.T. (2012). International high-frequency base balance benchmark study. *The 2012 World Congress on Advances in Civil, Environmental, and Materials Research, Aug. 26-30, Seoul, Korea.*
- [3] Dadvand, P., Rossi, R. and Oñate, E. (2010). An object-oriented environment for developing finite element codes for multi-disciplinary applications. *Archives of Computational Methods in Engineering*, **17**:253–297.
- [5] Wardlaw, R.L, Moss, G.F. (1970). A standard tall building model for the comparison of simulated natural winds in wind tunnels. CAARC, C.C.662m Tech, 25.
- [6] Templin, J.T., Cooper, K.R., (1981). Design and performance of a Multi-Degree-of-freedom aeroelastic building model. *J. Wind Eng. Ind. Aerod.* **8**:157-175.
- [7] Melbourne, W.H. (1980). Comparison of measurements on the CAARC standard tall building model in simulated model wind flows. *J. Wind Eng. Ind. Aerod.* **6**(1-2):73-88.
- [8] Whitbread, R.E. (1975). The measurement of non-steady wind forces on small-scale building models. In: *Proceedings of fourth IAWC conference. Heathrow: Cambridge University Press, Cambridge.* P.567-74
- [9] Blackmore, P.A. (1985). A comparison of experimental methods for estimating dynamic response of buildings. *J. Wind Eng. Ind. Aerod.* **18**(2):197–212.
- [10] Braun, A.L., Awruch, A.M. (2009). Aerodynamic and aeroelastic analyses on the CAARC standard tall building model using numerical simulation. *Computer & Structures.* **87**:564-581.
- [11] Dagnew, L., Bitsualmalk, G., Merrick, R. (2009). Computational evaluation of wind pressure on tall buildings. *11th Americas Conference in Wind Engineering. San Juan, Porto Rico.*
- [12] Zang, Y., Habashi, W., Khurram, R. (2015). Predicting wind-induced vibrations of high-rise buildings using unsteady CFD and modal analysis. *J. Wind Eng. Ind. Aerod.* **136**:165–179

Mitigation of structural demand to wind turbines: experimental investigation of three control strategies

C.T. Georgakis¹, J. Chen², N. Caterino³ and M. Spizzuoco⁴

¹Department of Engineering, Aarhus University, Aarhus, Denmark

²Department of Structural Engineering, Tongji University, Shanghai, China

³Department of Engineering, University of Naples "Parthenope", Naples, Italy

⁴Department of Structures for Architecture and Engineering, Univ. of Naples Federico II, Naples, Italy

Corresponding author: N. Caterino, nicola.caterino@uniparthenope.it

Abstract

The adoption of wind turbines to produce electric energy nowadays represents one of the most promising alternatives to the use of the exhausting fossil fuel stocks. The actual tendency is toward the design of taller towers, that can produce more power because excited by stronger winds. There is the need of designing these structures in a cost effective way, aiming to reduce the wind induced growing structural demand.

Three different control systems are investigated and compared herein to this aim, on the basis of the experimental results gathered at the Structural Dynamics Laboratory of the Denmark Technical University. Two of these are passive and have been designed as in Georgakis and Chen (2013a, 2013b). The third one is semi-active (Caterino 2015, Caterino et al. 2014, 2016).

A tuned rolling-ball damper (TMD - Figure 1) was adopted in the first case (Chen and Georgakis 2013a) to reduce vibrations of a prototype 1/20-scale wind tower model. The model was subjected to shaking table tests, by applying three accelerograms at the base, each being equivalent to a different wind load case (namely "overspeed", "extreme operating gust - EOG", "parking"). The rolling-ball damper consists of a glass container, attached to the top of the model, with single or multiple rolling steel balls inside. Five configurations of such damper were tested: one using a one-layer container with one steel ball inside, the other using a two-layer container with three to six smaller steel balls inside each layer. The damper with three balls in a one-layer container had better control effectiveness than that with only one ball because of the impact effect and the rolling friction, but the control effectiveness of the damper cannot be improved further when the number of balls is increased beyond three. The results highlight that peak values of structural demand cannot significantly be dampened through such passive strategy, especially for impulsive load cases (EOG), mainly because the mass of TMD needs time before being effectively able to contrast the structural motion. The strategy results to be so effective in reducing the standard deviation of the top displacement and the base moment demand, up to 25% in respect to the uncontrolled response.

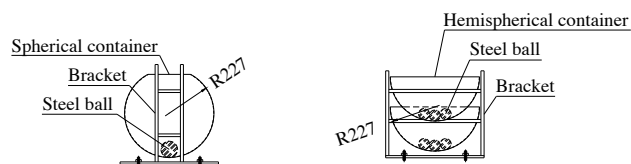


Figure 1. Rolling-ball damper.

The same setup has been re-used using water rather than steel balls inside the glass container (Chen and Georgakis 2013b). The spherical tuned liquid damper (TLD - Figure 2) consisted of two-layer hemispherical containers, partially filled with water: various water depths were investigated to examine the control effectiveness under the above load cases. For EOG load case, the experimental results showed that all the TLD could significantly reduce the standard deviation of top displacement and base moment more than 36% in respect to the uncontrolled case, although they could not reduce their peak values.

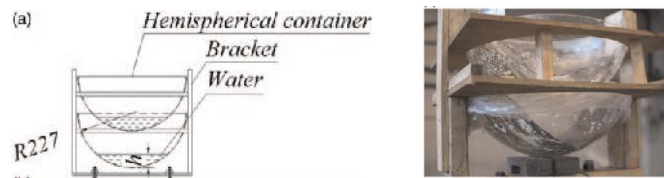


Figure 2. Spherical tuned liquid damper: drawing (left) and picture (right)

The third control technique is semi-active and based on the use of a cylindrical hinge at the base of the wind tower together with MR devices placed in parallel with linear springs, so as to realize a time-variant base restraint (Figure 3). The ‘stiffness’ of such devices can be in real time driven by a purposely written control logic (Caterino et al. 2014, 2016; Caterino 2015). The controller has to be programmed to instantaneously calibrate the MR devices to reduce the base bending moment, relaxing in selected intervals of time the base restraint. It also has to hold the top displacement within acceptable values so as to avoid detrimental increase of second order effects. The results of the experimental campaign demonstrated that significant reduction of base stresses in the turbine tower can be reached trading off a minor increase of the top displacement. For instance, when the EOG input is considered, the control system is able to reduce the peak base stress of 67% in respect to the “fixed base” case, at the cost of a 28% larger peak top displacement demand.

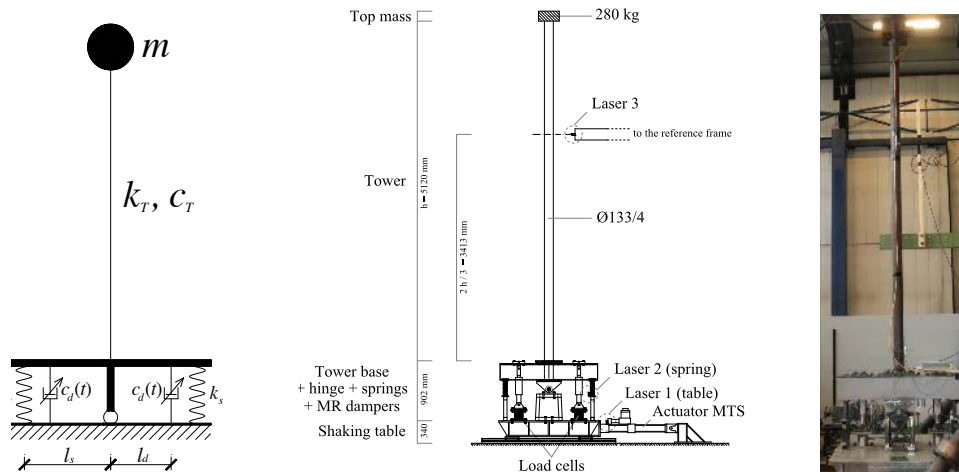


Figure 3. Smart base restraint including semi-active MR dampers: schematic idea, set-up drawing and picture

References

- Chen, J., and Georgakis, C.T. (2013a). Tuned rolling-ball dampers for vibration control in wind turbines. *Journal of Sound and Vibration* **332**, 5271–5282.
- Chen, J., and Georgakis, C.T. (2013b). Spherical tuned liquid damper for vibration control in wind turbines. *Journal of Vibration and Control* **0** (0), 1–11.
- Caterino, N., Georgakis, C.T., Trinchillo, F., Occhiuzzi, A. (2014). A Semi-Active Control System for Wind Turbines. In: Luo N, Vidal Y and Acho L (eds) *Wind Turbine Control and Monitoring. Advances in Industrial Control*. Springer International Publishing Switzerland. ISBN 978-3-319-08412-1.
- Caterino, N. (2015). Semi-active control of a wind turbine via magnetorheological dampers. *Journal of Sound and Vibration* **345**, 1–17, doi:10.1016/j.jsv.2015.01.022
- Caterino, N., Georgakis, C.T., Spizzuoco, M., and Occhiuzzi, A. (2016). Design and calibration of a semi-active control logic to mitigate structural vibrations in wind turbines. *Smart Structures and Systems* **18** (1).

Experimental study on the aerodynamics of rectangular prisms with a forebody screen

A. Giachetti¹, C. Mannini¹ and G. Bartoli¹

¹ CRIACIV/Department of Civil and Environmental Engineering, University of Florence, Italy

Corresponding author: A. Giachetti, andrea.giachetti@unifi.it

Abstract

Understanding the wind effects on permeable building envelopes represents a challenging task. Previous two-dimensional studies on section models proved that the presence of oscillating flow in the cavity may interfere with the aerodynamics of the supporting body. This work presents some advances concerning the incoming turbulence and wind direction effects. It also introduces the ongoing investigations on more realistic three-dimensional geometries concerning tall buildings.

1 Introduction

The request to reach high aesthetic and energetic standards makes the building envelope one of the crucial elements in the design of a modern building. From a wind-loading point of view, a permeable building envelope can be considered as an additional layer fixed to one or more faces of the main building structure, which creates an internal cavity somehow connected to the exterior. In order to properly define the wind loads acting on such building facades, it is necessary to measure and/or evaluate both external and internal pressures. Since the internal cavity is connected to the exterior, the wind-driven internal and external flows may mutually interact, and the study of the resulting fluid-dynamic system is expected to be difficult.

One of the most complicated aspects to take into account is the reliability of the study of such geometries on scaled models, being the internal cavity gaps usually one order of magnitude smaller than the building itself. Moreover, the cavity between the building face and the external layer can be connected to the exterior in several ways, and compartmentalized with horizontal and/or vertical sub-structures. As shown in Giachetti (2017), at least in the two-dimensional case study, different configurations may lead to different aerodynamic behaviours of the whole systems.

Despite the many works carried out on permeable building envelopes (*e.g.* Gerhardt and Janser, 1994, Inculet and Davenport, 1994, Lou *et al.*, 2012,), the inadequacy of current wind loading codes clearly shows that the flow mechanisms acting on the system “building + façade” are not fully understood in certain configurations, thereby stressing the necessity of exploratory two-dimensional studies.

The current work focuses on a system with a laterally-opened airtight screen fixed in front of a square prism with a gap between 1/10 and 1/40 of the cross-wind section dimension. Results of the ongoing two- and three-dimensional experimental investigations are presented, especially those concerning the effect of the wind angle of attack and incoming turbulence.

2 Experimental set-up

The experimental campaign was carried out in the CRIACIV Boundary Layer Wind Tunnel. Tests were performed in smooth and turbulent flow. The first experiments concerned section models in two-dimensional flow conditions, while ongoing tests focus on the model of a tall building with an approaching turbulent boundary layer flow.

The two-dimensional models, characterized by a cross-section side length $D = 0.12$ m and a span length of 1.24 m, were mounted vertically in the 2.4×1.6 m test section and confined by large circular end plates. The three-dimensional tests are carried out on a square prism with a 1:1:5 side ratio. The reproduced approaching boundary layer is characterized by a flow exponent typical of an urban environment ($\alpha \approx 0.3$). The screens were made of stainless steel foils of 1 mm.

The models were equipped with pressure taps and high-frequency force balances. For instance, in the case of the section model two force balances were placed at the section-model extremities behind the end plates, while 44 pressure taps were installed around the middle section. Nevertheless, due to the limited thickness, it was not possible to equip the screen with pressure taps.

Finally, the models were fixed to the wind tunnel through a rotating system in order to perform tests at different angles of attack.

3 Results

Figure 1 reports the mean pressure coefficients around the middle section of the two-dimensional models for a wind flow perpendicular to the screened face, for both smooth (1a) and turbulent (1b) approaching flows. In particular, in turbulent flow the difference between internal and external pressures in correspondence of the cavity extremities seems to indicate an aerodynamic interaction similar to that encountered in smooth flow. Moreover, preliminary studies conducted by varying the angle of attack indicate that for any direction the wind drives an internal air flow in the cavity. These results represents the basis for an extension of the study to a more realistic three-dimensional building geometry.

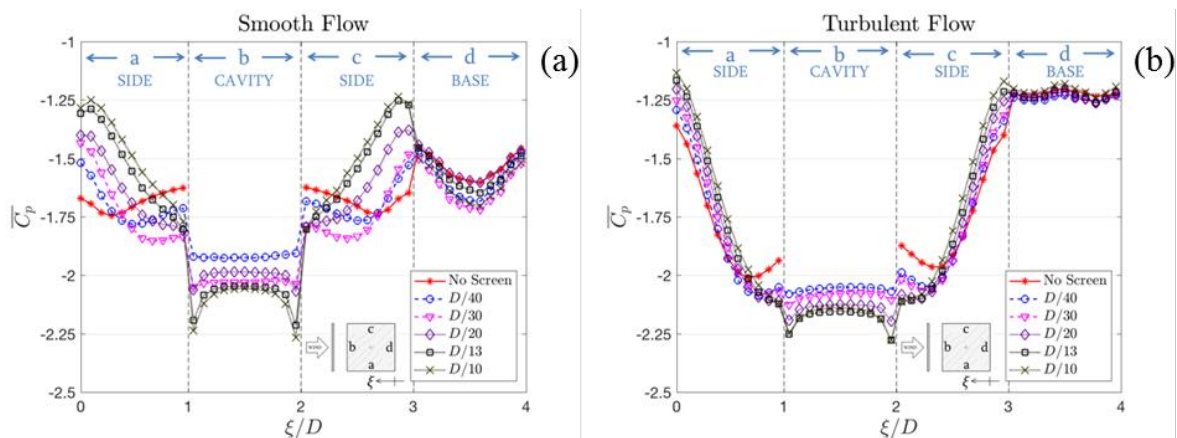


Figure 1. Mean pressure coefficients around the middle section of the square cylinder equipped with an airtight screen in smooth (a) and turbulent (b) flow (turbulence intensity of 13-15%, integral length scale of about $2D$).

References

- Gerhardt, H. J., Janser, F., (1994). Wind loads on wind permeable facades. *Journal of Wind Engineering and Industrial Aerodynamics* **53**, 37–48.
- Giachetti, A., 2017. Wind effects on permeable building envelopes : a two-dimensional exploratory study. *PhD thesis*, University of Florence – TU Braunschweig (under revision).
- Inculet, D. R., Davenport, A. G., 1994. Pressure-equalized rainscreens: A study in the frequency domain. *Journal of Wind Engineering and Industrial Aerodynamics* **53**, 63–87.
- Lou, W., Huang M., Zhang M., Lin N., 2012. Experimental and zonal modeling for wind pressures on double-skin facades of a tall building. *Energy and Buildings* **54**, 179–191.

Aerodynamic instability of cables fitted with pipes

S. Giappino¹, A. Manenti¹ and S. Muggiasca¹

¹ Department of Mechanical Engineering, Politecnico di Milano, Italy

Corresponding author: Sara Muggiasca, sara.muggiasca@polimi.it

Abstract

The present paper describes the aerodynamic study performed on a cable provided by a fitting with circular shape (pipe) and dimensions comparable to the ones of the cable. Experimental tests were carried out in the high velocity low turbulence test section of the Politecnico di Milano wind tunnel. Typical galloping instability was observed, due to asymmetry introduced by the fitting, but also a strong torsional instability occurred. This phenomenon is not generally significant for cables, but it can appear when fittings change substantially the shape of the cable: for this reason the study devoted a particular attention to this instability.

1 Introduction

Cables are structures very sensitive to the wind actions and they may suffer from different kinds of flow-structure interaction: vortex shedding and galloping (Belloli et al. 2012, Williamson & Govardhan 2004, Matsumoto et al. 2010). These problems are often observed on cables characterized by low structural frequencies, small structural damping and inclination with respect to the wind as stays of a cable-stayed bridge, hangers of suspended bridges or spoke cables of an observation wheel. Vortex shedding on circular cylinders is a well-known phenomenon that induce vibration perpendicular to the flow and it is generally experienced at low wind velocity. At higher wind velocities other aerodynamic phenomena may occur as ice-galloping, rain-wind induced vibration, high-speed vortex excitation and dry inclined cable galloping. When fittings are applied on this kind of flexible cables, giving rise to a geometrical asymmetry, instability can occur: asymmetries generate lift force on the cable and if the slope of the lift force as a function of the angular position is negative this can be indicative of a possible instability (Den Hartog 1932). Torsional instability due to negative slope of the moment coefficient with respect of the angle of attack is generally not relevant for cables but when fittings with dimensions comparable to the dimensions of the cable, are coupled to the cable itself, also the moment coefficient must be considered. Fittings with relevant dimension are, for example, dehumidification air pipes applied to hangers of suspended bridges or pipes that contain power cables for illumination system for spokes of observation wheel. In the present paper particular attention was devoted to torsional instability for a cable coupled to with a cylindrical fitting, by means an experimental study performed in the Politecnico di Milano wind tunnel.

2 Experimental set-up

Wind tunnel tests were performed in the high velocity low turbulence tests section of the Politecnico di Milano wind tunnel. The model was a cable covered with a HDPE tube and a helical fillet coupled to a cylindrical tube (see Figure 1 (a)): the main cable external diameter was 0.093m, the added tube diameter was 0.063m and the gap between the two cables was 0.024 m. Other configurations in terms of fittings cable diameter and relative gap were considered obtaining similar results. Both static and dynamic tests were performed on the model to characterize its aerodynamic behaviour. Static tests set-up was realized positioning the model vertically in the wind tunnel test section. The turntable on the floor allowed for an easy variation of the angle of attack while the aerodynamic forces on the model

were measured using two force balances placed at the ends. Dynamic tests set-up was realized suspending the model horizontally in the tests section, free to oscillate cross-flow (vertical direction, rigid translation of the cable model) and to rotate around a fix point. The two d.of. were considered separately. The dynamic response of the model was measured trough accelerometers.

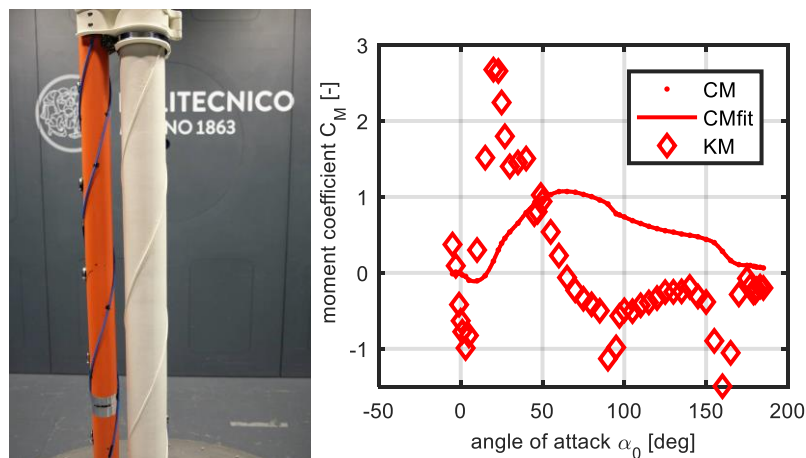


Figure 1. Model in the wind tunnel tests section (a) Moment coefficient measured at $U=30\text{m/s}$

3 Results

During the static tests aerodynamic coefficients were measured for different wind velocities and different angles of attack: as an example in Figure 1 (b) is reported the moment coefficient and the trend of its derivative for $U=30\text{m/s}$: it is possible to note that the moment coefficient derivative is negative, reaching a value of -1.0, for wind angles of attack of 0 deg. This configuration was tested also with the dynamic set-up observing torsional instability at a wind velocity equal to 16.7 m/s.

A sensitivity analysis was also performed in order to evaluate the influence of the gap between the two cables on the system stability.

References

- Belloli, M., Giappino, S., Muggiasca, S., Zasso, A., 2012, Force and wake analysis on a single circular cylinder subjected to vortex induced vibrations at high mass ratio and high Reynolds number, *Journal of Wind Engineering and Industrial Aerodynamics*, 103, pp. 96-106.
- Den Hartog, J.P., 1932. Transmission Line Vibration Due to Sleet. *Transaction, AIEE*, 1074-1076.
- Matsumoto M., Yagi T., Hatsuda H., Shima T., Tanaka M., Naito H., 2010. Dry galloping characteristics and its mechanism of inclined/yawed cables. *Journal of Wind Engineering and Industrial Aerodynamics* 98(2010), 317–327
- Williamson, C.H.K., Govardhan, R., 2004, Vortex-induced vibrations, *Annual Review of Fluid Mechanics*, 36, pp. 413-455

Cyclist aerodynamics: a comparison between wind tunnel tests and CFD for helmet design

S. Giappino¹, S. Omarini¹, P. Schito¹, C. Somaschini¹, M. Belloli¹, M. Tenni²

¹Department of Mechanical Engineering, Politecnico di Milano, Italy

²MET Helmets, Italy

Corresponding author: Stefano Giappino, stefano.giappino@polimi.it

Abstract

During the last decades a particular attention to the aerodynamic optimization of professional bike riders and their equipment, with a large use of experimental investigation as well as numerical simulations. Large studies have been carried out in wind tunnels all over the world by professional cycling teams to study the best set-up for time trial competitions. The standard approach is to compare different part of the equipment or different position and find out the optimized configuration by trial and error procedure. This paper presents an attempt of helmet design based on CFD calculations and the experimental validation of numerical results.

1 Introduction

It is well established that wind resistance is responsible for most of the metabolic cost of cycling in level ground. Aerodynamic drag is about 80% of the total resistive force in road racing at 30 *km/h* and up to 94% in time trial competitions at 50 *km/h*, so that it becomes important to reduce it to improve cycling performance [1–3].

Blocken et al. [4] performed CFD simulations of the riders to study rider positions and drafting effects as function of the distance between bikes.

So that different techniques are used nowadays to evaluate aerodynamic drag in cycling: on one side track testing allows a natural athlete's behavior while, on the other side, wind tunnel testing is the most accurate and reliable technique. In case of wind tunnel testing, particular attention should be given to the simulation of the pedaling with an adequate resistance, since significant differences are found between static and in effort tests [3]. Wind tunnel results showed a good agreement with track values considering also that the rolling resistance was not included in the wind tunnel measurements.

CFD calculations showed good agreement with wind tunnel experiments but using as reference tests on mannequins because spinning wheels and pedaling are very challenge to be simulated using a computational approach.

All these comparisons are made in terms of integral force, drag and side forces when side wind effects are included. CFD presents a great advantage: it can be used as a design tool, because it defines the flow field and the local pressure on the whole surface of the considered body, on the other hand it is very complicated to measure the pressure on the rider, bike and equipment. This work presented in this paper tries to overcome this issue by proposing a new experimental set-up able to measure the pressure on a real helmet, worn by an athlete during wind tunnel testing. This local measurement let us validate the CFD results in terms of local pressure distributions.

2 CFD and experimental set-up

The numerical analysis is conducted using the geometry of a biker and the CAD model of the helmet and of the visor. The rider geometry is obtained by means of a three-dimensional scan. As can be seen

in Figure 1, the geometry reproduces the upper-body of a real athlete, while some minor details, as the hairs (that will be shaded by the helmet), the hands, the legs and the bicycle are neglected.

The helmet and the visor are placed correctly on the rider head and this geometry is used as a reference for the CFD analysis as can be seen in Figure 1. The numerical analysis is conducted resolving steady state RANS with a $k\omega$ -SST turbulence closure model.

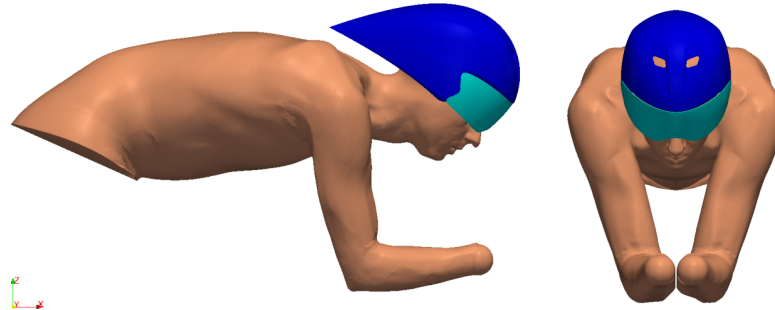


Figure 1. Geometry of the rider and the helmet: side view (left), front view (right).

The wind velocity is defined on the right side of the domain, and the wind speed is coherent with the speed of a professional athlete: in particular the wind speed is 14m/s. The pressure distribution on the surface together with the visualization of the path-lines and the oil flow pattern shown in Figure 2, allows to define possible directions for the improvement of the aerodynamic design of the helmet for achieving the drag reduction.

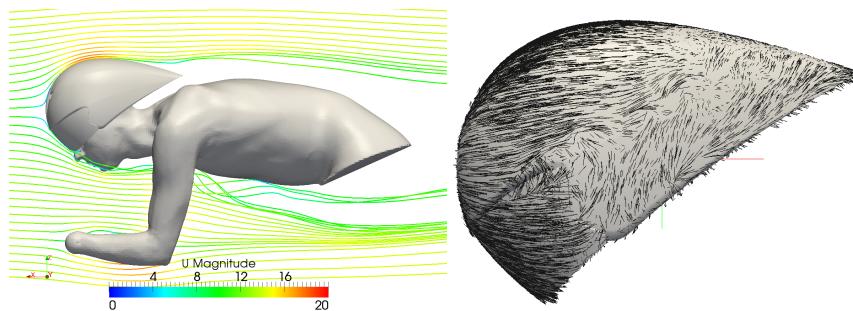


Figure 2. Path-lines coloured by velocity magnitude around the cyclist symmetry plane (right); oil flow on the helmet and visor to display the local velocity direction.

In the full paper will be presented the improvement steps and the final version of the helmet design, the comparison with the wind tunnel tests realized on an instrumented version of the helmet. Figure 3 shows two views of the helmet instrumented with the pressure taps.



Figure 3. Instrumented helmet for pressure measurements

3 References

- S. Padilla, I. Mujika, F. Angulo, J.J. Goiriena Scientific approach to the 1-h cycling world record: a case study, *Journal of applied physiology*, 89 (2000), pp. 1522-1527
- J. García-López, J.A. Rodríguez Marroyo, C. Juneau, J. Peleteiro, A.C. Martínez, J.G. Villa, Reference values and improvement of aerodynamic drag in professional cyclists, *Journal of Sports Sciences*, 26 (2008), pp. 277-286
- G. Gibertini, G. Campanardi, D. Grassi, Cycling aerodynamics: a complex problem, in: 13th International Conference on Wind Engineering (ICWE13), 2011
- B. Blocken, T. Defraeye, E. Koninckx, J. Carmeliet, P. Hespel Cfd simulations of the aerodynamic drag of two drafting cyclists *Computers and Fluids*, 71 (2013), pp. 435-445

Extreme wind speed prediction – the Australian experience

John B. Holmes¹

¹JDH Consulting, Mentone, Victoria, Australia

Corresponding author: john.holmes@jdhconsult.com

Abstract

The greatest source of uncertainty in the prediction of wind loads on structures is undoubtedly the estimation of extreme wind speeds at the high return periods associated with low risk of exceedance of wind loads. In the loading of quasi-static structures, the wind speed is squared, so that errors in wind speed estimation are effectively doubled. For structures with significant resonant dynamic response, for which the response relation increases with wind speed to a higher power than two, the magnification of the errors in wind speed is even greater.

The emergence of limit-states structural design from the 1980s onwards has led to some countries adopting very high return periods for wind speeds for ultimate limit states. For example, the national wind loading standard in Australia, AS 1170.2, adopted a return period of 1000 years for most structures in the 1989 edition. The wind load factor for wind loads calculated in this way was (and still is) 1.0. In 2002, a system was introduced in which the return period, R , varies with the importance of the structure; for example, for farm buildings, R would be taken as 100 years, and for post-disaster buildings, such as hospitals, as 2000 years.

To predict extreme wind speeds, wind engineers must rely on data collected by bodies such as national meteorological agencies – in Australia it is the Bureau of Meteorology. Over periods of 40 - 50 years, anemometer locations often will be changed several times, the instrument itself may be changed, as may be the method of acquiring data (for example, with the introduction of automatic weather stations (AWS) with digital sampling from the 1990s). The surrounding terrain often changes significantly over time, particularly at airports in, or near, urban areas. In the case of Australia where a peak gust speed is used as a basic wind speed, the effective gust duration is another factor that may require correction. The introduction of the 3-second moving average gust, as mandated by the World Meteorological Organisation in the 1980s, means that corrections to the shorter duration gust used in Australian standards are required.

In a large country like Australia with several climate zones, there are several mechanisms that can generate high wind speeds: tropical cyclones, extratropical depressions, cold fronts, severe thunderstorm downdrafts, and occasionally tornados. Since strong winds generated by these mechanisms generally will follow different probability distributions, it is necessary to separate high gusts into defined storm types before extreme-value analysis.

Assuming all the above corrections have been made and procedures have been followed, there remains the problem of extrapolating data from a station recorded over, say, 50 years, to make predictions to return periods of 500 to 1000 years for ultimate limit states design. Although Gumbel's classic text (1958) on extreme value theory discusses sampling errors and confidence limits for long-return-period predictions using the Type I Extreme Value Distribution, assessment of statistical sampling errors is often lacking in published analyses of extreme wind speeds in recent decades. This paper will discuss the sampling errors for predictions using the distributions adopted for the main wind

region covering the majority of Australia not affected by tropical cyclones – known as ‘Region A’ in AS/NZS 1170.2.

Between 1989 and 2002, the wind gust speed versus return period for Region A was given in AS 1170.2-1989 by Equation (1):

$$V_R = 29.2 + 3.0 \log_e R \text{ m/s} \tag{1}$$

This is the high-return period approximation to the Type I, or Gumbel, Extreme Value Distribution with a mode of 29.2 m/s and scale, or slope, of 3.0 m/s. As a special case of the Generalised Extreme Value (GEV) Distribution, the shape factor (k) is 0. Figure 1(a), on the left, shows the 80% confidence limits obtained by simulating 50 samples of 50 years of annual maxima (2500 in total), and fitting each sample to the Gumbel Distribution using the Method of Moments. It can be seen that the predictions of V_{1000} can be up to 4 m/s from the correct value of 50 m/s (from Eq (1)). Even the V_{50} predictions can depart from the correct value of 41 m/s by up to 2.5 m/s.

Since 2002, the GEV with a shape factor, k , fixed at +0.1 has been used for Region A in the Australian/ New Zealand standard, giving for high return periods:

$$V_R = 67 - 41 R^{-0.1} \text{ m/s} \tag{2}$$

A similar ‘bootstrapping’ approach in which the excesses above a threshold of 25 m/s were simulated with the corresponding Generalised Pareto Distribution, produced Figure 1(b). Again 50 groups of 50 samples each were simulated. The 80% confidence limits for V_{500} are 2.3 – 3.7 m/s. The two figures below illustrate that even relatively high sample sizes of 50 years will result in wide confidence limits for the return periods required for structural design for ultimate limit states. The full paper will show how these sampling errors can be reduced by combining data from nearby stations, and will give examples of correction, storm-type separation, fitting and predictions for Australian data.

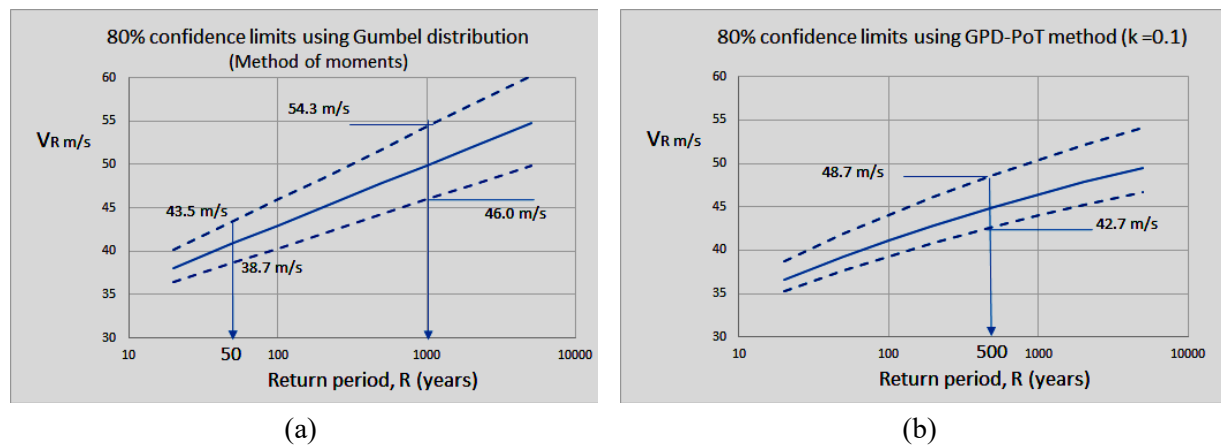


Figure 1. Confidence limits for predictions in Australia using 50-years samples.

Computational simulation of windblown sand erosion, transport, and sedimentation around dunes

M. Horvat^{1,4}, L. Bruno^{1,4}, S. Khris^{2,4}, A. Lo Giudice^{2,3,4}

¹Department of Architecture and Design, Politecnico di Torino, Italy

²Optiflow Company, Marseille, France

³Department of Mathematical Sciences “Giuseppe Luigi Lagrange”, Politecnico di Torino, Italy

⁴Windblown Sand Modelling and Mitigation joint Research Group

Corresponding author: M. Horvat, marko.horvat@polito.it

Abstract

Aeolian processes induced by windblown sand are of interest in several research fields, from mathematical physics to Earth sciences and civil and environmental engineering. From the engineering perspective, the accurate simulation and prediction of aeolian events is a key element in arid environments, with respect to human activities and infrastructures.

Aeolian processes represent a multi-disciplinary field since they deal with the interaction among subfields such as blowing wind, air suspended particles and bed-particles. Such an interaction takes place in windblown sand Erosion, Transport, Sedimentation and Avalanching (ETS-A). Windblown sand Erosion from the Earth surface occurs if the shear stress induced by the wind exceeds a given threshold value (Raffaele et al 2016) sand grains are entrained into the lower part of atmospheric boundary layer. Windblown sand Transport occurs in different modes of motion of the sand particles in function of their dimensions (Shao, 2008). Among all transport mechanisms responsible of sand motion, *saltation* largely prevails in term of mass (Kok et al., 2012). Windblown sand Sedimentation results from the out of balance between inertial, gravity and aerodynamic forces acting on the sand particles in air. Avalanching occurs if the sedimented sand accumulates along a profile with steepest slope exceeding the sand angle of repose (A. Lo Giudice et al, 2018). The overall ETS-A phenomena involve changes in the Earth surface at different spatial and time scales, i.e. the formation and evolution of sand seas, dunes, ripples and sand accumulation around obstacles (Wiggs, 2001).

The accurate prediction of the phenomena above currently remains an open issue. In situ full scale observations and measurements (e.g. Baddock et al, 2011), wind tunnel tests (e.g. Ferreira and Fino, 2012) and computational simulations (e.g. Bruno and Fransos, 2015, Preziosi et al, 2015) may be used.

The present study develops within the computational approach. The Erosion Transport and Sedimentation (ETS) model developed and implemented by the members of the SMaRT project (Preziosi et al., 2015) is a segregated model that accounts for all the phenomena described above.

The windblown sand is described by the distribution field of the variable φ_s , which is defined as the volume ratio of the sand inside the volume of air.

$$\frac{\delta \varphi_s}{\delta t} + \nabla \cdot (\varphi_s \mathbf{v}_s + \mathbf{q}_{coll}) = 0, \quad (1)$$

where $\mathbf{v}_s = f(\mathbf{v}_f) - \omega_{sed} \mathbf{k}$. \mathbf{v}_f is the wind velocity, ω_{sed} is the settling velocity and \mathbf{k} is unit vector in the direction of the gravity.

The wind field is obtained solving the Reynolds Averaged Navier-Stokes (RANS) equations consisting of mass and momentum conservation equations for an incompressible flow. This set of equations is complemented by the $k-\omega$ SST turbulence model taking into account turbulent phenomena. A Reynolds Averaged approach is justified by the fact that the interest is in the mean long-term prediction of transport processes (Bruno and Fransos, 2015).

Boundary condition on the interface between the sand and the wind (i.e. saltation flux, q_s) can be calculated by semi empirical models, such as modified Bagnold type models in which sand flux is a function of the effective shear velocity u_{eff} (Raffaele et al., 2018), defined as: $q_s \propto u_{eff} \propto f(u^*) - f(u_t^*)$. The model shown by the following equation has been selected to define the wind-sand interaction at the interface: $q_s = \frac{\omega \alpha \hat{\rho}_f}{gd} \beta (u^{*2} - u_t^{*2})$.

In the present study, free model parameter tuning is carried out by referring to the fundamental setup of sand transport over a flat sand bed (Zhang et al., 2007). The model validation is carried out comparing the computational results with the experimental measures of the sinusoidal dune morphodynamics (Ferreira and Fino, 2012).

Acknowledgments

The study has been developed in the framework of the MSCA-ITN-2016-EID research project Sand Mitigation around Railway Tracks (SMaRT, www.smart-eid.eu). The SMaRT project has received funding from the European Union Horizon 2020 research and innovation program under grant agreement No 721798. The authors wish to thank the other researchers of the SMaRT consortium (N. Coste, E. Delboulbe, C. Nash, R. Nuca, L. Preziosi, G. Wiggs) for the helpful discussions about the topics of the paper. The contribution given by SMaRT partner organizations (Ansaldo STS, Astaldi, Salcef group) is acknowledged as well.

References

- Baddock, M.C., Wiggs, G.F.S., and Livingstone, I. (2011) A field study of mean and turbulent flow characteristics upwind, over and downwind of barchan dunes, *Earth Surface Processes and Landforms* **36**-11, 1435-1448
- L. Bruno, D. Fransos (2015) Sand transverse dune aerodynamics: 3D Coherent Flow Structures from a computational study, *Journal of Wind Engineering & Industrial Aerodynamics* **147**, 291-30
- Ferreira, A.D., Fino, M.R.M. (2012) A wind tunnel study of wind erosion and profile reshaping of transverse sand piles in tandem, *Geomorphology* **139–140**, 230–241
- Kok, J.F., Parteli, E.J.R., Michaels, and T.I., Karam, D.B. (2012). The physics of wind-blown sand and dust. *Reports on Progress in Physics* **75**, 106901
- Lo Giudice, A., Giammanco, G., Fransos, D. and Preziosi, L. (2018) Modelling Sand Slides by a Mechanics-Based Degenerate Parabolic Equation, *Mathematics and Mechanics of Solids*, in press
- Preziosi, L., Fransos, D. and Bruno, L. (2015) A Multiphase First Order Model for Non-Equilibrium Sand Erosion, Transport and Sedimentation, *Applied Mathematical Letters* **45**, 69-75
- Raffaele, L., Bruno, L., Pellerey, F., and Preziosi, L. (2016). Windblown sand saltation: A statistical approach to fluid threshold shear velocity. *Aeolian Research* **23**, 79–91
- L. Raffaele, L. Bruno, G.F.S. Wiggs (2018) Uncertainty propagation in aeolian processes from threshold shear velocity to sand transport rate, *Geomorphology* **301**, 28–38
- Shao, Y. (2008). *Physics and Modelling of Wind Erosion*. Second edn. Springer
- Wiggs, G.F.S. (2001) Desert dune processes and dynamics, *Progress in Physical Geography* **25**-1, 53-79
- Zhang, W., Wang, Y., and Lee S.J. (2007) Two-phase measurements of wind and saltating sand in an atmospheric boundary layer, *Geomorphology* **88**-1–2, 109-119

Application of aerodynamic modification on slender structures for wind energy harvesting

Gang Hu¹, K. C. S. Kwok¹ and K. T. Tse²

¹School of Civil Engineering, The University of Sydney, Sydney, New South Wales 2006, Australia

²Department of Civil and Environmental Engineering, The Hong Kong University of Science and Technology, Hong Kong, China

Corresponding author: Gang Hu, ghuaust@gmail.com

Abstract

This paper presents effects that fitting fins to the corners of a square prism galloping-based piezoelectric energy harvester (PEH) has on its performance, based on results from a series of wind tunnel model tests. The results show that attaching fins to the leading edge significantly improves the efficiency of the harvester, achieving a maximum power 2.5 times that attained by a plain square prism PEH. In addition, two aerodynamic optimization strategies including attaching small diameter cylindrical rods on circular cylinder and placing splitter plates in the leeward side of circular cylinder are applied on a vortex-induced vibration (VIV)-based wind energy harvester. The two strategies produce a significant enhancement of wind energy harvesting capability.

1 Introduction

The past few years saw a number of studies on piezoelectric energy harvesters (PEHs) being developed as sustainable power sources. The majority of these PEHs are designed to harvest energy from flow-induced vibrations such as vortex-induced vibration (VIV), flutter, and galloping. Different strategies to improve the efficiency of these PEHs have since been proposed and studied, both theoretically and experimentally. To enhance the efficiency of the wind energy harvester, aerodynamic modification of the bluff body is one of the most effective approaches.

2 Wind tunnel experiments and results

The performance of a PEH—with fins attached onto the corners of a square prism—was modelled and investigated in an open-circuit wind tunnel (Hu et al., 2016a). Fins were attached to the square prism in three configurations as shown in Figure 1: fins attached to all four corners, fins attached to leading edges only, and fins attached to trailing edges only, and their performances were compared to that of a plain (fin-less) square prism. The fins had length $l = 0.4$ cm, which corresponds to an l/D ratio of $1/6$. The fins were always attached at 45° with the horizontal.

For the VIV-based wind energy harvester, attaching small diameter cylindrical rods on the circular cylinder or placing splitter plates in the leeward side of the circular cylinder of a VIV-based wind energy harvester were also tested (Hu et al., 2016b; Song et al., 2017). Two small diameter cylindrical rods with diameter d were bonded to two sides of a circular cylinder parallel to the circular cylinder axis and symmetrical to the oncoming flow direction, as shown in Figure 2. The attachment locations of the rods were defined by the circumferential angle θ . For the splitter plate, different lengths in the streamwise direction was tested.

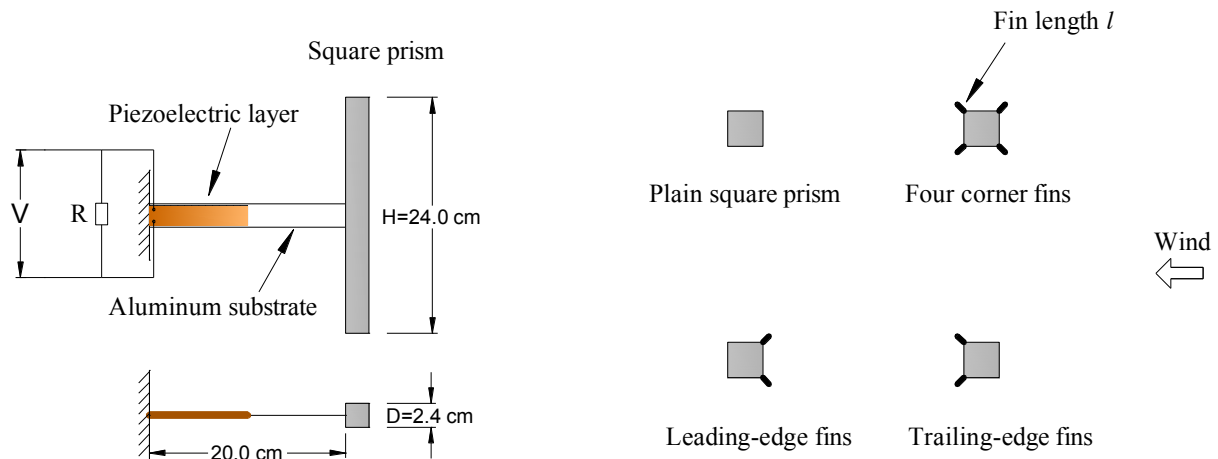


Figure 1 Sketch of galloping-based piezoelectric energy harvester and different fin configurations (Hu et al. 2016).

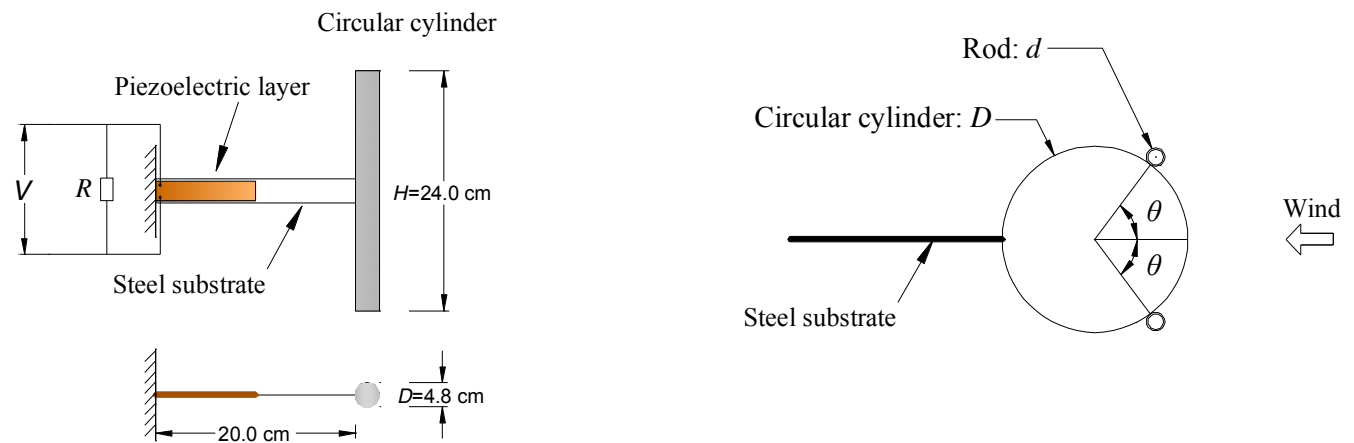


Figure 2 Sketch of piezoelectric energy harvester and rod attachment configuration (Hu et al., 2016b).

Test results show that leading-edge fins significantly improve the efficiency of the harvester with maximum improvement ratio of harvest power reaching 150% compared to a plain square prism. On the other hand, attaching two small-scale cylindrical rods on two sides of the circular cylinder parallel to the cylinder axis and symmetrical to the oncoming flow at the circumferential location $\theta = 60^\circ$ significantly expands the aeroelastic unstable range of the circular cylinder. Similarly, placing the splitter plates with a proper length dramatically expands the instability range. The wind energy harvester with these two configurations harnesses wind energy beyond the VIV onset wind speed and is sustained over the range of wind speed tested.

References

- Hu, G., Tse, K.T., Kwok, K.C.S., 2016a. Enhanced performance of wind energy harvester by aerodynamic treatment of a square prism. *Appl. Phys. Lett.* 108. <https://doi.org/10.1063/1.4944555>
- Hu, G., Tse, K.T., Kwok, K.C.S., Song, J., Lyu, Y., 2016b. Aerodynamic modification to a circular cylinder to enhance the piezoelectric wind energy harvesting. *Appl. Phys. Lett.* 109, 1–6. <https://doi.org/10.1063/1.4967497>
- Song, J., Hu, G., Tse, K.T., Li, S.W., Kwok, K.C.S., 2017. Performance of a circular cylinder piezoelectric wind energy harvester fitted with a splitter plate. *Appl. Phys. Lett.* 223903, 1–5.

Life-cycle cost-based wind design of tall buildings

Laura Ierimonti¹, Ilaria Venanzi¹ and Luca Caracoglia²

¹Department of Civil and Environmental Engineering, University of Perugia, Perugia, Italy

²Department of Civil and Environmental Engineering, Northeastern University, Boston, Mass., USA

Corresponding author: Laura Ierimonti, ierimonti@strutture.unipg.it

Abstract

An automated and computationally cost-effective procedure, designated Life-Cycle Cost Wind Design (LCCWD) and recently proposed by the authors, has been proposed for the design of wind-excited tall buildings. The LCCWD is based on the evaluation of the life-cycle cost associated with various levels of wind-induced damage through the PEER equation. The best design configuration is obtained by comparing the lifetime cost of different design alternatives. All the peculiarities involved in the design of high-rise buildings can be taken into account by the procedure: uncertainties in the wind load characterization, wind directionality effects, modeling of the response (vibration modes with nonlinear mode shapes, torsional effects, etc.). Moreover, the long-term monetary benefits associated with the installation of a control system can be considered. The present work is aimed at enhancing the investigation of the potentialities of the LCCWD procedure through the consideration of several sources of uncertainty, numerous damage states, different design alternatives and cost models.

Introduction

Life Cycle Cost Analysis (LCCA) is devoted to quantifying the monetary losses expected in structures during their lifetime (Wen et al., 2001; Cui and Caracoglia, 2015). In the framework of the LCCA, the LCCWD procedure has been recently proposed by the authors (Ierimonti et al., 2017), which is specifically devoted to wind-excited tall buildings. By exploiting the PEER integral equation considering suitable fragility models, it relates the probability of exceeding specific damage states to the repair costs needed to restore the structure to its original functions after a strong wind event. In non-hurricane prone regions, the main monetary losses can be related to failure of drift-dependent and acceleration-dependent nonstructural elements. The LCCWD considers various design options:

- I. The structural system, with reference to the structural members, the materials and the geometry of the building.
- II. The building's orientation, considering the wind exposure and the geographical location.
- III. The structural control system, which is often employed in tall buildings to reduce wind-induced vibration.
- IV. The typology, number and location of nonstructural elements, which can be considered as integrated elements of the design process as they significantly influence the life-cycle costs.

1 LCCWD: damage and cost analysis

The outline of the LCCWD procedure (Figure 1.a), developed for each design alternative of steps I-IV, can be summarized as follows:

1. Select the structural model and, if applicable, the control system model (e.g. TMD, etc. CS).
2. Identify the wind hazard model: wind tunnel tests, mean-wind speed annual maxima and direction-dependent joint probability distribution $f(V_{ref}, \theta + \delta)$, where V_{ref} is the reference height (building top floor), θ is the mean-wind incidence angle and δ is the building orientation.

3. Evaluate structural response through engineering demand parameters inducing damage *EDP*.
4. Select the damage states related to: direct losses associated with nonstructural components; indirect losses related to occupant’s discomfort (business downtime). Hence, evaluate the corresponding complementary cumulative distribution function (CCDF), i.e. the fragility function $P[DS_j | EDP(V_{ref}, \theta, cs)]$, also accounting for the presence of the control system, where DS_j represents the j^{th} selected damage state.
5. Compute the annual damage probability in a generic direction of the building ($h=x,y$) as a function of the building orientation δ and height z .

$$P_{j,cs}^h(\delta, z) = \iiint P[DS_j | EDP(V_{ref}, \theta, cs)] f[EDP(V_{ref}, \theta, cs)] f(V_{ref}, \theta + \delta) dEDP dV_{ref} d\theta \quad (1)$$

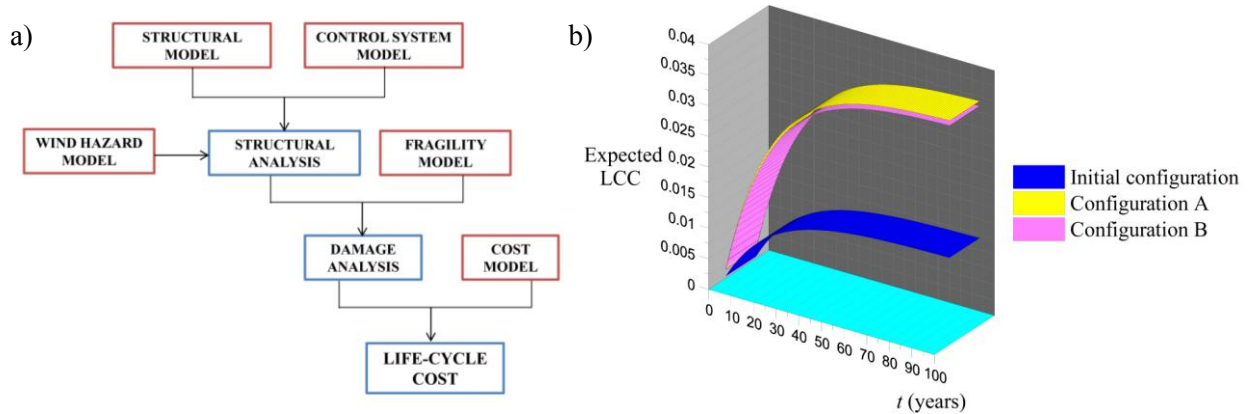
6. Calculate the expected life-cycle cost ($E[\cdot]$) by considering: the loading occurrence number (I); the total number of loading occurrences (L) between time 0 and time t ; each j^{th} damage state; the deterministic cost C_j associated with the j^{th} damage state; the yearly discount rate (λ):

$$E[C_{cs}(t)] = C_{0,s} + C_{0,cs} + E \left[\sum_{z=1}^H \sum_{h=x,y} \sum_{l=1}^L \sum_{j=1}^K \tilde{n}_j^h(z) C_j e^{-\lambda t} P_{j,cs}^h(\delta, z) \right] \quad (2)$$

where \tilde{n} is the number of damage-sensitive elements at height z .

2 The case study: preview of the results

The efficiency of the LCCWD approach is demonstrated by making use of a case study, i.e. a 180-m high tall building, for which wind tunnel load data are available. Full-scale wind speeds and direction data records for the specific site location where the building is built, are used. The structural analysis is carried out in the frequency domain and considers modal superposition with nonlinear mode shapes and torsional response. As an example, Figure 1.b) illustrates various cost-based design alternatives different for typology, number and location of nonstructural elements (step IV).



References

Wen, Y., Kang, Y., (2001). Minimum building life-cycle cost design criteria. I: Methodology. *Journal of Structural Engineering*, ASCE 127, 330-7.

Cui, W., Caracoglia, L., (2015). Simulation and analysis of intervention costs due to wind-induced damage on tall building. *Engineering Structures* 87, 183–197.

Ierimonti, L., Caracoglia, L., Venanzi, I., Materazzi, A.L. (2017). Investigation on life-cycle damage cost of wind-excited tall buildings considering directionality effects. *Journal of Wind Engineering & Industrial Aerodynamics* 171, 207-2018.

An approximate model for large-scale fluctuations in tornado-like vortices

Mohammad Karami¹, Luigi Carassale², Horia Hangan¹, Maryam Refan¹

¹The Wind Engineering, Energy and Environment (WindEEE) Research Institute, Western University, London, Ontario, Canada N6A 5B9

²Department of Civil Environmental and Architectural Engineering, University of Genova, Italy

Corresponding author: Mohammad Karami, mkarami3@uwo.ca

Abstract

Analytical modelling of tornado-vortices is much attractive since it provides a better understanding of the evaluation of tornadic wind loads on structures. Tornadoes present two type of fluctuations: (i) large scale fluctuations due to intrinsic instabilities present in the flow and (ii) small scale turbulent fluctuations. Herein we attempt a reconstruction of the large scale fluctuations (or Coherent Structures - CS) in tornado vortices using modal analysis.

The use of proper orthogonal decomposition (POD) method to identify typical or recurrent flow patterns, possibly associated to some specific physical phenomenon, has been experimented by several authors. To reconstruct the fluctuating flow field by using POD technique, the following steps are necessary:

1. Subtract mean velocity $\bar{V}(x)$ from the velocity field $V(x, t)$ to obtain the fluctuating velocity field, $V'(x, t)$:

$$V'(x, t) = V(x, t) - \bar{V}(x) \quad (1)$$

2. Obtain the set of modes $\varphi(x)$ of fluctuating velocity field $V'(x, t)$. In POD method, the modes $\varphi(x)$ are eigenvectors of the covariance matrix of $V'(x, t)$. It should mentioned that the modes are enumerated in such a way that their corresponding eigenvalues are sorted in decreasing order. This means that the first modes have higher eigenvalues of the other modes.
3. Select the modes that represent the large scale fluctuations (n). In POD method, the eigenvalues of modes represent the turbulent kinetic energy of the flow. Therefore, the first modes that have higher eigenvalues represent the coherent structures of the flow, i.e. large scale fluctuations.
4. Obtain the principal components $S(t)_k$ ($k = 1, \dots, n$) of those modes that represent large scale fluctuations:

$$S(t)_k = \varphi(x)_k^T \times V'(x, t) \quad (2)$$

where k is the number of the modes that represent coherent structures. Note that this is matrix product and thus principal components are only function of time.

5. Reconstruct the large scale fluctuating velocity field (V_{cs}') from the modes that represent the coherent structures:

$$V_{cs}'(x, t) = \sum \varphi(x)_k \times S(t)_k \quad (3)$$

To better understand the POD method as well as its application for extraction of coherent structures out of the flow, this method is applied on the velocity field of tornado-like vortex. The flow is simulated experimentally in a 1/11 scaled model of WindEEE Dome (MWD) at Western University. Using PIV method, the velocity field is measured in a horizontal plane at a height of 7cm above the ground.

Figure 1 shows the first five POD modes, $\varphi(x)$, of the vorticity fields. As we can see, POD decomposes the flow into a few simple modes. Modes 1 and 2 represent two vortices and mode 3 shows a single mode. Mode 4 and 5 shows four small vortices. Figure 2 shows the contribution of each mode to the energy. We can see that the first two modes have the most contribution into the energy. This suggests that we can approximate the fluctuation by the reconstructing the flow field based on the two first POD modes.

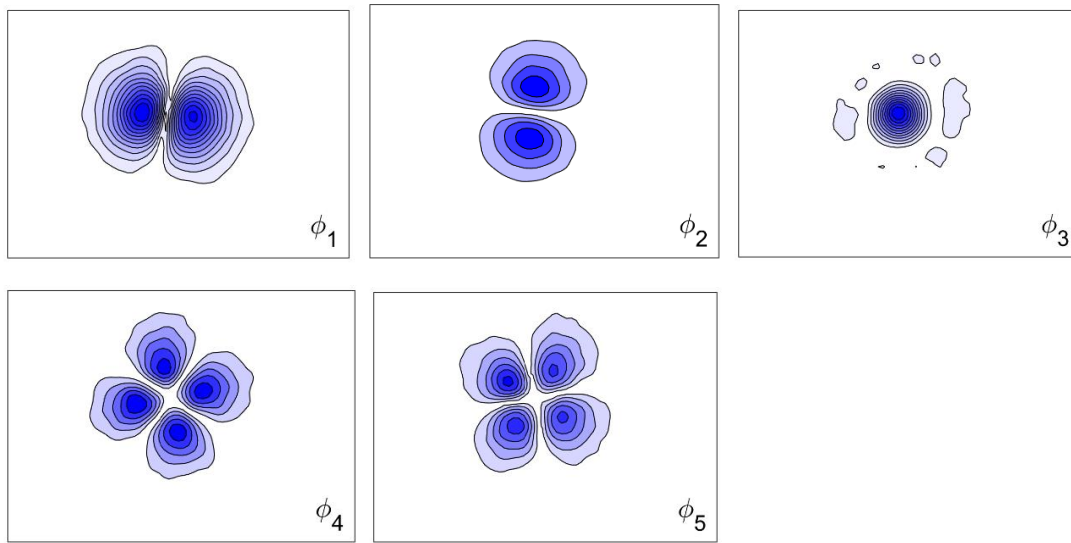


Figure 1. The first five POD modes of vorticity field at $S=0.22$ and height=7cm above ground.

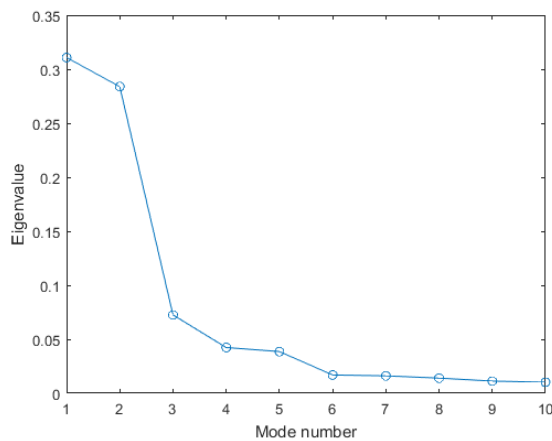


Figure 2. Eigenvalues of POD modes.

Characteristics of unsteady aerodynamic force on tall building

YC Kim¹, YL Lo² and CH Chang²

¹Department of Architecture, Tokyo Polytechnic University, Japan

²Department of Civil Engineering, Tamkang University, Taiwan

Corresponding author: YC Kim, kimyc@arch.t-kougei.ac.jp

Abstract

Characteristics of unsteady aerodynamic force on a vibrating tall building was evaluated under two oncoming flows. Surface pressures and tip displacements were measured. In an across-wind direction, large and clear differences were found between static and vibrating models, but only small differences were found in an along-wind direction. The fluctuating generalized force coefficients of the vibrating model were larger than those of the static model, showing the largest value near the resonant velocity. Two peaks in power spectra of the generalized force coefficients were observed during the lock-in range, and the reason why the Strouhal component disappears in the power spectra of tip displacement was discussed.

1! Introduction

There are two representative methods to evaluate the characteristics of unsteady aerodynamic forces experimentally: forced vibration method and free vibration method. In the forced vibration method, the experimental model vibrates forcibly in the flow using predetermined forcing frequencies and amplitudes. Then, by cancelling the inertia force, if necessary, it is possible to measure the unsteady aerodynamic force only and directly. In the free vibration method, on the other hand, the experimental model is supported elastically with springs and damping devices, and oscillates freely in the flow. Then, the measured pressures are used to evaluate the characteristics of unsteady aerodynamic forces by comparison with those of the static model. One of the advantages of this method is that conventional aeroelastic devices can be used.

In this study, characteristics of unsteady aerodynamic forces on a tall building with an aspect ratio of 9 was investigated using the free vibration method under low-turbulence (LTF) and boundary-layer (BLF) flows. A square section model of 0.07m width and depth and 0.63m height was used, and length and time scales were 1/400 and 1/40 respectively. Surface pressures and tip displacements were measured, and two Scruton numbers Sc were considered only for the BLF.

2! Results and discussion

Figure 1 shows the amplitude dependency of damping ratios of the system. Damping ratios were evaluated using two methods, the logarithmic decrement method (open triangle in Figure 1) and wavelet transform (solid circle in Figure 1). Damping ratios from the wavelet transform are similar to the envelop of damping ratios from the logarithmic decrement method. Damping ratios increase with increasing normalized displacements, showing a maximum value of about 2 ~ 2.2% at $\sigma/B \approx 0.025$ regardless of Scruton number. After reaching the maximum value, the damping ratios decrease with increasing normalized displacements. Increasing tendency of the damping ratios is well known, but it is also pointed out from the full-scale measurement that the damping ratios do not necessarily increase with amplitude continuously. According to Tamura (2012), damping ratios decrease with increasing displacement when the structural elements are not damaged after reaching their maximum. In the experiment, similar tendency was observed.

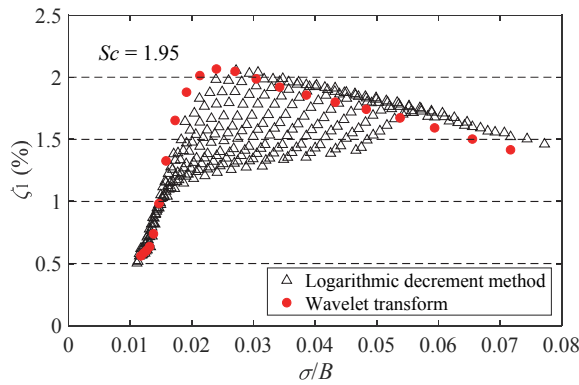


Figure 1. Amplitude dependence of damping ratio

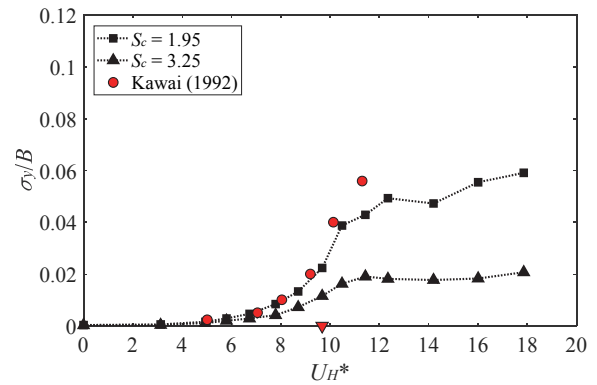


Figure 2. Normalized cross-wind displacements in BLF

Fluctuating displacements increase with normalized velocity, showing the largest slope near the resonant velocity. In Figure 2, the resonant velocity in BLF is 9.7 (red inverse triangle). The fluctuating displacements for small Sc are larger than those for large Sc , and when the Sc is large, the fluctuating displacements become almost constant after $U_H^* = 12$. The present results agree well with previous results (Kawai, 1992).

Figure 3 shows the power spectra of the generalized force coefficients. Vortex shedding components are well identified, but when the normalized velocity is higher than the resonant velocity the system's natural frequency is also clearly observed.

Figure 4 shows the relationship between power spectra of force and displacement through a displacement mechanical function. It is clearly identified that the Strouhal component shown in force disappeared in the displacement, which comes from the characteristics of displacement mechanical function.

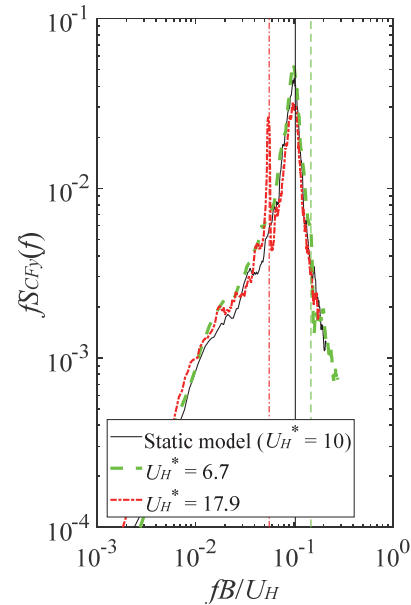


Figure 3. PSD of generalized force in BLF

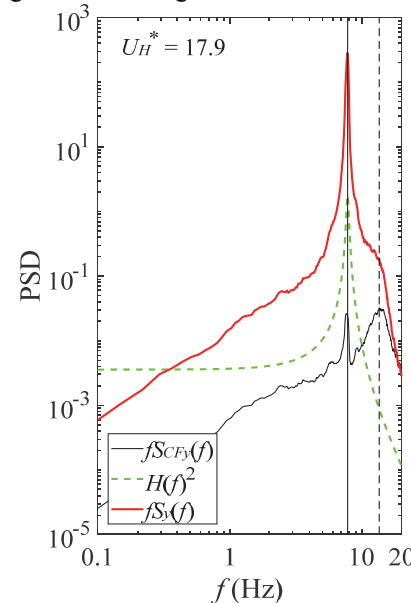


Figure 4. PSD of generalized force and displacement

3! Conclusion

Unsteady aerodynamic forces are well observed near the resonant velocity, and two peaks in power spectra of the generalized force coefficients were observed during the lock-in range, and the reason why the Strouhal component disappears in the power spectra of tip displacement was discussed.

References

Kawai H. (1992). Vortex Induced Vibration of Tall Buildings, *Journal of Wind Engineering and Industrial Aerodynamics* **41-44**, 117-128.

Tamura Y. (2012). Amplitude Dependency of Damping in Buildings and Critical Tip Drift Ratio, *International Journal of High-Rise Building* **1(1)**, 1-13.

Uncertainty quantification in RANS simulations for predicting wind loads on buildings

G. Lamberti¹ and C. Gorlé¹

¹Department of Civil & Environmental Engineering, Stanford University, USA

Corresponding author: G. Lamberti, giacomol@stanford.edu

Abstract

Computational fluid dynamics (CFD) simulations can provide a powerful tool to quantify pressure loads on buildings and assess wind hazards. However, CFD simulations of the atmospheric boundary layer (ABL) can be strongly influenced by uncertainty in the inflow conditions and turbulence model. Uncertainty quantification (UQ) methods can propagate these uncertainties to the quantities of interest to provide predictions for the wind pressure coefficients in terms of mean values and confidence intervals. This presents significantly more meaningful information to designers and engineers than the outcome of a single deterministic CFD simulation.

In the present work we quantify uncertainty in the time-averaged pressure coefficients predicted by RANS simulations of a wind tunnel experiment of a high-rise building. The experiment was originally performed at the wind tunnel of the Politecnico di Milano (PoliMi) (Amerio, L., 2018), and subsequently repeated at the Wall of Wind (WoW) facility of Florida International University (Figure 1). The objective is to predict the distribution of the time-averaged pressure coefficient on the building's lateral facade with 95% confidence intervals, and compare the results to the experimental data.



Figure 1: test section of PoliMi wind tunnel (left) and WoW wind tunnel (right).

The uncertainty in the inflow condition is characterized using 3 uncertain parameters: the reference wind speed, the atmospheric boundary layer (ABL) roughness length, and the model orientation. The uncertainties in these parameters are propagated to the quantities of interest using a polynomial chaos expansion (PCE) approach (Smith, R. C., 2013). The result, shown in Figure 2, shows that the largest discrepancy with the experimental data appears in the regions of flow separation, where uncertainty related to the turbulence model might be dominant. To incorporate quantification of the turbulence model uncertainties, the inflow UQ framework is combined with a method that introduces perturbations in the Reynolds stress tensor (Gorlé et al., 2012; Emory et al., 2013).

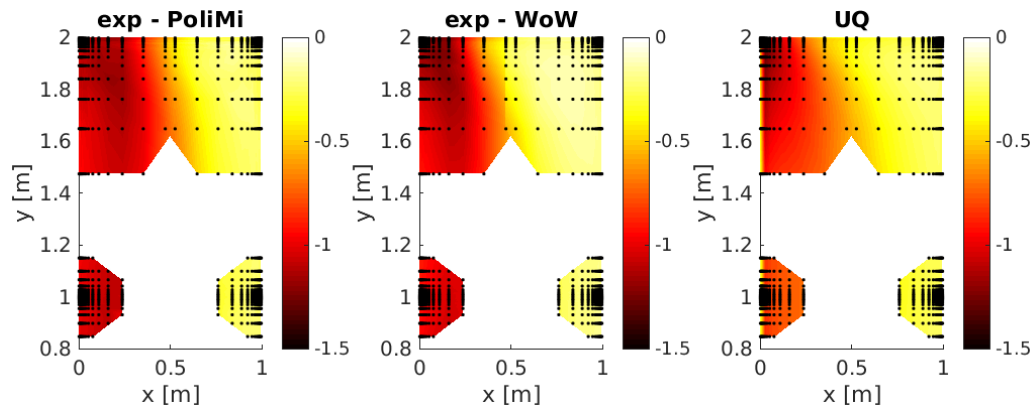


Figure 2: time-averaged pressure coefficient distribution on the building facade: PoliMi data (left), WoW data (center) and mean values from the CFD inflow UQ study (right).

The Reynolds stress perturbations introduced make the turbulence more one- (c1c), two- (c2c), or three- (c3c) component. For each of these perturbations the inflow UQ study is repeated to obtain the results shown in Figure 3. The framework is capable to provide a prediction that encompasses the wind tunnel data, but the uncertainty is rather high. The results confirm that the uncertainty in the turbulence model is dominant in the region of flow separation, while the inflow uncertainty is more significant where the flow is attached. Future work will focus on calculating root mean square and peak pressure distributions from the RANS averaged flow field, and apply the UQ framework to these new quantities of interest.

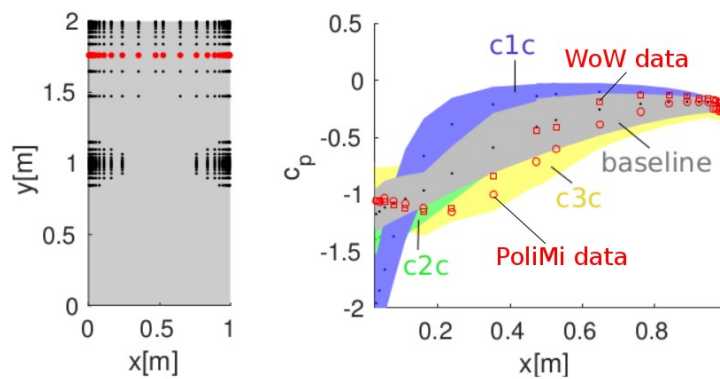


Figure 3: pressure tap locations on the model (left); mean and plausible intervals for the time-averaged pressure coefficient on the row of taps indicated in red (right). The shaded regions indicate the result of the inflow UQ for the baseline and three perturbed simulations.

References

- Amerio, L., 2018. Experimental high resolution analysis of the pressure peaks on a building scale model façades (Ph.D. thesis, unpublished). Milano: s.n.
- Smith, R. C. 2013. Uncertainty quantification: theory, implementation, and applications. Vol.12. SIAM.
- Gorlé, C., Emory, M., Larsson, J., and Iaccarino, G., 2012. Epistemic uncertainty quantification for RANS modeling of the flow over a wavy wall. Center for Turbulence Research, Annual Research Briefs.
- Emory, M., Larsson, J., and Iaccarino, G., 2013. Modeling of structural uncertainties in Reynolds-averaged Navier-Stokes closures. Physics of Fluids 25(11).

Effects of amplitude on the spectral characteristics of motion-induced force for oscillating 5:1 rectangular cylinder

Siyuan Lin¹, Haili Liao¹, Nikolaos Nikitas² and Qi Wang¹

¹Department of Bridge Engineering, School of Civil Engineering, Southwest Jiaotong University, China

²School of Civil Engineering, University of Leeds, UK
Corresponding author: Siyuan Lin, linsiyuan01@gmail.com

Abstract

The 5:1 rectangular cylinder can be seen in lots of engineering applications as a benchmark bluff section. Having a better understanding of the motion-induced force characteristics would be a key to predict post-critical flutter response for bridges and improve our understanding of flutter instabilities. Combined with forced motion test and pressure measurement of the cylinder, the effects of motion amplitude on the 5:1 rectangular cylinders has been investigated in a series of wind tunnel tests. After integrating the pressure on the surface of the cylinder, the motion-induced force can be extracted using the low pass filter. The spectral characteristics of self-excited lift, moment and drag under different amplitudes of single pitching and heaving motion were summarized. It can be found the second order harmonics dominate in all kinds motion type regardless of amplitude. While for the high order harmonics for moment is more prominent than lift. The heaving amplitude has little influence on the high order harmonics in the characteristics of self-excited force. While larger pitching amplitude would increase the high order harmonics nonlinearly.

1 Introduction

Due to the simple geometry of rectangular cylinders with an aspect ratio of 5:1, loads of researches have been done concerning its aerodynamic properties around the world. Under the framework of BARC(Bruno, Salvetti et al. 2014) (Bruno et al, 2014), the aerodynamic coefficients, spanwise correlation of the aerodynamic forces, effects of flow fields on the aerodynamic force and etc. have been investigated by adopting wind tunnel tests or CFD simulations. Even though there are many researches for stationary and oscillating rectangular cylinders (Haan and Kareem 2009; Mannini, Marra et al. 2017), there are few reports on the spectral characteristics of motion-induced force for rectangular cylinders. The goal of the present research work is to investigate experimentally and describe the amplitude effects on the spectral characteristics of motion-induced force for 5:1 rectangular cylinders.

2 Wind tunnel tests

These wind tunnel tests were conducted in the second test section of XNJD-1 wind tunnel, which is a closed circuit low speed wind tunnel located in Southwest Jiaotong University. The model was driven by a forced motion test rig as shown in Fig.1. The pressure around the rectangular cylinder model, which has width of 0.5m and depth of 0.1m (shown in Fig.2), was measured using the Scanivalve DSM 3400 measurement system and ZOC 33/64 PxX2 pressure measurement module.



Fig 1. Forced motion test rig

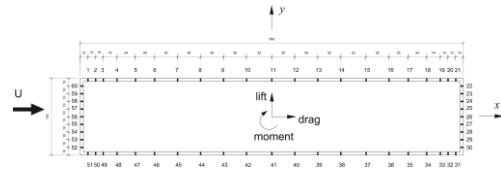


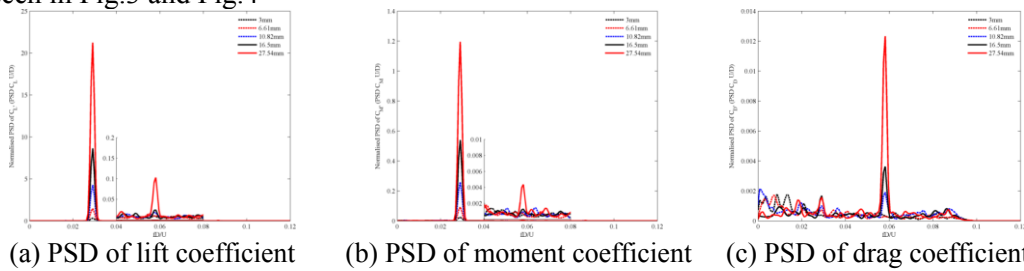
Fig 2. Arrangement of pressure taps around the cylinder

3 Spectral characteristics of motion-induced force

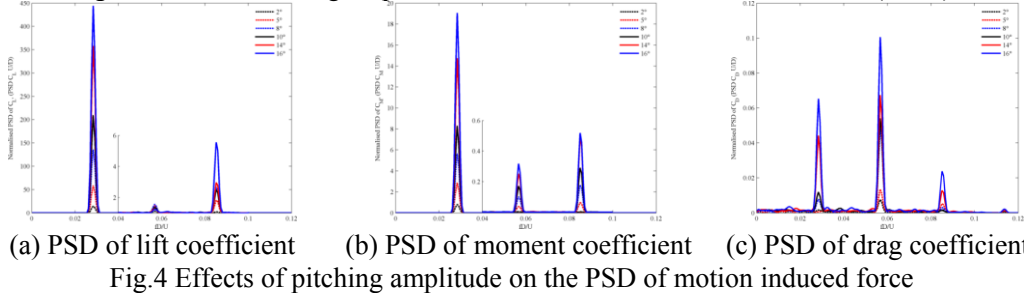
The force from the integration of pressure around the cylinder can be expressed as,

$$F = \bar{F} + \tilde{F} = \bar{F} + F_v + F_m \tag{1}$$

Where \bar{F} the mean is aerodynamic force, F_v is the vortex-induced force and F_m is the motion-induced force. The spectral characteristics of self-excited lift drag and moment can be obtained by performing the FFT with Matlab script. The spectral characteristics under different motion amplitudes can be seen in Fig.3 and Fig.4



(a) PSD of lift coefficient (b) PSD of moment coefficient (c) PSD of drag coefficient
Fig.3 Effects of heaving amplitude on the PSD of motion-induced force(Ur=6)



(a) PSD of lift coefficient (b) PSD of moment coefficient (c) PSD of drag coefficient
Fig.4 Effects of pitching amplitude on the PSD of motion induced force

4 Concluding remarks

The second order harmonics dominate in the drag PSD regardless of the type and amplitude of motion. The increment in heaving motion amplitude contributes less to the high order components in the PSD of lift and moment. Larger amplitude of pitching motion would make high order term in the moment PSD more prominent than the lift PSD, where the odd order component is larger in quantity than even one.

References

Bruno, L., Salvetti, M.V. and Ricciardelli, F. (2014), Benchmark on the Aerodynamics of a Rectangular 5:1 Cylinder: An overview after the first four years of activity, *Journal of Wind Engineering & Industrial Aerodynamics*. **126**(1), 87-106.
 Haan, F.L. and Kareem, A. (2009), Anatomy of Turbulence Effects on the Aerodynamics of an Oscillating Prism, *Journal of Engineering Mechanics*. **135**(9), 987-999.
 Mannini, C., Marra, A.M., Pigolotti, L. and Bartoli, G. (2017), The effects of free-stream turbulence and angle of attack on the aerodynamics of a cylinder with rectangular 5:1 cross section, *Journal of Wind Engineering and Industrial Aerodynamics*. **161** 42-58.

A model extension for vortex-induced vibrations

F. Lupi¹, H.-J. Niemann¹ and R. Höffer¹

¹Faculty of Civil and Environmental Engineering, Department of Wind Engineering and Flow
Mechanics, Ruhr-Universität Bochum, Germany

Corresponding author: F. Lupi, francesca.lupi@rub.de

Abstract

The paper presents free-vibration wind tunnel tests performed at WIST Boundary Layer Wind Tunnel at Ruhr-Universität Bochum (Germany) on a 3D aeroelastic cylindrical model with circular cross-section. The aim of the tests is to validate a model extension to the original spectral method developed by Vickery&Basu in 1983, able to calculate the maximum oscillation of a structure subjected to vortex-induced vibration in the lock-in region. The peculiarity of the extension is the application of an experimental curve for the negative aerodynamic damping. It was previously developed by the authors through forced vibration wind tunnel tests. The model extension is linear. In fact, linear – in case iterative – approaches are usually preferred for the design of structures. However, limitations due to linearization of an intrinsically non-linear phenomenon are unavoidable. Strengths and weaknesses of the linear approach are discussed in the paper.

1 Introduction

This work represents a further development of previous papers written by the authors (Lupi et al., 2017-2018), dealing with modelling vortex resonance. Firstly, wind tunnel experiments in forced vibrations performed at Ruhr-Universität Bochum (Germany) allowed the development of a new aerodynamic damping model. It was then applied to 27 full-scale chimneys with promising results. This paper validates through free-vibration wind tunnel tests the model extension to calculate the maximum oscillation of a structure with circular cross-section subjected to vortex-induced vibration in the lock-in region. It is a linear model, based on the original spectral method developed by Vickery&Basu in 1983. Strengths and weaknesses of the linear approach are discussed in the paper.

2 Wind tunnel tests in free-vibrations

The wind tunnel tests are performed at WIST Boundary Layer Wind Tunnel at Ruhr-Universität Bochum. It is an open circuit wind tunnel with a test section of 1.8 m in width and 1.6 m in height (Figure 1a). The models for free-vibration tests are cantilever beams with circular cross-section. Two models with constant, but different diameters are used: $d_1 = 32$ mm for the model n.1 and $d_2 = 50$ mm for the model n.2 (the latter is shown in Figure 1b). Mass and damping of the models are varied, in order to explore the lock-in region for different Scruton numbers ($Sc = 2.8 \div 22.5$). The experiments are performed in smooth flow with turbulence intensity $I_v = 4.5\%$.

Figure 2 shows some exemplary measurements for $Sc = 17.78$. This relatively high Scruton number shows a typical "intermittent" behaviour in the resonant zone, as shown in the figure. In fact, a stable resonant oscillation only occurs in case of very low mass and damping. The intermittency is caused by the fluctuation of the turbulent wind speed around the mean. Capturing and modelling such a non-linear, quasi-stationary behaviour, a sort of detuning between motion-induced force and natural frequency of the system (see, for example, a similar approach in (Náprstek&Fischer, 2017)) is a challenge and goes beyond the purpose of this paper. Instead, the linear approach described in the

paper reproduces the largest amplitude of oscillation in the lock-in range as function of the Scruton number.

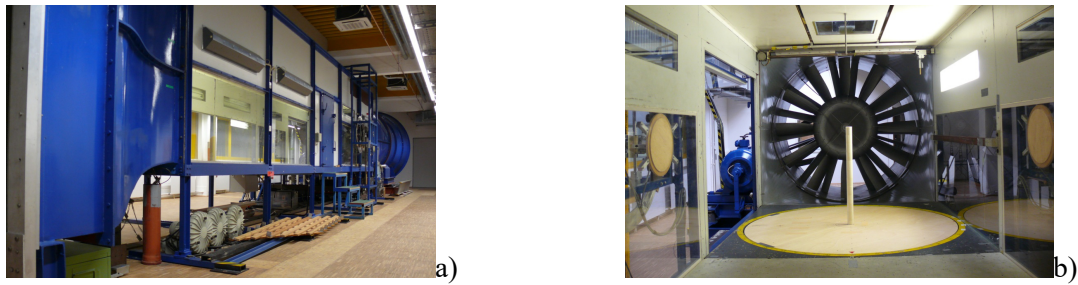


Figure 1. WIST Boudary Layer Wind Tunnel at Ruhr-Universität Bochum, Germany.

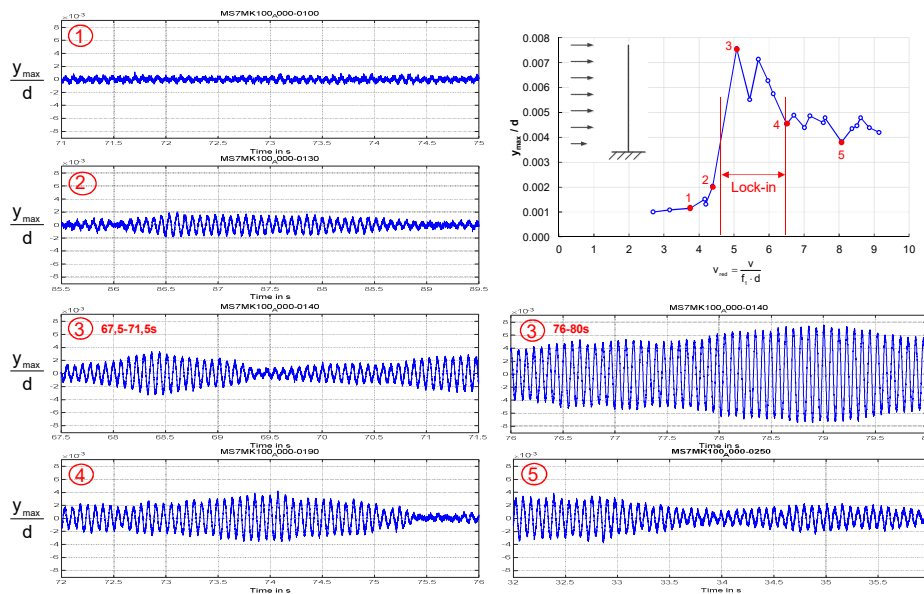


Figure 2. Time histories of tip oscillation, $Sc = 17.78$

3 Acknowledgements

The authors would like to acknowledge the Alexander von Humboldt Foundation (Germany) and the CICIND / International Committee on Industrial Chimneys for the interest and support to this research.

References

- Lupi F., Niemann H.-J., Höffer R. (2017) A novel spectral method for cross-wind vibrations: Application to 27 full-scale chimneys. *Journal of Wind Engineering and Industrial Aerodynamics* **171**, 353-365.
- Lupi F., Niemann H.-J., Höffer R., (2018) Aerodynamic damping model in vortex induced vibrations for wind engineering applications. *Journal of Wind Engineering and Industrial Aerodynamics* (accepted for publication).
- Náprstek J, Fischer C. (2017). Analysis of the quasi-periodic response of a generalized van der Pol nonlinear system in the resonance zone. *Computers and Structures*, <http://dx.doi.org/10.1016/j.compstruc.2017.07.021>
- Vickery B.J., Basu R.I. (1983) Across-wind vibrations of structures of circular cross-section. *Journal of Wind Engineering and Industrial Aerodynamics*, Vol. **12**, 49–97.

Aerodynamic effect of non-uniform turbulent wind profiles for long-span bridges

Tor M. Lystad^{1,2}, Aksel Fenerci² and Ole Øiseth²

¹Bridge Department, Norconsult, Sandvika, Norway

²Department of Structural Engineering, Norwegian University of Science and Technology, Trondheim, Norway

Corresponding author: Tor M. Lystad, tor.martin.lystad@norconsult.com

Abstract

Long-span bridges are often designed based on the assumption of wind field homogeneity. At the Hardanger Bridge the wind field along the bridge span is monitored through 8 triaxial ultrasonic anemometers. Simultaneously recorded profiles for mean wind velocity and turbulence intensity along the span are used to investigate the effect of non-uniform wind profiles on the aerodynamic behaviour of the Hardanger Bridge. Extreme non-uniformity is considered using Monte Carlo simulations to generate extreme, but realistic wind profiles based on the variability of the measured wind field. Girder section forces and aerodynamic stability is considered, and significant effects on the behaviour is found.

1 Introduction

Since 2013 the Norwegian University of Science and Technology has been monitoring the wind field along the Hardanger Bridge girder through 8 triaxial ultrasonic anemometers. The Hardanger Bridge is located in complex terrain, typical for the west coast of Norway. The measured wind field display large non-uniformity along the bridge span, challenging the validity of the homogeneity assumption widely used in bridge aerodynamics.

The effect of idealised non-uniform mean wind velocity profiles on the buffeting response and the aerodynamic stability of long-span bridges were studied by (Arena et al. 2014; Zhang 2007), showing possible significant effects on the aerodynamic behaviour. A non-uniform mean wind velocity profile measured from terrain model wind tunnel tests of the Stonecutters Bridge surroundings was also investigated in (Hu et al. 2017), without any significant impacts to the bridge behaviour. In this paper, non-uniform profiles of mean wind velocity and turbulence intensity measured in full-scale at the Hardanger Bridge site is investigated. A measure of the variability of the recorded non-uniformity is obtained by fitting the measured wind profiles to a chosen shape function using linear regression. Profiles of mean wind velocity and corresponding turbulence intensity is generated through Monte Carlo simulations from the joint probability distribution of the fitted shape function coefficients. The effect of simulated extreme non-uniform wind profiles on the buffeting response and the aerodynamic stability of the Hardanger Bridge are shown.

2 Non-uniform wind profiles

Simultaneously recorded along span profiles of 10-minute mean wind velocity and turbulence intensity from the Hardanger Bridge full-scale measurement program has been used to investigate the effect of wind field inhomogeneity on the aerodynamic bridge response. Only strong wind profiles with a mean wind velocity averaged along the span above 15 m/s are used. The measured mean wind velocity and turbulence intensity profiles are fitted to a shape function consisting of a linear part and a

harmonic part. To be able to compare the effect of the non-uniformity alone, the wind profiles are normalized to be energy equivalent.

Based on the observed shape of the recorded wind profiles, the mean wind velocity can be represented by the following shape function:

$$U(x) = U_0 + a_1 x - a_2 \left[1 - \cos\left(\frac{\pi}{L}\right)\right] \quad (1)$$

where U_0 is the midspan mean wind velocity, L is the span width, a_i are fitted coefficients and $-L/2 \leq x \leq L/2$. Analogously the profile for turbulence intensity can be represented by the following shape function:

$$I(x) = I_0 + b_1 x + b_2 \left[1 - \cos\left(\frac{\pi}{L}\right)\right] \quad (3)$$

where I_0 is the midspan turbulence intensity and b_i are fitted coefficients.

By fitting the recorded wind profiles to the shape functions shown above, an assumed gaussian joint probability distribution of the fitted coefficients can be achieved. Based on this fitted distribution, profiles for mean wind velocity and corresponding turbulence intensity can be generated using Monte Carlo simulations. Simulated profiles for mean wind velocity is shown in Figure 1a and for along wind turbulence intensity in Figure 1b. Extreme non-uniform profiles are highlighted.

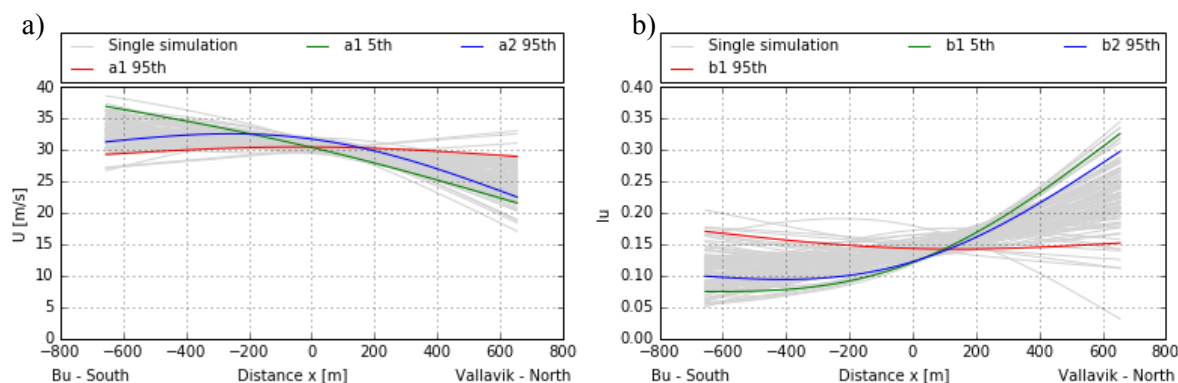


Figure 1. Simulated wind profiles, a) Mean wind velocity, b) Along wind turbulence intensity.

3 Bridge response to extreme wind profiles

The effect of the wind field non-uniformity along the Hardanger Bridge is investigated by calculating the bridge response to simulated extreme non-uniform wind profiles. The response is calculated using a multimodal approach in the frequency domain, adjusted to be able to handle non-uniformity in the mean wind velocity and turbulence intensity. By comparing the response to extreme non-uniform profiles and energy equivalent uniform profiles, differences in girder section forces up to 25 % and effects on the flutter instability limit up to 5 % was found.

4 References

- Arena, A., Lacarbonara, W., Valentine, D. T., and Marzocca, P. (2014). "Aeroelastic behavior of long-span suspension bridges under arbitrary wind profiles." *Journal of Fluids and Structures*, 50, 105–119.
- Hu, L., Xu, Y., Zhu, Q., Guo, A., and Kareem, A. (2017). "Tropical Storm – Induced Buffeting Response of Long-Span Bridges : Enhanced Nonstationary Buffeting Force Model." *Journal of Structural Engineering*, 143(6), 4017027.
- Zhang, X. (2007). "Influence of some factors on the aerodynamic behavior of long-span suspension bridges." *Journal of Wind Engineering and Industrial Aerodynamics*, Elsevier, 95(3), 149–164.

A comparative analysis of construction costs of onshore and shallow- and deep-water offshore wind farms

C. Maienza¹, A.M. Avossa¹, F. Ricciardelli¹, F. Scherillo² and C.T. Georgakis

¹Department of Engineering, University of Campania “Luigi Vanvitelli”, Italy

²Seapower srl, Italy

Department of Engineering, Aarhus University, Denmark

Corresponding author: C. Maienza, carmela.maienza@unicampania.it

Abstract

Capital and operation and maintenance costs (fixed and variable) are the main key parameters of wind power economics. The capital costs of a wind power project are split into several components that, as reported by the International Renewable Energy Agency (IRENA, 2012), are shown in Table 1. In particular, the capital cost of offshore wind projects is almost twice than of onshore wind projects. This higher cost is mainly due to the expensive foundations at sea, due to shipping and construction site setup costs, and to the laying of cables at sea. Moreover, turbines in shallow water and especially in deep water, require additional protection against the harsh marine environment and to corrosion, such to contain maintenance costs. In a typical wind generator, the largest cost is that of the tower, as shown in Table 2 (IRENA, 2012). Then, the other most expensive components of the turbine are the rotor blades and the gearbox which, together with the tower, sum up to 60% of the overall turbine cost.

Table 1. Comparison of capital cost breakdown for typical onshore and offshore, 2011

Capital cost breakdown	Example for detailed cost items	Onshore	Offshore
Capital investment costs (USD/Kw)		1750-2450	3300-5000
Turbine	Keys in hand from manufacturer	65-84%	30-50%
Grid connection	Cabling; Substations	9-14%	15-30%
Construction	Foundation (Onshore and Shallow Water Offshore: fixed tower; Deep Water Offshore: floater, anchoring, mooring); Trasportation; Installation	4-16%	15-25%
Other	Development; Licensing; Consultancy	4-10%	8-30%

Table 2. Example of costs split (%) of a 5 MW RE Power MM92 wind turbine

Tower	26%	Gearbox	13%	Brake system	1%
Rotor blades	22%	Generator	3%	Nacelle housing	1%
Rotor hub	1%	Yaw system	1%	Cables	1%
Rotor bearings	1%	Pitch system	3%	Screws	1%
Main shaft	2%	Power converter	5%	Other	12%
Main frame	3%	Transformer	4%		

According to Brown et al. (2015), wind farms are connected to electricity grids via transmission lines and distribution networks. If the grid connection point is not far from the wind farm (e.g. onshore and shallow water offshore farms), the connection is usually a High Voltage Alternating Current (HVAC) connection. The transmission capability of HVAC system reduces with distance because of dielectric losses, so it is reasonable to use High Voltage Direct Current (HVDC) connections in case of deep water offshore farms (for distances in excess of 50 km), because transmission capability is independent of distance.

In offshore installations, distance and therefore travelling time from holding port to site affect the final cost, as also does the use of purpose-built vessels and cranes. In addition, deep-water offshore

installations turn out to be more expensive than shallow-water ones due to the high cost of construction and installation of the floater, of the mooring lines and of the anchoring system.

According to the International Renewable Energy Agency, operations and maintenance costs (O&M) contribute for around 25-30% to the total costs of a project. Besides, O&M costs are divided into fixed and variable. Fixed costs include administration, insurance, grid access fees and service contracts for scheduled maintenance, whereas variable costs include scheduled and unscheduled maintenance not covered by fixed contracts, replacement of parts and materials. O&M costs for offshore wind farms are significantly higher than for onshore ones, and in particular in the case of deep-water installations. This is due to the higher costs associated with maintenance, both for the difficult accessibility and for the higher expected failure rate of components.

Through the analysis of onshore, shallow- and deep-water offshore turbine projects from the National Renewable Energy Laboratory (NREL, 2015), it is possible to compare the costs split that characterize their economic, and Table 3 shows the percentages of their capital expenditures.

Table 3. Capital expenditures (%) for onshore, shallow. (SW) and deep-water (DW) offshore turbines

Capital expenditures	Examples for detailed cost items	Onshore	Offshore (SW)	Offshore (DW)
Turbine	Tower; Rotor; Nacelle	71,6	31,8	22,1
Development	Progress reports; Quality verification	0,9	1,4	1
Engineering & Management	Design process; Administration; Consultancy fees	1,1	1,6	2,2
Substructure & Foundation	Fixed; Floater, Anchoring and Mooring	3,5	14,7	36,2
Site Access, Port & Staging	Site preparation; Creation of access roads; Use of vessels	2,8	0,5	0,6
Assembly & Installation	Construction site and equipment	2,5	19,3	11,1
Plant Commissioning	Electrical tests	/	0,8	0,8
Electrical infrastructure	Transmission and integration systems; Export cable	8,8	8,6	10,5
Contingency	Loss of generator; Failure of a transmission line	6	6,4	6,4
Construction Finance	Loans	2,9	8,7	7
Insurance	Business interruption; Transit physical-damage coverage	/	1	1
Decommissioning	Disassembly of the wind farm	/	5,1	1,2

For the onshore case, reference is made to the average characteristics of 68 wind farm projects completed in 2015 in the United States; these include several hundreds of 2 MW turbines. For the offshore, shallow-water case, reference is made to the average characteristics of 14 wind farm projects completed in 2015 in the United States; the average turbine capacity of the turbines was 4.14 MW. Finally, for the offshore deep-water case, capital expenditures were formulated based on a combination of empirical data and scalability ratios.

Within this topic, the aim of the paper is to highlight the typical costs of different wind farms, through a specific analysis of the aspects that characterize the wind economy. Moreover, a comparative analysis of the costs affecting the various typologies of wind turbines and the main economic key parameters will be carried out to evaluate the best hypothetical field of investment. This is the counterpart of the wind resource available, that can be drawn from mean wind maps. Comparison of resource and installation costs in the three different situations considered gives a picture of the possible evolution of the wind energy industry for the years to come.

References

Brown, C., Poudineh, R. and Foley, B. (2015). *Achieving a cost-competitive offshore wind power industry: What is the most effective policy framework?*, Oies paper EL 15, Oxford Institute for Energy Studies.

International Renewable Energy Agency (IRENA) (2012). *Renewable Energy technologies: cost analysis serie*. Volume 1: Power sector, Issue 5.5. Wind Power

National Renewable Energy Laboratory (NREL) (2015). *2015 Cost of Wind Energy Review*

A numerical analysis of different approaches for rotation modelling on the aerodynamic drag of a spoked cycling wheel

Fabio Malizia¹, Hamid Montazeri^{1,2} and Bert Blocken^{1,2}

¹ Building Physics Section, Department of Civil Engineering, KU Leuven, Kasteelpark Arenberg 40 - bus 2447, 3001 Leuven, Belgium

² Building Physics and Services, Department of the Built Environment, Eindhoven University of Technology, P.O. Box 513, 5600 MB Eindhoven, The Netherlands

Corresponding author: Fabio Malizia, fabio.malizia@kuleuven.be

Abstract

Wheels account for about 10% of the total aerodynamic drag of a cyclist. While different types of wheels are commercially available, spoked wheels are commonly used in cycling races. This paper presents computational fluid dynamics (CFD) simulations of spoked wheels, and systematically evaluates different boundary conditions that are usually used for rotation modelling of wheels, namely (i) rotational moving wall, (ii) moving reference frame (MRF) and (iii) sliding mesh. Steady and unsteady Reynolds-Averaged Navier-Stokes (RANS) CFD simulations are thus performed for an isolated wheel. Moreover, the impact of the volume enclosing the wheel, where the MRF is applied, on the predicted wheel drag is evaluated. The evaluation is based on validation with wind-tunnel measurements of force coefficients. The results of this study can be used for accurate CFD simulations of cyclist aerodynamics.

1 Introduction

In the 2017 Tour de France, 10 different manufacturers provided the wheels for the 22 teams in the race (Arthur, 2017), while each manufacturer had several wheels in their catalogue. The wheels are selected among the large variety of commercially available options based on their performance in terms of aerodynamic drag, weight, inertia and stiffness (Kyle, 1995). The aerodynamic performance of wheels is of significant importance since the drag of both wheels is responsible for about 10% of the total cyclist resistance (Greenwell et al., 1995). It is usually evaluated using wind-tunnel tests (Greenwell et al., 1995; Kyle, 1995, 1991; Tew and Sayers, 1999) and more recently using CFD simulations (Godo et al., 2010).

CFD is capable of computing forces and moments acting on each single wheel's component (rim, tyre, spokes and hub) and providing fundamental information that can be used by designers to improve the aerodynamic performance of wheels. Nevertheless, one critical aspect in the CFD simulations of wheels is appropriate rotation modelling approaches. To the best of our knowledge, the impact of different rotation modelling approaches on the accuracy of CFD simulations of cycling wheel aerodynamics has not yet been investigated.

2 Methodology

In this study, CFD simulations are first validated with the wind-tunnel measurements by Tew and Sayers (1999). The Campagnolo Shamal wheel has a 19 mm rim width and a 61 mm depth, spanning from the tyre to the rim edges (Fig. 1a). The spoke's cross section is approximated to a rectangle of 3 mm × 1 mm (Fig. 1b). The computational domain has a cross-section of 8.6 m × 7.8 m. The upstream and downstream length of the domain are 3.9 m and 7.4 m, respectively. The computational grid consists of about 13.2 million cells, while about 246,000 surface cells are used on the wheel (Fig. 1b). The mean

velocity inlet boundary condition is a uniform profile (48 km/h), accordingly to the experiment (Tew and Sayers, 1999). The 3D RANS equations are solved in combination with the $k-\omega$ SST turbulence model. It should be noted that the good performance of the $k-\omega$ SST turbulence model has been already shown in previous studies on cycling aerodynamics, e.g. Defraeye et al. (2010).

Three approaches are evaluated to model the rotation of the wheel: (i) the rotational wall approach (RW), (ii) the moving reference frame approach (MRF) and (iii) the sliding mesh approach (SM). The latter two methods are applied on a volume surrounding the wheel, as shown in Fig. 1a and Fig. 1c. Moreover, the impact of the volume enclosing the wheel, where the MRF is applied, on the predicted wheel drag is evaluated. (Fig. 1c).

3 Results

The CFD results show a good agreement with the wind-tunnel results in terms of the drag coefficient with a deviation of about 1.8 % at 0° yaw angle. Further and more detailed information about the different approaches will be provided in the full paper.

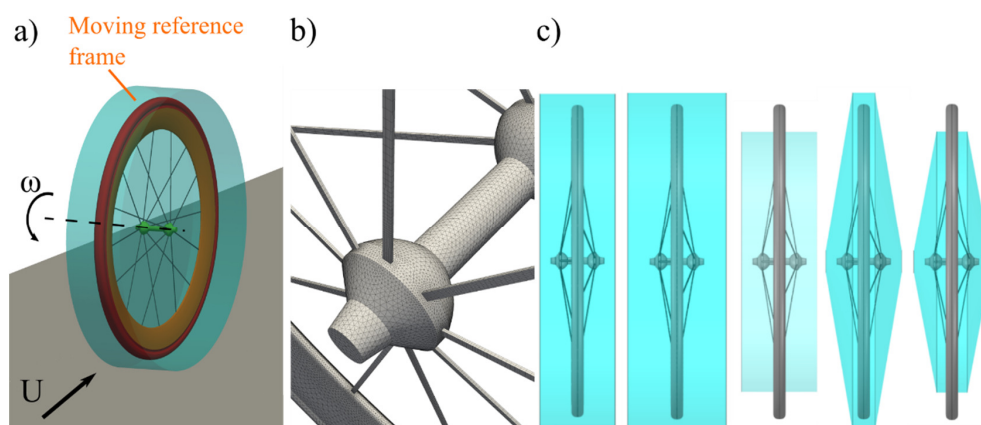


Figure 1 a) volume enclosing the spoked wheel where the moving reference frame condition is applied; b) part of the computational grid; c) different volumes (light blue) around the wheel, where the MRF can be applied.

References

- Arthur, D., 2017. Tour de France bikes 2017 [WWW Document]. URL <http://road.cc/content/feature/224475-tour-de-france-bikes-2017> (accessed 12.29.17).
- Defraeye, T., Blocken, B., Koninckx, E., Hespel, P., Carmeliet, J., 2010. Computational fluid dynamics analysis of cyclist aerodynamics: Performance of different turbulence-modelling and boundary-layer modelling approaches. *J. Biomech.* 43, 2281–2287.
- Godo, M., Corson, D., Legensky, S., 2010. A Comparative Aerodynamic Study of Commercial Bicycle Wheels using CFD. 48th AIAA Aerosp. Sci. Meet. Incl. New Horizons Forum Aerosp. Expo. 35, 1–31.
- Greenwell, D.I., Wood, N.J., Bridge, E.K.L., Addy, R.J., 1995. Aerodynamic characteristics of low-drag bicycle wheels. *Aeronaut. J.* 99, 109–120.
- Kyle, C.R., 1995. Aero wheel performance. *Cycl. Sci.*
- Kyle, C.R., 1991. New aero wheel tests. *Cycl. Sci.* 27–30.
- Tew, G.S., Sayers, A.T., 1999. Aerodynamics of yawed racing cycle wheels. *J. Wind Eng. Ind. Aerodyn.* 82, 209–222. [https://doi.org/10.1016/S0167-6105\(99\)00034-3](https://doi.org/10.1016/S0167-6105(99)00034-3)

Some topics about wind engineering that Curtain Walling design might be longing for in standards

Giampiero Manara¹

¹Department of Structural and Building Physics Analysis, Permasteelisa S.p.A, Italy

Corresponding author: g.manara@permasteelisagroup.com

1 Introduction

Curtain walling (CW) is assuming a leading role in tall building architectural design.

From a structural standpoint, the wind action is the main loading condition, governing all the dimensioning of any CW single component. The wind action is sensitive, in turn, to any CW local shape discontinuity, which may magnify the load intensity on a micro-scale. As a matter of fact, a peculiarity of CW engineering is that the structural safety check must take care both of macro and micro conditions. As far as wind loads are concerned, the structural engineer has to cope with some common issues:

- to define wind loads either during an initial tender phase, when no wind tunnel test has been developed yet, or for a building that will never have a wind tunnel test;
- to define wind loads on components that have not been simulated in the wind tunnel model.

Published standards are the only support to this activity, but this presentation will show some frequent cases that are still missing in standards. Examples from the everyday design work will be shown.

2 Canopies and sunshades projecting from façades

Canopies are frequently added to façades, to shield the building entrance, and the façade itself influences the wind action on canopies.

They can be placed at different heights along the building surface and with different orientations as far as the wind direction is concerned.

These conditions can produce completely different loads, as reported by N.J. Cook in his book [1] and shown in the figure here below.

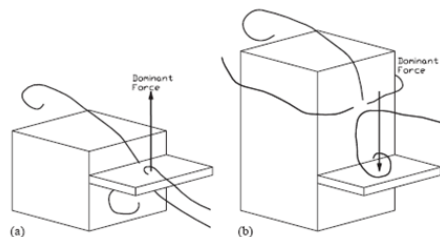


Figure 1. Wind action on canopies at different heights of a façade (N.J. Cook).

Only the German National Annex to the EN 1991-1-4 (Eurocode 1 about wind) and the Swiss norm SIA 261 include some data about these components, but they consider just a limited scenario of cases.

The general text of Eurocode 1 ignores canopies, as like as the ASCE-7 (US standard) does.

Sunshades have become essential on façades, for energy reasons. They can have dimensions, orientations (horizontal, vertical, inclined), positions, gaps from the façade (i.e. space between the element and the surface of the façade), and distance between them, extremely variable. Each of these parameters can influence the pressure coefficient. There are few studies on this type of elements and no mention in the standards.

3 Buildings with rounded corners

The wind action analysis of cylindrical buildings having a circular cross section is supported by clear rules in the Eurocode 1, based on Reynolds' number. On the other hand, if we are dealing with non-circular buildings having locally rounded corners, no rule can be found in the standards.

A plan view of a non-circular building featuring rounded corners is shown in the following sketch.

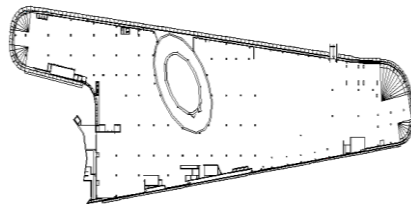


Figure 2. Non-circular building having rounded corners.

No true circular cylindrical shape can be defined in this case, but experience has taught that certain rounded areas can give rise to strong effects of wind suction, very similar to those of circular cylindrical buildings, whereas others can produce opposite results.

Rounded corners are very frequent in modern architecture, but no hint can be found in the standards.

4 Correlation of peak values at the building corners

It is well known that building corners can give rise to strong local alterations in the wind flow, with intense suction effects, but positive pressures as well. However, it is also known that the pressure values on the two sides of the corner do not all reach their peak at the same instant, because of lack of correlation.

On consequence, combination factors could be defined to decrease the combined effect, but this is not regulated in any current standard.

5 Pressure on cladding elements with more than one skin

Wind load sharing in double skin cladding elements is a complex topic. This involves not only double skin façades having two glazed surfaces, but also shadow box elements whenever any ventilation hole has been opened, ventilated cladding etc.. Eurocode EN 1991-1-4 gives some guidance, at clause §7.2.10, but this proved to be very poor, compared to the actual possible configurations. Some recent in-house tests on shadow box panels have shown unexpected results, although the test procedure should be carefully questioned.

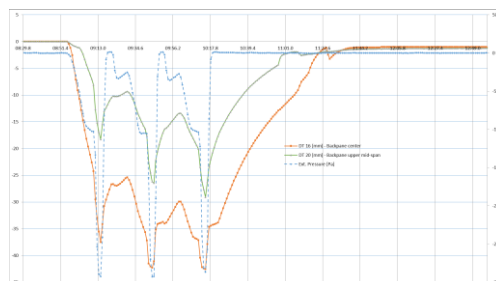


Figure 3. Applied pressure & displacement at panel centre vs. time.

References

Cook N. J., (1990). *The designer's guide to wind loading of building structures. Part 2: static structures*. Building Research Establishment Report, Butterworths.

Numerical investigation of transverse galloping in turbulent flow

Claudio Mannini¹

¹Department of Civil and Environmental Engineering, University of Florence, Italy

Corresponding author: Claudio Mannini, claudio.mannini@unifi.it

Abstract

This paper attempts to model the complicated effects of incoming turbulence on the unsteady galloping instability of a rectangular cylinder, which arises due to the interference of vortex-induced vibration and quasi-steady galloping. As a first step, a purely quasi-steady nonlinear model is considered. Then, a modified version of the nonlinear wake-oscillator model proposed between the 70's and the 80's by Prof. Y. Tamura is considered. In both cases, turbulence is included in the model by synthesizing a random field of partially-correlated flow velocity fluctuations.

1 Introduction

Slender bluff bodies immersed in an airstream and allowed to vibrate in the transverse degree of freedom can be prone to vortex-induced vibration (VIV) and galloping. If the mass-damping parameter is sufficiently low, the ranges of excitation of the two phenomena tend to approach, and a peculiar type of instability occurs, which one may call “unsteady galloping”. In this case, large amplitude of vibration are exhibited in a range of flow speed where no excitation is predicted by the classical theories of VIV and galloping (Mannini et al., 2014). This phenomenon was shown to be an issue for rectangular cylinders with a cross-sectional side ratio close to one.

While the main characteristics of unsteady galloping are now fairly clear in smooth flow (Mannini et al., 2016, 2018a), a recent experimental wind tunnel campaign in various turbulent flows underscored a complicated behaviour of a rectangular cylinder with a side ratio of 1.5. In particular, several features still need to be understood, such as the progressive delay of the instability onset beyond the vortex-resonance flow velocity (Mannini et al., 2018b). Free-stream turbulence also seems to be able to interact in a nonlinear way with the unsteady wake and with the quasi-steady wake undulations, transferring energy from the vortex shedding frequency to the natural frequency, thereby promoting the onset of sustained vibrations at flow speeds significantly lower than the quasi-steady galloping threshold.

In the present work, the effect of turbulence on the galloping instability of a rectangular cylinder is studied through numerical analyses, focusing on the unsteady features of the phenomenon.

2 Quasi-steady approach

As a first step, the contribution of turbulence is included in a purely quasi-steady nonlinear model, where the transverse force per unit length at the spanwise station z can be expressed as:

$$F_y(z, t) = \frac{1}{2} \rho [V + u(t)]^2 DC_{F_y}(\alpha) \quad (1)$$

$$C_{F_y}(\alpha) = -\sec(\alpha) [C_L(\alpha) + C_D(\alpha) \tan(\alpha)] \quad (2)$$

$$\alpha(t) = \text{atan} \left[\frac{w(t) + \dot{y}}{V + u(t)} \right] \quad (3)$$

where ρ is the air density, D the cross-wind section dimension of the cylinder; V the mean wind speed, $u(t)$ and $w(t)$ the longitudinal and vertical turbulent velocity fluctuations respectively; α the apparent angle of attack; C_L , C_D and C_{Fy} the lift, drag and transverse force coefficients respectively; y denotes the transverse direction, and the overdot the derivative with respect to time t .

A partially correlated vectorial random field of velocity fluctuations is synthesized following the Weighted-Amplitude Wave Superposition method, and time-domain calculations are performed. The first results show the tendency of the unsteady flow to mitigate the galloping instability, in a way that has not been observed in the experiments indeed.

3 Nonlinear wake-oscillator model

In a second step, the contribution of turbulence is considered in a nonlinear wake-oscillator model, originally proposed by Tamura and Matsui (1979) for a two-dimensional circular cylinder, then extended to the case of an elastic continuous beam by Tamura and Amano (1983), and finally applied to the case of an elastically-suspended rigid square cylinder by Tamura and Shimada (1987). The modified version of such a model has recently been proved to capture the main features of the interference of VIV and galloping in a smooth airflow (Mannini et al., 2018a). An appealing feature of this model is the fact that it is built on some physical bases, and consequently all the parameters have a clear physical meaning.

Once again, turbulence is included in the nonlinear differential equations of the model according to a quasi-steady perspective, employing the synthetic random field of partially-correlated flow velocity fluctuations. The steady force coefficients measured both in smooth and in turbulent flow are employed. The roles of external and parametric excitation are emphasized.

The first results reveal that the model is able to predict a reduction of the oscillation amplitude due to incoming turbulence. Nevertheless, it does not seem able to explain the delay of the instability onset observed in the experiments in turbulent flow.

References

- Mannini, C., Marra, A. M., and Bartoli, G. (2014). VIV-galloping instability of rectangular cylinders: Review and new experiments. *Journal of Wind Engineering Industrial Aerodynamics* **132**, 109–124.
- Mannini, C., Marra, A. M., Massai, T., and Bartoli, G. (2016). Interference of vortex-induced vibration and transverse galloping for a rectangular cylinder. *Journal of Fluids and Structures* **66**, 403–423.
- Mannini, C., Massai, T., and Marra, A. M. (2018a). Modeling the interference of vortex-induced vibration and galloping for a slender rectangular prism. *Journal of Sound and Vibration* (in press).
- Mannini, C., Massai, T., and Marra, A. M. (2018b). Unsteady galloping of a rectangular cylinder in turbulent flow. *Journal of Wind Engineering Industrial Aerodynamics* **173**, 210–226.
- Tamura, Y., and Matsui, G. (1979). Wake-oscillator model of vortex-induced oscillation of circular cylinder. *5th International Conference on Wind Engineering, Jul. 8-14, Forth Collins, US, pp. 1085–1094*.
- Tamura, Y., and Amano, A. (1983). Mathematical model for vortex-induced oscillations of continuous systems with circular cross section. *Journal of Wind Engineering Industrial Aerodynamics* **14** (1-3), 431–442.
- Tamura, Y., and Shimada, K. (1987). A mathematical model for the transverse oscillations of square cylinders. *1st International Conference on Flow-Induced Vibration, May 12-14, Bowness-on-Windermere, UK, pp. 267–276*.

Flow separation delay and drag reduction through contoured transverse grooves

A. Mariotti¹, G. Buresti¹ and M.V. Salvetti¹

¹Dipartimento di Ingegneria Civile e Industriale, Università di Pisa, Italy

Corresponding author: A. Mariotti, alessandro.mariotti@for.unipi.it

Abstract

The results of several investigations aimed at assessing the performance of contoured transverse grooves as a method to delay flow separation are described. The physical mechanism at the basis of this passive technique is the local relaxation of the no-slip boundary condition, with a consequent reduction of the viscous losses and an increase of the downstream near-wall momentum. Numerical simulations and experiments showed that the application of one groove transverse to the flow direction may delay boundary layer separation both in laminar and turbulent conditions. As a consequence, significant increases of the pressure recovery in plane diffusers and decreases of the drag of boat-tailed axisymmetric and two-dimensional bluff bodies were obtained. It is shown that robust configurations may be devised provided the shape and dimension of the grooves are suitably chosen in order to assure the appearance of steady and stable local flow recirculations.

1 Geometry and physical mechanism

The delay of boundary layer separation over curved solid surfaces immersed in internal or external flows is of great importance in many engineering applications in order to attain desired characteristics of the aerodynamic forces. Different techniques may be used to achieve this objective, and the present one belongs to the class of passive control methods. The idea is to introduce a small and suitably-shaped cavity transverse to the flow (i.e. a “contoured transverse groove”) to produce a local steady and stable flow recirculation, avoiding the necessity of any active stabilization method and producing on the outer flow an effect that is analogous to a local relaxation of the no-slip boundary condition.

The geometry of a typical groove, shown in Figure 1, is characterized by the presence of an initial sharp edge and semi-elliptical contour – in order to fix and promote the start of the desired local recirculation region – and by a final spline tangential to the basic surface. The chosen shape avoids the presence of sources of local perturbations, such as, e.g., downstream sharp edges; however, to assure the steadiness of the flow and the absence of cavity oscillations, the depth of the groove must be definitely smaller than the thickness of the incoming boundary layer. Referring to Figure 1, the parameters defining the geometry of a groove are the starting point, s , the total length, t , the depth h , and the length of the ellipse axis in the streamwise direction, a .

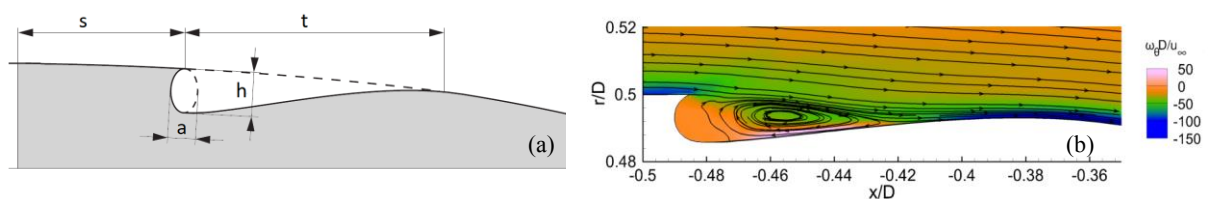


Figure 1. Sketch of the groove geometry (a); mean velocity streamlines and vorticity field in the groove region (b)

2 Main results and conclusions

The use of contoured grooves as a passive flow control method has been successfully assessed for both internal and external flow. In our previous works, the grooves introduced in the diverging walls of plane diffusers were found to significantly reduce flow separation and to increase the pressure recovery (see e.g. Mariotti et al., 2015, and the references herein).

As for external flows, the method is found to be effective to reduce the drag of axisymmetric boat-tailed bluff bodies (see e.g. Mariotti et al., 2017) and two-dimensional ones. In both cases the considered geometry has a cross-section with a 3:1 elliptical forebody and a rectangular main part followed by a circular-arc boat tail; the Reynolds number, based on the body length and freestream velocity, is $Re=lu_\infty/\nu = 5.5 \times 10^5$. The wake of the axisymmetric configuration is characterized by the shedding of hairpin vortices and the two-dimensional one by a strong alternate vortex shedding. When no groove is present, the boat-tail geometries imply flow separation along their lateral surface. As demonstrated by wind tunnel tests and Large Eddy Simulations, the introduction of one suitably contoured transverse groove on the lateral wall produces a significant boat-tail drag reduction (of the order of 9.7% for the 2D case and up to 29% for the axisymmetric one) due to a significant delay of the flow separation and a consequent increase of the base pressure (see for instance Figure 2). Moreover, the wake width is reduced, as can be seen for a two-dimensional case in Figure 3; consequently, the Strouhal number related to the vortex shedding is increased.

As expected, the flow within the grooves is found to be steady and the separation-delay effect to be connected with the enhanced near-wall momentum present in the boundary layers immediately downstream of the grooves.

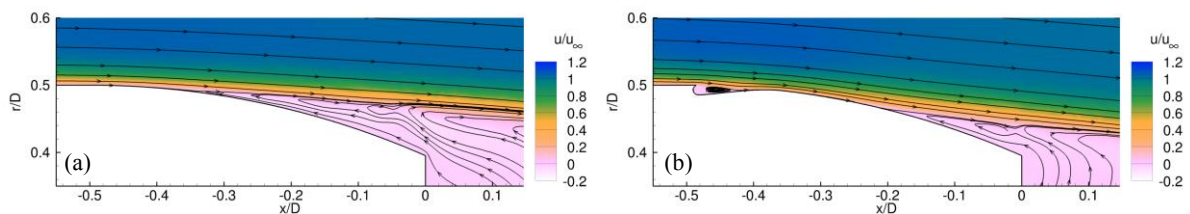


Figure 2. Mean velocity streamlines and streamwise velocity field for an axisymmetric boat-tailed bluff body: reference boat tail (a) and boat tail with groove (b).

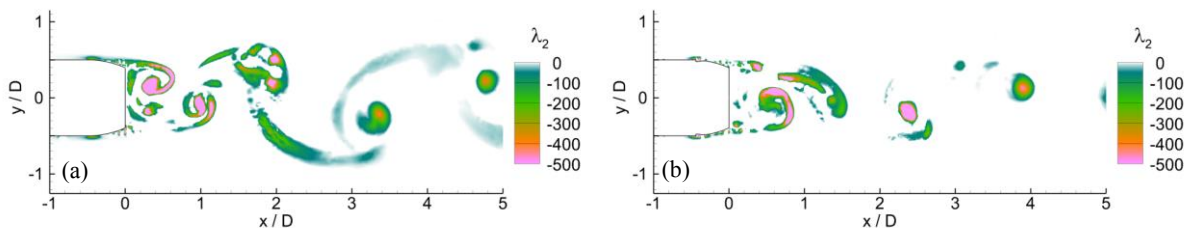


Figure 3. Vortex indicator on the plane $z/D=0$ downstream of a two-dimensional boat-tailed bluff body: reference boat tail (a) and boat tail with groove (b).

3 References

- Mariotti, A., Buresti, G., and Salvetti, M. V. (2015). Use of multiple local recirculations to increase the efficiency in diffusers. *Eur. J. Mech. B/Fluids* **50**, 27–37.
- Mariotti, A., Buresti, G., Gaggini G., and Salvetti, M. V. (2017). Separation control and drag reduction for boat-tailed axisymmetric bodies through contoured transverse grooves. *Journal of Fluid Mechanics* **832**, 514–549.

Experimental Study on the Effect of Secondary Vortices at Trailing Edge on Motion-Induced Excitation

Kazutoshi Matsuda¹, Kusuo Kato¹, Nade Cao¹ and Ryoya Higashimura¹

¹Department of Civil Engineering and Architecture, Kyushu Institute of Technology, Japan¹

Corresponding author: Kazutoshi Matsuda, matsuda@civil.kyutech.ac.jp

Abstract

According to the results of conventional wind tunnel tests on rectangular cross sections with side ratios of $B/D=2-8$ (B : along-wind length (m), D : cross-wind length (m)), motion-induced vortex excitation was confirmed. The generation of motion-induced vortex excitation is considered to be caused by the unification of separated vortices from the leading edge and secondary vortices at the trailing edge. Spring-supported test for $B/D=1.18$ was conducted in a wind tunnel at Kyushu Institute of Technology. Critical wind speeds were confirmed around reduced wind speeds $V_r=V/fD=2$ and $V_r=8$ (V : wind speed (m/s), f : natural frequency (Hz)). Because the reduced critical wind speed in motion-induced vortex excitation is calculated as $V_r=1.67 \times B/D=1.67 \times 1.18=2.0$, vibrations around $V_r=2$ were considered to be motion-induced vortex excitation. In this study, smoke flow visualizations were performed for side ratios of $B/D=0.5-6.0$ in order to find out the relation between side ratios of rectangular cross sections and secondary vortices at trailing edge in motion-induced vortex excitation. Spring-supported tests were also carried out in order to obtain the response characteristics of the models.

1 Introduction

According to Shiraishi and Matsumoto (1983), the vortices separated from rectangular cross sections in wind tunnel tests are broadly classified into Kármán vortices and motion-induced vortices (vortices separated from the leading edge). Kármán vortices are accompanied by interference of the two separated shear layers at both the top and bottom surfaces of the structures. Motion-induced vortices are shed separately from the leading edges of the top and bottom surfaces, because the separated shear layers at the top and bottom surfaces are excited alternately due to the vibration of the rectangular cross section. In order to clarify the relation between the generation of motion-induced vortex and the side ratios B/D , a visualization test for the smoke flows around the cross section was performed by providing a forced oscillation on models of the rectangular cross sections of $B/D=0.50-6.0$. By conducting a smoke flow visualization test, this research aims to clarify in what cases the secondary vortex at the trailing edge forms on the cross sections where the motion-induced vortex excitation was recognized. Moreover, based on the results, this research aimed to verify whether or not the secondary vortex at the trailing edge is essential for the generation of motion-induced vortex excitation.

2 Experimental Setup

Smoke flow visualizations around the model during oscillating condition were conducted in a small-sized wind tunnel (0.4m high \times 0.4m wide \times 2.0m long) at Kyushu Institute of Technology. Figures 1 and 2 show the schematic illustration of experimental setup for smoke flow visualization and the forced oscillation system, respectively. Spring-supported tests were also performed in order to get the response characteristics of the models.

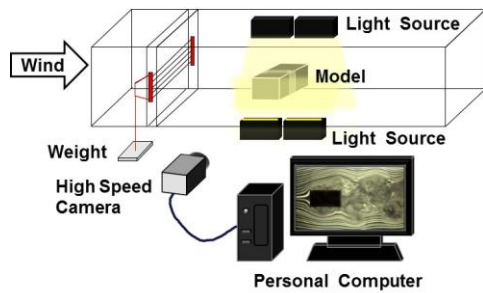


Figure 1. Schematic illustration of experimental setup for smoke flow visualization

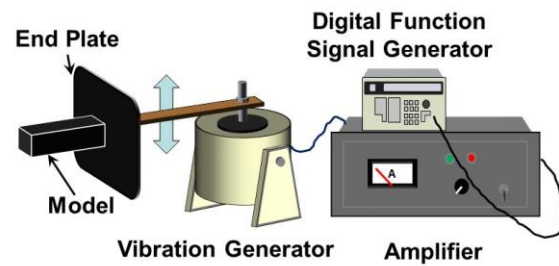


Figure 2. Forced oscillation system

3 Experimental Results and Discussion

Figure 3 shows a typical wind tunnel test result. Though the secondary vortex at the trailing edge for the model with a side ratio of $B/D=1.0$ was recognized at the amplitude more than $2\eta/D=0.06$ as shown in Figure 3(a), based on the spring-supported test of this model shown in Figure 3(b), the motion-induced vortex excitation was observed to form at an amplitude of less than $2\eta/D=0.06$ at a reduced wind speed of 1.67. There was a hysteretic behaviour observed in between $V_r=2.3$ and $V_r=2.8$. It is clear that the generation probability for the secondary vortex at the trailing edge tends to gradually increase, as the amplitude of oscillation becomes larger. The same goes for $B/D=0.5-1.5$. The results for $B/D=2.0, 4.0$ and 6.0 will be shown in the full paper.

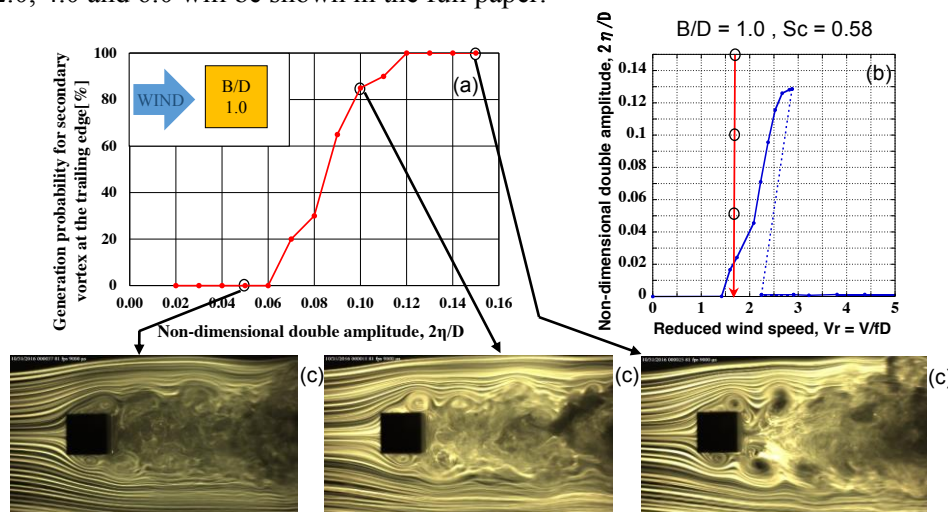


Figure 3 $B/D=1.0$, (a) Generation probability for secondary vortex at the trailing edge at $V_r=1.7$, (b) Relation between V_r and $2\eta/D$, (c) Flow visualization test results of forced-oscillating model at the top displacement

4 Conclusions

At a critical wind speed of the motion-induced vortex excitation of the cross sections whose side ratio is $B/D=0.62-1.5$, there are amplitude ranges where the secondary vortex at the trailing edge does not form clearly. Therefore, it is considered that the secondary vortex at the trailing edge is not always essential for the generation of the motion-induced vortex excitation of each cross section.

References

- Shiraishi, N., and Matsumoto, M. (1983). On classification of vortex-induced oscillation and its application for bridge structures, *Journal of Wind Engineering and Industrial Aerodynamics* 14, 1-3, 419-430.

Wind-wave loading and response of OWT monopiles in rough seas

Agota Mockutė¹, Claudio Borri¹, Enzo Marino¹ and Claudio Lugni²

¹Department of Civil and Environmental Engineering, University of Florence, Italy

²CNR-INSEAN – Maritime Research Institute - National Research Council, Italy

Corresponding author: Agota Mockutė, amockute@dicea.unifi.it

Abstract

The increasing size of offshore wind turbines makes them more susceptible to the effects of wave nonlinearities which may lead to dangerous resonant amplifications that are still not fully understood. This study focuses on the comparison of three hydrodynamic loading models – Morison equation, slender-body theory and FNV theory – to be used in hydro-aero-elastic models predicting the dynamic response of a monopile-supported offshore wind turbine in very rough seas. Preliminary findings on fixed monopile show that all three models perform equally well in capturing the peak loading even in very steep waves but all omit the highly nonlinear secondary loading cycle which used to be associated with ringing – a dangerous dynamic amplification of the response. Nonetheless, recent studies show that the two phenomena are not directly linked, therefore the dynamic response of the structure is currently being studied.

1 Introduction

Wind energy has become an important player in the energy sector, but with more accurate hydrodynamic loading modelling the price of the substructure could be driven down. As the size of the offshore wind turbines (OWTs) grows, their natural frequencies lower and are likely to match third order wave frequencies, which may prompt dangerous nonlinear resonant amplifications, known as ringing. In this study three hydrodynamic loading models – Morison equation, slender-body theory, and FNV theory – are compared in rough seas. To understand the importance of nonlinearities and to contribute to a better understanding of these complex phenomena the study is first assessing the models on a fixed cylinder in steep regular waves before considering the dynamic structural response.

2 Methodology

The combined wind-wave action and the global system response in the final phase is to be computed by coupling aero-hydro-servo-elastic simulator FAST and the hydrodynamic models used in this study. The wave kinematics are modelled as linear, 2nd, 3rd and 5th Order Stokes and Fourier approximation. Fully nonlinear wave kinematics are simulated with second order Boundary Element Method model, initiated directly with nonlinear analytic Rienecker-Fenton theory. The three compared hydrodynamic loading models are: Morison equation consisting of linear inertia (M) and quadratic drag (d); slender-body theory suggesting three slender-body terms (A , I , D) to correct Morison inertia term to third order; and FNV (Faltinsen-Newman-Vinje) perturbation theory derived directly to third order.

3 Results and Discussion

First the case of fixed rigid cylinder was analysed, where the highly nonlinear secondary load cycle (slc) has been observed. Numerous experiments were recreated numerically and here we report only Stansberg (1997), illustrated in Figure 1. It can be seen that all models behave very well despite the high

wave steepness (the drag component d on the slender-body theory is added for comparison only, therefore $M+A+I+D+d$ curve can be ignored). The biggest discrepancy is seen at time $t \approx [0.8-1.4]$ s, where secondary load cycle is experimentally observed but none of the models capture it. The fact that not even FNV theory, which is derived directly to third order and takes flow nonlinearities and diffraction into account, managed to capture the secondary load cycle indicates that slc is caused by either effects of higher order than third, or three-dimensional effects. Nonetheless, recent studies confirmed that the two phenomena are not directly linked as it was previously thought; meaning that omitting slc does not directly lead to overlooking ringing as well. Therefore the next natural step is to look at the dynamic response of the cylinder, which is the focus of the presented study.

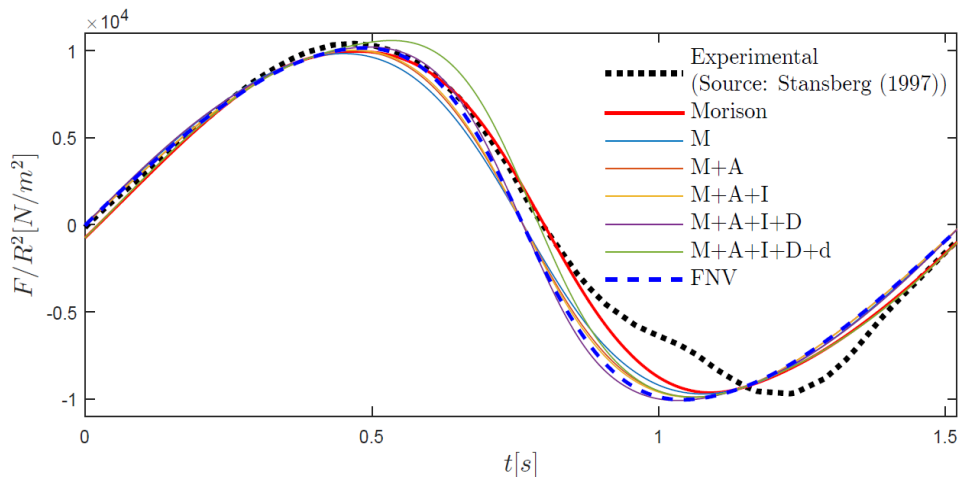


Figure 1. Comparison of normalised horizontal force over one period. Parameters: cylinder radius 0.1 m, water depth 10 m, wave period 1.52 s, nondimensional wave steepness $ka = 0.282$.

Ringing-like response has been observed in past studies even with Morison equation, but only when fully nonlinear wave kinematics were used – the amplifications were omitted with linear or weakly nonlinear waves. No scientific consensus has been reached on which order of nonlinearities ringing is actually associated with, or whether the nonlinearities in wave kinematics or forcing model trigger it. Therefore it is of major relevance to see how different hydrodynamic loading models perform when modelled in linear, weakly nonlinear and fully nonlinear waves; and how it influences the modelled dynamic response of the cylinder in waves of increasing steepness. This study will present the three aforementioned hydrodynamic loading models with linear, 2nd/3rd/5th Order Stokes and fully nonlinear potential flow kinematics as input, in waves of increasing steepness on a bottom-fixed cylinder with one degree of freedom, before considering irregular waves and a full OWT including action of wind.

4 Conclusions and Ongoing Work

Comparing three hydrodynamic loading models – Morison equation, slender-body and FNV theories – on a fixed cylinder has shown that all models behave similarly by recreating the loading peak very well but none managing to capture the nonlinear secondary load cycle. Nonetheless, secondary load cycle was recently unlinked from ringing, therefore a cylinder in motion is being studied before moving to irregular waves and real-scale OWT monopile in severe sea conditions. The ultimate goal of this contribution is to give an insight in the use of wave loading models on monopiles in rough seas and to assess their effects on the dynamic response to the coupled wind and waves actions.

References

- Stansberg, C. T. (1997) Comparing ringing loads from experiments with cylinder of different diameters - an experimental study. *BOSS '97 Behaviour of offshore structures, vol. 2*.

Design optimization of a reduced model of a wind mill tower for wind tunnel testing

M. Cid Montoya¹, S. Hernández¹, C. López¹, A. Álvarez¹ and J.Á. Jurado¹

¹Structural Mechanics Group, School of Civil Engineering, University of La Coruña, La Coruña, Spain
Corresponding author: M. Cid Montoya, miguel.cid.montoya@udc.es

Abstract

This presentation describes a research carried out for the design of a reduced model of a wind mill tower to be built and tested in the boundary layer wind tunnel of the University of La Coruña. It is well known that one of the many requirements of a reduced model is its capability of reproduce the natural frequencies and vibration modes of the real structure at the reduced length scale. In this research, a technique developed by the authors in a previous work based on the use of optimization algorithms that allows to minimize the error between these dynamic properties of the reduced model and the target values is used. The numerical results are presented.

1 Introduction

Although in the early years of wind mills towers steel was the material used to build these constructions, more recently several companies have created designs using prefabricated segments of reinforced or prestressed concrete for towers that can be up to 120 m. tall. During the construction phases and after completion, but before installing blades, they can be subjected to aeroelastic phenomena, for instance, vortex shedding excitation. Hence, wind tunnel test using reduced models can be very convenient to anticipate the performance of the real constructions.

This presentation is related to the design of a reduced model representing a wind mill tower 80 m. high made of prefabricated reinforced concrete segments to be tested in the boundary layer wind tunnel of the University of La Coruña. Its design needs to maintain dynamic similarity with the real construction and the procedure used to achieve this is presented in the next paragraphs.

2 Description of wind mill tower and reduced model

A picture of the real construction appears in Figure 1a and the finite element model generated to obtain the natural frequencies and natural modes of the real tower appear in Figure 1b. The reduced model was designed to be built using a central span of aluminium and cladding modules of plastic material created in a 3D printing machine, as shown in Figure 2.



Figure 1. Real tower and finite element model.

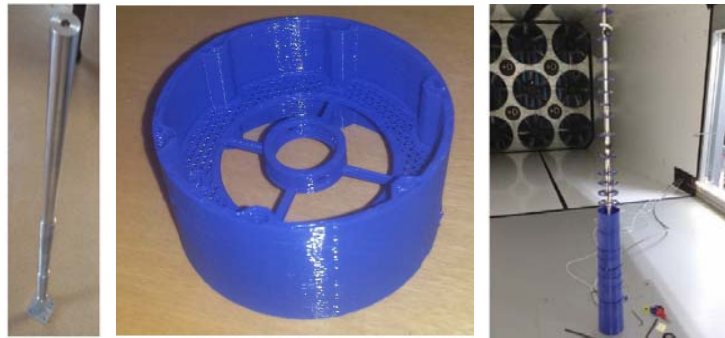


Figure 2. Reduced model of wind mill tower. (a) Spine (b) Cladding module (c) Construction of the model

3 Design optimization of the reduced model

The reduced model was defined as a central spine with 4 segments of different diameters and 14 cladding modules that dynamically behaves like lumped masses. They constitute the set of design variables of the optimization problem, that was developed in the authors' previous work Cid Montoya et al. (2018) and it was formulated for this particular case as follows

$$\min F(\mathbf{D}, \mathbf{M}) = \sum_{i=1}^{N_{\omega}} \left| \delta_i(\omega_{R,i}^2, \omega_{m,i}^2) \right|, \quad (1)$$

where \mathbf{D} is a vector containing the set of diameters of the spine segments, \mathbf{M} is a vector with the masses of the cladding modules, N_{ω} is the number of modes considered to be optimized (3 in this case), $\omega_{R,i}$ and $\omega_{m,i}$ are the i -esime natural frequency of the real structure and the reduced model, and δ_i stands for relative error. Therefore the aim of the optimization problem is to minimize the error of the first three natural frequencies of the model, which is initially designed using the traditional design process (Davenport et al. (1969), Isyumov (1999)), with regards to the real structure. Table 1 shows the result of the optimization procedure. The value of the frequencies are normalized due to the necessary privacy asked by the wind mill construction company.

Table 1. Numerical results of the optimization process normalized to the first frequency of the real structure.

Structure	f_1 [Hz]	f_2 [Hz]	f_3 [Hz]
Real structure (target)	1.000	5.074	13.544
Initial design of the model	1.149	6.105	17.562
Relative error of the initial design	14.872	20.331	29.671
Final design (optimized model)	0.998	5.064	13.773
Relative error of the final design	0.150	0.197	1.695

References

Cid Montoya, M., King, J. P. C., Kong, L., Nieto, F. and Hernández, S. (2017). A method for improving the dynamic response of full bridge reduced-scale models in aeroelastic wind tunnel tests by using optimization algorithms. *Journal of Wind Engineering Industrial Aerodynamics* **167**, 198-216.

Davenport, A.G., Isyumov, N., Fader, D.J. and Bowen, C.F.P. (1969) A study of wind action on a suspension bridge during erection and on completion. BLWTL-3-69, University of Western Ontario.

Isyumov, N., (1999). editor. Wind Tunnel Studies of Buildings and Structures. ASCE Manuals and Reports on Engineering Practice No. 67.

Transitional shear layers on rectangular sections

Daniel M. Moore¹, Chris W. Letchford² and Michael Amitay¹

¹Dept. of Mechanical, Aerospace & Nuclear Eng., Rensselaer Polytechnic Institute, Troy, NY, USA

²Dept. of Civil & Environmental Eng., Rensselaer Polytechnic Institute, Troy, NY, USA

Corresponding author: Daniel M. Moore, moored7@rpi.edu

Abstract

The present work implements 2D Particle Image Velocimetry measurements in an effort to study the transition process of the separated shear layer on rectangular sections. Inspection of the average and fluctuating vector fields enable quantitative definitions of important length scales such as transition lengths and reattachment lengths. The effect of free stream Reynolds number is examined in detail which, among other points, show clear trends of increasingly rapid transition lengths over the wind speeds investigated. Additionally, transitional shear layer dynamics are discussed for sections exposed to inclined winds. It is shown that under small angles of attack, relatively large changes in shear layer trajectory result in significant alterations to the global loads felt by the body.

Introduction

Introduced in 2008, the Benchmark on Aerodynamics of Rectangular Cylinders (BARC) aimed to address the fundamental fluid physics that govern the aerodynamic performance of the 5:1 rectangular cylinder. While many research teams contributed to this benchmark study, the collection of data pertaining to the unsteady behaviour on the BARC varied significantly. Specifically, the study appears to have two open areas yet to be completely understood. First, it can be shown that proper prediction of the true center of the recirculating region alongside the body is not easily calculated (Bruno, Salvetti, and Ricciardelli 2014). The second issue pertains to the variation of the lift coefficient for the BARC under inclined winds (Schewe 2013). The present work aims to address these two issues through close inspection of the shear layers' development by changing two parameters, the Reynolds number and angle of attack. Through collecting high spatial resolution flow field information around the BARC geometry, the authors aim to explore the transition process with the hope of elucidating the fundamental fluid mechanics involved with this ubiquitous shape.

Experimental Setup

A modular two dimensional rectangular prism was constructed out of 5 aluminium square tubes with side dimensions of $h = d = 50.8\text{mm}$ and $w = 508\text{mm}$. Each module was fabricated such that they were easily bolted together from the downstream side. The final product formed a rectangle with various aspect ratios ranging from $d/h = 1:1$ to $5:1$ in integer counts. However, the width remained constant. The final assembly was then mounted on a test rig with end plates in the Large Wind Tunnel at the Center for Flow Physics and Control (CeFPaC) at Rensselaer Polytechnic Institute. Tests were carried out covering a range of Reynolds numbers between 1.3×10^4 to 1.2×10^5 based on the model's thickness and the free stream wind speed. 2D Particle Image Velocimetry (PIV) was employed to document the flow field near the prisms' leading edge.

Results

Preliminary results provide indication of the level of detail captured using PIV techniques. Figure 1 shows the baseline case at a Reynolds number of 1.3×10^4 which displays several interesting features of the BARC geometry. The upper half of the figure displays the time-averaged streamlines which show the reattachment point just upstream of the trailing edge at approximately $x/h \approx 3.9$. Additionally, the average vorticity field is shown on the lower half of the figure showing the rapid spatial diffusion of vorticity that spreads from the leading edge along the body. Finally, the inset image consists of an instantaneous vorticity shot captured near the leading edge corner. The instantaneous vorticity very clearly shows the roll-up of a coherent structure which is the first observable feature in the transition process for the separated shear layer (Lander 2017). The full paper will explore the various parameters which are important to the transition process of separated shear layers and their contributions to the global loads on rectangular sections.

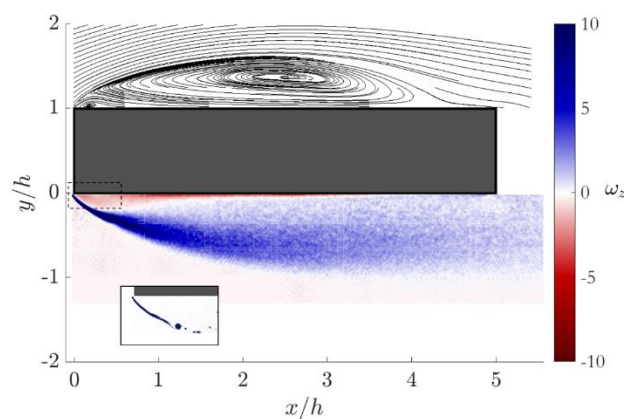


Figure 1: Baseline data for the BARC geometry. Streamlines on the upper half. Average span wise vorticity plotted on the lower half. Wind is left to right.

References

- Bruno, Luca, Maria Vittoria Salvetti, and Francesco Ricciardelli. 2014. "Benchmark on the Aerodynamics of a Rectangular 5:1 Cylinder: An Overview after the First Four Years of Activity." *Journal of Wind Engineering and Industrial Aerodynamics* 126: 87–106. <http://dx.doi.org/10.1016/j.jweia.2014.01.005>.
- Lander, Daniel Chapman. 2017. "Influence of Freestream and Forced Disturbances on the Shear Layers of a Square Prism." Rensselaer Polytechnic Institute.
- Schewe, Günter. 2013. "Reynolds-Number-Effects in Flow around a Rectangular Cylinder with Aspect Ratio 1 : 5." *Journal of Fluids and Structures* 39: 15–26.

CFD applications for Building and Environment

Marco Mulas¹, and Rossano Zucca¹

¹Vento CFD, Cagliari, Italy

Corresponding author: Marco Mulas, marco.mulas@vento-cfd.com

Abstract

We present a novel Computational Fluid Dynamics (CFD) software developed for the Building and Environment applications. The technical noveltries are represented by a fully automated and extremely quick Cartesian Grid generator and by the use of the Immersed Boundary method. The result is an easy workflow that takes less than 15 minutes to prepare the application, no matter of the geometrical complexity of the object of the simulation.

The software focuses on 3 outdoor wind applications: the evaluation of the wind load on constructions, the so called pedestrian comfort analysis on urban districts, and the trasport and diffusion of contaminants on cities and environmental sites, both in steady-state and transient modes.

The equation for the contaminant is decoupled from the solution of the 5 thermo-fluid dynamic equations (conservation of mass, equation of motion and conservation of energy), and it can be solved on an available, previously computed solution, in frozen mode.

A fully implicit solution algorithm drives the iterative method to the steady-state solution. In case a transient analysis is of interest, the same solution algorithm is used to follow the time evolution time-step after time-step.

The software has been validated against available wind tunnel data for a variety of applications. The figure 1 shows the flow pattern on a 3D model of a high rise building located in a urban block that was analysed in a wind tunnel¹

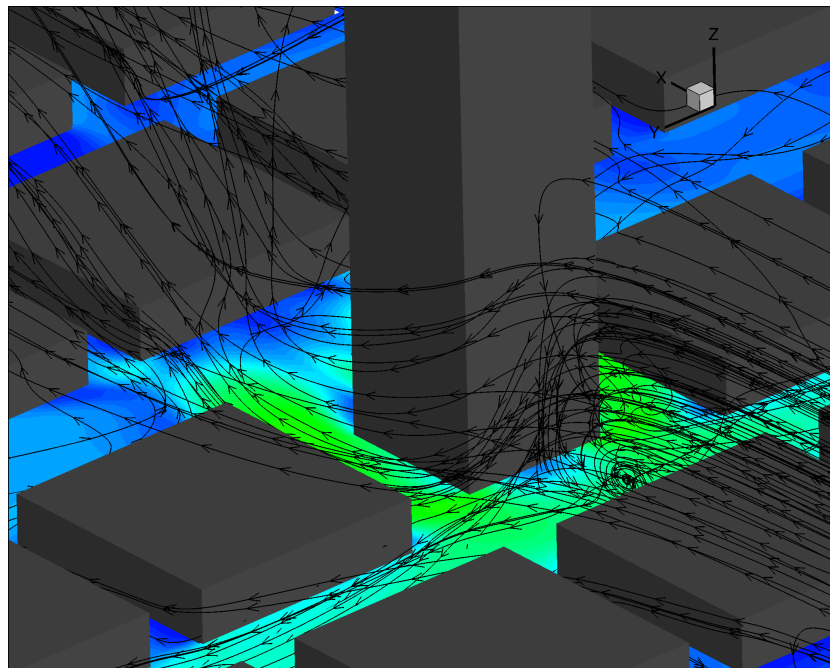


Figure 1. the velocity magnitude on a horizontal section and streamlines.

1 R. Yoshi et al.: “Cooperative project for CFD prediction of pedestrian wind environment in the Architectural Institute of Japan”, Journal of Wind Engineering and Industrial Aerodynamics, 95, 2007.

The figure 2 shows the comparison between wind tunnel measurements and the computed solution on the street immediately downstream of the tall building and orthogonal to the wind direction.

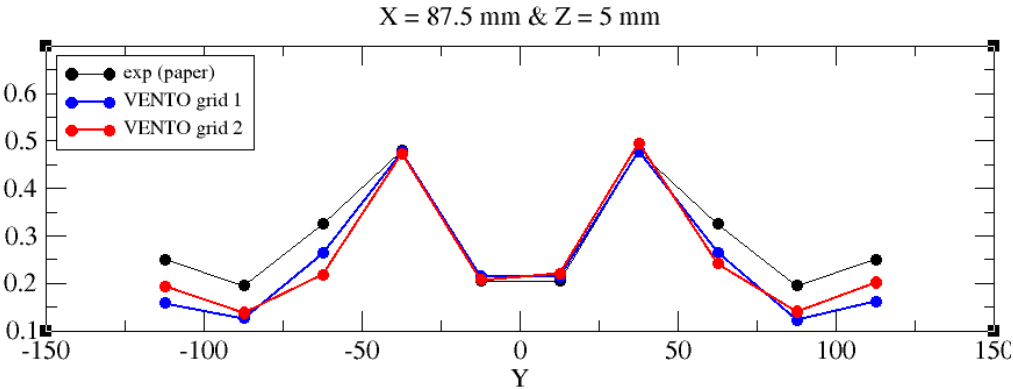


Figure 2. comparison between the computed solutions and wind tunnel data

A critical database for the Strouhal number of bridge decks

Bernardo Nicese¹, Claudio Mannini¹, Antonino Maria Marra¹ and Gianni Bartoli¹

¹Department of Civil and Environmental Engineering, University of Florence, Italy

Corresponding author: Bernardo Nicese, bernardo.nicese@unifi.it

Abstract

This paper represents a first step towards a prenormative study on the Strouhal number of bridge decks. The main goal of the work is to identify, where possible, a range of values of this important parameter for the most common typologies of deck cross sections to be used for the preliminary design of bridge structures. With this aim in mind, data available in the literature are critically reviewed, collected and classified.

1 Introduction

In the last decades, the construction of slender bridge structures characterized by limited mass per unit length and low frequencies of oscillation has become more and more common. As a consequence, the study of vortex-induced vibration (VIV) of bridge decks due to the wind action is a crucial design issue. In particular, the Strouhal number (St) is a parameter of utmost engineering importance, as it allows the estimation of the VIV critical wind speed.

It is well known that the Strouhal number depends on several factors: geometry of bridge deck cross section, angle of attack of the air flow, incoming flow turbulence characteristics, and Reynolds number. In particular, concerning the cross section geometry, a key role is played by the presence of lateral barriers, screens and other non-structural details. As a result, the estimation of the Strouhal number without specific wind tunnel tests is a complicated task. Indeed, presently the available codes do not allow any accurate enough prediction of this parameter for the preliminary design of bridge structures.

This paper reports a few results of an ongoing prenormative study about the Strouhal number for several typologies of bridge deck cross sections (Fig. 1). As a first step, a large number of data available in the scientific literature have been collected and categorized on the basis of some selected key influencing factors.

A synthetic example of the resulting database is reported in Table 1. Therein, both the results of experiments (either in the wind tunnel or at full scale) and computational fluid dynamics (CFD) calculations can be found. All of the values of the Strouhal number reported are made homogeneous considering the height D of the deck without non-structural details (barriers, screens, etc.) as reference dimension.

From the analysis of the data, an estimation of ranges of values for the Strouhal number for the various bridge deck typologies seems viable. Nevertheless, the need of extending the data collection and of considering additional parameters in the classification is also apparent, in order to make smaller the range of Strouhal number values to consider in a preliminary VIV analysis of bridge decks.

Table 1. Strouhal number data for various bridge deck cross sections. B and D denote respectively the width and the height of the bridge deck. The Strouhal numbers have been determined through full-scale tests (FULL), wind tunnel experiments (WT), or numerical simulations (CFD). α is the angle of attack of the air flow (positive nose up).

Cross section	Bridge	B/D	Method	α	Configuration	St
Quasi-streamlined box girder (Fig. 1a)	Storebælt East Bridge (Brusiani et al., 2013; Fradsen et al., 2001)	7.75	FULL	-	-	0.08-0.15
			WT	0°	Bare	0.11
			CFD	0°	Bare	0.14
Single box girder (Fig. 1b)	Storebælt East Bridge approach spans (Larose et al., 2006; Schewe et al., 1998)	3.69	FULL	-	-	0.22
			WT	0°	Bare	0.16-0.22
	Ikara Bridge (Larose et al., 2006)	5.50	FULL	-	-	0.20
			WT	0°	Bare	0.16
Twin-box girder (Fig. 1c)	Xihoumen Bridge (Li et al., 2011)	11.04	FULL	-	-	0.094-0.107
	Stonecutters Bridge (Larose et al., 2003)	13.63	WT	0°	Bare	0.20
	General twin-box study (Laima et al., 2013)	10.28	WT	0°	Bare	0.15
				-5°	Bare	0.17-0.21
				0°	Bare	0.20
				+3°	Bare	0.20-0.22
	General twin-box study (Matsuda et al., 2001)	10	WT	+5°	Bare	0.21-0.24
-4°				Bare	0.15	
-4°				Barriers	0.12	
0°				Bare	0.14	
0°				Barriers	0.11	
Trapezoidal box girder with lateral cantilevers (Fig. 1d)	Sunshine Skyway Bridge (Ricciardelli et al., 2001)	6.73	WT	+4°	Bare	0.09
				+4°	Barriers	0.09
				-5°	Bare	0.24
	CRIACIV section inspired by Sunshine Skyway Bridge (Mannini et al., 2010)	6.43	WT	0°	Bare	0.21
				+5°	Bare	0.24
				CFD	0°	Bare
	Volgograd Bridge (Corriols et al., 2010)	2.06	CFD	0°	Bare	0.133
0°				Barriers	0.116	

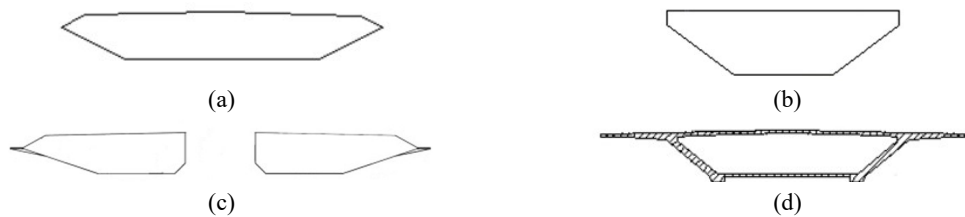


Figure 1. Schematics of the bridge deck section geometries that have been considered.

Synthetic turbulence generation using spectral methods

Luca Patruno, Mattia Ricci

Department of Civil, Chemical, Environmental and Materials Engineering,
University of Bologna, Italy

Corresponding author: Luca Patruno, luca.patruno@unibo.it

Abstract

The generation of synthetic turbulence represents a crucial step in the setup of Computational Fluid Dynamics (CFD) simulations which involve the use of scale resolving approaches to turbulence modelling. Numerous applications which involve the generation of synthetic turbulent fluctuations can be found in the literature, ranging from the coupling of RANS and LES in hybrid zonal approaches to Computational Aeroacoustics. In particular, in the field of Computational Wind Engineering, the development of unsteady boundary conditions, representative of the flow field expected on site, is of great importance for both wind load assessment and pollutant dispersion problems. In this contribution, some recent results obtained in the development of synthetic turbulence generation procedures based on spectral methods are presented.

1 Introduction

The generation of synthetic turbulence, fostered by the continuous growth of the available computer power, is receiving increasing attention in the scientific community due to the rapid spreading of scale resolving approaches to turbulence modelling. Review papers summarising available techniques for the generation of unsteady inflow conditions have been presented by Tabor and Baba-Ahmedi (2005) and, more recently, by Wu (2017).

Roughly speaking, it can be said that unsteady inflow conditions can be generated by following two main approaches: recycling/rescaling methods and synthetic turbulence generation. Following the first approach, velocity fluctuations applied at the inlet are extracted from the numerical simulation itself and, properly rescaled, are used as inflow condition. The second approach, can be itself subdivided into three groups depending on the strategy followed in order to obtain the random fluctuations. In the first one, turbulent fluctuations are generated by superposition of randomly distributed coherent structures. In the second one, digital filters are adopted in order to obtain random fields characterised by target statistical properties while the third group, which collects the so called “spectral methods”, assumes that random fluctuations can be seen as a superposition of harmonic functions as proposed by Kraichnan (1970).

A study regarding the mechanisms underlying some of the currently available spectral methods have been proposed by Patruno (2016). Starting from such results, it is found that a complete control over the generated turbulent field and its compliance with the linearised Euler’s equations require to consider the realisability of each harmonic component that, by superposition, contributes to its definition

In the present contribution, such realisability conditions are described and new methodologies which can be used in order to obtain synthetic turbulent fields, approximatively characterised by prescribed target properties, are presented. Special attention is devoted to the role played by the divergence-free condition and Taylor assumption when such random fields are used as inflow conditions for CFD simulations.

2 Spectral synthesis

When spectral methods are adopted, the starting point is always represented by the work proposed by Kraichnan (1970). In particular, the random field is built as:

$$\mathbf{u}(\mathbf{x}, t) = \sum_{n=1}^N \mathbf{p}^n \cos(\mathbf{k}^{nT} \mathbf{x} + \omega^n t) + \mathbf{q}^n \sin(\mathbf{k}^{nT} \mathbf{x} + \omega^n t), \quad (1)$$

where $\mathbf{u}(\mathbf{x}, t)$ is the random velocity field which depends on the space position, \mathbf{x} , and time, t . The index n spans all the N considered harmonic contributions, \mathbf{p}^n and \mathbf{q}^n are amplitude vectors, \mathbf{k}^n is a wavevector and ω^n is a circular frequency. By leaving the form presented in Eq. (1) unchanged, available spectral methods allow to obtain \mathbf{p}^n , \mathbf{q}^n , \mathbf{k}^n and ω^n in order to impose some target characteristics to the obtained random field. In order to impose the divergence-free condition, it can be demonstrated that \mathbf{p}^n and \mathbf{q}^n must lie in the null space generated by \mathbf{k}^n . In particular, the well-known Modified Discretizing and Synthesizing Random Flow Generator (MDSRFG) requires to evaluate the aforementioned quantities as:

$$(\mathbf{p}_i^n)^2 + (\mathbf{q}_i^n)^2 = 2E_i(f^n) \quad (2)$$

$$\omega^n = 2\pi f^n; \quad |\mathbf{k}| = 2\pi f^n / U, \quad (3)$$

where U is the wind speed and \mathbf{E} is a vector collecting the prescribed variance of each velocity component at the frequency f^n . Such choice allows to impose target time spectra to the obtained velocity field and, when a single harmonic component is considered, it leads to the distribution of \mathbf{k} over circular orbits as shown in Figure 1.

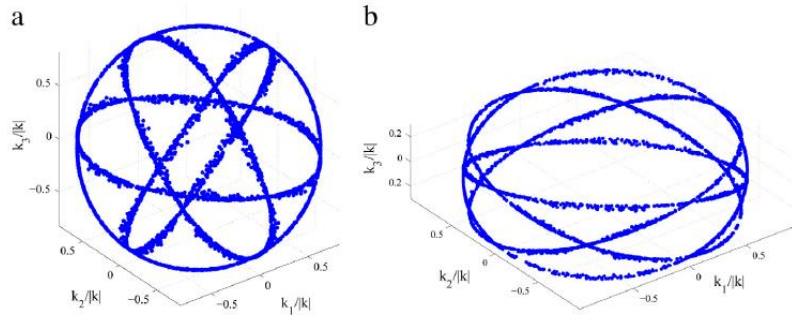


Figure 1: Orbits described by \mathbf{k} when using MDSRFG: (a) $E_1 = E_2 = E_3$ and (b) $E_1 = E_2 = E_3/20$.

As is can be seen from Eq. (3), only the module of \mathbf{k} is explicitly controlled while only by controlling all its components, separately, it is possible to impose the spectral content along all spatial directions and, thus, the correlations of the obtained random fields. It is shown that such aspect leads to the definition of appropriate realisability conditions which link \mathbf{k} to \mathbf{E} , so constraining the harmonic contributions which can be actually used to build the synthetic field.

References

- Tabor, G., Baba-Ahmedi, M. (2005). Inlet conditions for large eddy simulation: a review. *Comp. Flu.* **39**, 553-567.
- Wu, X. (2017). Inflow turbulence generation methods. *Annual Review of Fluid Mechanics* **49**, 23-49.
- Kraichnan, R. (1970). Diffusion by a random velocity field. *Physics of Fluids* **13**, 22-31.
- Patrino, L., Ricci, M. (2017). On the generation of synthetic divergence-free homogeneous anisotropic turbulence. *Comput. Methods Appl. Mech. Engrg.* **315**, 396-417.

Simultaneous vibration suppression and energy harvesting under wind excitation in tall buildings equipped with the tuned mass damper inerter (TMDI)

Francesco Petrini¹, Zixiao Wang² and Agathoklis Giaralis²

¹ Department of Structural and Geotechnical Engineering, Sapienza University of Rome, Rome, Italy

² Department of Civil Engineering, City, University of London, London, UK

Corresponding author: Francesco Petrini, francesco.petrini@uniroma1.it

Abstract

An adaptive tuned mass damper inerter (TMDI) for simultaneous vibration suppression and energy harvesting (EH) in tall buildings under wind excitation is presented. A 305m high building is selected as case-study: the TMDI is first optimized for vibration suppression specifically focusing on minimizing across-wind floor acceleration, then EH potential is investigated by partially replacing the damping produced by the dashpot of the TMDI system by the one produced by an electromagnetic harvester.

1 Introduction

The constantly increasing cost of land in downtown metropolitan areas as well as sustainability requirements in building construction leads to the need for designing and constructing ever more lightweight tall/slender buildings. These structures optimize space and material usage while minimizing visual impact in congested urban environments. Nevertheless, they can be particularly susceptible to oscillations in the cross-wind direction (i.e., within the normal plane to the wind direction) due to vortex shedding generated at their edges; this is especially true for structures with rectangular floor-plan and high height-to-width aspect ratios. In such buildings, ensuring that floor accelerations remain below a certain threshold becomes a dominant structural design requirement to achieve acceptable performance in terms of occupants comfort at a serviceability limit state.

In this context, over the past two decades, tuned mass dampers (TMDs), among other devices and configurations for supplemental damping, have been widely used in practice for vibration mitigation in wind-excited tall buildings to meet occupants' comfort criteria prescribed by the relevant building codes and guidelines. In its simplest form, the classical linear passive TMD comprises a mass attached towards the top of the building whose oscillatory motion is to be controlled (primary structure) via linear stiffeners, or hangers in case of pendulum-like TMD implementations, in conjunction with linear energy dissipation devices (dampers). Stiffness and damping properties of the TMD are optimally designed/tuned to control the fundamental vibration mode of a given primary structure for a pre-specified attached mass. Nevertheless, as the slenderness level of the building increases, peak floor accelerations are more and more influenced by higher modes of vibrations and, therefore the classical TMD becomes less efficient to meet serviceability requirements as it can only suppress a single (the first) mode. In this regard, TMDs become less efficient. At the same time, the effectiveness of the TMD for vibration control depends heavily on the attached mass. The latter can rarely exceed 0.5% to 1% of the total building mass in tall buildings as it becomes overly expensive to accommodate its weight and volume due to structural and architectural limitations, respectively.

Recently, the authors (Giaralis and Petrini 2017) addressed the above drawbacks of the TMD to suppress wind-induced vibrations in the across wind direction of tall buildings by incorporating an inerter device in the so-called tuned mass-damper-inerter (TMDI) configuration originally developed for suppressing vibrations in base-excited structures (Marian and Giaralis 2014). The inerter is a two-terminal device with negligible mass/weight which develops a resisting force proportional to the

relative acceleration of its terminals by a scalar coefficient termed “inertance” (Smith 2002). Previous work by the authors (Giaralis and Petrini 2017) demonstrate that appreciable gains in reducing peak top floor accelerations in typical tall/slender benchmark buildings are achieved by optimally designed TMDIs compared to TMDs for a fixed attached mass. These gains are attributed partly to the mass-amplification effect and partly to higher-modes-damping effect endowed to the TMD by the inerter in the TMDI configuration. Both these effects are leveraged through the inertance property.

In this contribution, the potential benefits of replacing the damping device of the TMDI by an electromagnetic motor (EM) coupled with energy harvesting circuitry, in wind-excited tall buildings is numerically explored in conjunction with the use of inerter devices with varying inertance. The consideration of the EM makes possible to readily vary the damping property of the TMDI through the motor/circuitry functionalities. The varying EM damping property together with the varying inertance leverage the vibration control capabilities of the TMDI, as well as its potential to transform part of the kinetic energy into electricity as discussed in Marian and Giaralis (2017) for the case of harmonically excited single degree-of-freedom structures.

Herein, a linear reduced-order structural system is developed, defined by a diagonal mass matrix and full damping and stiffness matrices, which captures faithfully the dynamic properties of a detailed finite element model corresponding to a benchmark 74-storey building with square floor plan. A TMDI with varying damping and inerter properties is added to the structural system by elementary operations to the mass, damping, and stiffness matrices assuming ideal linear inerter behavior. The wind action is represented by an analytical spectral density matrix modelling correlated across-wind induced forces accounting for vortex shedding and the structural analysis step is undertaken in the frequency domain for efficiency. Starting from an optimally designed TMDI defined via a standard numerical optimization search to minimize peak top floor acceleration, the peak top floor acceleration and the available energy for harvesting are quantified as both TMDI damping and inertance properties are judiciously let to vary. The reported numerical results obtained for various TMDI topologies and for a pre-specified attached mass demonstrate that allowing for variations to both damping and inertance properties of the TMDI leads to a smart/adaptive lightweight tall/slender building in which, depending on the occupancy over day and night, users’ comfort requirements can be relaxed to achieve potentially higher energy generation levels depending on the intensity of the wind loading.

References

- Giaralis, A. and Petrini, F. (2017). Wind-induced vibration mitigation in tall buildings using the tuned mass-damper-inerter (TMDI). *Journal of Structural Engineering ASCE*, **143**(9), article number 04017127
- Marian, L., and Giaralis, A. (2014). Optimal design of a novel tuned mass-damper–inerter (TMDI) passive vibration control configuration for stochastically support-excited structural systems. *Probabilistic Engineering Mechanics* **38**, 156–164
- Marian L and Giaralis A. (2017). The tuned mass-damper-inerter for harmonic vibrations suppression, attached mass reduction, and energy harvesting. *Smart Structures and Systems*, **19**, 665-678.
- Smith, M.C. (2002). Synthesis of Mechanical Networks: The Inerter. *IEEE Transactions On Automatic Control*, **47**(10), 1648-1662

Some advances in the study of classical-flutter-based generators

Luca Pigolotti¹, Claudio Mannini¹ and Gianni Bartoli¹

¹CRIACIV / Department of Civil and Environmental Engineering, University of Florence, Italy

Corresponding author: Luca Pigolotti, luca.pigolotti@dicea.unifi.it

Abstract

This work focuses on wind-energy harvesting from two-degree-of-freedom vibrations induced by the classical-flutter instability. The main features of the system response, both at the incipient motion and during the large-amplitude limit-cycle oscillations, are discussed. The results point out some peculiar (and non-intuitive) behaviours, ruled by the still-air frequency ratio and the damping of the translational motion component, the latter simulating the operation of a conversion apparatus.

1 Introduction

Vibrations triggered by the classical-flutter instability represent an effective source for wind-energy harvesting. The flutter-based technology considers systems that perform two-degree-of-freedom (heaving and pitching) spontaneous oscillations, without any external control of the motion.

In the perspective of outlining some design guidelines for improving the performance of flutter-based generators (Pigolotti et al., 2017a), the present work reviews some peculiar features encountered during wide and systematic, numerical and experimental, campaigns of investigation (Pigolotti et al., 2017b,c). In particular, the effects of frequency-ratio parameter ($\gamma_n = n_{\alpha 0}/n_{\eta 0}$ pitching-to-heaving uncoupled frequency ratio in still air) and ratio-to-critical heaving damping (ξ_{n0}) are highlighted, since they play a significant role in both the critical and post-critical response of the system.

2 Methodology of investigation

Parametric numerical analyses were conducted in the frequency-domain through a linearized approach (Pigolotti et al., 2017b), using Theodorsen's model for the self-excited loads. The cut-in velocity of the device corresponds to the critical-flow speed, and high-performance systems require an as low as possible instability threshold. Therefore, the analytical model allowed efficiently exploring the influence of the governing parameters on the critical condition, so to identify a design procedure for developing potential optimal configurations.

Wind-tunnel tests were conducted in the CRIACIV laboratory to investigate the post-critical response of a flat-plate sectional model, with an elongated rectangular cross-section of 25:1 width-to-depth ratio (Pigolotti et al, 2017c). A specific large-amplitude setup was developed, which enabled a fine setting of the governing parameters. In particular, the linear viscous damping in the heaving component was increased (up to 18%) through eddy-current dampers, simulating the operation of an energy-conversion apparatus. Moreover, the frequency ratio was controlled by adjusting the stiffness of the heaving and/or pitching elastic suspension.

3 Main features of the response

Among all parameters describing the classical-flutter problem, the system is very sensitive to the frequency ratio γ_n . Indeed, this parameter rules the main characteristics of the motion, that is the

amplitude ratio and phase difference between pitching and heaving motion components. This behaviour was suggested by the linear analyses, and confirmed by the wind-tunnel experiments (Fig. 1). For low-damped configurations with γ_n lower than unity, the system is characterized by an out-of-phase motion with large heaving amplitude compared to pitching rotations, while the in-phase motion occurring for γ_n larger than unity shows a marked pitching component.

Furthermore, a peculiar behaviour occurs when the heaving damping $\xi_{\eta 0}$ is increased. In particular, while the configuration with $\gamma_n < 1$ shows a reduction of the motion amplitude and a delay of the instability threshold, the configuration with $\gamma_n > 1$ exhibits a destabilizing effect of damping. Indeed, the critical condition is anticipated, and the pitching amplitudes increases while the heaving amplitudes only slightly alters. These different behaviours make the response of the two configurations more similar, shifting the amplitude ratio toward a ‘virtual common pattern’ (Fig. 1a). The pitching-to-heaving phase difference also varies with a damping increment (Fig. 1b); for both values of γ_n , the configurations tend toward a quadrature-of-phase motion. Therefore, the system response seems to saturate as $\xi_{\eta 0}$ achieves high values.

These behaviours highlighted by the experimental measurements of the post-critical response have also been suggested by the linear analyses, although the characteristics of the incipient motion at the instability threshold are qualitatively different from those at the limit cycle.

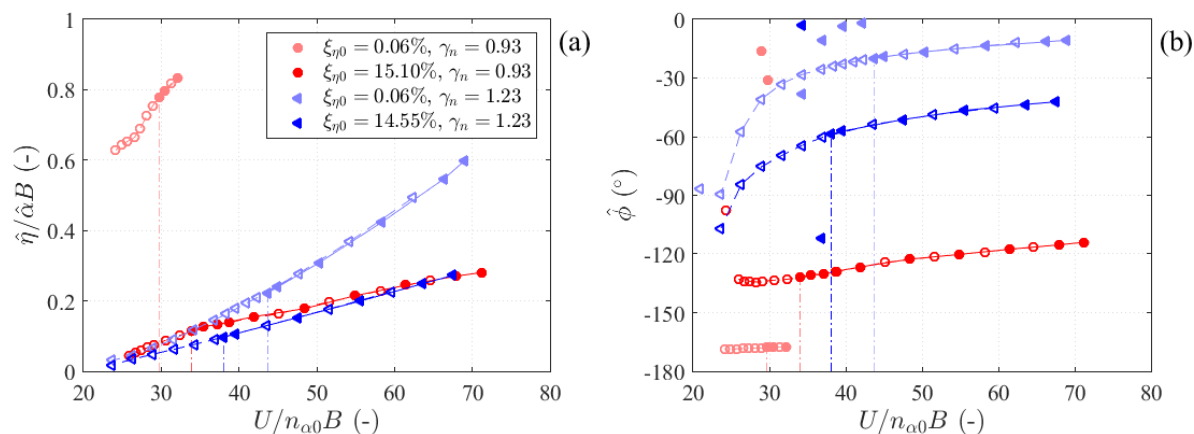


Figure 1. Amplitude ratio (a) and pitching-to-heaving phase difference (b). Vertical dash-dot lines indicate the instability threshold. Filled and empty markers connected by solid and broken lines, represent limit-cycle oscillations for, respectively, increasing and decreasing flow speed (U). $n_{\alpha 0}$ is the still-air uncoupled pitching frequency, and B is the cross-section chord.

References

- Pigolotti, L., Mannini, C., and Bartoli, G. (2017). Critical and post-critical behaviour of two-degree-of-freedom flutter-based generators. *Journal of Sound and Vibration*, **404**, 116–140.
- Pigolotti, L., Mannini, C., Bartoli, G., (2017). Destabilizing effect of damping on the post-critical oscillations of flat plates. *Meccanica*, **52**, 3146–3164.
- Pigolotti, L., Mannini, C., Bartoli, G. (2017). Experimental study on the flutter-induced motion of two-degree-of-freedom plates. *Journal of Fluids and Structures*, **75**, 77–98.

A semi-probabilistic framework for windblown sand action

Lorenzo Raffaele^{1,2}, Luca Bruno^{1,2}

¹Department of Architecture and Design, Politecnico di Torino, Italy

²Windblown Sand Modeling and Mitigation joint research group, Italy-France-UK

Corresponding author: Lorenzo Raffaele, lorenzo.raffaele@polito.it

Extended Abstract

Windblown sand results from the interaction between physical subsystems such as wind, air suspended particles and bed-particles. The study of these phenomena is intrinsically multi-disciplinary, and it involves several research fields, from mathematical physics to Earth sciences, civil and environmental engineering. The engineering interest in windblown sand is driven by the harmful interactions that windblown sand can have with a number of structures and infrastructures in desert and arid environments, such as pipelines, industrial facilities, single buildings, towns, farms, roads, and railways. In particular, the windblown sand accumulation on railways is the key design challenge threatening safety and serviceability issues. Windblown sand effects on railways have been recently categorized by Bruno et al (2018) into *Sand Limit States* (SLS). SLS are set as threshold performance levels in analogy with Civil Engineering common practice. SLS are further classified into Sand Ultimate Limit States (SULS) and Sand Serviceability Limit States (SSLS) as follows: i. attaining SULS involves service interruption and/or passengers unsafe conditions; ii. attaining SSLS involves railway partial loss of capacity and/or passenger discomfort. *Sand Mitigation Measures* (SMMs) are artefacts properly designed to avoid any such condition. The so-called Path SMMs (Bruno et al 2018) are located along the windblown sand path, upwind the infrastructure to be protected. They are intended to trap incoming sand flux by promoting its sedimentation around them.

Windblown sand saltation is the main mode of particles transport in terms of mass. Saltation initiates when the wind shear stress τ exceeds the threshold shear stress τ_c , which depends on sand features. The effects of the variability of sand subsystem on the threshold shear velocity u_{*c} has already been investigated in a number of study reviewed e.g. in Raffaele et al. (2016). The amount of saltating particles is expressed by the sand transport rate Q [kg/ms], defined as the integral over the vertical direction of the sand flux q [kg/m^2s]. A number of semi-empirical models (Q -models) to obtain Q has been formulated in the literature so far (see e.g. Kok et al., 2012). Because of their concise form and sound physical basis, *modified Bagnold type* models are widespread in the literature and the most employed in the practice. The evaluation of the time-cumulated amount of transported sand is expressed by means of the sand drift (D) in order to take into account the variability of the wind subsystem in average (Fryberger and Dean, 1979). The probabilistic evaluation of D is firstly introduced in Raffaele et al. (2017), where the aleatory uncertainties of both the wind and sand subsystems are taken into account. However, even among modified Bagnold type models, different Q -models give rise to heterogeneous predictions (Raffaele et al, 2018). According to the Authors, the introduction of a new epistemic Q model uncertainty is required to account for such a scattering.

In this study, the Authors first propose a framework for the definition and quantification of the sand action in semi-probabilistic terms. The definition of sand action is established in analogy to other environmental actions in civil engineering field, e.g wind action (EN 1991-1-4, 2005), or windblown snow (EN 1991-1-3, 2002). The incoming windblown sand is defined as the amount of sand carried by the incoming wind undisturbed by any obstacle, in analogy to the incoming mean wind velocity in wind engineering practice. The incoming sand can be expressed by its flux q , its transport rate Q or the drift potential D . Conversely, the local windblown sand action is generally defined as the amount of sedimented sand around a given obstacle. Analogously to the incoming sand, the sedimented one can

be expressed by the sedimentation flux $s(x, t)$ at the solid surface, the sedimentation rate $S(t) = \int_{-\infty}^{\infty} s dx$, or the time-cumulated sedimentation volume $V(T) = \int_0^T S dt$. The local sand action is related to the incoming windblown sand by a black box function \mathcal{F} . It mainly depends on the sand morphodynamics around the obstacle that depends in turn on the local wind flow and the obstacle geometry, analogously to the aerodynamic coefficients for wind action. Given the lack of a closed form of \mathcal{F} , its semi-empirical expression can be obtained by wind tunnel tests and/or computational simulations. Figure 1a shows the conceptual scheme of the modelling framework, where the incoming windblown sand and the local sand action are expressed by the incoming drift potential DP_{in} , and the time-cumulated sedimentation volume V , respectively, so that $V = \mathcal{F}D$. This conceptual scheme can be generalised in the case of multiple obstacles arranged in series, e.g. for a path SMM upwind a railway embankment (Figure 1b).

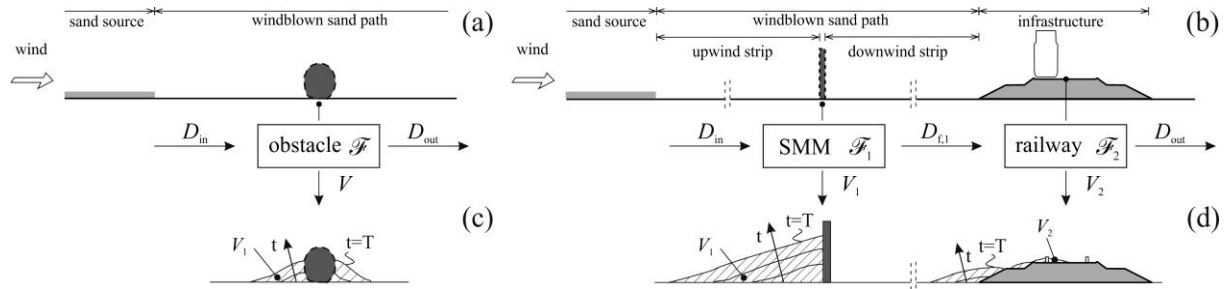


Figure 1. Windblown sand action conceptual scheme for single obstacle (a), for mitigated railway (b), sedimented sand action (c,d)

The design value of the local sand action V_d on a single obstacle is defined by the semi-empirical expression

$$V_d = \gamma V_k = \gamma_{dp} \gamma_{sd} V_k = \gamma_{dp} \gamma_{sd} \mathcal{F} D_{in,k} ,$$

where the values V_k and $D_{in,k}$ are characteristic ones with an intended probability of non-exceedance. The partial factor γ accounts for both sand action inborn uncertainties defined by the partial factor γ_{dp} , and modelling uncertainties defined by γ_{sd} . For a deterministic \mathcal{F} and a nominal sand resistance of the infrastructure, the partial factor γ results from the uncertainties affecting the incoming windblown sand only. The full paper will detail the general framework components and a tentative application to a benchmark application will be given.

References

- Bruno, L., Horvat, M., Raffaele, L. (2018). Windblown Sand along Railway Infrastructures: a review of Challenges and Mitigation Measures, *Journal of Wind Engineering and Industrial Aerodynamics*, submitted
- Fryberger, S., Dean, G. (1979). *A Study of Global Sand Seas*.
- Kok, J.F., Parteli, E.J.R., Michaels, T.I., and Karam, D.B. (2012). The physics of wind-blown sand and dust. *Reports on Progress in Physics*.
- Raffaele, L., Bruno, L., Pellerey, F., and Preziosi, L. (2016). Windblown sand saltation: A statistical approach to fluid threshold shear velocity. *Aeolian Research* **23**, 79-91.
- Raffaele, L., Bruno, L., Fransos, D., and Pellerey, F. (2017). Incoming windblown sand drift to civil infrastructures: A probabilistic evaluation. *Journal of Wind Engineering and Industrial Aerodynamics* **166**, 37-47.
- Raffaele, L., Bruno, L., Wiggs, G.F.S. (2018). Uncertainty propagation in aeolian processes: From threshold shear velocity to sand transport rate. *Geomorphology* **301**, 28-38.

Wind-induced fatigue verification standard methods

M.P. Repetto¹, M. Damele¹

¹Department of Civil, Chemical and Environmental Engineering, University of Genoa, Italy

Corresponding author: M.P. Repetto, repetto@dicca.unige.it

Abstract

Wind-induced fatigue is a key issue in design of many slender structures; despite this reality, suitable engineering and standards procedures are almost completely lacking. Working in this field, the author has carried out a wide research project aimed at formulating a general procedure for determining the wind-induced fatigue damage. Thanks to some relevant hypotheses, a closed form solution of the alongwind-induced fatigue damage has been obtained. The formulation has been progressively simplified, in order to be suitable for engineering verifications and standard format. The research is aimed to derive an analogous method for the crosswind-induced fatigue. The method has been applied to a particular type of structure, sensitive to turbulence induced fatigue: highway sign supports. The comparison between the inspection and the simplified closed form solution shows an excellent agreement, showing that probabilistic approach can have the potentiality of catching the main features of the wind-induced fatigue phenomenon, giving good results with simplified procedures.

1 Introduction

Wind-induced actions can produce large vibrations of structures at moderate and frequent wind velocities, leading to accumulation of fatigue damage. Severe damage and even collapse has been observed for different structural types, such as wind turbines, cranes, poles and towers. Nevertheless, standards procedures aren't effective, making this sector a major wind engineering shortcoming.

This research is aimed at proposing a general procedure for determining the wind-induced fatigue damage, taking into account the aerodynamic actions and structural responses. The complete probabilistic method has been progressively simplified, introducing a hierarchy of hypotheses, in order to develop a closed form solution of the wind-induced fatigue, suitable for engineering calculations and code provisions, aimed at evaluating the total fatigue damage and the fatigue life of structures and structural elements. The general method has to consider both alongwind and crosswind-induced fatigue. The paper will describe the complete closed form solution that concerns fatigue damage due to alongwind and crosswind turbulence, discussing the main analytical features and the simplifying hypotheses adopted. Every input parameter may be evaluated using actual codes.

The method is applied to real structures of a specific type which is particularly sensitive to turbulence-induced fatigue: highway sign support structures. Results have been compared with benchmark inspections in situ at the critical joints of the structure. The comparison between the effective benchmark and the simplified closed form solution shows a surprisingly good agreement; this makes the probabilistic approach an appropriate methodology to catch the main features of the wind-induced fatigue phenomenon. Good results may be obtained by simplified procedures, reasonably expressed in standard format.

2 Wind-induced fatigue damage analytical assessment

Using a quasi-steady theory and dealing with the structure as a linear system, the wind-induced stress s at a point M of the structure in a ΔT time interval is a stochastic stationary Gaussian process, given by the sum of s , the mean static stress, and s' , the fluctuating stress, schematized here as a bi-

modal process (Repetto, 2005; Repetto and Solari, 2006), obtained by summing the low frequency quasi-static part and the high frequency resonant part of s' . This two different parts of spectral content may be considered as uncorrelated. Adopting the S-N approach, the fatigue damage is evaluated by the Palmgren-Miner linear rule referred to the nominal stress (Miner, 1945). $D(1)$ is the mean total damage in the unit time and collapse conventionally occurs after a mean time T_F such that $D(T_F) = 1$. T_F is referred to as the mean fatigue life.

The solution of mean total damage in the unit time is very difficult. This difficulty may be partially overcome by introducing three further simplifying hypotheses. First, the density function of the mean wind velocity \bar{u} is given by the hybrid Weibull model (Takle and Brown, 1978; Solari, 1996). Second, the basic stress parameters –the mean value \bar{s} , the standard deviation σ , the expected frequency ν , the expected frequency of the quasi-static part ν_Q , and the normalized variance of the resonant part λ_D – are linked with the mean wind velocity \bar{u} by an approximate power law, depending on \bar{u}_{ref} , which is the reference mean wind velocity associated with the design return period R (Holmes, 2002; Repetto and Solari 2009). Third, in accordance with the code provisions usually adopted for steel details, the fatigue S-N curve is given by a trilinear function on a bi logarithmic diagram (Eurocode 3, 2005).

Based upon the above hypotheses, the author demonstrated that the mean total damage in the unit time may be expressed by (Repetto and Solari, 2009):

$$\bar{D}(1) = \bar{D}_0(1) C_{BM} C_M C_{SN} \quad (1)$$

where $\bar{D}_0(1)$ is referred to as the 0 level solution, C_{BM} is the bi-modal factor, C_M is the mean stress factor, and C_{SN} is the fatigue curve factor. The 0 level solution adopts three classic simplifications traditionally used in the technical literature: 1) the stress process is narrow band; 2) the stress process is zero mean; and, 3) the fatigue S-N curve is simplified as a straight line with m_1 slope, $\forall \Delta$. Due to these hypotheses, the analytical expression of $\bar{D}_0(1)$ is obtained in closed form, using the Gamma Function $\Gamma(\bullet)$ (Davis, 1965); the expressions of the factors C_{BM} , C_M and C_{SN} are obtained analytically in closed form too, removing the traditional hypothesis of the 0 level solution, one by one. The bi-modal factor satisfies the condition $C_{BM} \leq 1$, C_{BM} tending to 1 when the stress is narrow-band. The mean stress factor satisfies the condition $C_M \geq 1$, C_M tending to 1 when the mean stress is null. The fatigue curve factor satisfies the condition $C_{SN} \leq 1$, taking into account the trilinear trend of the S-N curves; it is worth notice that C_{SN} depends on the stress, on the S-N curve and on the wind parameters (Repetto and Solari, 2012).

The formulation explained in the previous part is earned both for alongwind and crosswind turbulence, since they have the same probabilistic properties, formulating input parameters equations for both evaluations. The author worked on the simplification of this formulation in order to be consistent with standards. Moreover, this formulation has been generalized to every different structural material, with every different slopes of fatigue S-N curves. The method considers that incoming wind velocity has always the worst direction for safety's sake (unidirectional analysis) (Repetto and Solari, 2004).

3 Highway signs support structures

Wind-induced fatigue response of a particular slender structure, the highway signs support structure, has been analysed, since many real examples of this kind experienced fatigue problems. This is reflected by inspection reports, which often indicate many damaged welded joints. The analysis conducted is based on the procedure proposed by the authors and the results has been compared with the inspections and the results of current codes. The latter have shown unreliable and rough outcome, while the application of the proposed method, compared with the real cases examined, leads to accurate fatigue life prediction. This analysis furnishes a key for the interpretation of collapses and damage causes of this kind of structures, highlighting the critical aspects of their aerodynamic behaviour and suggesting some remarks on the current state-of-the art on design against wind-induced actions.

References

- Davis, P.J. (1965). *Gamma function and related functions*. In Abramowitz, M., Stegun, I.A. (Eds.). Handbook of mathematical function. Dover Publication, New York.
- Eurocode 3. *Design of steel structure – Part 1-9: Fatigues*, UNI EN 1993-1-9:2005.
- Holmes, J.D. (2002). Fatigue under along-wind loading - closed-form solutions. *Eng. Struct.*, **24**, 109-114.
- Miner M. (1945). Cumulative Damage in Fatigue. *Trans. A.S.M.E.*, **67**, A159.
- Repetto M.P., Solari G., (2004). Directional wind-induced fatigue of slender vertical structures, *J. Struct. Eng.*, ASCE, **130**(7), 1032-1040.
- Repetto, M.P. (2005). Cycles counting methods for bi-modal stationary Gaussian processes. *Prob. Eng. Mech.*, **20**, 229-238.
- Repetto, M.P., Solari, G. (2006). Bimodal alongwind fatigue of structures. *J. Struct. Eng.*, ASCE, **132**(6), 899-908.
- Repetto, M.P., Solari, G. (2009). Closed form solution of the alongwind-induced fatigue damage to structures, *Eng. Struct.* **31**, 2414-2425.
- Repetto M.P., Solari G., (2012). Closed-Form Prediction of the Alongwind-Induced Fatigue of Structures, *J. Struct. Eng.*, ASCE, **138**, 1149-1160.
- Solari, G. (1996). *Wind speed statistics*. In Lalas, D.P., Ratto, C.F. (Eds.). Modeling of the atmospheric flow fields. World Scientific Publishing, Singapore.
- Take, E.S., Brown, J.M. (1978). Note on the use of Weibull statistics to characterize wind speed data. *J. Appl. Meteorol.*, **17**, 556-559.

Effect of Solidity on Aerodynamic Performance of Vertical Axis Wind Turbines

Abdolrahim Rezaeiha¹, Hamid Montazeri^{1,2}, Bert Blocken^{1,2}

¹ Building Physics and Services, Department of the Built Environment, Eindhoven University of Technology, P.O. Box 513, 5600 MB Eindhoven, The Netherlands

² Building Physics Section, Department of Civil Engineering, KU Leuven, Kasteelpark Arenberg 40 – Bus 2447, 3001 Leuven, Belgium

Corresponding author: A. Rezaeiha, a.rezaeiha@tue.nl

Abstract

Vertical axis wind turbines (VAWTs) are promising for wind energy harvesting in the urban environment mainly because of their omnidirectional capability. However, currently their aerodynamic performance is not comparable with horizontal axis wind turbines (HAWTs). Therefore, to make them an ideal candidate, they need to be further improved. The aerodynamic performance of VAWTs depends on several geometrical parameters, such as solidity. However, the impact of solidity on blade aerodynamics and turbine wake has not yet been comprehensively investigated. Therefore, the current study intends to systematically study the effect of solidity on aerodynamic performance of VAWTs with different number of blades operating at various tip speed ratios to provide a deeper insight into its impact on dynamic loads on blades, turbine performance and wake. High-fidelity unsteady Reynolds-averaged Navier-Stokes (URANS) simulations extensively validated with experimental data are employed. The results show that for fixed-rotational-speed urban VAWTs, which frequently operate at high tip speed ratios, a low solidity value is more favorable. On the other hand, an optimal VAWT is a high-solidity variable-rotational-speed (fixed λ) rotor operating at a low tip speed ratio regime.

1 Introduction

Vertical axis wind turbines have recently received growing interest for wind energy harvesting in the urban environment mainly due to their omni-directional capability. However, their aerodynamic performance is currently lower than HAWTs and they require performance improvement. Solidity (defined as $\sigma = nc/d$, where d is turbine diameter, n number of blades and c blade chord length) is an important geometrical parameter, which significantly affects the aerodynamic performance of VAWTs. An optimal rotor design (i.e. optimal σ) will maximize the output power. However, the optimal σ is highly dependent on the operating conditions, i.e. tip speed ratio λ . The impact of σ has been numerically and experimentally studied (Eboibi, Danao, & Howell, 2016; Li et al., 2016). However, to the best of our knowledge, (i) the studied range of σ was very limited, (ii) the dependency of σ on λ was not well addressed, and (iii) the focus was mainly on the average turbine performance rather than detailed analyses of blade aerodynamics and turbine wake. Therefore, the current study intends to address these gaps to support optimal design of VAWTs. High-fidelity CFD simulations extensively validated with experimental data are employed.

2 Computational settings and parameters

H-type VAWTs with the symmetric NACA0018 airfoil, $d = 1$ m, $n = 2-4$, $c = 2.25-18$ cm, and $\sigma = 0.09-0.36$ are studied. The freestream velocity is 9.3-18.6 m/s. The turbine rotational velocity is 46.5-102.3 rad/s corresponding to $\lambda = 2.5-5.5$. Chord-based Reynolds number is $0.77 \times 10^5 - 6.4 \times 10^5$. The approach-flow and incident-flow total turbulence intensities are 5% and 4.42%, respectively. The turbulent length scale is 1 m. The two-dimensional computational domain is $35d \times 20d$. The distance from the turbine center to domain inlet and outlet are $10d$ and $25d$. The blockage ratio (d/W) is 5%. The computational grid consists of approximately 400,000 quadrilateral cells with a maximum and average y^+ value of 3.8 and 1.4, respectively. The boundary conditions are uniform velocity inlet, zero gauge pressure outlet, symmetry sides, no-slip walls and sliding grid interface for the rotating grid. Incompressible URANS simulations are performed using ANSYS Fluent 16.1 with the 4-equation transition SST turbulence model, due to the transitional nature of the flow. 2nd order discretization in time and space and SIMPLE scheme for pressure-velocity coupling are employed. The transient simulations are performed with azimuthal increment of 0.1° for 20 revolutions of the turbine to ensure the results have reached a statistically steady state condition. The

results are sampled at the 21st turbine revolution. Extensive solution verification and validation are presented in Ref. (Rezaeiha, Kalkman, & Blocken, 2017; Rezaeiha, Montazeri, & Blocken, 2018).

3 Results and conclusions

Fig. 1 shows the power coefficient versus λ and σ for a 2-bladed VAWT. Fig. 1a reveals that a low-solidity VAWT will operate optimally at high λ while a high-solidity VAWT is optimum at low λ . The optimal λ decreases by increasing σ . This implies that a fixed-rotational-speed VAWT (i.e. the dominant design) is operating sub-optimally under the majority of operating conditions. In addition, for an urban VAWT, which most frequently operates at high λ regime due to low mean wind speed in the urban environment, a low solidity is favorable. Note that for fixed-rotational-speed urban VAWTs, high λ is unavoidable because, given their small size, they are preferred to rotate relatively fast to keep a sufficiently high Re ($>10^5$) and avoid the unwanted consequences of operating at low Re regime, i.e. large laminar separation bubble on blade and the consequent load fluctuations. Fig. 1b shows that the optimal σ decreases by increasing λ . In addition, the value of C_p delivered at the optimal σ slightly decreases for higher λ . This implies that, from an aerodynamic point of view, an optimal VAWT is a variable-rotational-speed rotor (fixed λ) with high solidity operating at a low λ regime. For the case of small-size urban VAWTs, the high solidity (high c) will help to keep Re in the desired regime. Fig. 1c exhibits turbine C_p in λ - σ space which can serve as a design guide for VAWTs for different operating conditions. Further and more detailed results and discussion for the 2-, 3- and 4-bladed VAWTs will be presented in the full paper.

The conclusions of this study are: (i) low solidity is favorable for fixed-rotational-speed urban VAWTs due to their inevitable high tip speed ratio, (ii) solidity of fixed-rotational-speed VAWTs needs to be selected with special attention to the wind conditions of potential installation sites and (iii) the optimal design for VAWTs needs to include variable rotational speed, high solidity and low tip speed ratio. The results of this study can help to design optimum VAWTs and more widespread wind energy harvesting.

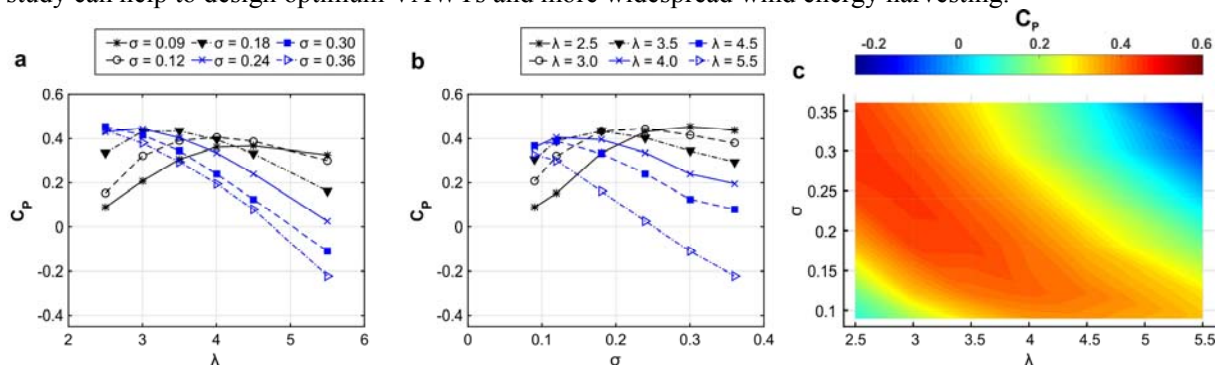


Figure 1. Power coefficient versus tip speed ratio and solidity for a 2-bladed VAWT (based on 36 simulations).

4 Acknowledgement

The authors acknowledge support from the EU Horizon 2020 (H2020-MSCA-ITN-2014), the TU1304 COST ACTION “WINERCOST, the partnership with ANSYS CFD, the NWO and FWO 12M5316N.

References

- Eboibi, O., Danao, L. A. M., & Howell, R. J. (2016). Experimental investigation of the influence of solidity on the performance and flow field aerodynamics of vertical axis wind turbines at low Reynolds numbers. *Renewable Energy*, 92, 474-483.
- Li, Q., Maeda, T., Kamada, Y., Murata, J., Shimizu, K., Ogasawara, T., . . . Kasuya, T. (2016). Effect of solidity on aerodynamic forces around straight-bladed vertical axis wind turbine by wind tunnel experiments (depending on number of blades). *Renewable Energy*, 96, 928-939.
- Rezaeiha, A., Kalkman, I., & Blocken, B. (2017). CFD simulation of a vertical axis wind turbine operating at a moderate tip speed ratio: guidelines for minimum domain size and azimuthal increment. *Renewable Energy*, 107, 373-385.
- Rezaeiha, A., Montazeri, H., & Blocken, B. (2018). Towards accurate CFD simulations of vertical axis wind turbines at different tip speed ratios and solidities: guidelines for azimuthal increment, domain size and convergence. *Energy Conversion and Management*, 156(C), 301-316.

Predicting microscale wind conditions to improve ship navigation in the largest vault in the world

A. Ricci^{1,2}, B. Blocken^{1,3}

¹ Building Physics and Services, Department of the Built Environment, Eindhoven University of Technology, P.O. Box 513, 5600 MB Eindhoven, The Netherlands

² Department of Civil, Chemical and Environmental Engineering (DICCA), University of Genoa, via Montallegro 1, 16145 Genoa, Italy

³ Building Physics Section, Department of Civil Engineering, KU Leuven, Kasteelpark Arenberg 40 - bus 2447, 3001 Leuven, Belgium

Corresponding author: A. Ricci, a.ricci@tue.nl

Abstract

This paper presents 3D steady RANS simulations performed for part of the Port of Amsterdam for 24 reference wind directions. The CFD results have been validated by field measurements by four 2D ultrasonic anemometers for a period of five months. A software application has been developed to convert the macroscale wind conditions at the reference weather station to the local wind conditions near and in the newly built vault in the Port of Amsterdam, the so-called IJmuiden vault.

1 Introduction

The macroscale wind conditions by standard weather stations show considerable differences with the local microscale wind conditions in harbor basins (Blocken et al., 2015). This is often caused by the local-scale forcing effects (e.g. buildings) and the influence of terrain roughness on the local wind flow. Knowledge of microscale port wind conditions is important for maneuvering and mooring of ships and also for optimizing the harbor design. In particular, the increasing ship sizes cause a larger ship inertia which renders the navigation through the harbor and especially through vaults by the tugboat pilots more difficult (Burlando et al., 2014). For this purpose, an accurate transformation tool based on numerical simulation with Computational Fluid Dynamics (CFD) has been developed to convert the macroscale wind conditions at the reference weather station to the local wind conditions near and in the newly built vault in the Port of Amsterdam, the so-called *IJmuiden vault*. The results of this transformation can be used in two ways: first to provide realistic simulations to train tugboat pilots, second as input for a real-time software application that provides the local wind conditions based on standard weather station recordings to help the tugboat pilots to guide the ship more precisely through the vault.

2 Field measurements

Field measurements of wind speed with 2D ultrasonic anemometers have been performed at four different positions, termed *IJm1*, *IJm2*, *IJm3* and *IJm4*, from 5th of July to 5th of December 2017 (Fig. 1). All the stations have been installed at a height of about 10 m above the ground level. The gathered field measurements were 1-min data and successively averaged into 10-min data. Field measurements have been used to validate the CFD results, in terms of mean wind speed and wind direction, as described in Sections 3 and 4.



Figure 1. Positions of the 2D ultrasonic anemometers installed in the IJmuiden vault.

3 CFD simulations

A high-resolution computational grid has been developed for a large part of the Port of Amsterdam. The grid covers an area of 225 km² and 74 million control volumes. 3D steady RANS simulations with realizable k - ϵ turbulence model have been performed for 24 reference wind directions (θ) using ANSYS Fluent 16.1. Five different roughness length (z_0) values, according to the roughness classification of Davenport updated by Wieringa (1992), have been taken into account by the standard wall functions, in terms of roughness height (k_s), and imposed on the bottom of the computational domain.

4 Validation of CFD results and software application

Fraction of data within a factor 1.3 ($FAC1.3$) has been used to validate the simulated data with the measured data, in terms of wind amplification factor (K). The comparison shows that 71% of simulated data is within 30% of deviation from the mean measured data. Based on the satisfactory agreement between simulated and measured data, a real-time software application has been developed for practical use by the Amsterdam Port Authority. The software, including the CFD results of 24 reference wind directions, allows the user to calculate the data of wind speed, wind direction and turbulence intensity at every position in the harbor (at 10 m above MSL) as a function of measured values at the reference position (KNMI) (Fig. 1). The results of this transformation can be used first to provide realistic simulations to train tugboat pilots, second to help the tugboat pilots to guide the ship more precisely through the vault.

References

- Blocken, B., van der Hout, A., Dekker, J., Weiler, O. (2015). CFD simulation of wind flow over natural complex terrain: Case study with validation by field measurements for Ria de Ferrol, Galicia, Spain. *Journal of Wind Engineering and Industrial Aerodynamics* **147**, 43-57.
- Burlando, M., Pizzo, M., Repetto, M.P., Solari, G., De Gaetano, P., Tizzi, M. (2014). Short-term wind forecast for the safety management of complex areas during hazardous wind events. *Journal of Wind Engineering and Industrial Aerodynamics* **135**, 170-181.
- Wieringa, J. (1992). Updating the Davenport roughness classification. *Journal of Wind Engineering and Industrial Aerodynamics* **41-44**, 357-368.

Experimental tests on the wave-induced response of a Tension Leg Platform supporting a 5MW wind turbine

L. Riefolo¹, M. Vardaroglu², A.M. Avossa², D. Vicinanza², F. Ricciardelli², G.R. Tomasicchio³

¹ Department of Civil and Environmental Engineering, Politecnico di Milano, Milano, Italy

² Department of Engineering, University of Campania “Luigi Vanvitelli”, Italy

³ Department of Engineering, University of Salento, Lecce, Italy

Corresponding author: L. Riefolo, luigia.riefolo@polimi.it

Abstract

The interest for the dynamic response of offshore wind turbines, when subjected to given environmental conditions, has rapidly expanded in the last years. The investigation of the dynamic behaviour is a complex topic that needs to be examined through dedicated physical models. Nowadays, the demand has increased for quality physical model tests to optimise the design of innovative floating wind turbines, and to collect reliable and accurate data for further calibration and verification of numerical models. Tension Leg Platform (TLP) wind turbines represent one potential method for accessing offshore wind resource in moderately deep water. Although numerous TLP concepts have been developed and presented in the literature (Pegalajar-Jurado et al., 2016; Bachynski and Moan, 2012), it is essential to improve the knowledge on the TLP concept, and its performance in various environmental conditions.

The present paper summarises the experience gained from wave basin experiments aimed at investigating the dynamic response of a TLP wind turbine, under different wind and wave conditions. The tests were performed at the Danish Hydraulic Institute (DHI) within a wider test program funded in the framework of the EU-Hydralab IV Integrated Infrastructure Initiative. The 1:40 Froude-scaled model was subjected to regular and irregular waves, and to steady wind loads. Measurements were taken of the hydrodynamics, of the displacements of the floating structure, and of the wave induced forces at critical sections of the structure and of the tendon lines. First, free vibration tests were performed to obtain the natural periods. Then, displacements, rotations, accelerations, and forces were measured under regular waves for different wind conditions. Statistical and spectral analyses were carried out to investigate the dynamic behaviour of TLP wind turbine.

The physical model was built with reference to the prototype MIT/NREL for TLP model (Jonkman et al., 2009). Model tests were carried in the DHI deep-water wave basin in Hørsholm, Denmark. The wave basin is 20 m long and 30 m wide with an overall water depth of 3 m and a 6 m deep pit. The floating structure was placed at the centre of the pit, and at a distance of 8 m from the wave maker. The TLP model was constructed out of plastic and it was composed by four main components: the floater, the cover, the tower and the leg assembly. TLP was tested under long crested regular and irregular, orthogonal and yaw (20°) waves, and under a steady wind load. An overview of the setup instrumentation, and a summary of the properties of the TLP are given in Figure 1 and in Table 1.

In the paper the dynamic response of the turbine will be investigated, both in the time and frequency domains. The statistical and spectral characteristics of the displacement and acceleration components, of the structural forces and of the tendon stresses will be analysed, and their variability with sea state and conditions drawn.

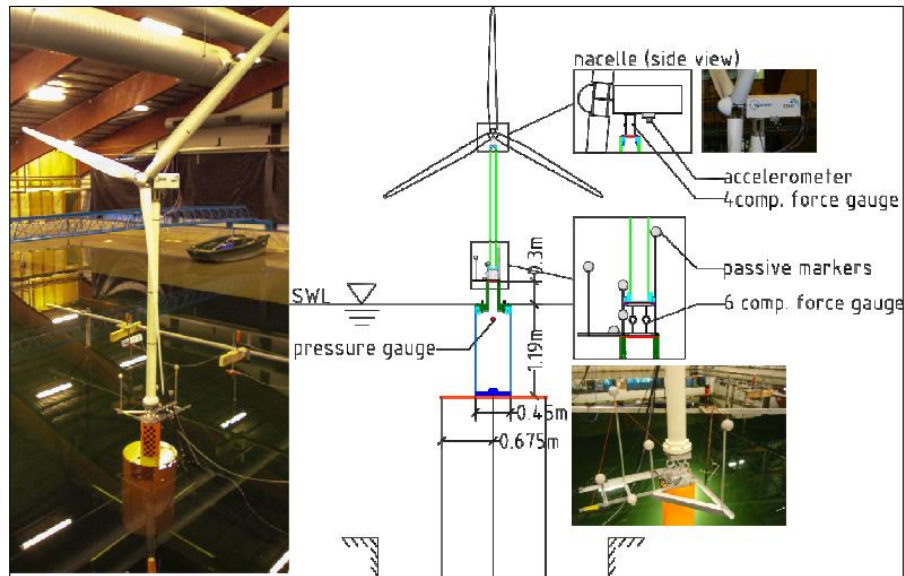


Figure 1. Overview of the setup and instrumentation of the TLP wind turbine.

Table 1. Summary of properties of the MIT/NREL model.

	Prototype scale	Unit	Scale factor	Model scale
Diameter of the platform	18	m	λ	0.45
Draft	47.89	m	λ	1.20
Radius to fairleads	27	M	λ	0.67
Depth to fairleads	47.89	M	λ	1.20
CM location below still water level	40.61	m	λ	1.01
Tower height (hub level)	90	m	λ	2.25
Tower mass	347500	kg	λ^3	5.30
Mass of floating system including ballast	8600000	kg	λ^3	131.10
Water displacement	12180	m ³	λ^3	0.19
Roll mass moment inertia	5.72×10^8	kgm ²	λ^5	5.44
Unstretched line length	151.70	m	λ	3.79
Line diameter	0.1270	m	λ	0.0032
Line mass density	116	kg/m	λ^2	0.0707

1 References

Bachynski E., Moan T. (2012). Design considerations for tension leg platform wind turbines, *Marine Structures* 29, 89–114.

Jonkman, J., Matha, D., (2009). A Quantitative Comparison of the Responses of Three Floating Platforms, *Proceedings of European Offshore Wind Conference and Exhibition Stockholm, Sweden, September 14–16*.

Pegalajar-Jurado A., Hansen A.M., Laugesen R., Mikkelsen R.F., Borg M., Kim T., Heilskov N.F., Bredmose H., (2016). Experimental and numerical study of a 10MW TLP wind turbine in waves and wind, *Journal of Physics: Conference Series* 753 092007.

Mixture model in high-order statistics for peak factor estimation on low-rise building

F. Rigo¹, T. Andrianne¹ and V. Denoël²

¹Wind Tunnel Lab, Dept. of Aerospace and Mechanical Engineering, University of Liège, Belgium

²Stochastic and Structural Dynamics, Dept. of Urban and Environmental Engineering, University of Liège, Belgium

Corresponding author: F. Rigo, francois.rigo@uliege.be

Abstract

To design reliable structures, extreme pressures and peak factors are required. In many applications of Wind Engineering, their statistical analysis has to be performed taking into account the non-Gaussianity of the wind pressures. With the increasing precision and sampling frequency of pressure sensors, large short and local peak events are more usually captured. Their relevance is naturally questioned in the context of a structural design.

Furthermore, the increasing computational power allows for accumulation and analysis of larger data sets revealing the detailed nature of wind flows around bluff bodies. In particular, in the shear layers and where local vortices form, it is commonly admitted that the Probability Density Function (PDF) of measured pressures might exhibit two or more significant components. These mixed flows can be modelled with mixture models [Cook (2016)]. Whenever several processes coexist, and when one of them is leading in the tail of the statistical distribution, as will be seen next in the context of corner vortices over a flat roof, it is natural to construct the extreme value model with this leading process and not with the mixed observed pressures. It is therefore important to separate the different processes that can be observed in the pressure histories. Once this is done, specific analytical formulations of non-Gaussian peak factors can be used to evaluate the statistics of extreme values [Kareem and Zhao (1994), Chen (2009)].

The separation of mixed processes is usually done by means of the PDF of the signals [Cook (2016)]. This information is of course essential to perform an accurate decomposition but it might be facilitated by considering higher rank information like auto-correlations and higher correlations like the triple or quadruple correlation. Indeed, the two phenomena that need to be separated and identified might be characterized by significantly different timescales, which are not reflected in the PDF. In this paper, the large negative pressures measured on a flat roof are analyzed and decomposed into two elementary processes, namely, the flapping corner vortex and the turbulent flow detaching from the sharp upstream edge.

The full paper will finally show that an accurate decomposition of the recorded pressures into their underlying modes provides a more meaningful evaluation of the extreme pressures.

1 Introduction

The setup made by [Blaise et al (2017)] consists of a square plan-form low-rise building (sides of 45 m and a height of 25 m), uniformly instrumented by 121 pressure taps in a quarter of its roof (see Figure 1(a)), sampled at 500 Hz. The model is placed at an incidence of 45° in the atmospheric boundary layer test section of the wind tunnel (WT) of the University of Liege. Scaling parameters are: $\lambda_L = 1/100$ (geometry), $\lambda_U = 1/3.5$ (velocity) and $\lambda_T = 1/28.6$ (time). Every measurement is converted in full scale. A total of 13 h of measurement has been taken in the WT, corresponding to 371.8 h full scale. This long information allows to draw precise PDF tail, necessary to study the extreme values. The flow around this low-rise building is characterized by corner vortices, that roll in a cone shape. The 2 cones on both corners have a main axis, recognizable by in the ridgelines of the standard deviation of the pressure coefficient $\sigma(C_p)$, in Figure 1(b). Figure 1(c) shows a map of the mean value

of peak factor of the pressure coefficient $\mu_g(C_p)$, the highest values happening were the vortex cone touches the roof.

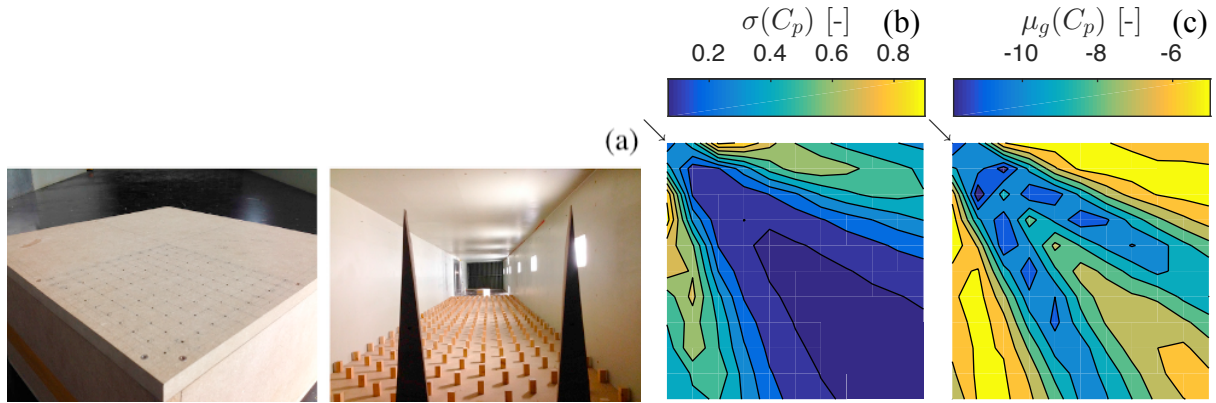


Figure 1. Model inside the WT (a), map of standard deviation (b) and peak factor (c) of pressure coefficient.

2 Methodology

Figure 2(a) shows the recorded pressure coefficient at tap 34 (inside corner vortices and separated region), with non-Gaussian behaviour. Two modes in the PDF are identifiable in Figures 2(b)-(c): (i) mode 1 corresponding to the turbulent background flow (as the one present on the roof region without vortex) and (ii) mode 2 to the vortices fluctuation (separated flow). Using a skew-Gaussian for the 2 modes and a skew hyperbolic secant to represent the tail, as suggested by [Cook (2016)], the PDF decomposition was simple for this tap because of its clear double bump.

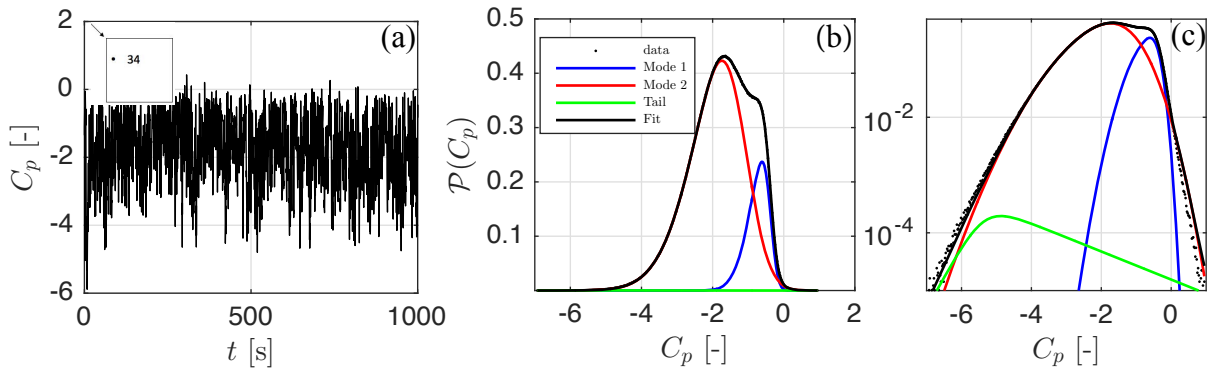


Figure 2. Time history (a), PDF in linear (b) and log (c) scale of the pressure coefficient at tap 34.

3 Results and conclusions

By going through the taps along the corner, the two bumps are getting closer and merge, mode 2 becoming more and more important compared to mode 1. The method proposed by [Cook (2016)] is not robust anymore to identify initial values of the fitting algorithm. By looking at the autocorrelation function in Figure 3(b), the shape shows a break between two exponential decay functions, at around 0.4 s. This suggests also a decomposition in 2 modes, as before: (i) the turbulent background of mode 1 with a longer memory time than (ii) mode 2. The value of the autocorrelation at the origin is the variance. Variances of both modes are identified and are used in the PDF decomposition algorithm, to make it more robust (see Figure 3(a)). The same procedure is done using the triple correlation (with 2 delays) to decompose skewness of both modes. Figure 3(c) shows the map of the relative importance of variances of modes 1 and 2. Mode 1 is more present at the extremities of the vortex cone. Once PDFs are decomposed, one can access the statistical properties of a given mode. It allows to correct

the value of skewness and kurtosis used in the extreme value model of [Kareem and Zhao (1994)]. More precise estimation of peak factor is then obtained, compared to those obtained with the whole PDF, not robust in the model because of its strong non-Gaussianity.

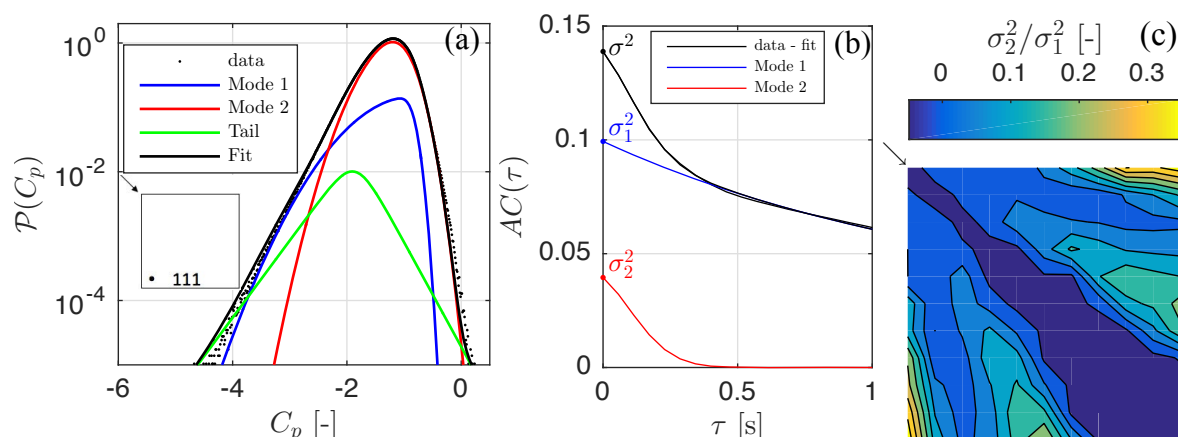


Figure 3. PDF (a) and autocorrelation function (b) of the pressure coefficient at tap 111, map of relative importance of variance of mode 2 compared to 1 (c).

References

- Kareem, A., and Zhao, J. (1994). Analysis of non-Gaussian surge response of tension leg platforms under wind loads. *J. offshore Mech. and Arctic Eng.*, ASME, **116**, 137-144.
- Chen, X. and Huang, G. (2009). Evaluation of peak resultant response for wind-excited tall buildings. *Engineering Structures* **31**, 858-868.
- Cook, J. (2016). Short communication: On the Gaussian-Exponential Mixture Model for pressure coefficients. *Journal of Wind Engineering and Industrial Aerodynamics* **153**, 71–77.
- Blaise, N., Andrienne, T. and Denoël, V. (2017). Assessment of extreme value overestimations with equivalent static wind loads. *Journal of Wind Engineering and Industrial Aerodynamics* **168**, 123–133.

Vortex induced vibrations of rectangular cylinders arranged on a grid

F. Rigo¹, V. Denoël² and T. Andrianne¹

¹Wind Tunnel Lab, Dept. of Aerospace and Mechanical Engineering, University of Liège, Belgium

²Stochastic and Structural Dynamics, Dept. of Urban and Environmental Engineering, University of Liège, Belgium

Corresponding author: F. Rigo, francois.rigo@uliege.be

Abstract

A grid arrangement made of one hundred rectangular cylinders fixed to the facade of a house generates strong and disturbing mono-harmonic noise. The cross-flow vibration of the rectangular cylinders is identified as the origin of the noise. The present article proposes a complete investigation of the Vortex Induced Vibration (VIV) combined with a grid effect. It is based on in situ measurements, numerical (finite elements and Computational Fluid Dynamics (CFD)) and extensive wind tunnel (WT) modelling. A comparison between unsteady pressure tap measurements and CFD results allows to understand the vortex shedding process and synchronization type depending on the wind incidence and spacing of the cylinders. On the basis of this multi-approach parametric investigation, a deep understanding of the VIV-grid phenomenon enables to propose two mitigation techniques. These techniques are tested and their effectiveness is reported in terms of vibration amplitude and acoustic intensity.

1 Introduction

Figure 1 shows the grid made of rectangular aluminium cylinders, concealing the terrace of the house. The phenomenon was rapidly identified as VIV of the cylinders, interacting inside the grid arrangement, for given wind conditions (direction and intensity). The purpose of this study is to characterise the phenomenon and propose a mitigation technique.



Figure 1. Grid arrangement on the facade of the house.

2 Methodology

Figure 2 shows measurements performed on the real grid during seven half days, to cover a large distribution of wind speeds and incidences. In this preliminary observation, three cylinders were instrumented with accelerometers, two filled with sand and one was empty. An anemometer is used to monitor the wind conditions. It appears that strong vibrations take place when the wind speed is above 5 m/s with a preferred 50° incidence. The vibration amplitude of the empty cylinder is more important than the filled one due to a lower weight and damping. A 1:1 scale model of the grid including ten cylinders was built and tested at the Wind Tunnel Laboratory of ULiège. This allowed to perform a parametric study of the grid by changing the wind incidence [Knisely (1989)] and the cylinders spacing to obtain typical VIV responses and a Strouhal number map in the space of parameters [Zdravkovitch (1984) and Sumner et al. (2007)]. The cylinders were instrumented by accelerometers and pressure taps to understand the flow in the grid arrangement. In parallel, a finite element model of the grid was used to characterise the dynamic properties of the grid. A CFD model allowed to deeper understand the flow between cylinders and the interaction between shear layers and cylinders, as a function of the spacing. Wind conditions of the real grid were reproduced and compared with the WT model, the latter showed critical condition at 5 m/s and 0° . The VIV curve *in situ* was a mixing of WT VIV curves between 0° and 50° .

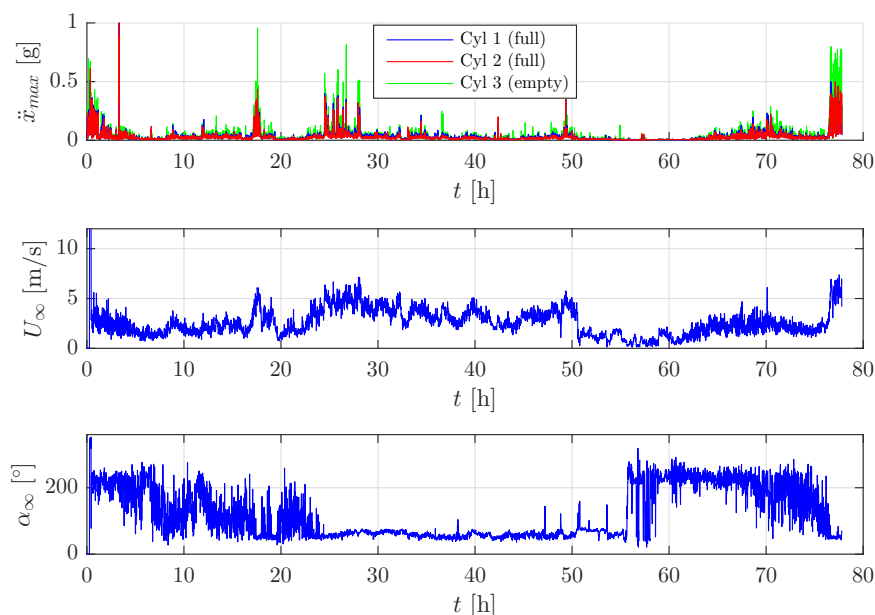


Figure 2. *In situ* measurement: peak response during 7 half days, correspondence U_∞ - α_∞ during event.

3 Results

After a deep analysis of the VIV-grid phenomenon, two mitigation techniques were proposed and tested: (i) solution 1 consists in adding a horizontal beam, riveted to the cylinders, while (ii) solution 2 is performed by adding sand in the cylinders. The first solution has the effect to stiffen and add damping to the structure and the second solution adds damping and weight but reduces the structural modal frequencies. Figure 3 shows the VIV curve obtained for the initial grid and the two solutions. Solution 2 allowed to reduce the vibration amplitude and the noise intensity but at a lower critical speed. Solution 1 was retained because vibration and noise amplitude were reduced, and the critical speed was higher (15 m/s), which is rather unlikely in the present landscape. The noise intensity *in situ* were higher than the one in the WT because of the terrace, playing as a guitar soundboard.

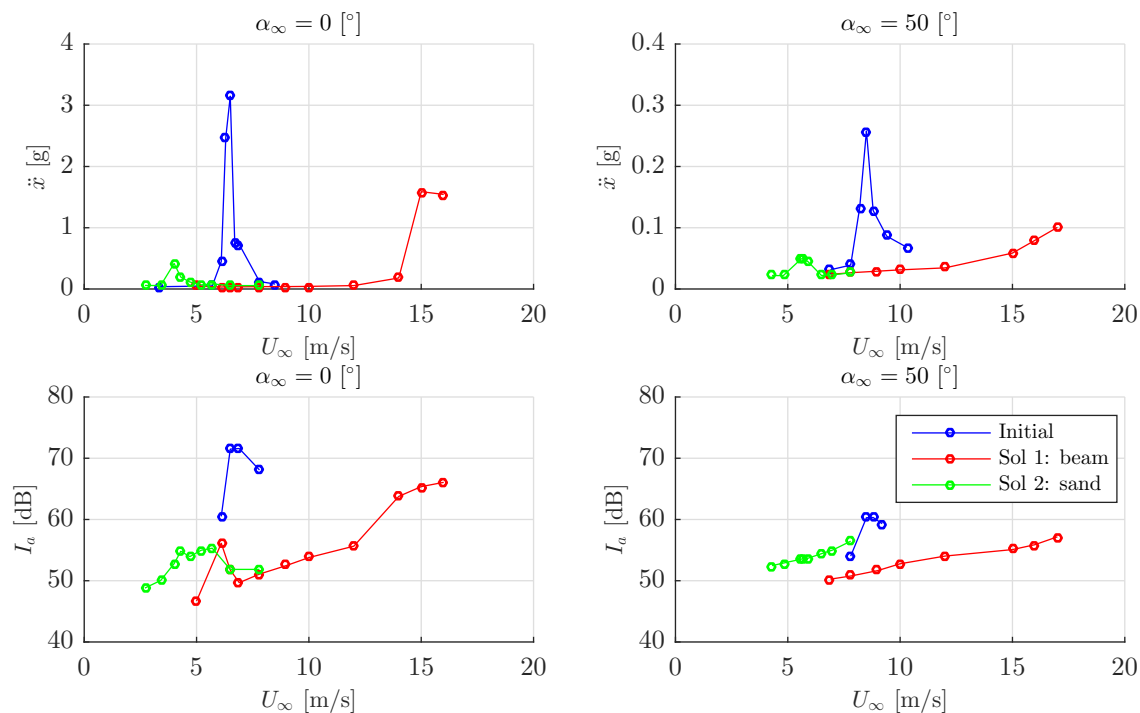


Figure 3. Wind tunnel model: VIV curve \ddot{x}_{rms} and acoustic intensity I_a vs U_∞ at $\alpha_\infty = 0^\circ - 50^\circ$ for the initial and solution models.

References

- Knisely, C. W. (1989). Strouhal numbers of rectangular cylinders at incidence: a review and new data. *Journal of Fluids and Structures* **4**, 371-393.
- Zdravkovich, M. (1984). Kareem, A., and Zhao, J. (1994). Flow induced oscillations of two interfering circular cylinders. *Journal of Sound and Vibration* **101**, 511-521.
- Sumner, D., Richards M. and Akosile, O. (2007). Kareem, A., and Zhao, J. (1994). Strouhal number data for two staggered circular cylinders. *Journal of Wind Engineering and Industrial Aerodynamics* **96**, 859-871.

The interplay between background atmospheric boundary layer winds and downburst outflows. A first physical experiment

Djordje Romanic¹ and Horia Hangan¹

¹Wind Engineering, Energy and Environment (WindEEE) Research Institute, Western University,
Canada

Corresponding author: Djordje Romanic, dromanica@uwo.ca

Abstract

The research presented in this paper is on the interaction between downburst outflows and background atmospheric boundary layer (ABL) winds close to the surface. Downbursts are buoyancy-driven downdrafts of cold air that originates from thunderstorms (typically cumulonimbus clouds) and result in a vigorous starburst outflows upon reaching the surface. There are neither satisfactory analytical models nor experimental results on the highly complex interaction between these two wind systems. One of the advanced modes of the WindEEE Dome operation enables the simultaneous generation of downburst and ABL flows. In accordance with the WindEEE Dome capabilities, an experiment is designed to address this important question on the relationship between ABL and downburst flows.

1 Introduction

Downbursts were first investigated after several commercial airplane crashes in the 1970s (Fujita 1981; 1985). Later, it has been shown that downbursts are also extremely damaging not only to airplanes but also to the built environment on the surface. Although large progress has been made in understanding these severe windstorms in the meantime, there are still a number of unknown facets associated with this phenomena. One of these is the coupling between the microscale downburst and the macroscale synoptic winds.

The parent cloud as well as the developing downburst are not an isolated system, but instead both are embedded into the background atmospheric boundary layer (ABL) flow. That is, the cloud-downburst system constantly interacts with the ABL winds, which, in turn, are characterized with the pronounced velocity shears during the atmospheric conditions favourable for development of thunderstorms. Note that the velocity shear indicates that both speed and direction of wind are changing with height. Currently there are neither satisfactory analytical models nor experimental results on the nonlinear interaction between the two wind systems. An attempt to combine the flows through a linear vector summation is physically inaccurate, as recently demonstrated at the European Wind Engineering Conference in Liège, Belgium (Romanic et al., 2017). A new approach is therefore needed.

2 WindEEE Dome

The Wind Engineering, Energy and Environment (WindEEE) Dome (Hangan 2010; Hangan et al., 2017) at Western University in London, Ontario, Canada (<http://www.eng.uwo.ca/windeee/>) is the world's first three-dimensional testing chamber capable of physically replicating time-dependent, straight, sheared or swirl winds of variable directionality, such as downbursts and tornadoes. The simulation of these large spectra of atmospheric flows is achieved through manipulating 106 individually controlled fans and 202 louvers. 100 fans are positioned along the peripheral walls of the testing chamber, out of which 60 are installed in a matrix of 15 fans per row times 4 rows. This 60-fan wall will be used to produce the ABL flows (Figure 1). Each of the 60 fans is 0.8 m in diameter with the

nominal wind speed of approximately 25 m s^{-1} . The 6 fans in the upper chamber are 2 m in diameter and they are used to produce the impinging jet-like downburst (Figure 2). The downburst jet runs through a bell mouth of 4.5 m in diameter that connects the upper plenum with the testing chamber of the WindEEE Dome.

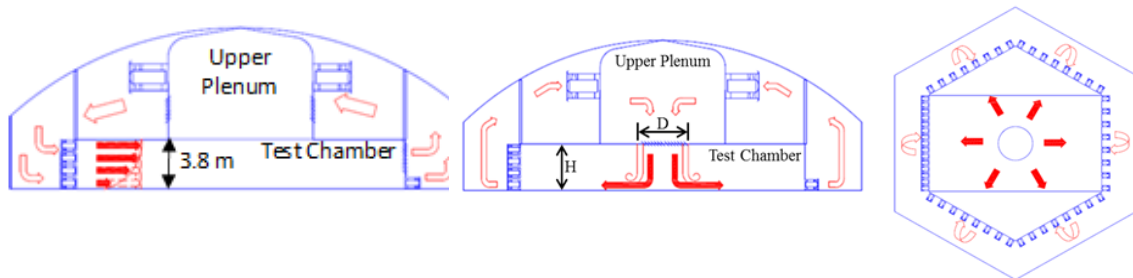


Figure 1. Schematics of ABL flow (left) and downburst (right) flows in WindEEE Dome.

3 Experiment setup

One of the advanced modes of the WindEEE Dome operation enables the simultaneous generation of downburst and ABL flows. Recognizing this unique capability of WindEEE Dome, an experiment has been designed that would address the question on the relationship between the ABL and downburst winds. The experiment setup is portrayed in Figure 2. The velocity measurements are conducted using a set of ten Cobra Probes with a sampling frequency of 2500 Hz. Five Cobra Probes always face the centre of the testing chamber (i.e., the downburst centre), while the other five probes are oriented towards the 60-fan wall (i.e., facing the ABL flow). Note that due to the circular symmetry of the bell mouth, downbursts in the WindEEE Dome are symmetric around the vertical axis, which also enables the independent measurements of ABL and downbursts flows. Since Cobra Probes measure the flow within a 45° cone, the obtained ABL and downburst time series can be combined to obtain the overall flow field. The experiments are performed for different radii (R) from the downburst centre as well as for the different azimuth angles (θ ; see Figure 2). The experiment is designed to reveal the full three-dimensional picture of the flow—namely, five probes at different heights (z) plus different radii plus different azimuth angles plus two sets of probes that independently measure ABL and downburst winds. The measurements were repeated several times in order to test for repeatability and to build the necessary statistical significance of the results.

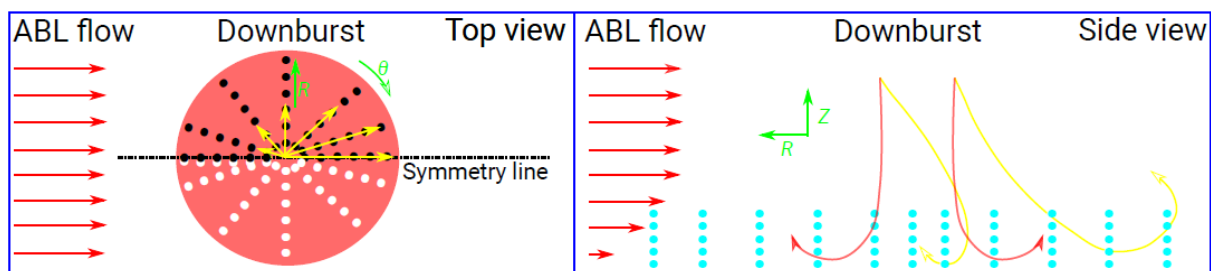


Figure 2. Conducted experiment in the WindEEE Dome; the red downburst represents a downburst flow without ABL winds and the yellow arrows are a schematics of a downburst influenced by the ABL flow; in left panel black and white dots represent the downburst and ABL Cobra Probes, respectively; in right panel both sets of probes are indicated with cyan color.

References

- Fujita, T.T. (1981). Tornadoes and downbursts in the context of generalized planetary scales. *Journal of the Atmospheric Sciences* **38**, 1511–1534.
- Fujita, T.T. (1985). *The downburst: microburst and macroburst*. Satellite and Mesometeorology Research Project, Department of the Geophysical Sciences, University of Chicago.
- Hangan, H. (2010). Current and future directions for wind research at Western: A new quantum leap in wind research through the Wind Engineering, Energy and Environment (WindEEE) Dome. *Wind Engineers, JAWE* **35**, 277–281.
- Hangan, H., Refan, M., Jubayer, C., Romanic, D., Parvu, D., LoTufo, J., and Costache, A. (2017). Novel techniques in wind engineering. *Journal of Wind Engineering and Industrial Aerodynamics* **171**, 12–33.
- Romanic, D., Parvu, D., and Hangan, H. (2017). Influence of background winds and storm motion on downburst outflow. *7th European and African Conference on Wind Engineering (EACWE 2017)*, Jul. 3–6, Liège, Belgium.

Field measurement of gas dispersion in the Atsugi area

Ryoji Sasaki¹, Koichi Miyashita¹ and Ryuichiro Yoshie²

¹Wind Engineering Institute Co., Ltd., Japan

²Tokyo Polytechnic University, Japan

Corresponding author: Ryoji Sasaki, sasaki@wei.co.jp

Abstract

The prediction of gas dispersion is important for environmental assessment. A field study was conducted on the gas dispersion in the urban area of Atsugi city in Japan. The release point of the gas was set on the rooftop of a building. The sampling points were located on the ground surface. We compared the gas concentrations from the field measurements with the theoretical plume model. The field results agree with the plume model. Furthermore, it is found that the wind direction at the release point affects the accuracy of predicting gas dispersion.

1 Introduction

The prediction of gas dispersion is important for environmental assessment. The prediction method using wind tunnel tests and Computational Fluid Dynamics (CFD) has not yet been validated, because of the lack of sufficient wind speed and gas concentration data in urban areas. For the purpose of this study, we did a preliminary field measurement of gas dispersion at Tokyo Polytechnic University over a 300-m wide area. It was shown that the wind speed and gas concentration data of the field measurement agreed well with the values of wind tunnel tests and CFD (Miyashita et al., 2015). As the next step, we performed a similar field measurement for a wider area (Atsugi city, Japan).

2 Field measurement

The field measurement was conducted in the Atsugi area, which is approximately 5 km wide. In the test area, Sagami River flows in a north-south direction and the topography is mostly flat. The field measurement was carried out from August 5 to August 8, 2014.

Figure 1 shows the locations of the release point and 37 sampling points. The release point was set on the rooftop of a building, which was approximately 24 m high, as shown in Figure 2(a). An ultrasonic anemometer, a pyranometer, and a doppler lidar were set at the release point. In this study, PMCH (Perfluoro-Methyl Cyclo Hexane, C_7F_{14} , $M=350$) was used as the tracer gas. The sampling points were located on the ground surface as shown in Figure 2(b), and the height of the sampler was 1.5 m. The sampling time for 1 run was 30 min. We performed 8 runs per day, totalling to 32 runs in the study.

3 Results

Figure 3 illustrates the distribution of gas concentration over the test area. The arrows in the figure show the wind direction at the release point. It is shown that the high-concentration area extends along the wind direction. However, Figure 3(c) indicates that there is a gap in the high-concentration area. It is thought that the gap is related to the atmospheric stability or the fluctuation of wind direction.

Figure 4 shows a comparison of the results from this study and the plume model. Figure 4(a) and (b) indicate that the results agree with each other. Furthermore, it is found that the wind direction at the release point is important in predicting the gas dispersion.

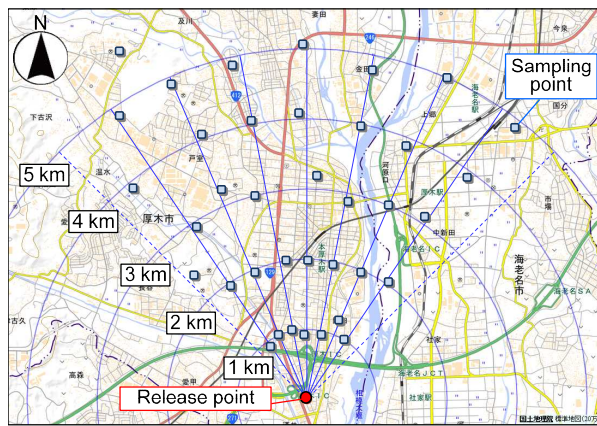


Figure 1. Location of the release and sampling points

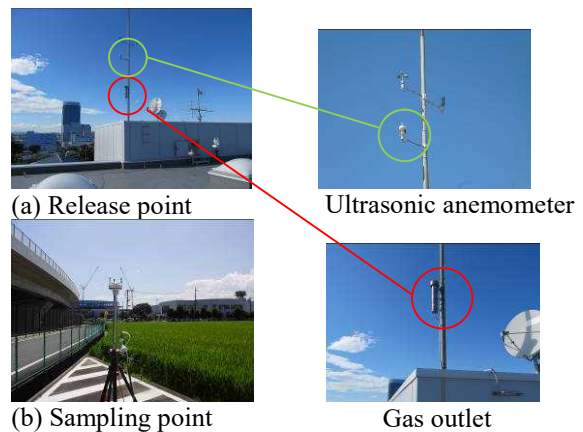


Figure 2. Overview of points

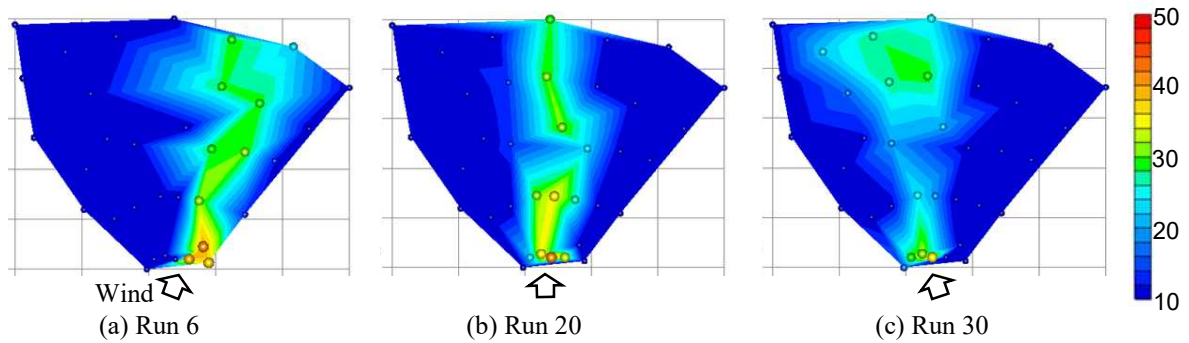


Figure 3. Distribution of gas concentration (ppq [Log-scale])

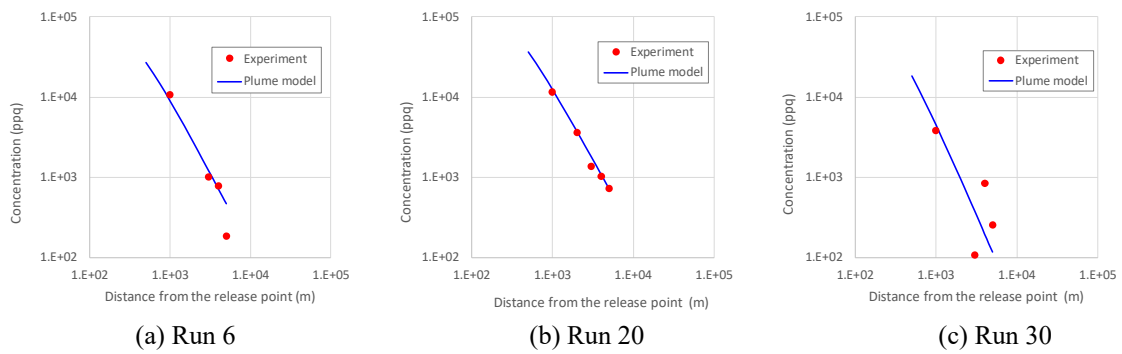


Figure 4. Comparison of concentrations between the experimental results and plume model

References

Miyashita, K. et al. (2015). Full scale experiment of gas dispersion in an urban area and its prediction by wind tunnel experiment and large eddy simulation, Part 1-4, *Wind Engineers, JAWE*, Vol 40 No.2, pp.87–94. [in Japanese]

Definition of wind loads on the Riyadh Western Metro Station

Paolo Schito¹, Lorenzo Rosa¹ and Alberto Zasso¹

¹Department of Mechanical Engineering, Politecnico di Milano, Italy

Corresponding author: Paolo Schito, paolo.schito@polimi.it

Abstract

Design of large modern structures can be strongly affected by wind actions, in terms of dynamic loading as well as peak façade cladding load. The definition of the wind forcing can be defined by means of CFD analysis as well by wind tunnel tests using a scaled model instrumented with pressure taps. The density and the distribution of pressure taps on the building surface is critical, as well as the averaging of the surface pressure time history for the definition of the wind actions. Dynamic actions are calculated using a modal approach, while pressure excitation is computed according to time equivalent area averaging. The definition of the time equivalent area averaging is carefully analysed, in order to provide pressure values consistent with the forcing area.

1 Introduction

Many strategies can be adopted for the calculation of wind loads on structures. In the present case the study is carried out using CFD calculation for the definition of the aerodynamic actions on the structure and using the Standard recommended approach to compute the wind loads, and in a following stage through wind tunnel tests using the high frequency pressure integration technique (HFPI). The practical basis of this approach is to develop an analytical modal approach considering as input the pressure data acquired simultaneously over the surface of the structure and the modal information (modal masses, mode shapes and frequencies) obtained from a finite element model of the structure.

The structure that has been considered is the Riyadh Western Metro Station (Figure 1): it is a very light structure, mainly in steel, with length larger than $300m$ and a height up to $25m$. The particular shape of the building and in particular of the smaller dome that acts as a cantilever produces very particular dynamic response of the structure.



Figure 1. Rendering of the Riyadh Western Metro Station.

CFD analysis is carried out using an incompressible steady-state RANS approach, with boundary conditions able to reproduce and maintain the incident wind profile. Wind speed is assumed to be the 3 second gust wind speed.

For the experimental test, the wind tunnel model must be instrumented with pressure taps at enough locations to fully describe the overall wind loading at any instant in time. The time histories of the pressures should be filtered by a moving average filter in order to spread the measured local value on an effective surface area appropriate for the calculation of the total external pressure force.

The response of the structure caused by the turbulent wind is then calculated in correspondence of the nodes of the FE model. The analysis is carried out, in the time domain, using step by step numerical integration of the motion equations of the structure, known the pressure measurements, properly filtered, in correspondence of the pressure taps.

The overall structural loads are then shown as equivalent forces acting as a static load on each node of the FE model and the simultaneous external pressures acting as a static pressure on loading-areas in which the external surface has been divided (typical on the external shell elements).

Since it is impractical to analyse every possible wind pressure pattern might occur, certain loading scenarios that tend to stress the structure in important ways must be properly selected. This operation is done considering different markers that are generally selected in accordance with the structural engineer in order to find the most severe and representative load conditions to be applied to the structure.

Example of markers are the instants of time in which a total base force or a base total moment reaches its maximum/minimum, or a combination of maximum/minimum of the base forces.

Applying these wind loads to the structural finite element model of the building (FEM) it is then possible to calculate the overall deflections of the structure. The structural engineer can finally review these deflections in order to assess the potential for excessive shearing in structure.

As an example of results, Figure 2 shows the whole instant values of wind-induced total load (external pressure + inertial contribution) in terms of the shear force F_y TOT vs F_x TOT at the base of the structure calculated for each wind exposure angle tested during the wind tunnel tests. In other words, this figure shows all the possible combinations of wind-induced loads (shear forces) at the base of the structure predicted by the numerical calculation. The figure is obtained considering the pressure values calculated for all the wind exposures tested in the wind tunnel, resulting in a corresponding statistical base of equivalent full scale time that is very wide. From this figure, it is possible to highlight the worst load conditions to which the structure is subjected. The selected points on the boundary of the region, numbered in the figures, represent real instantaneous relative maximum values reached by the corresponding shear/bending moments at the building base and can be considered as characteristic load cases. The external envelope of the points of each cloud graph, together with the others selected markers, are the reference base for selecting true wind load distributions that are the extreme values reached during a physically simulated event.

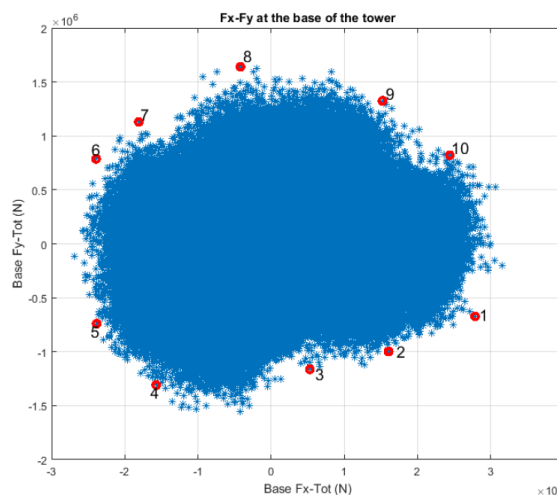


Figure 2. Predicted shears F_y TOT vs F_x TOT at base of a structure for all exposure angles.

Characterization of mean wind profiles and surface roughness assessment from wind LIDAR measurements

V. Sepe¹, F. Rizzo², F. Ricciardelli³ and A.M. Avossa³

¹Department of Engineering and Geology, University “G. D’Annunzio” of Chieti-Pescara, Italy

²CRIACIV: Inter-University Research Centre for Building Aerodynamics and Wind Engineering, Italy

³Department of Engineering, University of Campania “Luigi Vanvitelli”, Italy

Corresponding author: V. Sepe, v.sepe@unich.it

Abstract

To evaluate wind loading on medium- to high-rise structures, an accurate representation of the mean wind profile and of the structure of turbulence is required. Wind models are currently incorporated in Codes of Practice, which have been theoretically derived and experimentally calibrated. Nevertheless, the limited amount of data makes such calibration questionable at times. Wind LIDARS have recently appeared and are becoming more and more common for the assessment of wind power and for the monitoring of wind characteristics. They provide a direct measurement of the wind velocity at the site and at the height of interest and offer the possibility of analyzing the spatial distribution of mean and fluctuating wind speed. In this paper, wind LIDAR measurements are used to characterize the vertical wind profile under different stability condition, and to calibrate surface roughness to be used in wind models.

1 Introduction

To evaluate wind loading on medium- to high-rise structures, an accurate representation of the characteristics of strong winds in the Atmospheric Boundary Layer (ABL) is needed. On the other hand, lower winds contribute to fatigue damage accumulation, and are therefore of interest for Structural Engineers. Several theoretical and empirical models have been proposed to describe the vertical distribution of mean wind speed, the calibration of which is based on the knowledge of the underlying surface roughness. Although the topic is well established, there is still no common consensus on what is the most appropriate wind model, especially for Code of Practice implementation, and on how to calibrate surface roughness. Recently, observations of wind speed profiles through Doppler Lidar anemometry are becoming available. These provide a direct measurement of the wind velocity at the site and at the height of interest, in a range of several hundred meters above the ground, and with a sampling rate up to 1 Hz. In addition, wind LIDARS, and in particular wind scanners also offer the possibility of analysing the spatial distribution of mean and fluctuating wind speed.

In spite of the inaccuracies associated with space averaging and with non-synchronous measurement of continuous beam LIDARS, wind LIDARS measurements are becoming a useful tool for Wind Engineering and for Wind Energy, e.g. to identify the vertical mean wind profile and the structure of turbulence in the ABL.

2 LIDAR measurements

At the beginning of October 2015 a pulsed wave WindCube V2 wind LIDAR manufactured by Leosphere was installed at 10 m of elevation at the Aversa site; the device is located on the roof of a 2-story building belonging to the School of Science and Technology of the University of Campania “Luigi Vanvitelli”. The Aversa site (40°58’00’’N, 14°12’00’’E) is located 15 km North of Napoli, at

an elevation of 50 m and at a minimum distance from sea of 15 km. The surroundings are characterised by a flat orography and densely built areas with low- to medium-rise constructions. Measurements started being taken on October 9, 2015 and were stopped at the end of 2017. In particular, the measurements taken until July 27, 2016 have been used for the analyses. The device is able to measure simultaneously the volume-averaged instantaneous three components of the wind speed at 12 elevations from 40 m to 300 m of vertical distance from the instrument, with a sampling rate of 1 Hz. For this particular experiment elevations of 50, 60, 70, 80, 90, 100, 110, 120, 150, 200, 250 and 300 m were selected. Ten-minute averages of the horizontal speed were calculated from the measurements; these are 144 for each day of measurements, with a total of 42,048 for the 292 days of measurement.

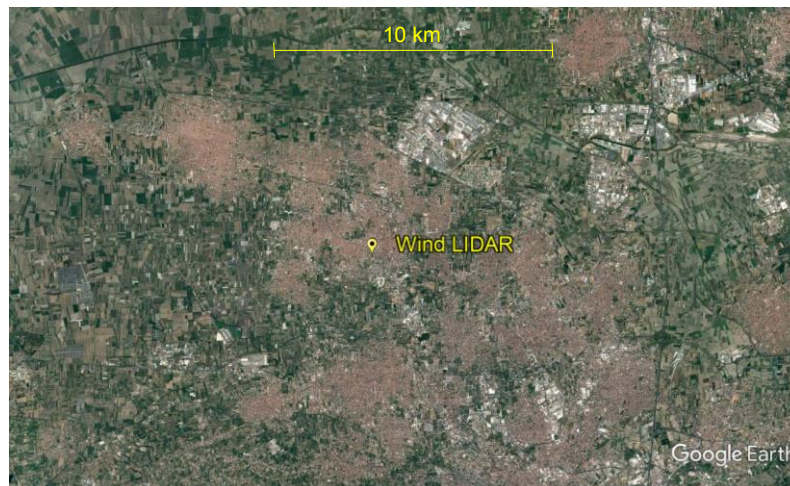


Figure 1. Aversa site.

3 Expected result

The flat terrain around the site of measurement allows neglecting any orography effect, therefore analysing only atmospheric stability and roughness effects. The vertical profiles of wind velocity are evaluated and will be analysed in the paper, with reference to atmospheric stability and site roughness. For neutral conditions, the available wind models (in particular the logarithmic profile and the linearized Deaves & Harris profile) will be discussed, with particular attention to the implications associated with Code implementations.

References

- Drew, D.R., Barlow J.F., Lane, S.E. (2013). Observation of wind speed profiles over Greater London, UK, using a Doppler lidar, *J. Wind Eng. Ind. Aerodyn.*, 121, 98-105.
- Lane, S., Barlow, J., Wood, C. (2013). An assessment of a three-beam Doppler lidar wind profiling method for use in urban areas, *J. Wind Eng. Ind. Aerodyn.*, 119, 53-59.
- Demartino C., Avossa A.M., Ricciardelli F., Calidonna C.R. 2017. Wind profiles identification using wind LIDARS: an application to the area of Lamezia Terme. *Proceedings of the 7th European and African Conference on Wind Engineering*, Liege, Belgium.
- Ricciardelli, F., Pirozzi S., and Mandara, A. (2016). *Comparison of wind LIDAR measurements with predictions from airport data*. 1stInternational TU1304 WINERCOST Conference, 21-22 April 2016, Ankara, Turkey
- Stull, R.B (1988). *An Introduction to Boundary Layer Meteorology*, Kluwer, Dordrecht.

Experimental study of wind loads on domed free roofs

Yasushi Uematsu¹ and Roma Yamamura¹

¹Department of Architecture and Building Science, Tohoku University, Japan

Corresponding author: Yasushi Uematsu, uematsu.yasushi@m.tohoku.ac.jp

Abstract

Design wind loads on domed free roofs have been investigated in a wind tunnel. Wind pressure distributions both on the top and bottom surfaces of the roof model were measured. The rise-to-span ratio, f/D , was varied from 0.1 to 0.4. First, the effect of the Reynolds number on the pressure distribution is examined. Then, the effects of f/D on the wind pressures and forces are made clear. Discussion is made of the design wind force coefficients for the main wind force resisting systems, in which focus is on the axial forces induced in the columns supporting the roof as the most important load effect, assuming that the roof is rigid and supported by four columns. Finally, the peak wind force coefficients for the design of cladding/components are proposed based on the maximum and minimum peak wind force coefficients irrespective of wind direction.

1 Introduction

Free roofs are widely used for structures providing shade and weather protection in public spaces. The roof is supported by columns and no walls. Being light and flexible, they are vulnerable to dynamic wind actions. Therefore, wind resistance is one of the most important technological problems, when designing these roofs. However, few studies have been made of the wind loads on domed free roofs, probably due to the difficulties in model making and pressure measurement.

The present paper experimentally investigates the design wind loads on domed free roofs. Wind pressure distributions both on the top and bottom surfaces are measured in a turbulent boundary layer. Based on the results, we propose the design wind force coefficients both for the main wind force resisting systems and cladding/components.

2 Wind Tunnel Experiment

Figure 1a shows a wind tunnel model made by using a 3D printer. The length scale of the model is assumed 1/100. The rise-to-span ratio, f/D , ranges from 0.1 to 0.4 with the diameter D being fixed to 150 mm. The roof of 2 mm thickness is supported by four columns of 6.5 mm diameter. The mean roof height H is 80 mm for all models. The coordinate system and notation are shown in Figure 1b. Nine pressure taps are installed both on the top and bottom surfaces along a centreline (Fig 1c), which provide the net wind forces on the roof. The tubing system is installed in the roof and columns. The wind direction is changed from 0° to 90°, providing the wind force distribution over the whole area.

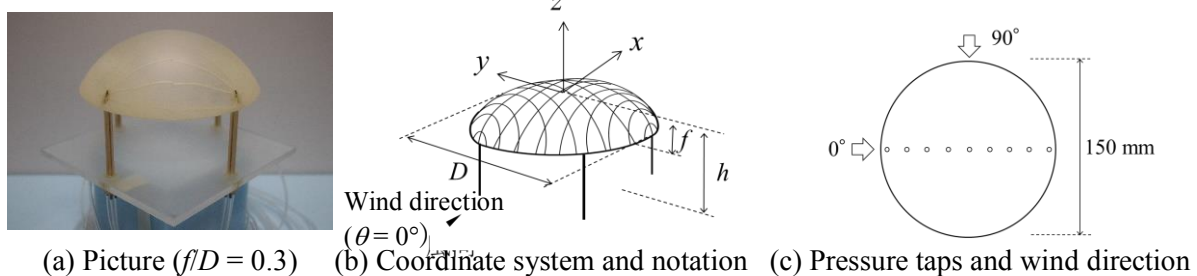


Figure 1. Experimental model

The wind tunnel flow is a turbulent boundary layer simulating a suburban exposure. The power law exponent of the mean wind speed profile is proximately 0.2. The wind tunnel speed U_H at the mean roof height is 9 m/s for $f/D = 0.1$ and 0.2 and 10 m/s for $f/D = 0.3$ and 0.4. The turbulence intensity I_{uH} at the mean roof height is approximately 0.16. Wind pressures at all taps are measured simultaneously at a sampling rate of 500 Hz. Each measurement is made for a time period of 10 minutes in full scale. The measurements are repeated 10 times. The statistical values of wind forces etc. are evaluated by applying an ensemble average to the results of these 10 runs.

3 Experimental Results and Discussion

3.1 Effect of Reynolds number on the pressure distribution

The Reynolds number Re is defined in terms of U_H and two times the radius curvature of the dome, corresponding to a circular cylinder. The wind speed U_H was varied from 3 to 11 m/s. The distributions of the mean wind force coefficients $C_{f,\text{mean}}$ for $\theta = 0^\circ$ were measured at various Re numbers. When $f/D = 0.1$, the distribution does not change with Re . This feature indicates that the wind flows along the roof surface without separation. On the other hand, when $f/D \geq 0.2$, the distribution changes with Re , which implies that the flow separates and the separation point shifts with Re . However, the distribution is hardly affected by Re when $Re > 1.0 \times 10^5$. This feature is consistent with the finding by Macdonald et al. (1988) for cylindrical structures. According to Macdonald et al., the results obtained under such a condition represent the practical situation in full-scale. Therefore, the measurements are made at $Re > 1.0 \times 10^5$ in the following sections.

3.2 Wind force coefficients for the main wind force resisting systems

First, the distributions of mean wind pressure coefficients both on the top and bottom surfaces of the model were measured. The results indicate that the distribution depends on the f/D ratio significantly. For discussing the design wind force coefficients for the main wind force resisting systems, focus is on the axial forces induced in the columns assuming that the roof is supported by four columns. Using the time history of wind pressure coefficients, we obtained the distribution of wind force coefficients at an instant when the maximum tension (Load case A) or the maximum compression (Load case B) was induced in the columns using a conditional sampling technique. Based on the results, we have proposed two sets of design wind force coefficients for the two load cases, A and B. In practice, the roof is divided into three zones by two straight lines perpendicular to the wind direction and constant values are provided to these three zones as a function of f/D . The coefficients are provided by applying spatial average to the distribution of wind force coefficients obtained from the conditional sampling technique. The design wind loads are provided by a gust effect factor approach. The gust effect factor is defined by the ratio of the maximum or minimum axial force to the mean axial force induced in the column.

3.3 Peak wind force coefficients for cladding/components

The distributions of the maximum and minimum peak wind force coefficients, $C_{f,\text{max}}$ and $C_{f,\text{min}}$, are obtained from the time history of wind force coefficients at all pressure taps for all wind directions. Because the roof is a rotationally symmetric structure, it is divided into a circular and two doughnut-shaped zones, R_1 to R_3 . Then, positive and negative peak wind force coefficients for the design of cladding/components are provided to these zones for each f/D ratio. Larger positive values are provided to the peripheral zone, while larger negative values are to the central zone.

References

- Macdonald, P.A., Kwok, K.C.S. and Holmes, J.D. (1988). Wind loads on circular storage bins, silos and tanks: I. Point pressure measurements on isolated structures. *Journal of Wind Engineering and Industrial Aerodynamics* **31**, 165-188.

Aerodynamic Optimization of Tall Buildings

Luca Viviani¹, Francesco Dorigatti¹, John Kilpatrick² and Jon Galsworthy²

¹ RWDI, Unit 1, Tilers Road, Milton Keynes, MK11 3LH, United Kingdom

² RWDI, 600 Southgate Drive, Guelph, Ontario, Canada, N1G 4P6

Corresponding author: Francesco Dorigatti, francesco.dorigatto@rwdi.com

1 Introduction

For tall or super tall buildings, it is not uncommon that across-wind excitation is the most critical source of lateral response. The natural frequencies of these structures are likely to be sufficiently low that they can be excited through vortex shedding at wind speeds related either to design or to serviceability return periods. Sometimes the across-wind response of tall buildings is found so onerous that any solution intervening only on the structural system would be impractical and, as such, the aerodynamic optimization of the shape of the building is warranted.

2 Mitigation of Across-Wind Excitation

Some cross sections, quite common in vertical building structures, are well known for being prone to across-wind excitation issues. Square or rectangular buildings with sharp corners are among those. If the risk of severe across-wind response is identified in the early stages of design, extensive measures such as tapering the building might still be viable (Irwin, 2008). However, if the wind consultant is involved in the design only at a relatively late stage of the process, introducing such radical alterations to the shape of the building can be difficult. Nonetheless, even in these circumstances some relatively minor geometry changes can be explored to mitigate severe across-wind responses. These include the alteration of the corner geometry, the opening of balconies and the introduction of porosity throughout the height of the tower (Gu and Quan, 2004; Tse et al., 2009). Experimental data collected by RWDI on commercial projects show how excessive across-wind excitation can be addressed effectively by implementing these minor geometry changes, while still meeting the client's requirements in terms of aesthetics and amount of sellable area.

This paper presents a number of case studies where mitigation of across-wind response on tall buildings was achieved through minor geometry changes. One of these case studies concerns a 380 m tall residential tower with a uniform rectangular cross-section of 50 m x 30 m. The building design originally had sharp corners and already included four refuge floors with permeable façade and a porous crown. The proposed site had an exposure corresponding to EN-1991-1-4 Category IV terrain. A 1:400 scale model of the building (Figure 1) was tested using the High Frequency Force Balance technique in RWDI's 2.7 by 2.1 m open-jet atmospheric boundary layer wind tunnel in Milton Keynes, UK. The wind tunnel data showed that the response of the tower was affected by severe across-wind excitation for wind blowing into the broader face, namely for winds in $\pm y$ direction (Figure 2). Given the magnitude of the response predicted for the design return period, it was soon clear that the structural system necessary to bear such loading would have been unreasonably massive, and aerodynamic mitigation options had to be investigated. The client not being keen to radically revise the building shape, a shaping workshop was carried out to investigate geometry changes of the corner areas only, with the purpose of mitigating the issue without significantly altering the original building design. Mitigation Options 1 and 3 introduced balconies on three corners of the building for most of the height of the tower, with slightly different geometries. Mitigation Option 2 had solid rounded

corners, with a radius of 3800 mm. Mitigation Options 4 and 5, finally, had corners chamfered with depths of 2800 mm and 3800 mm, respectively.

Figure 2 presents the plots of base overturning moment M_y for wind along the Y axis against the mean hourly wind speed at 600m height. The figure shows the considerable reduction of base overturning moment M_y achieved by all mitigation options. Considering the wind speed associated with the strength design return period, Option 2 gained a 45% reduction on the base moment M_y , while both Options 4 and 5 attained a reduction beyond 50%. Also, it is interesting to note that a reduced overall wind loading for strength design is associated with a shift to a lower value of the critical wind speed for vortex shedding. This has the collateral effect of increasing the serviceability level wind loads, and has the potential to aggravate the accelerations at the top of the building in the low ranges of return period. However, for the building presently considered, acceleration predictions remained within the criteria for human comfort.

3 Conclusions

Any of the mitigation measures that were tested for the case study presented was more welcome by the client than other options that would have required more severe geometry alterations. In the end, Option 2 was selected as it provided a sufficient reduction in overall wind loads for them to be compatible with the structural system and, at the same time, it minimized the loss of usable floor area compared to initial design that presented a sharp-corner rectangular section.



Figure 1 - Original model in the wind tunnel

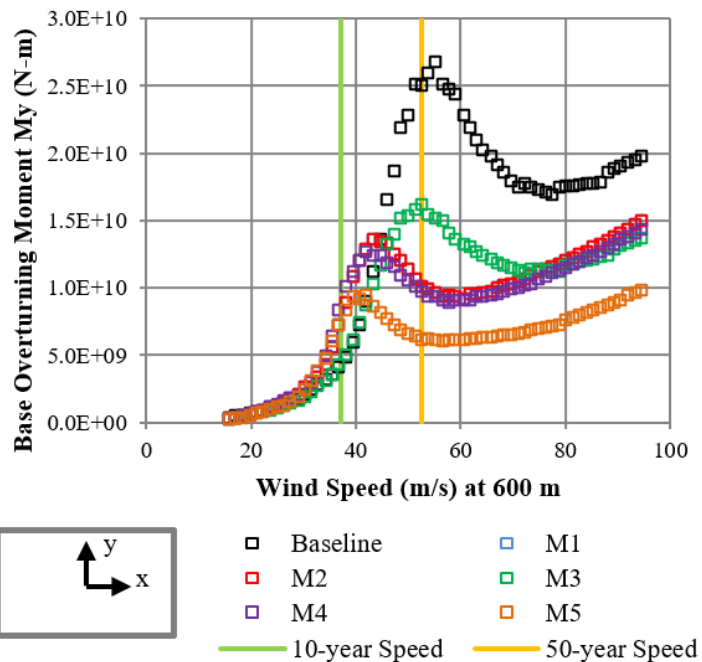


Figure 2 – Base overturning moment vs wind speed

References

Irwin, P.A. (2008). Bluff body aerodynamics in wind engineering. *Journal of Wind Engineering and Industrial Aerodynamics* **96**, 701–712.

Gu, M. and Quan, Y. (2004). Across-wind loads of typical tall buildings. *Journal of Wind Engineering and Industrial Aerodynamics* **92**, 1147-1165.

Tse, K.T. et al. (2009). Economic perspectives of aerodynamic treatments of square tall buildings. *Journal of Wind Engineering and Industrial Aerodynamics* **97**, 455-467.

Wind Pressures Distribution on a Porous Double Skin Façade System

A. Zasso¹, F. Perotti², L. Rosa¹, P. Schito¹, G. Pomaranzi¹ and N. Daniotti¹

¹Department of Mechanical Engineering, Politecnico di Milano, Italy

²Department of Civil and Environmental Engineering, Politecnico di Milano, Italy

Corresponding author: G. Pomaranzi, giulia.pomaranzi@mail.polimi.it

Abstract

Permeable double skin facades (permeable DSF) are part of modern architectural concepts. An accurate assessment of the wind loads and the porosity effects on this kind of facades is crucial for a correct design and performance evaluation. Measuring and predicting DSF airflow is not a straightforward task due to the interaction between the wind turbulence and the outer porous skin. Moreover, Eurocode and many other National Codes do not supply any prescription about such issue. In this paper the comprehensive experimental study of wind loads acting on the porous double skin facade of the *New Bocconi Campus*, currently under construction in Milan, is reported. Cladding loads assessment has been carried out performing wind tunnel tests on properly scaled rigid models able to reproduce the aerodynamic behaviour of the porous medium. Peak pressures for the inner facade have been estimated and compared to the ones expected forcing a standard glazed facade.

1 Introduction

Nowadays high efficiency facades such as ventilated double skins are often adopted in order to reduce the energy demand of the system. The impact of the double skin façade (now on DSF) on the inner face's pressure distribution has been very little investigated and neither the codes seem to propose a comprehensive section dedicated to the assessment of the wind load in this facade systems. Potential reduction of the wind pressure in the inner closed facade with respect to the standard glazed facade should be quantified since the cladding system can achieve up to 25% of the total building costs. When bespoke facade systems are involved, wind tunnel tests represent the only technique able to provide wind loads which are physically sound. The main objective of this research is focused on the assessment of cladding loads for the *New Bocconi Campus*, whose buildings are characterised by double skin porous facade systems. Ad-hoc wind tunnel tests have been commissioned to study the aerodynamic effect induced by porous outer skin on the pressures distribution acting on the inner glazed facade.

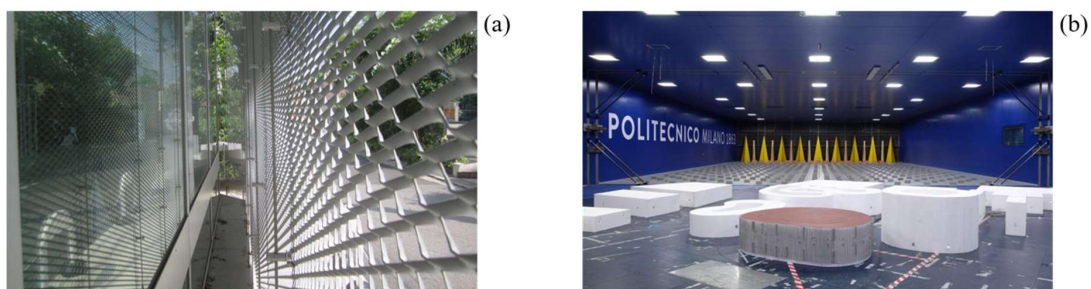


Figure 1. A porous double skin façade (a) and the New Bocconi Campus (b) in the Wind Tunnel.

In order to deeply understand the aerodynamic behavior of the porous media and to compute the pressure reduction in the inner facade, this research project is divided in two phases. In the first one, the buildings are tested as they would have a standard facade system to assess the wind loads acting on the

glazed facades without the porous media. Once the pressures distribution from this first stage is known, the attention may be focused on the building characterised by the worst condition in terms of wind load. Hence, during the second test, only the aforesaid structure is instrumented with pressure taps and the double skin porous facade is designed. The scaled porous model is able to reproduce the same aerodynamic effect of the porous facade at real scale provided that the same pressure loss coefficient is kept. By comparing the two tests outcomes, the beneficial effect of the porous medium in terms of peak pressures reduction is highlighted.

2 Results

An in-depth study of the time histories recorded in both tests has been conducted and the different nature of the signals has emerged. Inner facade's pressure distribution, acquired during the second stage where the DSF is modelled, is no more characterized by sharp and concentrated peaks, which appear smoothed instead. Moreover, those signals show higher correlation in space with respect to the corresponding ones which would act on a standard façade. Peak pressure distributions have been computed for both tests, according to the Cook and Mayne method, since the cladding design relies on such pressure values. Envelopes of negative peak pressures are shown in figure 2a, where the two tests results are compared. The aerodynamic effect induced by the porosity of the outer skin results in strong reduction with respect to the most severe peak values recorded on the no DSF model. The meaningful pressures exhibit reduction greater than 40%; making reference to the current practice in cladding design, which generally adopts on the safe side a unique dimensioning value, the decrease of the strongest suction from the no DSF test is equal to 63% (C_p increases from -3.21 to -1.18).

Looking at the percentage decreases of the envelope diagrams, shown in Figure 2b, it appears that the porous double skin system may play a very important role in the wind load reduction, since highest values are exhibited where the no DSF envelopes have the strongest peak pressures.

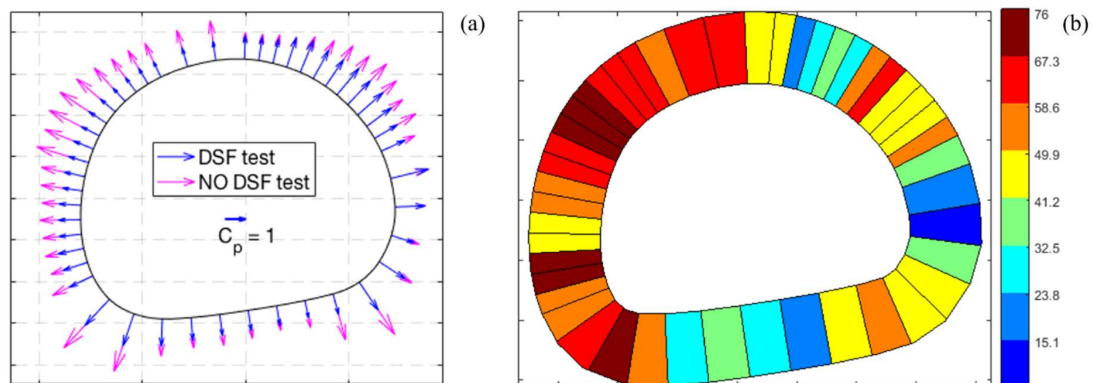


Figure 2. Envelope of the negative peak pressures for both tests (a) and the percentage decreases (b).

References

- Belloli, M., Rosa, L., & Zasso, A. (2014). Wind loads and vortex shedding analysis on the effects of the porosity on a high slender tower. *Journal of Wind Engineering and Industrial Aerodynamics*, 126, 75-86.
- Cook, N. J. (1986). *Designers guide to wind loading of building structures*. Butterworth Publishers, Stoneham, MA, 1986.
- Gerhardt, H. J., & Janser, F. (1994). Wind loads on wind permeable facades. *Journal of Wind Engineering and Industrial Aerodynamics*, 53(1-2), 37-48.

Numerical study of wind-induced pressure on a high-rise building with balconies: comparison of LES, RANS and experiments

Xing Zheng¹, Hamid Montazeri^{1,2}, Bert Blocken^{1,2}

¹ Building Physics and Services, Department of the Built Environment,
Eindhoven University of Technology, the Netherlands

² Building Physics Section, Department of Civil Engineering, KU Leuven, Belgium

Corresponding author: Xing. Zheng, x.zheng.1@tue.nl

Abstract

Information of the wind-induced pressure distribution on building facades is essential to evaluate infiltration, wind-induced natural ventilation and wind loads on building facades. Earlier studies have shown that geometrical details like balconies can significantly affect the pressure distributions on building facades. However, research on the impact of the façade geometrical details, such as balconies, is limited. This paper, therefore, presents a detailed CFD study to investigate the impact of balconies on the mean static pressure distribution on the facades of a high-rise building with balconies. To gain insight into the performance of Large-Eddy Simulations (LES) compared to steady Reynolds Averaged Navier-Stokes (RANS), LES and RANS CFD simulations are performed for three wind directions $\theta = 0^\circ$, 90° and 180° . The evaluation is based on the validation against wind-tunnel measurements of mean surface pressure. The results show that both LES and RANS can accurately predict the mean static pressure on the windward façade for $\theta = 0^\circ$. In this case, the average absolute deviations between the CFD results and wind-tunnel measurements are 0.076 and 0.099 for LES and RANS, respectively. Under the other two wind incident angles, LES has better reproductions of static pressure than RANS. The average absolute deviations for $\theta = 90^\circ$ are 0.104 and 0.298 by LES and RANS, respectively; for $\theta = 180^\circ$, the average absolute deviations are 0.043 and 0.161 by LES and RANS, respectively.

1 Introduction

Knowledge of the pressure coefficient distributions on building facades and roofs is important to evaluate wind-induced natural ventilation, infiltration, and wind loads on building facades and building components. Earlier studies have shown that façade geometrical details like balconies can significantly affect the near-façade airflow pattern and the pressure distributions on building walls (Stathopoulos and Zhu, 1988) (Montazeri and Blocken, 2013) (Murakami, 1990). However, research on the impact of balconies is limited. The present study, therefore, investigates the wind-induced mean pressure on the façade of a high-rise building with balconies. Previous studies using the steady RANS approach shown a good agreement between CFD and wind tunnel for the windward façade at $\theta = 0^\circ$ (Montazeri and Blocken, 2013). However, this is not the case for other wind directions as steady RANS is incapable of capturing the inherently transient behavior of separation, reattachment and von Karman vortex shedding in the wake. LES, on the other hand, can provide accurate descriptions of the mean and instantaneous flow field around bluff bodies. To gain insight into the performance of LES compared to steady RANS, LES and steady RANS CFD simulations are performed. The evaluation is based on validation with the wind-tunnel measurements by Stathopoulos and Zhu (1988).

2 Computational setup

A computational model is made of the reduced-scale building model (1:400) in the wind-tunnel measurement with the dimensions of width \times depth \times height = $0.152 \times 0.152 \times 0.3 \text{ m}^3$. The 3D steady

RANS equations are solved in combination with the realizable $k-\varepsilon$ turbulence model. The standard wall functions are applied for modeling flow parameters in the near-wall region. The LES simulation is performed with the WALE model ($C_{wale} = 0.325$) and Werner-Wengle wall treatment. The inlet vertical profiles (mean velocity U , turbulent kinetic energy k , and turbulence dissipation rate ε) in the simulations are based on the measured mean wind velocity and longitudinal turbulence intensity.

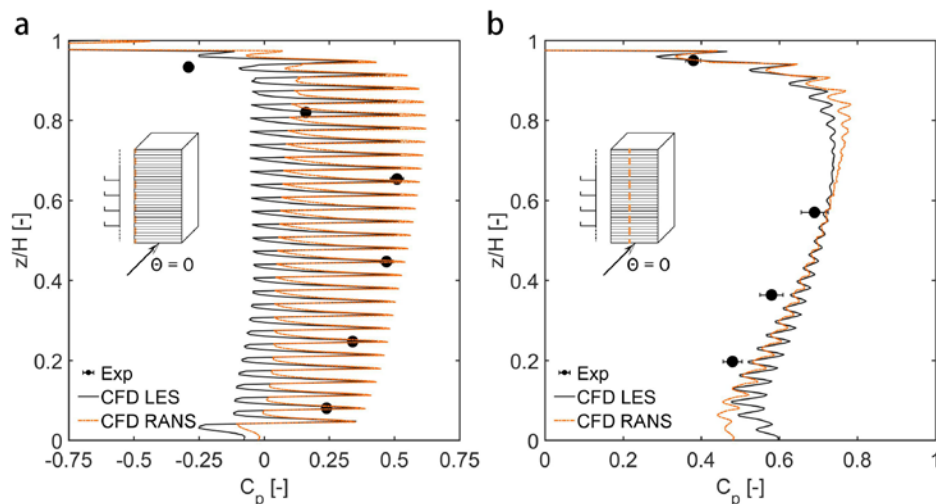


Figure 1. Comparison of C_p obtained by LES and RANS with wind-tunnel experiment data along edge line (a) and center line (b).

3 Results

The CFD results are validated with the measured mean pressure coefficients (C_p) along the “edge line” (0.0015 m to the edge of the building model) and the center line (0.0610 m to the edge) on the windward façade of the model (Fig. 1a&b). Good agreements are obtained along the center line, where the average absolute deviations are 0.032 and 0.026 for LES and RANS, respectively. At the edge line, the deviations increase to 0.119 and 0.171 for LES and RANS, respectively. However, under the other two wind incident angles, LES has better reproductions of static pressure than RANS. The average absolute deviations for $\theta = 90$ are 0.104 and 0.298 by LES and RANS, respectively; for $\theta = 180$, the average absolute deviations are 0.043 and 0.161 by LES and RANS, respectively. Detailed results will be published in the full paper.

Acknowledgements

Hamid Montazeri is currently a postdoctoral fellow of the Research Foundation - Flanders (FWO) and is grateful for its financial support (project FWO 12M5316N). The authors also gratefully acknowledge the partnership with ANSYS CFD.

References

- Montazeri, H., and Blocken, B. 2013. CFD Simulation of wind-induced Pressure Coefficients on buildings with and without balconies: Validation and Sensitivity Analysis. *Building and Environment* **60**, 137–49.
- Stathopoulos, T., and Zhu, X. 1988. Wind Pressures on Building with Appurtenances. *Journal of Wind Engineering and Industrial Aerodynamics* **31** (2–3), 265–81.
- Murakami, S. 1990. Computational Wind Engineering. *Journal of Wind Engineering and Industrial Aerodynamics* **36**, 517-538.

On effects of Correction Factor for VIV Amplitude from a Prototype Prism and 2D Section Model

Shuai Zhou, Lixin Tan and Shuisheng Li

China Construction Fifth Engineering Division Corp.LTD, China

Corresponding author: Shuai Zhou, zhoushuai2008@126.com

Abstract

Additional correction factor is required to predict the maximum vibration amplitude of 3D prototype structure according to the 2D section model result because of the differences in both mode shape and spanwise correlation of excitation forces between them. In this study, a 4.5m long rectangular prism with cross section of 50mm 70mm is taken as 3D prototype structure, its fundamental mode vortex-induced vibrations was measured in smooth and uniform flow wind tunnel test. The 1:1 2D section model having the same dimensions of cross-section as the prototype prism, was also tested in same flow condition and same equivalent mass, damping ratio, vibration frequency, scaling effects were eliminated. The prototype prism produces a roughly 20% higher maximum amplitude than the section model. For flexible rectangular prisms, the present study confirms that the combined three-dimensional (3D) effects due to mode shape and imperfect correlation of excitation forces .etc. contribute positively and disregarding the 3D effects may underestimates the maximum VIV amplitudes for section model tests. A correction factor of 1.2 for the VIV amplitude is suggested for similar practical use when converting the section model results to their corresponding fundamental mode prototype values.

1 Experimental setup

The comparison of main parameters of 3D prototype prism and 1:1 2D rigid section model are shown in Table.1.

Table.1 Main parameters of Case 1

Main parameters	Symbol	Units	Prototype prism tests	2D section model tests	Deviation
Flow condition	-	-	Uniform	Uniform	-
Cross section of prism	D	mm	70	70	0
	B	mm	50	50	0
	R	mm	4	4	0
Equivalent mass	M	Kg/m	3.51	3.56	1.4%
Natural frequency	f_0	HZ	12.89	12.91	0.2%
Damping ratio	ζ	%	0.581	0.588	1.2%
Scruton number	Sc	-	42.7	43.8	2.6%
Predicted VIV onset velocity	U	m/s	7.5	7.5	0

Where, $Sc=4\pi M\zeta/\rho D^2$ is Scruton number; R is the radius of model corner.

2 Results and Discussion

Fig.1 shows the comparison of maximum VIV amplitude between 3D prototype prism result and 1:1 2D section model. The expected agreements of VIV lock-in between them were observed, including onset velocities,

initial branches and lower branches. However, the fundamental mode maximum VIV amplitude of 3D prototype prism (Happened at middle point of the prism) reached at 0.036, a slightly higher than the 1:1 2D section model obtained 0.030, with the ratio of 1.2.

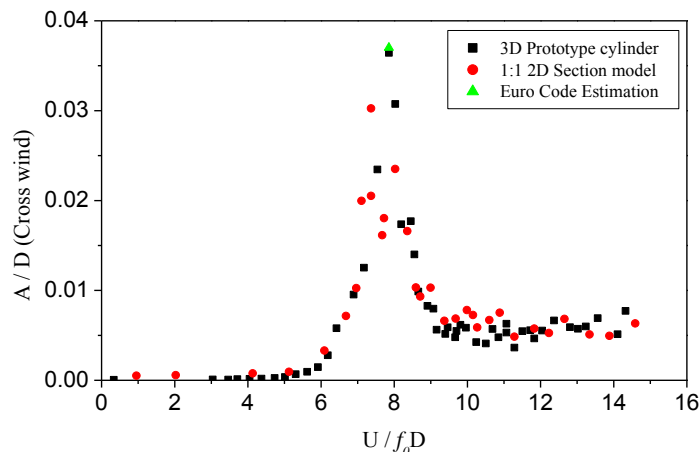


Fig.1 The comparison of maximum amplitude response between 3D prototype prism and 1:1 2D section model

3. Conclusions

This paper described the measurement results of the VIV amplitude from a 3D prototype rectangular prism and its 1:1 2D section model to assess the correction factor between them. Both the VIV onset velocity and lock-in range were observed to be coincided well for prototype prism and section model in velocity-amplitude curves.

Under the same structural parameters, the 3D prototype rectangular prism achieved higher maximum VIV amplitude than 2D section model by a factor of 1.2. The present study confirms that the combined three-dimensional (3D) effects due to mode shape and imperfect correlation of excitation forces contribute positively. In this case, the correction factor is suggested to be 1.2 when predicting the fundamental mode VIV amplitude of prototype rectangular prisms from section model measured results.

4. Acknowledgments

This study is mainly sponsored by the National Science Foundation of China with the program number No. 51708202, 51422806, 51478181, U1534206 which are greatly acknowledged.

References

- EN 1991-1-4:2004, Annex E.1.5.2.1 (2004), Eurocode-Basic of Structural Design, 1-1-4: 116–131.
- Govardhan R N. and Williamson C H K. (2006), Defining the modified griffin plot in vortex-induced vibration: revealing the effect of Reynolds number using controlled damping. *Journal of Fluid Mechanics*, 561, 147–180.
- Macdonald J. H. G., Irwin P. A., Fletcher M. S (2002). Vortex-induced vibrations of the Second Severn Crossing cable-stayed bridge—full-scale and wind tunnel measurements. *Proceedings of the Institution of Civil Engineers Structures & Buildings* 152, 123–134
- Ruscheweyh H., Practical experience with wind induced vibrations, *Journal of Wind Engineering and Industrial Aerodynamics*, 1990, 33: 211-218
- Sarpkaya, T. (2004), A critical review of the intrinsic nature of vortex-induced vibrations. *Journal of Fluids and Structures*, 19, 389–447.
- Zhang, Z.T., Ge, Y.J. and Chen, Z.Q. (2014), Vortex-induced oscillations of bridges: theoretical linkage between sectional model tests and full bridge responses. *Wind and Structures*, 19(3): 233-247.

AUTHOR INDEX

Álvarez A.	117	Chen J.	73
Amerio L.	1	Cheyne E.	41, 45
Amitay M.	119	Chiaracane A.	69
Andrienne T.	3, 143, 147	Churin P.	49
Antoun J. E. K.	17	Ciano M.	51
Argentini T.	7	Cid Montoya M.	53, 117
Astolfi D.	9	Cindori M.	55
Attrill S.	11	Coiro D. P.	57
Avossa A. M.	103, 141, 159	Como M.	59
Balbi A.	13	Damele M.	133
Barbanti G.	15	Daniotti N.	165
Barbato M.	17	Demartino C.	61
Bartoli G.	19, 27, 71, 75, 123, 129	Denis A.	63
Bayati I.	21	Denoël V.	3, 143, 147
Becchetti M.	65	Dorigatti F.	163
Belloli M.	21, 25, 79	Džijan I.	55
Bernini L.	21, 23	Egorychev O.	49
Bizzarrini N.	57	El-Batsh H. M.	65
Blocken B.	105, 137, 139, 167	Eltayesh A.	65
Bogunović Jakobsen J.	41	Facchinetti A.	21
Bordogna G.	25	Fenerci A.	67, 101
Borri C.	15, 69, 115	Ferri G.	69
Bruno L.	85, 131	Fontanella A.	21
Buccolieri R.	27	Freda A.	13
Buljac A.	29, 31	Frison G.	71
Buresti G.	111	Galsworthy J.	163
Burlando M.	33, 65	Garcia Navarro J.	37
Calise G.	57	Georgakis C. T.	73, 103
Calotescu I.	35	Giachetti A.	27, 75
Cammelli S.	37	Giappino S.	25, 77, 79
Cao N.	113	Giaralis A.	127
Caracoglia L.	89	Giberti H.	21
Carassale L.	91	Gioffrè M.	51
Castellani F.	9, 65	Gorlé C.	1, 95
Caterino N.	39, 73	Gribach J.	49
Chang CH	93	Grigoriu M.	51

Hangan H.	33, 91, 151	Mariotti A.	111
Hernández S.	53, 117	Marra A. M.	19, 71, 123
Higashimura R.	113	Massai T.	27
Höffer R.	69, 99	Matsuda K.	113
Holmes J. B.	83	Miyashita K.	155
Horvat M.	85	Mockutè A.	31, 115
Hu G.	87	Montazeri H.	105, 137, 167
Ierimonti L.	89	Moore D. M.	119
Jurado J. Á.	117	Muggiasca S.	25, 77
Juretić F.	55	Mulas M.	121
Karami M.	91	Nguyen-Sinh H.	37
Kareem A.	29	Nicese B.	123
Kato K.	113	Niemann H.-J.	99
Khris S.	85	Nieto F.	53
Kilpatrick J.	163	Nikitas N.	97
Kim YC	93	Øiseth O.	67, 101
Kozmar H.	29, 31, 55	Omarini S.	7, 79
Kwok K. C. S.	87	Patruno L.	125
Lamberti G.	1, 95	Perotti F.	165
Letchford C. W.	119	Petrangeli M.	7
Li S.	169	Petrini F.	17, 127
Liao H.	97	Piccardo G.	63
Lin S.	97	Pigolotti L.	129
Lo YL	93	Poddaeva O.	49
Lo Giudice A.	85	Pomaranzi G.	165
López C.	117	Pospíšil S.	31
Lugni C.	115	Pugliano G.	39
Lupi F.	69, 99	Quarta F.	27
Lystad T. M.	101	Raffaele L.	131
Macháček M.	31	Refan M.	91
Maienza C.	103	Reipas K.	11
Malizia F.	105	Repetto M. P.	13, 133
Manara G.	107	Rezaeiha A.	137
Manenti A.	77	Ricci A.	139
Mannini C.	19, 75, 109, 123, 129	Ricci M.	125
Marino E.	15, 115	Ricciardelli F.	61, 103, 141, 159

Riefolo L.	141	Zasso A.	1, 7, 21, 157, 165
Rigo F.	3, 143, 147	Zheng X.	167
Rizzo F.	159	Zhou S.	169
Robustelli U.	39	Zucca R.	121
Romanić D.	33, 151		
Rosa L.	157, 165		
Salveti M. V.	111		
Sasaki R.	155		
Scherillo F.	57, 103		
Schito P.	79, 157, 165		
Scotta R.	71		
Sepe V.	159		
Snæbjörnsson J.	41		
Solari G.	13, 33, 63		
Somaschini C.	79		
Spizzuoco M.	73		
Tan L.	169		
Tang V.	11		
Tarsitano D.	23		
Tenni M.	79		
Terzi L.	9		
Tomasicchio G. R.	141		
Tomasini G.	23		
Troise G.	57		
Tse K. T.	87		
Uematsu Y.	161		
Vardaroglu M.	141		
Venanzi I.	89		
Vicinanza D.	141		
Viviani L.	163		
Wang Qi	97		
Wang Z.	127		
Winkelmann U.	69		
Yamamura R.	161		
Yang W.	29, 97		
Yoshie R.	155		

SPONSOR



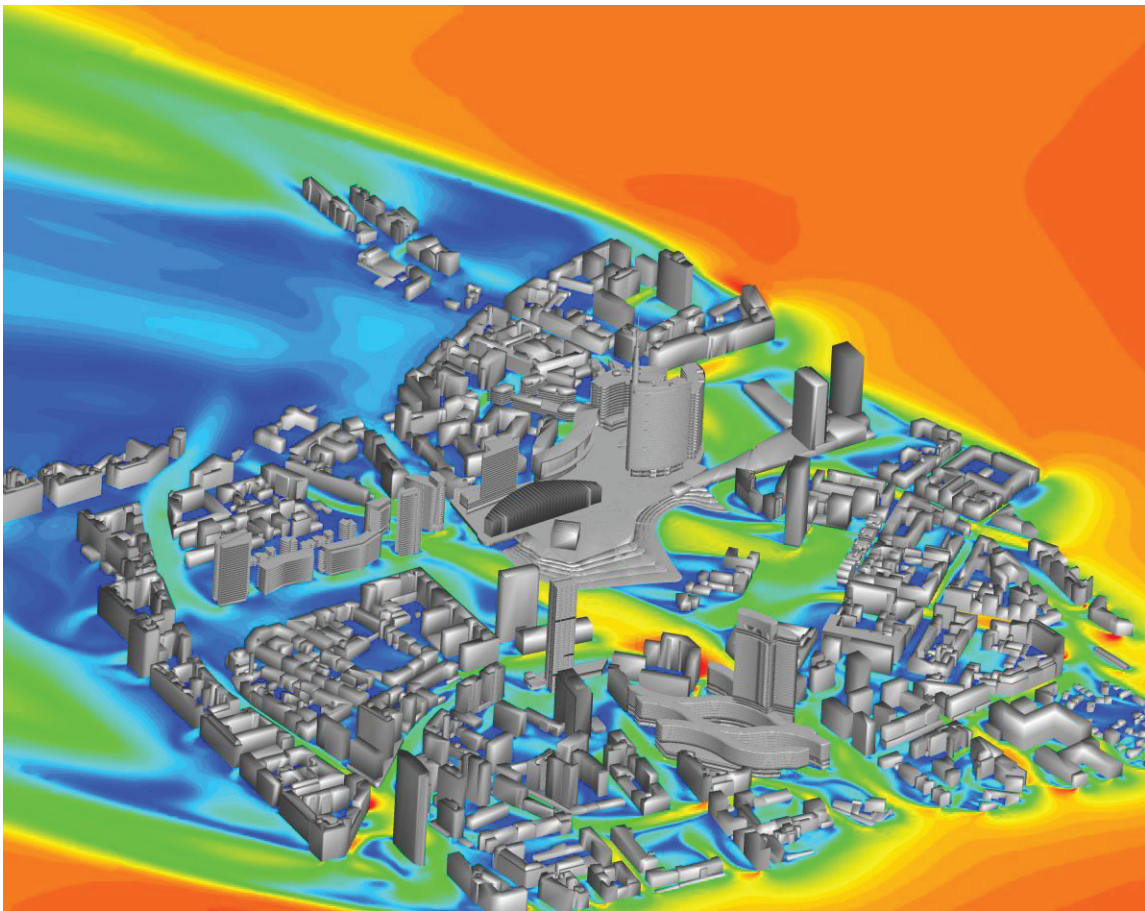
NAPOLI | IN-VENTO 2018

IN-VENTO 2018
XV Conference of the Italian Association for Wind Engineering
9-12 September 2018, Napoli, Italy

CSPFEA

ENGINEERING SOLUTIONS

CSPFea
via Zuccherificio, 5/D – 35042 Este (PD)
www.ingegneriadelvento.it
info@ingegneriadelvento.it



CSPFea è stata fondata da ingegneri civili strutturisti che, dopo un lungo impegno nell'attività professionale, hanno deciso di dedicarsi alla loro passione: i **software di analisi** e calcolo. Da quasi 15 anni ricerchiamo i migliori e più affidabili codici di calcolo per impararne le potenzialità ed i limiti e poterli distribuire alle migliori società di ingegneria italiane e svizzere ed ai più esperti professionisti nell'ambito del **calcolo strutturale e della simulazione**.

Ad oggi contiamo **più di mille clienti** che applicano le soluzioni software da noi distribuite nei più disparati campi applicativi: **ponti, tunnel, geotecnica strutturale, edifici in CA e acciaio, dighe, centrali nucleari, impianti e raffinerie**. Molti di loro sono già leader nel proprio settore applicativo e cercano un software strutturale reputabile e all'altezza delle sfide. In questi quindici anni abbiamo visto crescere anche molti neolaureati che hanno scelto le nostre soluzioni e oggi sono professionisti riconosciuti e ricercati per le loro alte competenze.



» VENDITA SOFTWARE

*Reputato nei settori:
Analisi strutturale sismica,
geotecnica, vento/clima,
Fire Safety Engineering,
structural BIM.*



» SUPPORTO TECNICO

*Supporto tecnico al
cliente a 360 gradi,
rapido ed accurato.*



» CORSI DI FORMAZIONE

*Corsi di formazione ed
affiancamento su progetto,
dedicata ai clienti utenti dei
software, per le tematiche
di modellazione ed analisi,
interpretazione dei risultati,
relazioni di calcolo*

» CORSI E TRAINING

*Dedicati ai nuovi clienti, alle Società di ingegneria
per i nuovi assunti, a tutti coloro che necessitano
approfondire tematiche di loro interesse. Forniamo
corsi base ed avanzati per ogni software, con cadenza
mensile nella sede di Este. Corsi presso gli Ordini degli
Ingegneri del territorio. Corsi dedicati in-house per
Società di Ingegneria ed Aziende.*

Il mondo dell'ingegneria, nel comparto AEC, sta cambiando rapidamente e in CSPFea crediamo che il **BIM** potrà essere un'enorme opportunità per gli ingegneri, poiché impone un modello digitale e un workflow numerico tra le discipline. Chi conosce le tecniche di modellazione può trarre un vantaggio dal BIM e dagli usi che se ne possono fare. Ci siamo evoluti fornendo strumenti di **Building Performance Simulation** che dal settore **strutturale** si estendono alla **fluidodinamica** degli edifici, al Green Building Performance, al **Fire Safety Engineering** e alla **simulazione delle folle** nei grandi ambienti.

I clienti riconoscono in CSPFea un **tutor fondamentale** per l'apprendimento dei software, dalle basi teoriche alle applicazioni avanzate.





Research

Professional Anemometers for Research Projects

The Gill Research range of 3-axis ultrasonic anemometers is particularly suited to applications such as fine scale Eddy Covariance or trace gas dispersion analysis studies, as well as no compromise high speed aerodynamic flow pattern work. R3 and HS anemometers are available with 50Hz or 100Hz output rates and will provide U, V, W vector, sonic temperature & speed of sound outputs.



Research RANGE

R3 professional 3D ultrasonic anemometers have an omni-directional head design, ideal for Eddy Covariance analysis and the study of turbulent air flows. R3 products will monitor wind speeds up to 45m/s and offer sonic temperature, speed of sound and U, V & W vector outputs, at an output rate of 50Hz for the R3-50 and 100Hz for the R3-100.

R3 50

R3 100

Wind Speed Range	45m/s (100mph)	45m/s (100mph)
Output Rate	50Hz	100Hz
Construction	Aluminium and Carbon Fibre	Aluminium and Carbon Fibre
Operational Temp	-40°C to +60°C	-40°C to +60°C
Weight	1.0kg (35oz)	1.0kg (35oz)

HS RANGE

HS professional 3D ultrasonic anemometers have a unique horizontal head design that allows for a more accurate measurement of vertical flows with minimal interruption from the anemometer geometry. Featuring a built-in inclinometer for simple positioning of the instrument on a tower or mast. A separate electronic interface allows easy access to the PRT and 6 analogue inputs.

HS anemometers will monitor wind speeds of 0-45m/s, the HS-50 provides a sampling rate of 50Hz and the HS-100 provides a faster 100Hz sample rate.



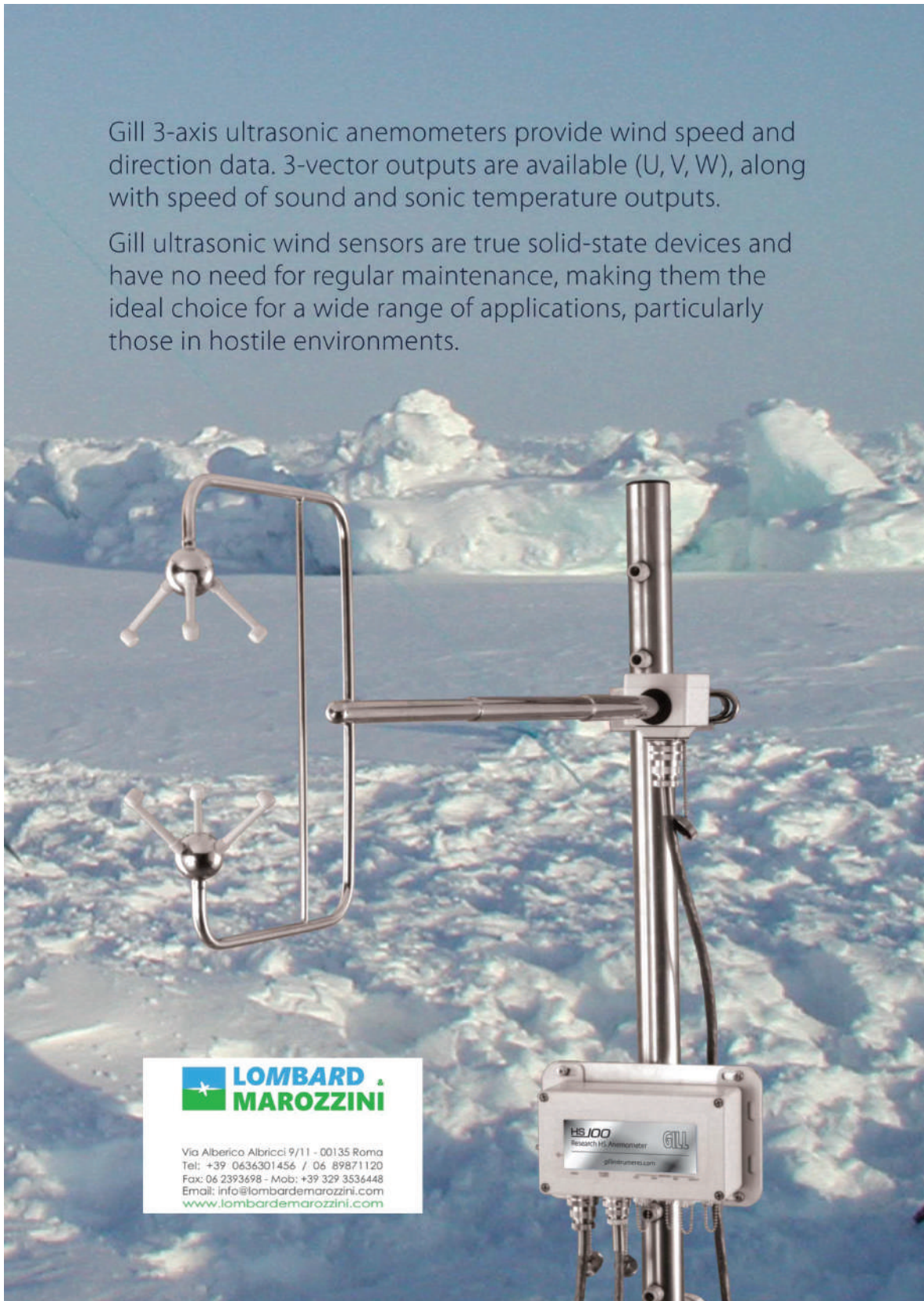
HS 50

HS 100

Wind Speed Range	45m/s (100mph)	45m/s (100mph)
Output Rate	50Hz	100Hz
Construction	Stainless Steel	Stainless Steel
Operational Temp	-40°C to +60°C	-40°C to +60°C
Inclinometer	Included	Included

Gill 3-axis ultrasonic anemometers provide wind speed and direction data. 3-vector outputs are available (U, V, W), along with speed of sound and sonic temperature outputs.

Gill ultrasonic wind sensors are true solid-state devices and have no need for regular maintenance, making them the ideal choice for a wide range of applications, particularly those in hostile environments.



**LOMBARD .
MAROZZINI**

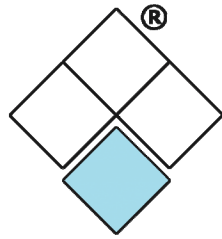
Via Alberico Albricci 9/11 - 00135 Roma
Tel: +39 0636301456 / 06 89871120
Fax: 06 2393698 - Mob: +39 329 3536448
Email: info@lombardemarozzini.com
www.lombardemarozzini.com



With over 1200 commercial LEOSPHERE coherent Doppler Lidar (laser radar) remote sensors now in operation globally, the technology has rapidly matured and is deployed onshore and offshore by meteorological offices, airports, the aviation industry, wind farm developers and operators, defense, port installations and research institutes.

LEOSPHERE is a world leader in atmospheric remote observations by Lidar. The company develops, sells and services a range of turnkey autonomous and networkable remote-sensing instruments allowing real-time key meteorological and atmospheric measurements such as wind, wind shear, wake turbulence, boundary layer height, clouds and aerosols.





SARTELCO[®] SISTEMI SRL

Founded over 25 years ago, Sartelco Sistemi qualifies as a value added partner for professional anemometry and meteorology.

The company provides professional weather instrumentation and services to Research Institutes, Universities, Ports, Airports, Wind Farm Developers and Operators (onshore and offshore), Wind Turbine Manufacturers, Public Companies and Industries.

The understanding and sharing customers' needs as well as a wide product portfolio and the cooperation with global professional partners are the key to Sartelco's operations.

From preliminary advice to the installation and maintenance services, from technical support to post-sales assistance, Sartelco Sistemi can constantly support customers with valuable suggestions and the most up-to-date procedures.

Sartelco Sistemi can also offer turn-key solutions.

Sartelco Sistemi is **ISO 9001:2015** certified.





ASSOCIAZIONE NAZIONALE PER L'INGEGNERIA DEL VENTO

Iawe member
INTERNATIONAL ASSOCIATION FOR WIND ENGINEERING



Università
degli Studi
della Campania
Luigi Vanvitelli

Scuola Politecnica e
delle Scienze di Base
Dipartimento di Ingegneria